DEVELOPMENT OF WEAK WAVES IN STEADY TWO-DIMENSIONAL SUPERSONIC FLOW WITH VIBRATIONAL RELAXATION

BY

R. P. HORNBY

A thesis presented to the University of Manchester
in support of an application for the degree
of Doctor of Philosophy

[1972]

ACKNOWLEDGEMENTS

I am deeply indebted to Professor Johannesen both for the opportunity to carry out this research and for the invaluable advice, encouragement and help given during the course of my stay and in the preparation of this thesis. I wish to express thanks to Dr. J.P. Hodgson for his enthusiastic support and guidance with the experiments and for many constructive suggestions. I am also grateful to Mr. C.G. Dain, my friend and colleague, for his help with the experiments and for numerous discussions of mutual benefit. I thank Dr. Gerrard and Mr. I. Sandler for their advice on computing. My gratitude to Mr. A. Ritson for making the wedge model and to all technicians at the Fluid Mechanics Laboratory who were involved in the experimental work. Finally I would like to thank Mrs. J. Davies for typing this thesis.

During the period of this research I was in receipt of a grant from the Science Research Council.

R. P. Hornby.

R.P. HORNBY
October 1972

PREFACE

The author graduated with a first class honours B.Sc. degree in Mathematics at the University of Manchester in June 1969. He then spent one year doing research in the Department of the Mechanics of Fluids at the University of Manchester and enrolled in October 1970 for a degree of Ph. D. in the same Department. The work described in this thesis was performed in the above Department between October 1970 and October 1972 and no part has been submitted in support of an application for any degree of this or any other University.

SUMMARY

The method of characteristics is used to solve the flow of a relaxing gas about a wedge of small angle. The results are presented in a concise similarity form that permits accurate extrapolation. A comparison is made with experimentally observed flows in CO_2 and N_2O. The available analytic techniques, valid for very weak wave flows, are described and a comparison between the method of characteristics and the method of matched expansions is presented.

CONTENTS

Part 1

CONTENTS (contd.)

Part 1 (contd.)

Part 2

.....

NOTATION

The use of subscripts and superscripts

The subscript ∞ will be used to denote a freestream variable. The subscripts f and e will be used to denote variables in the frozen and equilibrium states respectively.

The subscript α will be used to denote quantities relating to the alpha-shock and the alpha-gas.

The subscript o will be used to denote quantities at the wedge tip, immediately downstream of the alpha-shock.

The subscript w will be used to denote specific quantities on the wedge surface and the subscript ℓ will refer to quantities as predicted by the linear theory presented in section (1), Chapter 5.

In Chapter 5, section (4) the subscript ch will be used to denote variables on a negative characteristic.

Quantities with combinations of these subscripts have obvious meanings. For instance, $m_{f\infty}$ denotes the frozen freestream Mach number.

The subscript e when not used in combination with the ∞ subscript will refer to the equilibrium state downstream of the shock wave at infinity.

The superscript $*$ will be used to denote a critical quantity (defined in section (4), Chapter 1).

Subscripted quantities with special meanings are defined in the following list of notation

p	pressure
ρ	density
T	alpha-gas temperature
T_{vib}	vibrational temperature
T_c	characteristic temperature of vibration
a	sound speed
V	velocity magnitude
$\left\{ \begin{matrix} u \\ v \end{matrix} \right.$	x, y components of velocity
$\left\{ \begin{matrix} u_n \\ v_n \end{matrix} \right.$	x_n, y_n components of velocity
m	Mach number
$m_{n\infty}$	component of Mach number normal to shock wave at infinity

Notation (contd.)

σ	vibrational energy
$\bar{\sigma}(T)$	value of the equilibrium vibrational energy at temperature T.
$(\bar{\sigma}-\sigma)_{max}$	maximum value of $(\bar{\sigma}-\sigma)$ on a positive characteristic.
$(\bar{\sigma}-\sigma)_{max\infty}$	maximum value of $(\bar{\sigma}-\sigma)$ in the shock wave at infinity.
$(\bar{\sigma}-\sigma)_{a\infty}$	value of $(\bar{\sigma}-\sigma)$ immediately downstream of the alpha-shock in a partly dispersed shock wave at infinity
s	real gas entropy
s_a	alpha-gas entropy
$\underline{\Phi}$	relaxation frequency per unit density.
$\underline{\Phi}_c$	relaxation frequency per unit density at the characteristic temperature of vibration.
R	gas constant per unit mass of gas
c_{pa}	specific heat at constant pressure of the alpha-gas
c_{va}	specific heat at constant volume of the alpha-gas.
c_{vib}	vibrational specific heat
γ_f	$\frac{c_{pa}}{c_{va}}$
γ_e	$\frac{(c_{pa}+c_{vib})}{(c_{va}+c_{vib})}$
ν	Prandtl-Meyer function
θ	flow deflection relative to y = o
θ_w	wedge angle
ϕ	shock angle relative to y = o
ϕ^p	velocity potential
μ	Mach angle
k_s	shock curvature at wedge tip
ΔN	fringe shift
d	fringe spacing
λ	source light wavelength
D	width of shock tube working section
K	Gladstone-Dale constant
A	$\frac{(c_{pa}+c_{vib})}{c_{pa}V_\infty}$
b	$\frac{(M_{e\infty}^2-1)}{(M_{f\infty}^2-1)}$ (Chapter 5)
B	$\frac{(b-1)}{A\,b^{\frac{1}{2}}}$
C	$\frac{(\gamma_e+1)M_{e\infty}^4}{2(M_{e\infty}^2-1)(M_{f\infty}^2-1)^{\frac{1}{2}}}$

Notation (contd.)

$\bar{y}_\infty$	far-field shock wave development distance
y_D	shock wave development distance
$\bar{y}_\alpha$	far-field alpha-shock decay distance
$\bar{x}_w$	relaxation distance on wedge surface
x, y	rectangular Cartesian coordinates
x_n, y_n	rectangular coordinates with x_n measured normal to the shock wave at infinity
X	$x - \frac{y}{\tan\phi_0}$
Y	y
ξ	$x - (m_{\infty}^2 - 1)^{\frac{1}{2}} y$
$\bar{\xi}$	$x - (m_{\infty}^2 - 1)^{\frac{1}{2}} y$
$\bar{\xi}_i$	$\theta_w \bar{\xi}$
η	$y (m_{\infty}^2 - 1)^{\frac{1}{2}}$
η_i	$\theta_w^2 \eta$
ψ	$-x + x_w + \int_{y_w}^{y} \frac{dy}{\tan(\theta_{ch} + \mu_{ch})}$
x_{fr}, y_{fr}	x, y coordinates on a flow fringe

INTRODUCTION

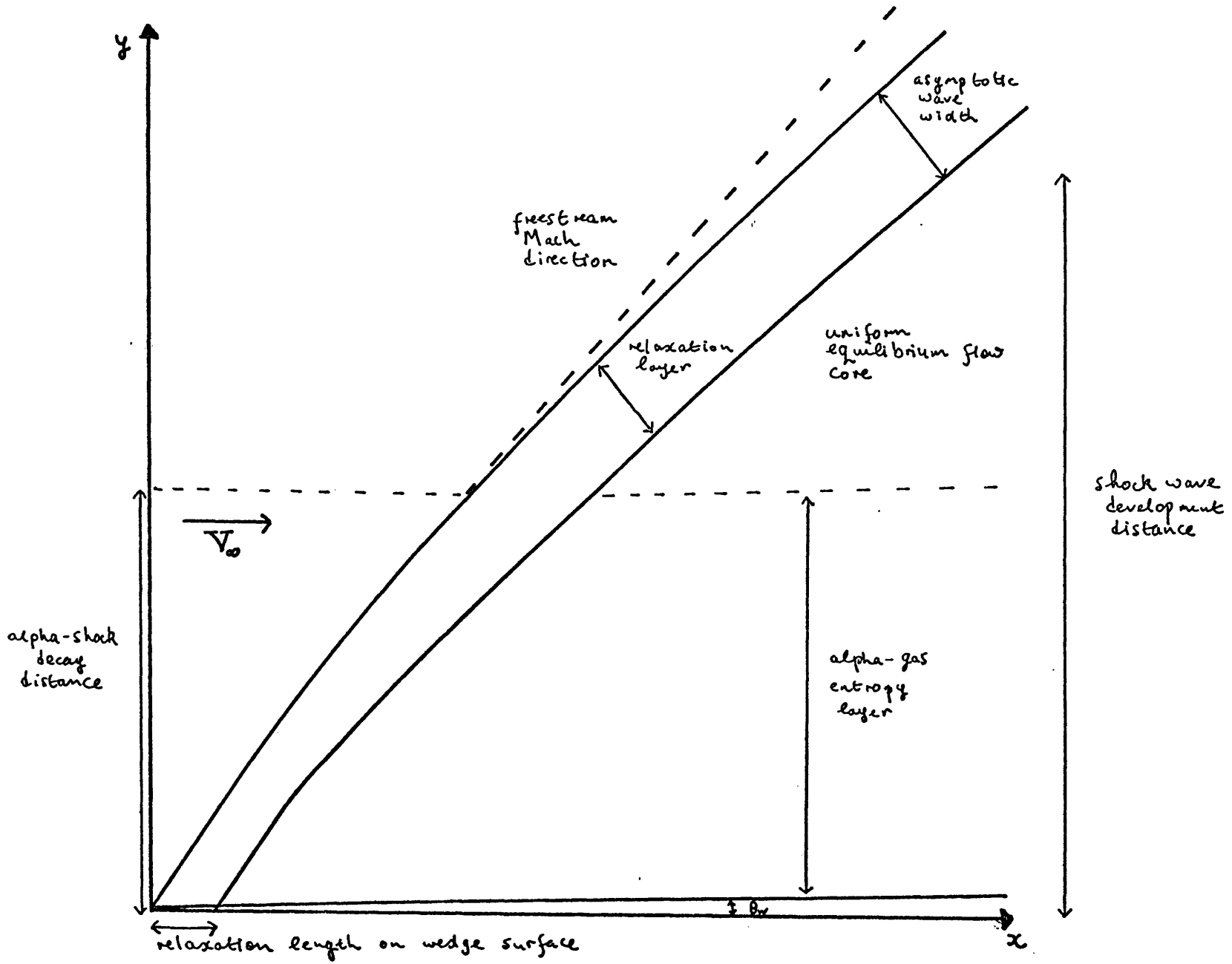

NON-EQUILIBRIUM RELAXING GAS FLOWFIELD
(for a fully dispersed shock wave at infinity)

INTRODUCTION

The assumption of Classical Gasdynamics, that the variations of fluid properties can be described by a set of equations derived considering the fluid to be everywhere in instantaneous equilibrium, is only justified when the characteristic times for the adjustment of the molecular energy states are very much smaller than the time taken by the fluid to encounter significant changes in its environment. When this equilibrium assumption is not true the full non-equilibrium processes occurring must be studied.

We shall consider a gas consisting of molecules with energy contributions from their translational, rotational and vibrational motions and shall neglect any effects due to dissociation, electronic excitation, etc. In particular we shall be concerned only with vibrational non-equilibrium (which leads to vibrational relaxation) and shall treat the rotational and translational modes as if they are everywhere in mutual thermodynamic equilibrium. The justification for this step lies in the fact that the latter two modes require relatively few collisions to attain equilibrium so that any non-equilibrium is exhibited only in flows with a correspondingly small characteristic time. This is equivalent to saying that non-equilibrium phenomena in the translational and rotational modes need only be considered in regions of high gradients, for instance in the viscous interior of shock waves. These regions are necessarily thin in comparison with the vibrational relaxation zones in which we are interested and can be treated as discontinuities in the flow. To the same approximation, we can assume that the vibrational modes remain 'frozen' through such discontinuities which are then completely akin to shock waves in an ideal gas and are determined by the 'frozen' shock relations with a specific heat ratio of $7/5$ (for all diatomic and linear molecules).

Intuitively, we expect all non-equilbirium flows to proceed towards an equilibrium state; in particular, we can assign to the vibrational energy an equilbirium value which is determined by the local translational and rotational temperature. The flow through the frozen shock wave therefore creates a departure from equilibrium in the vibrational energy which is the initial 'driving force' for the flow in the relaxation region downstream of the frozen shock. The rate equation, which is the additional equation we need when we introduce the energy in the vibrational mode as an extra variable, determines the manner in which the non-equilibrium process proceeds.

Let us consider the one-dimensional steady flow of a relaxing gas through a shock wave (which includes both the frozen shock and the accompanying relaxation region). The flow ahead of the shock wave is assumed to be in equilibrium. Johannesen (1961) has shown how these flows may be treated by interpreting the governing equations as those of ideal gas flow (with constant specific heats) with heat subtraction equal to the rate at which energy enters the vibrational modes. This allows one to define the artificial but extremely useful alpha-gas which has all the ideal gas properties. With this representation it is quite clear that the appearance of the initial discontinuity or alpha-shock is dictated solely by the frozen Mach number in the undisturbed gas. If this Mach number is less than or equal to 1 then there can be no alpha-shock so that all changes in the thermodynamic quantities proceed smoothly towards an equilibrium state. Such shock waves are called fully dispersed while those that include the initial discontinuity are called partly dispersed. Since the minimum value of the equilibrium Mach number is 1 (this value corresponds to no disturbance in the gas) fully dispersed waves are possible for the frozen Mach number range $1 \geq m_f > \sqrt{\frac{\gamma_e}{\gamma_f}}$. Physically, in this range, any convective effects, which tend to steepen the wave, can be balanced solely by the diffusive mechanisms of the relaxation (see Lighthill (1956)).

Fully dispersed shock waves can be produced experimentally in the shock tube and some of the early (though widely scattered) results were obtained by Griffith and Kenny (1957). Since then much work of predominantly academic interest has been done in determining the structure and appropriate relaxation times for these waves but it is only recently that Hodgson and Johannesen (1971) have shown that shocks of the strengths expected in sonic bangs are fully dispersed.

If we seek to generalize the results of the one-dimensional flow to consider relaxing gas flows with shock waves in any multi-dimensional physical coordinate space then we meet with considerable difficulty. For the flows are exceedingly complicated when more than 3 space coordinates are considered. For instance, if we wish to investigate a steady relaxing gas flow over a three-dimensional body surface then it is by no means clear what form the solution at large distances from the body will take without first solving for the whole flow. If the body curvature is rapidly varying over a typical gas relaxation length and the body is of suitable dimensions then the flow may never reach an equilibrium state. Indeed the confluence of many alpha-shocks may dictate that the solution at large distances from the body is not continuous. It is interesting to observe, however, that despite the intricate nature of three-dimensional steady and unsteady supersonic non-equilibrium flows, the necessary numerical characteristics methods for their solution are available (see Sauerwein (1966)) and await only the advent of larger and faster computer systems to be put into practice. Two-dimensional non-equilibrium flows are still difficult to deal with. In particular, we can isolate from the whole class of possible flows 2 analogous simple flows where the final wave motion is one-dimensional and under known conditions is either fully dispersed or partly dispersed. That is, we can consider the relaxing, steady gas motion of a supersonic stream over a wedge surface of small angle or correspondingly, the one-dimensional unsteady wave

motion due to an impulsively started piston advancing into a gas at rest.

The analogies in the gas motion in the (x, y) and (x, t) planes are well known (for instance, the piston path in the (x, t) plane 'corresponds' to the upper wedge surface in the (x, y) plane). The two flows are governed by similar sets of partial differential equations but whereas the unsteady flow equations are always hyperbolic, this is only true for the steady flow when the gas velocity is locally supersonic. We can specify the unsteady flow with 2 parameters namely the piston Mach number and vibrational specific heat; for the steady flow we need both the wedge angle, vibrational specific heat and the freestream Mach number. Nevertheless, the basic features of the two flows are very similar and can be understood by regarding the steady flow y coordinate as being 'time-like'. In particular very strong similarities exist in the very weak wave analyses for the two flows (see Blythe (1969)). This will be our justification for referring to analytic work on the unsteady problem when discussing the two-dimensional steady flow analysis. The initial (small 'time') flow in both cases is frozen, for large 'time' the resulting gas motion must be achieved by balancing non-linear convective steepening with the diffusive effects of viscosity and relaxation. The shock wave here is therefore fully dispersed or partly dispersed depending on whether the relaxation effects are sufficient in themselves to counteract any steepening.

We shall consider two-dimensional steady supersonic relaxing gas flows over thin wedges where the far-field flow is either a fully dispersed or partly dispersed shock wave motion. The corresponding unsteady flows have also been investigated in this Department by C.G. Dain . We choose the weak wave solutions and ensure that the wedge angle is less than the maximum wedge angle that permits supersonic flow in the tip region. In studying this flow we shall employ rectangular Cartesian coordinates with origin at the tip and x-axis aligned with the freestream. The shock

wave at the wedge tip must instantaneously deflect the flow through the wedge angle and must therefore be a frozen shock wave inclined at the appropriate wave angle. In order to classify later remarks we shall refer to any solutions that retain all terms in the appropriate governing inviscid equations as 'exact'. The conditions at the wedge tip are therefore known exactly and the flow near the tip may be considered frozen to a first approximation. At infinity (which is defined as both $x \to \infty$ and $y \to \infty$) we expect the balance set up between the opposing forces of convection and diffusion to maintain a shock wave of constant width and direction with equilibrium conditions occurring both upstream and downstream. Since all streamlines far downstream relative to the shock must be parallel to the wedge surface we can conclude that the shock wave at infinity resides at the equilibrium wave angle corresponding to a flow deflection equal to the wedge angle. The solution at infinity is also known exactly by integrating the conservation, rate and state equations normally through the non-equilibrium wave interior.

The frozen shock wave at the tip decays with distance from the wedge surface and the equilibrium shock angle is therefore less than the corresponding frozen shock angle. We therefore have the possibility of the normal frozen Mach number at infinity being greater than, equal to or less than 1. In the latter two cases the shock wave is fully dispersed while in the former it is partly dispersed.

Far downstream, although equilibrium conditions prevail and both pressure and flow angle are uniform throughout, the same is not true of any of the other flow variables (except, of course, the departure from equilibrium). This non-uniformity is referred to in the literature as an 'entropy layer' (see Sedney, South and Gerber (1962)) which is essentially a result of the entropy changes along the decaying alpha-shock. This interpretation is correct only for strong shocks; for weak shocks we shall show (see Chapter 2, section (4)) that the contributions to the total entropy

from the non-equilibrium processes in the relaxation region are much larger than the contributions due to non-equilibrium within the alpha-shock. This necessarily implies that the 'entropy layer' extends over the whole downstream flow whereas the layer in which the other flow variables are non-uniform has a smaller thickness based on the alpha-shock decay length.

Although the basic features of this flowfield are well known no generally applicable analytic solution has yet been presented and on closer inspection the problem is indeed complex. The questions we wish to answer such as the determination of the shock wave development and alpha-shock decay distances necessarily extend the analysis to distances which are far from the wedge surface. The characteristics of the flow are no longer straight lines as in the ideal case but have directions that are dependent on the local properties of the fluid. Analytic attempts based on Lin's (1954) perturbation procedure in characteristic coordinates by Clarke (1965) and Lick (1967) have failed to achieve the necessary balance between non-linear and diffusive effects at large distances and give essentially the same results as the linear theory for the alpha-shock decay. The method of matched asymptotic expansions (see, for instance, Ockendon and Spence (1969)) though producing a uniformly valid solution has been applied to only very weak wave flows and consequently throws no light, for example, on how non-linear effects modify the alpha-shock decay for waves that have nearly their maximum fully dispersed wave strength. We can perhaps indicate the nature of the problem by mentioning that even for the linear perturbation no general explicit inversion of the exact transformed equations has yet been found.

The problem must therefore be investigated numerically if any accuracy is desired and the 3 main methods available for solving hyperbolic relaxing gas flows are the method of characteristics, the method of integral relations and the finite difference method. Dejarnette (1966) has employed the finite difference technique of Lax to compute hypersonic non-equilibrium flows past bodies of prescribed profile. The equations include an artificial viscosity

term which 'smooths out' the alpha-shock but predicts the correct variation of conditions across it. The shock relations are therefore unnecessary. The calculations must proceed from a known data line (the conditions on which must be determined by some alternative method) and there is some initial instability. It is also found that a stability criterion must be applied generally throughout the flow. This requires that any new computed point does not lie outside the zone of influence predicted by the characteristic lines emanating from the known points. Dejarnette finds that the closer the finite difference grid is made to align itself with the characteristics the more accurate the results for a given mesh size. Comparison with the work of Sedney, South and Gerber (1962) (who use the method of characteristics) is found to be good except near the initial data line.

The method of integral relations has been applied by South (1964) to non-equilibrium flows past wedges and cones. The method consists of dividing the region between the body surface and alpha-shock wave into as many sections as the required accuracy demands. Usually 3 sectors are sufficient for good agreement with characteristics results. The equations of motions are written in divergence form and flow variables are approximated across the strips by polynomials whose degree is determined by the number of sectors. This is sufficient to reduce the complicated set of partial differential equations to a system of ordinary differential equations which can be solved numerically. Certain inconsistencies arise from the fact that the approximate differential equations are not equivalent to the correct x-momentum and streamline rate equation at the body surface. These exact equations can, however, be used to correct the surface vibrational energy and gas speed but must not be used as replacements for equations in the approximate system as this causes numerical instability. The step size on the body surface must be small enough to ensure that the necessary integrations will converge to sufficient accuracy but must also be controlled

by a stability scheme related to the characteristic directions in the flow.

The method of characteristics (which will be discussed in detail in Chapter 1 and Chapter 2) is well recognised as the most accurate, though somewhat more lengthy numerical scheme for flows of hyperbolic nature. There is no need, of course, for any reference to stability criteria (providing mesh lengths are not chosen inordinately large) and one has the advantage of being able at first hand to control the signal propagation in the gas. Our application of the method is also self starting, given the conditions at the tip, in that we determine the flow variables near the tip by a characteristic mesh scheme with iteration to the desired accuracy. The emphasis throughout will be on the use of exact results where possible, particularly in relation to the solution at infinity and initial tip gradients. Chapter 1 and Chapter 2 deal essentially with a description of the method of characteristics employed and its application in detail to a specific, though representative example. Chapter 3 deals with the analysis of the results of several flows which when appropriately scaled reveal approximate similarity curves. Chapter 4 applies the method to experimentally observed flows of CO_2 and N_2O past a thin wedge. Chapter 5 gives an account of the main analytic procedures for investigating the flow together with an example calculated by the method of matched asymptotic expansions and checked by characteristics. The application of Whitham's rule to shock decay in relaxing gas flow is also investigated.

The similarity curves which we present can be hopefully extended to flows of gases with very small vibrational specific heat (for example, air at room temperature) where numerical methods are necessarily inaccurate. The results are then of significance to the decay of sharp pressure signals superimposed on sonic bang profiles by atmospheric turbulence (see Crow (1969)).

CHAPTER 1

GOVERNING EQUATIONS AND ASYMPTOTIC SOLUTION.

INTRODUCTION

In Chapter 1 we shall be concerned with giving the major mathematical background necessary for solving the problem. Consequently section (1) presents the governing equations and boundary conditions together with the necessary characteristic form of the equations. Section (2) then discusses the various types of mesh scheme available as well as the checks needed to assess the progress of the calculations. Section (3) gives the exact solution at infinity. The characteristics solution must approach this at large distances from the wedge surface. Section (4) isolates those parameters on which the flow depends and determines the relations that must hold between them for fully dispersed or partly dispersed shock waves to exist at infinity.

SECTION (1)

Governing equations and boundary conditions

The equations governing the flow of an inviscid, non-heat-conducting, supersonic relaxing gas in two-dimensional Cartesian coordinates are

Continuity: $$\frac{\partial}{\partial x}(\rho u) + \frac{\partial}{\partial y}(\rho v) = 0$$

x-momentum: $$u\frac{\partial u}{\partial x} + v\frac{\partial u}{\partial y} = -\frac{1}{\rho}\frac{\partial p}{\partial x}$$

y-momentum: $$u\frac{\partial v}{\partial x} + v\frac{\partial v}{\partial y} = -\frac{1}{\rho}\frac{\partial p}{\partial y}$$

Energy : $$c_{pf}T + \sigma + \frac{1}{2}V^2 = \text{constant}$$

Rate : $$u\frac{\partial \sigma}{\partial x} + v\frac{\partial \sigma}{\partial y} = \rho\frac{\Phi}{\tau}(\bar{\sigma} - \sigma)$$

State : $$p = \rho RT$$

To solve this system of equations we must also specify the dependence of $\bar{\sigma}$ and $\frac{\Phi}{\tau}$ on the other thermodynamic variables. The equilibrium vibrational energy is a function of the gas temperature only so that

$$\bar{\sigma} = \bar{\sigma}(T).$$

The same is approximately true for the relaxation frequency, hence

$$\underline{\Phi} = \underline{\Phi}(T)$$

For the functional form of the temperature dependence for a general diatomic gas and for CO_2 see Johannesen et al. (1967).

We shall also have recourse to the streamline equations. Denoting distance along a streamline by ℓ and distance normal to a streamline by n these equations are

Continuity: $$\frac{1}{\rho}\frac{\partial \rho}{\partial \ell} + \frac{1}{V}\frac{\partial V}{\partial \ell} + \frac{\partial \Theta}{\partial n} = 0$$

ℓ-momentum: $$V\frac{\partial V}{\partial \ell} = -\frac{1}{\rho}\frac{\partial p}{\partial \ell}$$

n-momentum: $$\frac{\partial p}{\partial n} = -\rho V^2 \frac{\partial \Theta}{\partial \ell}$$

Energy: $$c_{pa}T + \sigma + \frac{1}{2}V^2 = \text{constant}$$

Rate: $$-V\frac{\partial \sigma}{\partial \ell} = \rho\underline{\Phi}(\bar{\sigma} - \sigma)$$

State: $$p = \rho RT$$

We shall apply these sets of equations to the steady flow of a uniform relaxing gas stream about a thin wedge of angle θ_w. We take the origin of the rectangular Cartesian coordinates at the wedge tip and x-axis parallel to the freestream direction. Denoting the freestream quantities by the subscript ∞ we employ the following system of non-dimensionalization

$$p = p_\infty \hat{p} \qquad \rho = \rho_\infty \hat{\rho} \qquad T = T_\infty \hat{T}$$

$$u = (RT_\infty)^{\frac{1}{2}}\hat{u} \qquad s = R\hat{s} \qquad \sigma = RT_\infty \hat{\sigma}$$

$$c_{pa} = R\hat{c}_{pa} \qquad \underline{\Phi} = \underline{\Phi}_\infty \underline{\hat{\Phi}}$$

$$\begin{Bmatrix} x \\ y \\ \ell \\ n \end{Bmatrix} = \frac{(RT_\infty)^{\frac{1}{2}}}{\rho_\infty \underline{\Phi}_\infty} \begin{Bmatrix} \hat{x} \\ \hat{y} \\ \hat{\ell} \\ \hat{n} \end{Bmatrix}$$

The 'hatted' quantities denote the non-dimensional variables.

The equations of motion in non-dimensional form are therefore

(Cartesian coordinates)

Continuity: $$\frac{\partial}{\partial \hat{x}}(\hat{\rho}\hat{u}) + \frac{\partial}{\partial \hat{y}}(\hat{\rho}\hat{v}) = 0$$

x-momentum: $$\hat{u}\frac{\partial \hat{u}}{\partial \hat{x}} + \hat{v}\frac{\partial \hat{u}}{\partial \hat{y}} = -\frac{1}{\hat{\rho}}\frac{\partial \hat{p}}{\partial \hat{x}}$$

y-momentum: $$\hat{u}\frac{\partial \hat{v}}{\partial \hat{x}} + \hat{v}\frac{\partial \hat{v}}{\partial \hat{y}} = -\frac{1}{\hat{\rho}}\frac{\partial \hat{p}}{\partial \hat{y}}$$

Energy : $$\hat{c}_{pa}\hat{T} + \hat{\sigma} + \frac{1}{2}\hat{V}^2 = \text{constant}$$

Rate : $$\hat{u}\frac{\partial \hat{\sigma}}{\partial \hat{x}} + \hat{v}\frac{\partial \hat{\sigma}}{\partial \hat{y}} = \hat{\rho}\hat{\Phi}(\hat{\bar{\sigma}} - \hat{\sigma})$$

State : $$\hat{p} = \hat{\rho}\hat{T}$$

(Streamline coordinates)

Continuity: $$\frac{1}{\hat{\rho}}\frac{\partial \hat{\rho}}{\partial \hat{\ell}} + \frac{1}{\hat{V}}\frac{\partial \hat{V}}{\partial \hat{\ell}} + \frac{\partial \Theta}{\partial \hat{n}} = 0$$

ℓ-momentum: $$\hat{V}\frac{\partial \hat{V}}{\partial \hat{\ell}} = -\frac{1}{\hat{\rho}}\frac{\partial \hat{p}}{\partial \hat{\ell}}$$

n-momentum: $$\frac{\partial \hat{p}}{\partial \hat{n}} = -\hat{\rho}\hat{V}^2\frac{\partial \Theta}{\partial \hat{\ell}}$$

Energy : $$\hat{c}_{pa}\hat{T} + \hat{\sigma} + \frac{1}{2}\hat{V}^2 = \text{constant}$$

Rate : $$\hat{V}\frac{\partial \hat{\sigma}}{\partial \hat{\ell}} = \hat{\rho}\hat{\Phi}(\hat{\bar{\sigma}} - \hat{\sigma})$$

State : $$\hat{p} = \hat{\rho}\hat{T}$$

We notice that the non-dimensionalized equations are exactly the same as the dimensional equations except for the absence of the factor R in the equation of state. It is understood that, unless specifically stated otherwise, from now on all variables are non-dimensionalized. The 'hats' will therefore be dropped for convenience.

The characteristic form of the equations of motion (that is, the form in which the system of partial differential equations reduces to a system of ordinary differential equations along specified directions) is most easily derived from the equations of motion in streamline coordinates. For the full derivation see Der (1963). The essential results are that there are 3 characteristic directions and the differential equations applying along them (or compatibility relations) are

on $\frac{dy}{dx} = \tan(\theta+\mu)$ (the negative characteristic or C^-) *

$$\frac{dp}{\rho V^2 \tan\mu} + d\theta = \frac{-(\gamma_f-1)\rho\Phi(\bar{\sigma}-\sigma)\,dy}{V^3 \sin\mu \sin(\theta+\mu)}$$

on $\frac{dy}{dx} = \tan(\theta-\mu)$ (the positive characteristic or C^+) *

$$\frac{dp}{\rho V^2 \tan\mu} - d\theta = \frac{-(\gamma_f-1)\rho\Phi(\bar{\sigma}-\sigma)\,dy}{V^3 \sin\mu \sin(\theta-\mu)}$$

on $\frac{dy}{dx} = \tan(\theta)$ (the streamline)

$$dp = -\rho\bar{V}\,d\bar{V}$$

and $$d\sigma = \frac{\rho\Phi(\bar{\sigma}-\sigma)\,dy}{\bar{V}\sin\theta}$$

To complete this system we have the energy and state equations, valid everywhere in the flow. That is

$$c_{pa}\bar{T} + \sigma + \tfrac{1}{2}\bar{V}^2 = \text{constant}$$

and $$p = \rho\bar{T}$$

---

* If we consider ideal gas flow and write the compatibility equations in terms of the Prandtl-Meyer function ν then $(\nu - \theta)$ is constant on a C^- and $(\nu + \theta)$ is constant on a C^+. This explains the rather awkward terminology.

If we choose $\gamma_f = 7/5$, $c_{pa} = 7/2$ then the above set of equations are valid for the flow of any linear gas molecule for which the single rate equation is an adequate description of the relaxation process (for applications of the rate equation to relaxation processes in O_2, CO_2 and N_2O see respectively Zienkiewicz and Johannesen (1963), Johannesen et al. (1962) and Bhangu (1966)).

The assumptions that the gas flow is inviscid and non-conducting are justified everywhere except on the wedge surface and in the interior of the alpha-shock wave. The effect of viscosity on the body surface is to modify the body contour by the appropriate displacement thickness which we shall neglect over the relaxation distances considered along the wedge surface (for an estimation of this thickness see Bardsley and Mair (1952)). The omission of a viscosity term in the equations for the flow through the alpha-shock necessitate the introduction of the frozen shock relations as extra boundary conditions. These relations are essentially the conservation equations applied across the thin region of translational and rotational non-equilibrium. They are (see Liepmann and Roshko (1967) p.85).

$$\bar{p} = 1 + \frac{2\gamma_f}{(\gamma_f+1)}\left(M_{f\infty}^2 \sin^2\phi_f - 1\right),$$

$$\bar{T} = 1 + \frac{2(\gamma_f-1)}{(\gamma_f+1)^2}\,\frac{\left(M_{f\infty}^2\sin^2\phi_f - 1\right)}{M_{f\infty}^2\sin^2\phi_f}\left(\gamma_f M_{f\infty}^2\sin^2\phi_f + 1\right),$$

$$\bar{\rho} = \bar{p}/\bar{T}, \qquad \bar{\sigma} = \bar{\sigma}_\infty,$$

$$\bar{V}^2 = \bar{V}_\infty^2 + 2c_{pa}(1-\bar{T}),$$

$$s = s_\infty + \log_e \bar{p}^{(\gamma_f-1)^{-1}} + \log_e \bar{\rho}^{-\frac{\gamma_f}{(\gamma_f-1)}}$$

and $$\tan\theta = \frac{2\cot\phi_f\left(M_{f\infty}^2\sin^2\phi_f - 1\right)}{\left(M_{f\infty}^2\left(\gamma_f + \cos 2\phi_f\right) + 2\right)}$$

The boundary condition to be applied at the wedge surface is

$$\theta = \theta_w$$

This set of characteristic equations and boundary conditions can be used to solve the flow of any relaxing gas over a wedge surface providing a suitable functional dependence on the temperature for both $\bar{\sigma}$ and $\underline{\Phi}$ is known.

We, however, are primarily concerned with the application of the characteristics method to weak wave relaxing gas flows and in particular in describing the shock wave development process. We therefore assume that

$$\underline{\Phi} = 1$$

and $$\frac{d\bar{\sigma}}{dT} = \left(\frac{d\bar{\sigma}}{dT}\right)_\infty = c_{v_{ib}}$$

These are good approximations only for very weak wave flows. They do, however, give our results far more generality without impeding in any way our methods for representing the shock wave development process. If, indeed, more accurate results are required, then it is a simple matter to insert the appropriate functional relationships for $\bar{\sigma}$ and $\underline{\Phi}$ into the computer program. The general structure of the program as developed with the assumptions above would remain unchanged.

To ascertain the variations of $\underline{\Phi}$ and $c_{v_{ib}}$ through the flows we shall be considering, we make use of Phinney's (1964) expressions for $\underline{\Phi}$ and $\bar{\sigma}$ valid for a diatomic gas. They are (reverting in this section to dimensional quantities)

$$\frac{\underline{\Phi}}{\underline{\Phi}_c} = \frac{T}{T_c}\, e^{-7.394\left(\left(\frac{T_c}{T}\right)^{\frac{1}{3}} - 1\right)}$$

$$\frac{\bar{\sigma}}{RT_c} = \left(e^{\frac{T_c}{T}} - 1\right)^{-1}$$

where T_c denotes the characteristic temperature of vibration of the molecule and $\underline{\Phi}_c$ is the relaxation frequency at this temperature.

Differentiating the expression for $\underline{\Phi}$ gives

$$\frac{d\underline{\Phi}}{\underline{\Phi}} = \left(1 + \frac{8}{3}\left(\frac{T_c}{T}\right)^{\frac{1}{3}}\right)\left(\frac{dT}{T}\right)$$

If we take $T_\infty = \frac{T_c}{2}$, that is $c_{v_{ib}} = 0.72R$ then for a shock wave that is just fully dispersed we have $\frac{dT}{T_\infty} = 0.026$. The percentage variation in $\underline{\Phi}$ through the shock wave is therefore about 11 per cent.

Similarly differentiating the expression for $\overline{\sigma}$ twice gives

$$\frac{d\,c_{v_{ib}}}{c_{v_{ib}}} = \frac{\left(2\left(\frac{T_c}{T}\right)e^{\frac{T_c}{T}} - 2\left(e^{\frac{T_c}{T}} - 1\right) - \left(\frac{T_c}{T}\right)\left(e^{\frac{T_c}{T}} - 1\right)\right)}{\left(e^{\frac{T_c}{T}} - 1\right)^2}\left(\frac{dT}{T}\right)$$

If we take $T_\infty = \frac{T_c}{2}$ and $\frac{dT}{T_\infty} = 0.026$ then we get a 1.6 per cent variation in $c_{v_{ib}}$ through the shock wave.

For linear triatomic molecules like CO_2 and N_2O (for which the maximum value of $c_{v_{ib}}$ is 4R) the percentage variations in $\underline{\Phi}$ and $c_{v_{ib}}$ are probably larger because $\frac{dT}{T_\infty}$ for shock waves that are just fully dispersed increases as $c_{v_{ib}}$ increases.

The assumptions of constant $\underline{\Phi}$ and $c_{v_{ib}}$ do allow us to consider many different gas flows from one characteristics calculation. For instance, a calculation for a value of $c_{v_{ib}}$ equal to 1R represents all different gas flows with freestream temperatures at which $c_{v_{ib}}$ equals 1R. In the following sections, therefore, it will be understood that these assumptions have been incorporated into the governing equations.

SECTION (2)

Characteristic mesh schemes, checks and starting processes for non-equilibrium relaxing gas flows

The choice of the correct characteristic mesh scheme to employ is extremely important because not only may it save computing time and therefore cost but it may also considerably improve the accuracy of the calculations. The choice should therefore be based on a sound knowledge of the physics of the flow and in particular on the role played by the characteristics in controlling the signal propagation into the gas.

Because the wedge angle is small, the attached frozen shock wave at the tip is weak and so a negative characteristic may be aligned approximately in the same direction. In this way we see that the gradients of the thermodynamic quantities along the negative characteristics are much smaller than the gradients along the positive characteristics which cut through the relaxation region along directions where the flow changes are rapid. Hence a suitable grid scheme would involve large step lengths along the negative characteristics and comparatively small step lengths along the positive characteristics. The direction of signal propagation into the gas must be recognized by building up the mesh scheme along the negative characteristics.

If we examine the characteristic compatibility relations given in section (1) then we see that the coordinates enter these equations only in conjunction with the departure from equilibrium. The negative characteristic compatibility relation is for instance

$$\frac{dp}{\rho V^2 \tan\mu} + d\theta = -\frac{(\gamma+1)\,\rho(\bar{\sigma}-\sigma)\,dy}{V^3 \sin\mu \sin(\theta+\mu)}$$

(here Φ has been put equal to 1).

This indicates that the step lengths should be chosen approximately inversely proportional to the departure from equilibrium. This is naturally

in accord with the idea that the closer the gas is to equilibrium the larger the step lengths we can employ. If we write the non-equilibrium term in the above compatibility relation in terms of x instead of y and use the rate equation we get

$$\frac{1}{\rho V^2 \tan\mu}\frac{d\phi}{dx} + \frac{d\theta}{dx} = \frac{-(\gamma+1)\left(\frac{\partial\sigma}{\partial x}\right)\cos\theta}{V^2 \sin\mu \cos(\theta+\mu)}$$

The changes in the flow are therefore intimately related to the changes in the vibrational energy along the streamlines. The most important streamline to consider is the wedge surface, from which signals are propagated into the whole flow. If we choose step lengths on the wedge surface with equal changes in the vibrational energy then we are dividing the total signal on the wedge surface into smaller signals distributed evenly over each step. This is the key idea in the formulation of our mesh scheme and will be developed in more detail in Chapter 2.

For non-equilibrium flows all 3 characteristics must be employed so that this immediately offers a choice of mesh scheme. For instance, one could employ either a streamline based mesh or a Mach line based mesh (figs.1(a), 1(b)). The streamline based method has the advantage of following fluid elements so that any conservation checks can be applied locally instead of over the whole flowfield. Both these methods rely on 2 input points but 3 input point methods have been developed by Sedney (see the review on non-equilibrium characteristic calculations by Sedney (1970)) due to his finding unexplained inaccuracy in the Mach line based and streamline based schemes. At first the errors were attributed to the linear interpolation that is necessary in these schemes. Consequently a 3 point non-iterative network was devised with error of second order in step length (fig. 1(c)). This scheme was developed from expansions about the centre 0 of the characteristic mesh in terms of the mesh lengths and seemed to correct the deficiencies in the Mach

line based network. However, this method proved unstable in calculating axisymmetric flows. As a remedy, a 3 point iterative scheme was introduced with interpolation along the previous Mach data line, (fig.1(d)). This method apparently corrected all the instabilities in the non-iterative method for axisymmetric flows and was successful for plane flows. The source of error in the Mach line based scheme is not now apparent since the 3 point iterative method also employs linear interpolation.

The present characteristic calculations make use of the Mach line based network and no instabilities of the type attributed by Sedney have been found despite the comparatively large step sizes used. Wood, Springfield and Pallen (1964) have used the same type of network to compute hypersonic relaxing gas flows and Johannesen, Zienkiewicz and Bird (1967) have used the streamline based scheme to determine the complicated unsteady flow behind a reflected partly dispersed shock wave. Neither group has reported any difficulty.

In his review Sedney (1970) advocates a method for starting the calculations that assumes a region of frozen flow at the body tip. This starting process is not advisable. One is impressing a region of uniform flow just where the flow gradient on the body surface is a maximum. This creates a weak discontinuity (that is one with first and higher order derivatives discontinuous) which can propagate out along a negative characteristic and by reflections influence the whole flow. Even if this has little effect on the accuracy one still has to decide how big this initial region should be. The accuracy of the calculations must to some extent be dependent on the starting process and this would mean that using this simple starting process would compel one to employ a far smaller step size than that required. The calculation procedure can quite easily be started by using the wedge tip gradients, series expansions for small values of the coordinates, or by an iterative method employing the characteristics (see Chapter 2, section (1)).

In some calculations errors have been directly attributable to the use of the real gas entropy as a dependent variable. Conservation checks of mass, momentum and energy applied by Feldmann and Widawsky (1962) to their computations of hypersonic non-equilibrium flows revealed substantial errors. The authors concluded that certain errors were inevitable and that corrections to the computed results must be made. Powers and O'Neill (1963) applied the mass conservation check to real gas hypersonic flow calculations and found similar large errors. They attributed these inaccuracies to the strong entropy gradients existing in the hypersonic flow and consequently modified their method by determining the local entropy from the equation for conservation of mass instead of by linear interpolation between 2 known points. This procedure, of course, reduces any errors in the mass conservation check since this is applied directly in the program. Perhaps a better test on any possible improvements in the calculations would have been to employ a momentum or energy conservation check. Wood, Springfield and Pallen (1964) were also conscious of employing entropy as a dependent variable in the compatibility relations for their hypersonic relaxing gas flow calculations.

In the present calculations the compatibility relations are employed in their simplest form with pressure and flow angle. The real gas entropy is never required since the alpha-gas model is used. The calculations are extensively checked. The convergence of the method is assessed by the use of different step sizes in a representative example and in every calculation checks are made to ensure that the integrated conservation equations are satisfied to a good approximation. For steady flows the integrated energy equation can be incorporated directly into the program so that a mass and momentum check is sufficient. In a Mach line based scheme these laws cannot, however, be applied over a single mesh length (this is possible with a streamline based scheme). Only the integrated effects over a whole character-

istic data line can be determined. A typical result is shown in fig.1(e). The characteristic data lines (which are the negative characteristics emanating from the wedge surface) are labelled with values according to their x-coordinate on the wedge surface. A closed contour is taken which comprises the wedge surface, characteristic data line and alpha-shock. The incoming mass and x-momentum are readily evaluated and denoted by mass$_{IN}$ and x-momentum$_{IN}$. The symbols mass and momentum refer to the integrated mass and x-momentum flux around the rest of the contour. In such checks there are 2 sources of error. There is the error in the characteristic calculations and the error in the step by step integration around the contour. These 2 errors may cancel as in fig.1(e). One source of error is then dominant, probably that in the characteristic calculations. In the early stages of the program development these checks were of great assistance in eliminating errors.

SECTION (3)

Exact solution at infinity and projection of the solution along the Mach lines and streamlines

In order to assess the progress of the characteristic calculations we need to have some idea of the asymptotic nature of the solution. For this particular flow we are fortunate in being able to determine this solution as accurately as we wish because, as has already been described, for large x and y we expect a shock wave at the equilibrium shock angle. The position of this shock wave in relation to the origin of coordinates at the wedge tip is, however, unknown. By a straightforward application of the conservation, rate and state equations along a direction normal to this shock we can completely determine the non-equilibrium structure of the interior to any desired accuracy. In particular we shall find an exact

expression for the maximum departure from equilibrium which holds for both fully dispersed and weak partly dispersed waves. This can be related (for very weak waves) to a gradient of the vibrational energy and hence to a wave thickness. The structure of the shock wave, once found, can be projected along any direction in the flow. Of particular interest are the Mach line and streamline directions, the former because the characteristic results are printed out along the Mach lines and the latter because any true diagram relating to the wave propagation is best observed along the streamlines.

We are interested in solutions where the shock wave at infinity may be partly dispersed as well as fully dispersed so we must include the possibility of a discontinuity or alpha-shock appearing if the normal frozen Mach number is greater than 1. This alpha-shock can be treated by applying the frozen shock relations to obtain the jump conditions across it. The structure of the relaxation region can then be found by applying the inviscid conservation, rate and state equations through the wave just as for a fully dispersed wave.

If we define

$$\Lambda_0 = \frac{\tan\theta_w \left((\gamma_e - 1) m_{e\infty}^2 + 2 \right)}{2}$$

$$\Lambda_1 = \left(1 - m_{e\infty}^2 \right)$$

$$\Lambda_2 = \frac{\tan\theta_w \left((\gamma_e + 1) m_{e\infty}^2 + 2 \right)}{2}$$

Then for the weak solution the equilibrium shock angle can be written explicitly as (see Appendix 1).

$$\cot\phi_e = \sqrt{\frac{4n_2^2}{9} - \frac{4}{3}n_1}\ \cos\left(\frac{1}{3}\cos^{-1}\left(\frac{-4\left(\frac{2n_2^3}{27} - \frac{n_1 n_2}{3} + n_0\right)}{\left(\frac{4n_2^2}{9} - \frac{4}{3}n_1\right)^{\frac{3}{2}}}\right)\right) - \frac{n_2}{3}$$

This is somewhat simpler than that given by Mascitti (1968).

Having found the appropriate wave angle as above, if $m_{f\infty}\sin\phi_e > 1$ then we determine the jump conditions across the alpha-shock by using the frozen shock relations for a shock wave inclined at angle ϕ_e to the horizontal.

That is, for instance

$$p = 1 + \frac{2\gamma_f}{(\gamma_f+1)}\left(m_{f\infty}^2\sin^2\phi_e - 1\right)$$

The structure of the relaxation region can now be determined by solving the conservation, rate and state equations. If we have $m_{f\infty}\sin\phi_e \leq 1$ then we can apply the following analysis immediately. The equations are, denoting the normal velocity as u_n and coordinates along and normal to the shock as y_n and x_n respectively (see fig.1(f)).

Mass : $\rho u_n = u_{n\infty}$

Momentum : $p + \rho u_n^2 = 1 + u_{n\infty}^2$

Energy : $c_{pa}\bar{T} + \sigma + \frac{1}{2}u_n^2 = c_{pa} + \bar{\sigma}_\infty + \frac{1}{2}u_{n\infty}^2$

Rate : $u_n \frac{d\sigma}{dx_n} = \rho(\bar{\sigma} - \sigma)$

State : $p = \rho T$

The assumption of constant specific heats gives

$$\bar{\sigma} = \bar{\sigma}_\infty + c_{vib}(T - 1)$$

The conservation equations of mass and momentum give (eliminating u_n)

$$p = 1 + u_{n\infty}^2 - \frac{u_{n\infty}^2}{\rho} \qquad 3.1$$

The conservation equations of energy and mass give (eliminating u_n)

$$c_{pa}\bar{T} + \sigma + \frac{1}{2}\frac{u_{n\infty}^2}{\rho^2} = c_{pa} + \bar{\sigma}_\infty + \frac{1}{2}u_{n\infty}^2 \qquad 3.2$$

From the equation of state

$$T = \frac{p}{\rho}$$

$$= \frac{(1+u_{n\infty}^2)}{\rho} - \frac{u_{n\infty}^2}{\rho^2} \quad \text{from 3.1} \qquad 3.3$$

Hence eliminating T from 3.2 gives

$$c_{pa}\left(\frac{(1+u_{n\infty}^2)}{\rho} - \frac{u_{n\infty}^2}{\rho^2}\right) + \sigma + \tfrac{1}{2}\frac{u_{n\infty}^2}{\rho^2} = c_{pa} + \bar{\sigma}_\infty + \tfrac{1}{2}u_{n\infty}^2$$

That is,

$$c_{pa}\left(\frac{1+u_{n\infty}^2}{\rho}\right) + \frac{u_{n\infty}^2}{\rho^2}\left(\tfrac{1}{2} - c_{pa}\right) + \sigma = c_{pa} + \bar{\sigma}_\infty + \tfrac{1}{2}u_{n\infty}^2$$

Inserting this expression into the rate equation gives (after eliminating u_n by the mass conservation equation)

$$\frac{u_{n\infty}}{\rho}\left(\frac{c_{pa}(1+u_{n\infty}^2)}{\rho^2} + \frac{2u_{n\infty}^2}{\rho^3}\left(\tfrac{1}{2} - c_{pa}\right)\right)\frac{d\rho}{dx_n} = \rho\left(c_{vib}(T-1) + c_{pa}\frac{(1+u_{n\infty}^2)}{\rho}\right.$$

$$\left. + \frac{u_{n\infty}^2}{\rho^2}\left(\tfrac{1}{2} - c_{pa}\right) - c_{pa} - \tfrac{1}{2}u_{n\infty}^2\right)$$

Eliminating T by 3.3 gives a first order differential equation for the density through the wave, viz.

$$\frac{u_{n\infty}}{\rho}\left(\frac{c_{pa}(1+u_{n\infty}^2)}{\rho^2} + \frac{2u_{n\infty}^2}{\rho^3}\left(\tfrac{1}{2} - c_{pa}\right)\right)\frac{d\rho}{dx_n} = \rho\left(\frac{c_{vib}(1+u_{n\infty}^2)}{\rho}\right.$$

$$- \frac{c_{vib}u_{n\infty}^2}{\rho^2} + \frac{c_{pa}(1+u_{n\infty}^2)}{\rho} + \frac{u_{n\infty}^2}{\rho^2}\left(\tfrac{1}{2} - c_{pa}\right)$$

$$\left. - (c_{pa} + c_{vib}) - \tfrac{1}{2}u_{n\infty}^2\right)$$

Multiplying both sides of the equation by ρ^4 gives

$$u_{n\infty}\left(c_{pa}(1+u_{n\infty}^2)\rho + 2u_{n\infty}^2\left(\tfrac{1}{2}-c_{pa}\right)\right)\frac{d\rho}{dx_n}$$

$$= \rho^3\Big(\big(c_{vib}(1+u_{n\infty}^2)+c_{pa}(1+u_{n\infty}^2)\big)\rho$$

$$-\left(c_{vib}u_{n\infty}^2 - u_{n\infty}^2\left(\tfrac{1}{2}-c_{pa}\right)\right)$$

$$-\left(\left(c_{pa}+c_{vib}\right)+\tfrac{1}{2}u_{n\infty}^2\right)\rho^2\Big)$$

That is

$$\frac{d\rho}{dx_n} = \frac{\rho^3\left(-\left(c_{pa}+c_{vib}+\tfrac{1}{2}u_{n\infty}^2\right)\rho^2+\left(c_{vib}+c_{pa}\right)\left(1+u_{n\infty}^2\right)\rho-\left(c_{vib}+c_{pa}\right)u_{n\infty}^2+\tfrac{1}{2}u_{n\infty}^2\right)}{u_{n\infty}\left(c_{pa}(1+u_{n\infty}^2)\rho-2u_{n\infty}^2\left(\tfrac{1}{2}-c_{pa}\right)\right)} \qquad 3.4$$

For a fully dispersed wave we can write the above equation more concisely by noticing that

$$\frac{d\rho}{dx_n} = 0 \qquad \text{when } \rho = 1 \text{ and } \rho = \rho_e$$

Hence the quadratic in ρ in the numerator of 3.4 must factorize. That is

$$\rho^2 - \frac{\left(c_{vib}+c_{pa}\right)\left(1+u_{n\infty}^2\right)}{\left(c_{pa}+c_{vib}+\tfrac{1}{2}u_{n\infty}^2\right)}\rho + \frac{\left(c_{vib}+c_{pa}\right)u_{n\infty}^2-\tfrac{1}{2}u_{n\infty}^2}{\left(c_{pa}+c_{vib}+\tfrac{1}{2}u_{n\infty}^2\right)} \equiv (\rho-1)(\rho-\rho_e)$$

Hence

$$\rho_e = \frac{\left(c_{vib}+c_{pa}\right)u_{n\infty}^2-\tfrac{1}{2}u_{n\infty}^2}{\left(c_{pa}+c_{vib}+\tfrac{1}{2}u_{n\infty}^2\right)} = \frac{(\gamma_e+1)m_{en\infty}^2}{\left((\gamma_e-1)m_{en\infty}^2+2\right)}$$

where

$$m_{en\infty} = \frac{u_n}{a_{e\infty}}$$

This, of course, is exactly what we would expect from a direct application of the equilibrium oblique shock equations.

The density distribution through a fully dispersed wave can therefore be written as

$$\frac{d\rho}{dx_n} = \frac{\rho^3(\rho-1)(\rho-\rho_e)\left(c_{pa}+c_{vib}+\tfrac{1}{2}u_{n\infty}^2\right)}{u_{n\infty}\left(\rho\left(c_{pa}(1+u_{n\infty}^2)\right)-u_{n\infty}^2(2c_{pa}-1)\right)} \qquad 3.5$$

We see that if

$$\rho = \frac{(2c_{pa}-1)u_{n\infty}^2}{c_{pa}(1+u_{n\infty}^2)} \qquad \text{then} \qquad \frac{d\rho}{dx_n} \to \infty$$

Hence we must always have

$$\frac{u_{n\infty}^2}{(1+u_{n\infty}^2)} \leq \frac{c_{pa}}{2c_{pa}-1}$$

That is $M_{fn\infty} \leq 1$ if the wave is to be fully dispersed.

Equation 3.5 can be solved analytically though not explicitly for ρ in terms of x_n. For approximations to equation 3.5 see Lighthill(1956).

For our purposes it is sufficient to integrate 3.5 numerically using a Simpson integration formula. To avoid difficulties at the wave end points where $\frac{dx_n}{d\rho}$ is large equation 3.5 is integrated from the inflexion point which is again found numerically, though to high accuracy, by maximizing 3.5.

If the shock wave is partly dispersed then 3.5 is applied through the relaxation region once the jumps across the alpha-shock have been determined. The analogous equation to equation 3.5 for the velocity has been given by Hodgson and Johannesen (1971). Their work, however, is mainly concerned with estimating fully dispersed wave widths for the strengths expected in sonic bangs and they give an analytic expression for the wave thickness.

Of importance in later calculations is the maximum value of the departure from local equilibrium of the vibrational energy in the shock wave at infinity. We shall denote this quantity as $(\bar{\sigma}-\sigma)_{max\infty}$. We shall need this in Chapter 2 when we define a suitable variable to describe the shock wave development process. The exact value of $(\bar{\sigma}-\sigma)_{max\infty}$ can be found as follows.

From the energy equation and the assumption of constant vibrational specific heat we can write

$$(\bar{\sigma} - \sigma) = \tfrac{1}{2}(u_n - u_{n\infty}^2) + (c_{pa} + c_{vib})(T - 1) \qquad 3.6$$

From the momentum equation, dividing by ρ gives

$$\frac{p}{\rho} + u_n^2 = \frac{(1 + u_{n\infty}^2)}{\rho}$$

The equation of state gives $T = \frac{p}{\rho}$ so

$$T + u_n^2 = \frac{(1 + u_{n\infty}^2)}{\rho}$$

By conservation of mass we get

$$T + u_n^2 = \frac{(1 + u_{n\infty}^2) u_n}{u_{n\infty}}$$

That is

$$T = \frac{(1 + u_{n\infty}^2) u_n}{u_{n\infty}} - u_n^2$$

Hence substituting into equation 3.6 for T,

$$(\bar{\sigma} - \sigma) = \tfrac{1}{2}(u_n^2 - u_{n\infty}^2) + (c_{pa} + c_{vib}) \left(\frac{(1 + u_{n\infty}^2) u_n}{u_{n\infty}} - u_n^2 - 1 \right) \qquad 3.7$$

Differentiating with respect to x_n gives

$$\frac{d(\bar{\sigma} - \sigma)}{dx_n} = u_n \frac{du_n}{dx_n} \left(1 - 2(c_{pa} + c_{vib}) \right) + \frac{(c_{pa} + c_{vib})(1 + u_{n\infty}^2)}{u_{n\infty}} \frac{du_n}{dx_n}$$

If we define $(\bar{\sigma}-\sigma)_{a\infty}$ as the departure from equilbirium of the vibrational energy immediately downstream of the alpha-shock in a partly dispersed shock wave at infinity, then assuming that $(\bar{\sigma}-\sigma)_{max\infty} > (\bar{\sigma}-\sigma)_{a\infty}$ (this restricts the result to weak partly dispersed shock waves) we have that $(\bar{\sigma}-\sigma) = (\bar{\sigma}-\sigma)_{max\infty}$ when

$$u_n = \frac{(c_{vib}+c_{pa})(1+u_{n\infty}^2)}{u_{n\infty}(2(c_{pa}+c_{vib})-1)}$$

Substituting back into 3.7 gives

$$(\bar{\sigma}-\sigma)_{max\infty} = \frac{(c_{pa}+c_{vib})^2(1+u_{n\infty}^2)^2}{2u_{n\infty}^2(2(c_{pa}+c_{vib})-1)^2} - \frac{1}{2}u_{n\infty}^2 - (c_{pa}+c_{vib})$$

$$+ \frac{(c_{pa}+c_{vib})^2(1+u_{n\infty}^2)^2}{u_{n\infty}^2(2(c_{pa}+c_{vib})-1)}$$

$$- \frac{(c_{pa}+c_{vib})(c_{pa}+c_{vib})^2(1+u_{n\infty}^2)^2}{u_{n\infty}^2(2(c_{pa}+c_{vib})-1)^2}$$

$$= \frac{(c_{pa}+c_{vib})^2(1+u_{n\infty}^2)^2}{2u_{n\infty}^2(2(c_{pa}+c_{vib})-1)} - \frac{1}{2}u_{n\infty}^2 - (c_{pa}+c_{vib})$$

Putting $u_{n\infty}^2 = \gamma_f m_{fn\infty}^2$ gives

$$(\bar{\sigma}-\sigma)_{max\infty} = \frac{\gamma_f^2 m_{fn\infty}^4(c_{pa}+c_{vib}-1)^2 - 2\gamma_f m_{fn\infty}^2(c_{pa}+c_{vib})(c_{pa}+c_{vib}-1)+(c_{pa}+c_{vib})^2}{2\gamma_f m_{fn\infty}^2(2(c_{pa}+c_{vib})-1)}$$

In Chapter 3 we shall simplify this expression by use of the small wedge angle expansions.

The solution as a function of x_n can be projected along the Mach lines or streamlines by expressing x_n in terms of coordinates measured along these directions in the following manner.

In the coordinate frame of reference (x_n , y_n), the positive characteristic directions are given by

$$\frac{dy_n}{dx_n} = \tan\left(\frac{\pi}{2} - \phi_e - \mu + \theta\right)$$

The variations of all the flow variables are known as functions of x_n so that by choosing suitable increments in the distance through the wave we can find the C^+ trajectories from

$$dy_n = \tan\left(\frac{\pi}{2} - \phi_e - \mu + \theta\right) dx_n$$

Similarly the C^- and streamlines from

$$dy_n = \tan\left(\frac{\pi}{2} - \phi_e + \mu + \theta\right) dx_n$$

and $$dy_n = \tan\left(\frac{\pi}{2} - \phi_e + \theta\right) dx_n \quad \text{respectively}$$

The solutions at infinity along the Mach lines and streamlines can therefore be built up step by step. The solutions can be iterated by choosing mean values of the gradients once a first approximation has been found.

SECTION (4)

The $(\theta_w$, $m_{f\infty}$, $c_{vib})$ space for fully dispersed and partly dispersed shock waves at infinity

To determine the flowfield we must first be able to specify which parameters control the flow.

The freestream pressure and relaxation frequency per unit density do not affect the physical nature of the flow field and just scale the coordinates. This fact is recognized by including these quantities in the non-dimensionalization of the coordinates. Certainly to determine the conditions at the wedge tip we need the frozen freestream Mach number

and the wedge angle.

Examination of the terms in the non-dimensionalized compatibility relations reveals that the only parameter unspecified is the vibrational specific heat, c_{vib} . If we make the assumption of a constant but different vibrational specific heat for each flow we consider (that is if we fix the vibrational specific heat at its freestream value) then the 3 parameters that we must specify are θ_w , $m_{f\infty}$ and c_{vib} .

We notice that we have made no assertion as to the nature of the gas except that the gas molecules be linear. The freestream temperature is defined implicitly by the vibrational specific heat. For instance, if we calculate a set of flows with $c_{vib} = 1.0$ then these calculations are valid for those gas flows with a freestream temperature for which $c_{vib} = 1.0$.

Next we would like to know for what values of these parameters the flow over a wedge will be fully dispersed, partly dispersed or just fully dispersed at infinity. We have mentioned that if the normal frozen Mach number at infinity ($m_{fn\infty}$) is less than or equal to 1, then the shock wave at infinity is fully dispersed. We can therefore recast the problem by inquiring the relationship between the parameters that would give the required normal frozen Mach number at infinity.

The relationship between θ_w , $m_{f\infty}$, c_{vib} and ϕ_e is given by the equilibrium oblique shock relation

$$\tan\theta_w = \frac{2\cot\phi_e\left(m_{f\infty}^2\frac{\gamma_f}{\gamma_e}\sin^2\phi_e - 1\right)}{\left(m_{f\infty}^2\frac{\gamma_f}{\gamma_e}\left(\gamma_e + \cos 2\phi_e\right) + 2\right)}$$

where $$\gamma_e = \frac{(c_{pa} + c_{vib})}{(c_{va} + c_{vib})}$$

If we rewrite this expression in terms of the normal frozen Mach number $m_{fn\infty}$ instead of wave angle ϕ_e then we shall be able to enforce the conditions stated above more easily.

Since $m_{fn\infty} = m_{f\infty} \sin\phi_e$ eliminating ϕ_e gives

$$\tan\theta_w = \frac{2\sqrt{1-\frac{m_{fn\infty}^2}{m_{f\infty}^2}}\left(\frac{\gamma_f}{\gamma_e} m_{fn\infty}^2 - 1\right)}{\left(\frac{m_{fn\infty}}{m_{f\infty}}\right)\left(m_{f\infty}^2 \frac{\gamma_f}{\gamma_e}\left(\gamma_e + 1 - 2\frac{m_{fn\infty}^2}{m_{f\infty}^2}\right) + 2\right)}$$

Simplifying this gives

$$\tan\theta_w = \frac{2\sqrt{m_{f\infty}^2 - m_{fn\infty}^2}\left(\gamma_f m_{fn\infty}^2 - \gamma_e\right)}{m_{fn\infty}\left(m_{f\infty}^2 \gamma_f(\gamma_e+1) - 2\gamma_f m_{fn\infty}^2 + 2\gamma_e\right)}$$

If we put $m_{fn\infty} = 1$ then we extract the relationship between the 3 parameters for shock waves at infinity that are just fully dispersed. That is

$$\tan\theta_w = \frac{2\sqrt{m_{f\infty}^2 - 1}\,(\gamma_f - \gamma_e)}{m_{f\infty}^2\left(\gamma_f(\gamma_e+1)\right) - 2(\gamma_f - \gamma_e)}$$

These curves are plotted in fig.1(h) for vibrational specific heats of 0.5 , 1, 2 and 3. Regions to the left of these curves are shock wave flows that are fully dispersed at infinity.

We are now in a position to define the flows we wish to compute. Naturally we want flows at constant Mach number and wedge angle as well as at constant vibrational specific heat so that we can ascertain the individual effects of the parameters. We therefore choose sets of flows at constant wedge angle and constant Mach number that 'cover' the region for which fully dispersed and partly dispersed shock waves at infinity exist. We can only hope to compute a representative sample of all the possible flows; to this end we choose frozen Mach numbers of 1.4 , 2.6 and 3.8. The flows that we have computed in this manner are registered in fig. 1(h).

The properties of the (θ_w , $m_{f\infty}$) curves will be discussed as follows.

<u>The maximum wedge angle that will give a certain normal frozen Mach number at infinity</u>

The relation between θ_w , $m_{f\infty}$, $c_{v,b}$ is

$$\tan\theta_w = \frac{2\sqrt{m_{f\infty}^2 - m_{fn\infty}^2}\,(\gamma_f m_{fn\infty}^2 - \gamma_e)}{m_{fn\infty}\,(m_{f\infty}^2\gamma_f(\gamma_e+1) - 2\gamma_f m_{fn\infty}^2 + 2\gamma_e)}$$

Taking $c_{v,b}$ as fixed (i.e. γ_e fixed) and $m_{fn\infty}$ fixed and differentiating w.r.t. $m_{f\infty}$ gives

$$\frac{d\tan\theta_w}{d m_{f\infty}} = (\gamma_f m_{fn\infty}^2 - \gamma_e)\left(2m_{f\infty}(m_{f\infty}^2\gamma_f(\gamma_e+1) - 2\gamma_f m_{fn\infty}^2 + 2\gamma_e) - 4(m_{f\infty}^2 - m_{fn\infty}^2)\gamma_f m_{f\infty}(\gamma_e+1)\right) \times m_{fn\infty}^{-1}(m_{f\infty}^2 - m_{fn\infty}^2)^{-\frac{1}{2}}\left(m_{f\infty}^2\gamma_f(\gamma_e+1) - 2\gamma_f m_{fn\infty}^2 + 2\gamma_e\right)^{-2}$$

This expression is zero when

$$m_{f\infty}^2\gamma_f(\gamma_e+1) - 2\gamma_f m_{fn\infty}^2 + 2\gamma_e - 2\gamma_f(\gamma_e+1)(m_{f\infty}^2 - m_{fn\infty}^2) = 0$$

(excluding $m_{f\infty} = 0$ and $m_{fn\infty} = \sqrt{\frac{\gamma_e}{\gamma_f}}$)

This gives

$$m_{f\infty}^2\left(\gamma_f(\gamma_e+1) - 2\gamma_f(\gamma_e+1)\right) = 2\gamma_f m_{fn\infty}^2 - 2\gamma_e - 2\gamma_f(\gamma_e+1)m_{fn\infty}^2$$

That is

$$m_{f\infty}^2 = \frac{2m_{fn\infty}^2\gamma_f\gamma_e + 2\gamma_e}{\gamma_f(\gamma_e+1)}$$

This gives the freestream frozen Mach number at which the maximum deflection occurs through a shock wave at infinity of fixed strength.

For frozen flow (i.e. at the wedge tip) this gives

$$M_{f\infty}^2 = \frac{2 M_{fno}^2 \gamma_f + 2}{(\gamma_f + 1)}$$

where $$M_{fno} = \frac{\bar{V}_\infty \sin \phi_{fo}}{a_{f\infty}}$$

The deflection itself can be easily found by substituting the expression for the Mach number into the equation for tan θ_w.

For Mach numbers greater than this value the gradient $\frac{d\theta_w}{dM_{f\infty}}$ is negative so that as $M_{f\infty} \to \infty$ $\theta_w \to 0$. The situation for Mach numbers less than this value is slightly more complicated. As $M_{f\infty} \to 1$ the wedge angle θ_w decreases until the flow behind the frozen shock at the tip becomes subsonic. If θ_w is decreased still further then the frozen shock becomes detached (see fig.1(g)). For smaller angles still the constant strength curves intersect. This is because for fixed Mach number and wedge angle there are 2 solutions for the wave angle and hence 2 wave strengths. For Mach numbers near unity these strengths are very nearly the same (since the wave angles are approximately equal) and hence appear as solutions in what for larger Mach numbers is essentially a weak solution domain.

Having established the regions of the (θ_w, $M_{f\infty}$) plane where the flows at infinity are fully dispersed, just fully dispersed or partly dispersed we are in a position to define a critical quantity which will have great importance in the presentation of the results in Chapter 3.

Definition of a critical quantity

The critical value of one of the parameters θ_w , $m_{f\infty}$ and $c_{v,b}$ is the value that it takes, for constant values of the other two parameters, at the maximum fully dispersed wave strength at infinity.

The corresponding critical value of any flow quantity is the value that it takes at the same point in the (θ_w , $m_{f\infty}$, $c_{v,b}$) space.

Critical values will be superscripted with a *.

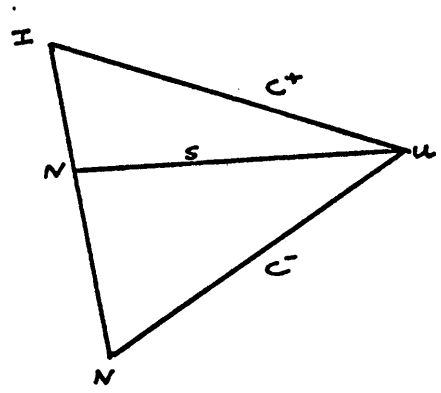

N, known point

U, unknown point

I, interpolated point

s, streamline

FIGURE 1(a). STREAMLINE BASED MESH

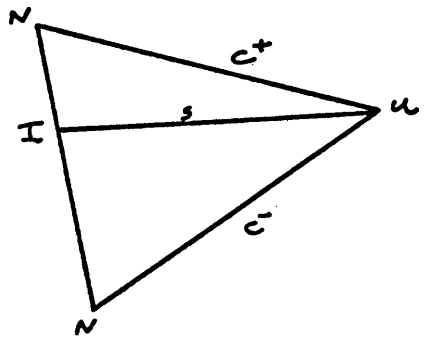

FIGURE 1(b). MACH LINE BASED MESH

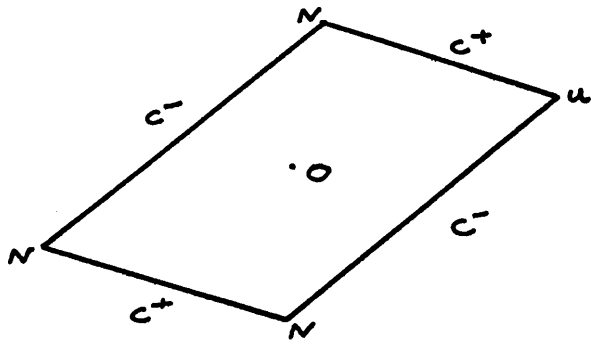

FIGURE 1(c). 3 POINT NON-ITERATIVE MESH

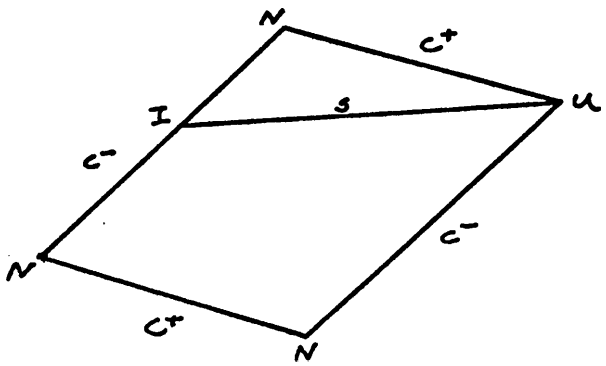

FIGURE 1(d). 3 POINT ITERATIVE MESH

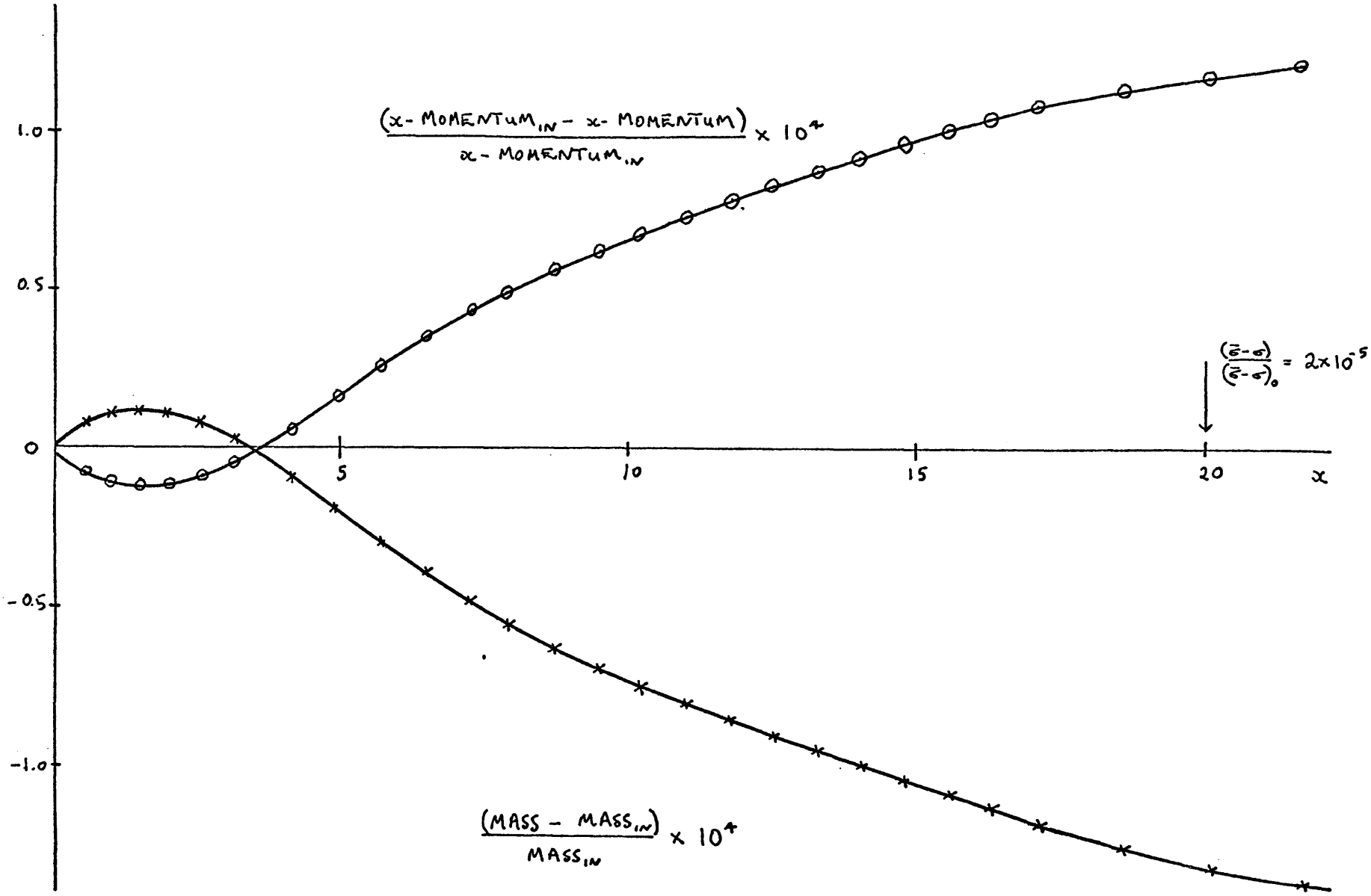

FIGURE 1(e). CONSERVATION CHECKS. ($\theta_w = 2.1°$, $M_{fw} = 3.8$ and $c_{vib} = 3.0$).

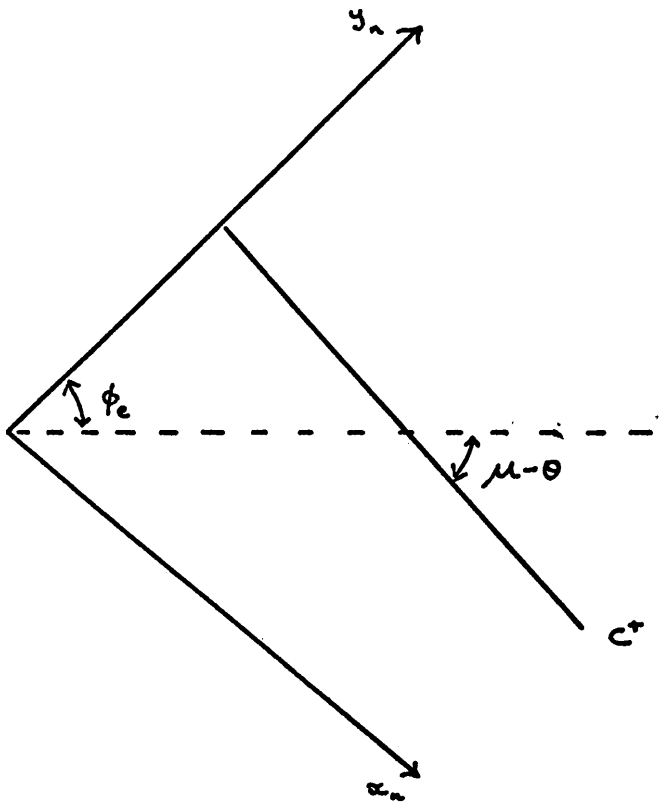

FIGURE 1(f). EQUILIBRIUM–SHOCK COORDINATE SYSTEM

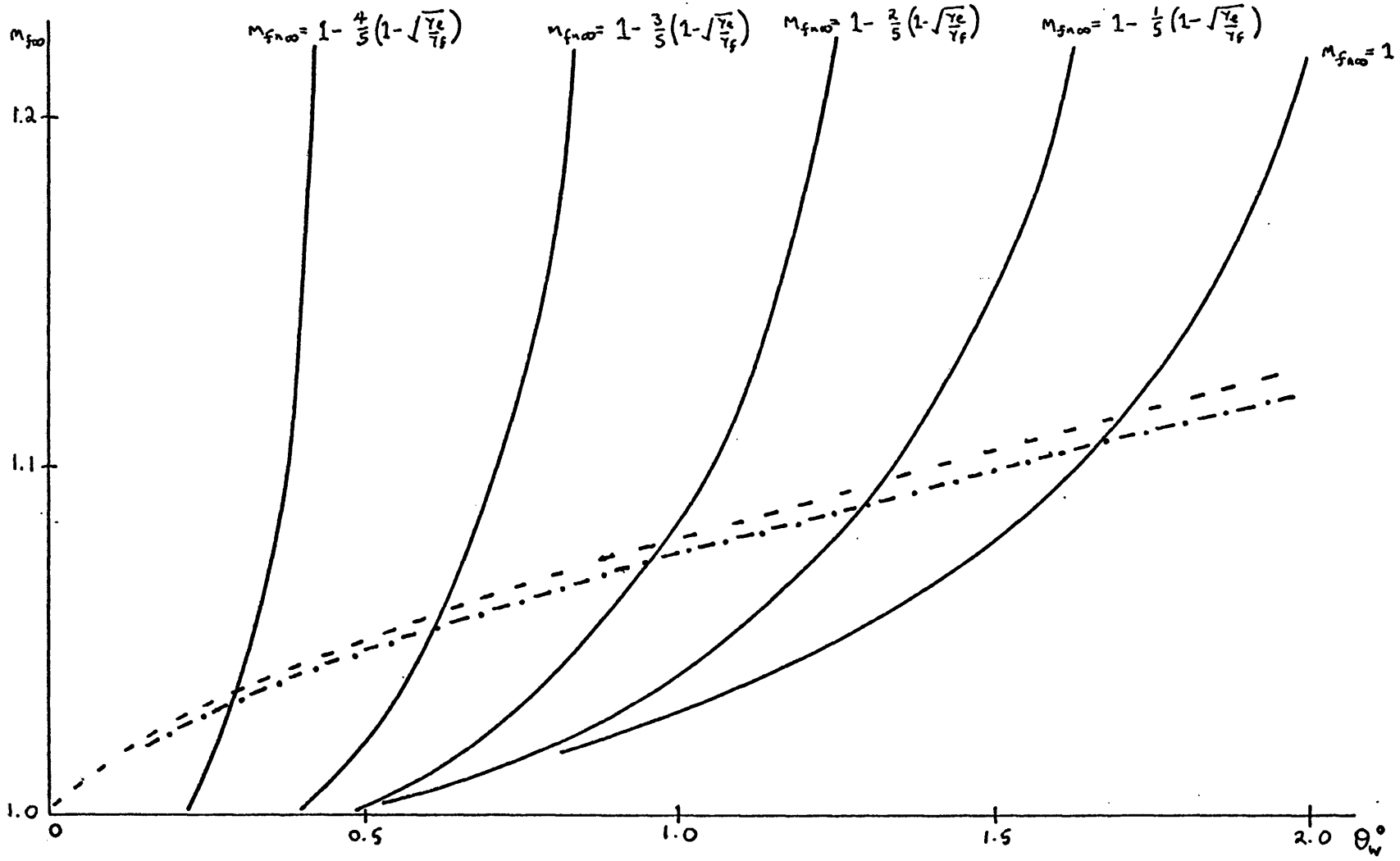

FIGURE 1(g). CONSTANT WAVE STRENGTH CURVES AT INFINITY. ($c_{w\infty} = 1.0$).

– – , *maximum wedge angle for supersonic flow at the wedge tip.*

– · – , *maximum wedge angle for an attached alpha-shock at the wedge tip.*

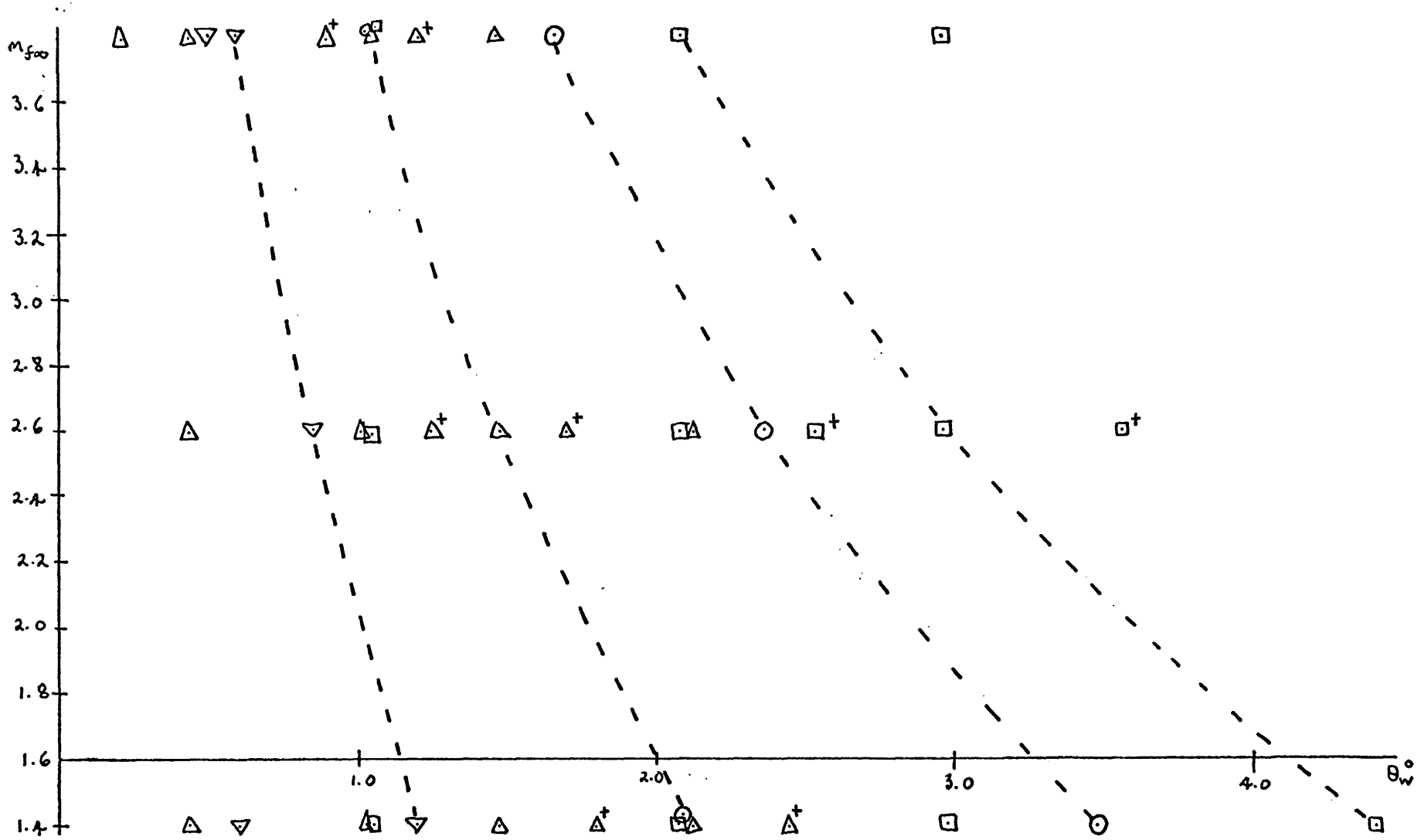

FIGURE 1(h). COMPUTED FLOWS.

□, $c_{vib} = 3$. ○, $c_{vib} = 2$. △, $c_{vib} = 1$. ▽, $c_{vib} = 0.5$.

+, *flows computed only for the variations along the alpha-shock.*

– –, *shock wave at infinity just fully dispersed.*

CHAPTER 2

GENERAL FLOW MESH SCHEME AND DECAY AND DEVELOPMENT PROCESSES

INTRODUCTION

Chapter 2 introduces the reader to the flow with a discussion in great detail of the flow given by $\theta_w = 2.00^o$, $m_{f\infty} = 1.49$ and $c_{w_b} = 2.12$. Section (1) gives details of the starting process and general mesh scheme and section (2) goes on to discuss the variations on the wedge surface and alpha-shock as well as the wave development process. Errors are assessed by calculations done with smaller step sizes and accurate diagrams of the characteristic mesh and shock wave development are presented. Section (3) deals with the very interesting distinction between real gas and alpha-gas entropy layers in the equilibrium flow far downstream from the shock wave. The order of magnitudes of the entropy productions on the wedge surface and at infinity are estimated in terms of the wedge angle. Section (4) utilises the first order wedge tip gradients to describe the initial shock wave development and alpha-shock decay. A simple solution for the pressure on the wedge surface is also given.

SECTION (1)

Starting process and general mesh scheme

The flow that we shall use as the main example to illustrate the essential shock wave development processes is representative of the fully dispersed wave flows computed (see fig. 2(a)). It incorporates all the important, general features of the computer program as well as being applicable to the shock tube flow of CO_2 at 600^oK.

In the last chapter the justifications for employing a thermodynamically controlled step size on the wedge surface were given. Here we shall give a detailed description of how this idea is put into practice.

The flow quantities at the wedge tip are easily obtained by use of the frozen shock relations with the flow deflection equal to the wedge angle. The flow boundaries are the alpha-shock, across which the frozen shock relations are valid, and the wedge surface where the flow direction is specified. In order to extend the calculations away from the wedge tip, an initial data line must be established. This can be done extremely accurately by employing small coordinate expansions in the tip vicinity but we shall employ a starting scheme that relies solely on the characteristics and which can be iterated to the desired accuracy. The convergence of this iteration scheme is checked analytically by extracting the first order tip gradients from the first approximation.

The characteristic relations given in Chapter 1 are

$$\frac{dp}{\rho V^2 \tan\mu} + d\theta = \frac{-(\gamma_f - 1)\rho(\bar{\sigma} - \sigma)\, dy}{V^3 \sin\mu \sin(\theta+\mu)} \quad \text{on a } C^-$$

$$\frac{dp}{\rho V^2 \tan\mu} - d\theta = \frac{-(\gamma_f - 1)\rho(\bar{\sigma} - \sigma)\, dy}{V^3 \sin\mu \sin(\theta-\mu)} \quad \text{on a } C^+$$

and $$d\sigma = \frac{\rho(\bar{\sigma} - \sigma)\, dy}{V \sin\theta} \quad \text{and}$$

$$dp = -\rho V\, dV \qquad \text{on a streamline}$$

These relations are employed in finite difference form with error of order the mesh length squared. The necessary iterations are accomplished by using the mean values of the coefficients of the differentials between successive mesh points. If no linear interpolation is employed then the error term is reduced to the order of the mesh length cubed (see Sedney (1970)).

For instance, between points 1 and 2, the negative characteristic relation is written as

$$\frac{(p_2 - p_1)}{\rho_1 V_1^2 \tan\mu_1} + (\theta_2 - \theta_1) = \frac{-(\gamma_f - 1)\rho_1(\bar{\sigma}_1 - \sigma_1)(y_2 - y_1)}{V_1^3 \sin\mu_1 \sin(\theta_1 + \mu_1)}$$

in the first approximation and as

$$\frac{(p_2 - p_1)}{\rho_{12} V_{12}^2 \tan\mu_{12}} + (\theta_2 - \theta_1) = \frac{-(\gamma_f - 1)\rho_{12}(\bar{\sigma}_{12} - \sigma_{12})(y_2 - y_1)}{V_{12}^3 \sin\mu_{12} \sin(\theta_{12} + \mu_{12})}$$

in a second approximation, where suffix 12 represents the average of the quantity at points 1 and 2.

The frozen shock relations, valid across the alpha-shock, are employed exactly. From these relations the changes in pressure along the alpha-shock can be related to the corresponding changes in flow angle by the differential relation

$$dp = \left(\frac{dp}{d\theta}\right) d\theta$$

where $$\frac{dp}{d\theta} = \frac{dp}{d\phi} \cdot \frac{d\phi}{d\theta}$$

$$\frac{dp}{d\phi} = \frac{2\gamma_f}{(\gamma_f + 1)} M_{f\infty}^2 \sin 2\phi$$

and $$\frac{d\theta}{d\phi} = \frac{(\gamma_f + 1) M_{f\infty}^4 \tan^2\theta \sin^2\phi}{(M_{f\infty}^2 \sin^2\phi - 1)^2 (1 + \tan^2\theta)} - \frac{2 \tan\theta}{\sin 2\phi (1 + \tan^2\theta)}$$

The equations of state and energy are applied exactly throughout the whole flow.

With reference to fig. 2(b) we first locate point 1 by assuming that this point determines a certain fraction of the total change in vibrational energy on the wedge surface. We evaluate the physical distance from the tip by the rate equation

$$d\sigma = \frac{\rho(\bar{\sigma} - \sigma)\, dx}{\bar{V} \cos\theta_w}$$

or $$dx = \frac{\bar{V} \cos\theta_w\, d\sigma}{\rho(\bar{\sigma} - \sigma)}$$

Applying this to the starting triangle gives

$$x_1 - x_0 = \frac{\bar{V}_0 \cos\theta_w (\sigma_1 - \sigma_0)}{\rho_0 (\bar{\sigma}_0 - \sigma_0)}$$

To find x_1 we must specify $(\sigma_1 - \sigma_0)$. The total change in vibrational energy on the surface is given approximately by

$$\bar{\sigma}(T_e) - \bar{\sigma}_\infty$$

where T_e denotes the equilibrium temperature far downstream behind the equilibrium-shock.

Since the difference between T_e and T_0 is small in relation to $T_0 - 1$ we can write

$$\bar{\sigma}_0 - \sigma_0 \approx \bar{\sigma}(T_e) - \bar{\sigma}_\infty$$

We therefore specify the change in vibrational energy per step along the wedge as equal to

$$\frac{1}{50}(\bar{\sigma}_0 - \sigma_0)$$

The fraction $1/50$ is chosen because this gives good accuracy as well as being amenable for use on the computer. The first physical step length is therefore given by

$$x_1 - x_0 = \frac{\bar{V}_0 \cos\theta_w}{50\,\rho_0}$$

The first approximation to the thermodynamics and geometry in the triangle 012 is to assume that the flow is uniform. A second approximation to the conditions at point 2 can be found by solving the negative characteristic relation along the line 12 in conjunction with the shock relation between pressure and flow angle.

That is we solve simultaneously the equations

$$\frac{(p_2 - p_0)}{\rho_0 \bar{V}_0^2 \tan\mu_0} + (\theta_2 - \theta_0) = \frac{-(\gamma_f - 1)\rho_0 (\bar{\sigma}_0 - \sigma_0)(y_2 - y_1)}{\bar{V}_0^3 \sin\mu_0 \sin(\theta_0 + \mu_0)}$$

and

$$(p_2 - p_0) - \left(\frac{dp}{d\theta}\right)_0 (\theta_2 - \theta_0) = 0$$

The geometry is given by

$$\frac{(y_2 - y_1)}{\sin(\theta_0+\mu_0)} = \frac{(x_1-x_0)\sin(\phi_0-\theta_0)}{\cos\theta_w \sin(\mu_0-\phi_0+\theta_0)}$$

and $$\frac{(z_2 - z_0)}{\sin\mu_0} = \frac{(x_1-x_0)}{\cos\theta_w \sin(\mu_0-\phi_0+\theta_0)}$$

where z is a distance coordinate along the alpha-shock. Hence solving for $p_2 - p_0$ gives

$$\frac{(p_2-p_0)}{(z_2-z_0)} = \frac{-(\gamma_f-1)\rho_0(\bar{\sigma}_0-\sigma_0)\sin(\phi_0-\theta_0)}{\bar{V}_0^3 \sin^2\mu_0 \left(\frac{1}{\rho_0\bar{V}_0^2\tan\mu_0} + \left(\frac{d\theta}{dp}\right)_0\right)}$$

$$= \frac{-(\gamma_f-1)\rho_0^2(\bar{\sigma}_0-\sigma_0)\cos(\phi_0-\theta_0)}{\bar{V}_0\left(\frac{\sin\mu_0\cos\mu_0\cos(\phi_0-\theta_0)}{\sin(\phi_0-\theta_0)} + \rho_0\bar{V}_0^2\sin^2\mu_0\cot(\phi_0-\theta_0)\left(\frac{d\theta}{dp}\right)_0\right)}$$

Since for weak waves $\phi_0 = \mu_0 + 0(\theta_0)$ the above expression is approximately equivalent to the analytically derived wedge tip gradient (see section (4)).

Having determined the pressure at point 2 all other quantities can be derived from the shock relations. A second approximation to the thermodynamics at point 1 (notice, however, that the value of the vibrational energy at point 1 has already been fixed) can be determined by employing the positive characteristic relation between points 1 and 3. The conditions at point 3 are found by linear interpolation between points 0 and 2. That is if k is the interpolating constant such that

$$k(p_2-p_0) = (p_2-p_0)$$

then

$$\frac{(p_1-p_0)-k(p_2-p_0)}{\rho_0\bar{V}_0^2\tan\mu_0} - (\theta_1-\theta_3) = \frac{(\gamma_f-1)\rho_0(\bar{\sigma}_0-\sigma_0)(y_1-y_3)}{\bar{V}_0^3\sin\mu_0\sin(\mu_0-\theta_0)}$$

But $\theta_1 \approx \theta_0$ so the above equation becomes

$$\frac{(p_1-p_0)-k(p_2-p_0)}{\rho_0 \bar{V}_0^2 \tan\mu_0} + k(\theta_2-\theta_0) = \frac{(\gamma_f-1)\rho_0(\bar{\sigma}_0-\sigma_0)(y_1-y_3)}{\bar{V}_0^3 \sin\mu_0 \sin(\mu_0-\theta_0)}$$

From the negative characteristic relation between points 1 and 2

$$(\theta_2-\theta_0) = -\frac{(p_2-p_0)}{\rho_0 \bar{V}_0^2 \tan\mu_0} - \frac{(\gamma_f-1)\rho_0(\bar{\sigma}_0-\sigma_0)(y_2-y_1)}{\bar{V}_0^3 \sin\mu_0 \sin(\theta_0+\mu_0)}$$

substituting for $(\theta_2-\theta_0)$ into the positive characteristic relation above gives

$$\frac{(p_1-p_0)-2k(p_2-p_0)}{\rho_0 \bar{V}_0^2 \tan\mu_0} = \frac{(\gamma_f-1)\rho_0(\bar{\sigma}_0-\sigma_0)(y_1-y_3)}{\bar{V}_0^3 \sin\mu_0 \sin(\mu_0-\theta_0)} + \frac{k(\gamma_f-1)\rho_0(\bar{\sigma}_0-\sigma_0)(y_2-y_1)}{\bar{V}_0^3 \sin\mu_0 \sin(\theta_0+\mu_0)}$$

Since

$$k = \frac{(\ell_1-\ell_0)\sin\mu_0}{(z_2-z_0)\sin(\mu_0+\phi_0-\theta_0)}$$

$$y_1-y_3 = -\frac{(\ell_1-\ell_0)\sin(\phi_0-\theta_0)}{\sin(\mu_0+\phi_0-\theta_0)}$$

and $y_2-y_1 = \frac{(\ell_1-\ell_0)\sin(\phi_0-\theta_0)}{\sin(\mu_0+\theta_0-\phi_0)}$ where $\ell = \frac{x}{\cos\theta_w}$

we get

$$\frac{(p_1-p_0)}{(\ell_1-\ell_0)} = -\left(-\frac{2\sin\mu_0}{\sin(\mu_0+\phi_0-\theta_0)}\frac{(p_2-p_0)}{(z_2-z_0)}\right.$$

$$+\frac{\rho_0 \bar{V}_0^2 \tan\mu_0 (\gamma_f-1)\rho_0(\bar{\sigma}_0-\sigma_0)\sin(\phi_0-\theta_0)}{\bar{V}_0^3 \sin\mu_0 \sin(\mu_0-\theta_0)\sin(\mu_0+\phi_0-\theta_0)}$$

$$\left.-\frac{\rho_0 \bar{V}_0^2 \tan\mu_0 (\gamma_f-1)\rho_0(\bar{\sigma}_0-\sigma_0)\sin(\phi_0-\theta_0)}{\bar{V}_0^3 \sin\mu_0 \sin(\mu_0+\theta_0)\sin(\mu_0+\phi_0-\theta_0)}\right)$$

For weak waves $\phi_0 = \mu_0 + O(\theta_0)$ so that approximately we have

$$\frac{(\phi_1 - \phi_0)}{(\theta_1 - \theta_0)} = \frac{1}{\cos(\phi_0 - \theta_0)} \frac{(p_2 - p_0)}{(\rho_2 - \rho_0)}$$

This is again the same result as given by the first order gradients. We can conclude, therefore, that the starting iteration process is likely to be rapidly convergent.

To obtain further approximations we proceed around the triangle in the same manner as before but employ the average values for the coefficients in the compatibility and shock relations. The iterations are continued until the pressure is 'correct' to 9 decimal places. The linear interpolation used between points 0 and 2, however, invalidates any precise statement of the accuracy.

Once the conditions at points 1 and 2 in the starting triangle have been determined the calculations can proceed as follows. With reference to fig. 2(c) we find the physical coordinates of point 4 just as we located point 1 in the first triangle. That is we have

$$x_4 - x_1 = \frac{\bar{V}_1 \cos\theta_w (\sigma_4 - \sigma_1)}{\rho_1 (\bar{\sigma}_1 - \sigma_1)}$$

where $$\frac{\sigma_4 - \sigma_1}{\bar{\sigma}_0 - \sigma_0} = \frac{1}{50}$$

In fig. 2(c) points 4, 5 and 6 are typical of the different types of mesh point in the characteristics network. Points 4 and 6 lie on the flow boundaries and are called body and shock points respectively. The mesh structure at these points is shown more closely in figs. 2(d) and 2(f). The boundary condition on the wedge surface necessitates the use of only 2 of the 3 characteristics in determining the unknown point. At the alpha-shock the shock relations together with the compatibility relation along

the negative characteristic are sufficient to determine the shock point. The major portion of the flow consists of points like 5 which are called field points (see fig. 2(e)). The pressure and flow deflection at the unknown point U can be found by solving the C^+ and C^- relations on the characteristics through the known points N, but the streamline relations (with linear interpolation between the two known points) must also be used to find the remaining thermodynamic quantities at U.

The solution is built up in layers along the negative characteristics. The first mesh point is a body point, followed by several field points and terminated with a shock point. Each step along the wedge surface has the same change in vibrational energy. From the rate equation the mesh lengths along the wedge surface are given by

$$dx = \frac{\bar{V} \cos\theta_w \, d\sigma}{\rho(\bar{\sigma} - \sigma)}$$

For fixed values of $d\sigma$, $dx \to \infty$ as $\sigma \to \bar{\sigma}$. It is therefore found convenient to terminate the thermodynamically controlled step size when 90 per cent of the change in vibrational energy on the wedge surface has taken place. The physical step size is then approximately 10 times its initial value. The calculations progress further downstream with a constant, though adjustable, physical step length on the wedge surface.

For wave flows that are fully dispersed at infinity, the shock points overshoot at a finite distance from the wedge surface. That is they iterate to pressures on the alpha-shock slightly below 1. The calculations can, however, be extended further downstream by computing up to the positive characteristic through the last shock point with the pressure greater than 1. A comparison between the solution at infinity and the characteristics can then be carried out along this last positive characteristic. Such a comparison is given in fig.2(g) for the flow $\frac{\theta_w}{\theta_w^*} = 1$, $M_{f\infty} = 2.6$, $c_{vib} = 1$. This procedure is sufficient to deal with wave flows which are partly

dispersed (here the program is terminated when the pressure jump across the alpha-shock overshoots its value at infinity) and just or nearly fully dispersed. For weaker wave flows the shock wave development distance can be many times the alpha-shock decay distance so that a new procedure is required to extend the calculations further above the wedge surface.

A typical case is illustrated in fig. 2(j). This represents the flow $\theta_w = 2.00^\circ$ ($\frac{\theta_w}{\theta_w^*} \simeq 0.6$), $M_{f\infty} = 1.49$, $c_{vib} = 2.12$. The pressure profiles are taken along the dashed lines. The wave development distance is approximately 2 times the alpha-shock decay length. Suppose that point 1 in fig. 2(h) is the shock point where the pressure first overshoots. Then we must extend the mesh above this point. We realize that if the flow at infinity is fully dispersed then the limiting direction of the decaying alpha-shock must be that of the freestream Mach line. Hence as soon as the pressure overshoots we equate all the thermodynamic variables to their freestream values. Since the last shock mesh length is rather large, facility is made for interpolating points like 2 so that approximately equal steps along the negative characteristics are maintained. The same procedure is used for all successive shock points though the computation of one more shock location (point 4) is all that is necessary. This is because the freestream characteristic (between points 1 and 4) has very nearly the same direction as the flow negative characteristic (between points 3 and 4) so that point 4 extends the mesh sufficiently to investigate the whole fully dispersed shock wave development.

We have, however, impressed slight discontinuities into the flow but these are not regarded as serious because they can only propagate into the flow along the positive characteristics. The main signals are channelled along the negative characteristics and the reflections along the positive

characteristics are weak in comparison. The propagation of these discontinuities into the flow will mean that iterating to the previous accuracy is not possible. We can only sensibly iterate down to the magnitude of the discontinuity inserted.

To illustrate the improvements obtained we can again refer to fig. 2(j). With the previous method we could have extended the calculations to a distance above the wedge of about 40. We can see that at this distance the shock wave is not fully developed. The modified method extends the calculations as far from the wedge surface as we wish. In particular at a distance of about 100 from the wedge surface the agreement between the characteristics solution and the solution at infinity is remarkably good.

SECTION (2)

Decay and development processes in the flow

In this section we shall deal with the methods adopted to extract all the relevant properties of the flow from the numerical characteristics results. In particular, we are interested in the modifications in alpha-shock propagation and shock wave development due to non-linear effects. The variations on the wedge surface, where simple solutions can be constructed, are also studied.

To illustrate the general nature of the flow (throughout this section we refer to the flow $\Theta_w = 2.00^\circ$, $M_{f\infty} = 1.49$, $c_{v,b} = 2.12$) the reader should see figs. 2(k) and 2 (i). The former is a scaled drawing of the actual characteristic mesh in a coordinate system that follows the initial frozen shock path. The physical (x, y) coordinate system involves distances that are both very large and very small (in each coordinate) on the same characteristic and hence is unsuitable. For the coordinate

system chosen we have

$$\underline{Y} = y$$

$$\underline{X} = x - \frac{y}{\tan \phi_o}$$

The initial frozen shock path is the line $\underline{X} = 0$ and the angle α corresponds to the angle

$$\beta = \tan^{-1} \frac{\tan \alpha \, . \tan \phi_o}{(\tan \alpha + \tan \phi_o)}$$

in the physical coordinate system. For instance when $\alpha = \frac{\pi}{2}$, $\beta = \phi_o$. This drawing clearly indicates how the bending of the negative characteristics (and consequently of the alpha-shock) modifies the location of the flow properties over large distances from the wedge surface. Notice how the physical step length along the wedge surface increases as do the shock mesh lengths further out in the flow. It is also interesting to observe how the characteristics are in fact 'self correcting'. That is they converge in regions of comparatively large gradients so reducing the step length. This effect can be seen by tracing the last few negative characteristics in the diagram. This diagram does not show the whole flowfield; the characteristics are traced to the point where the alpha-shock is replaced by a freestream Mach line.

Fig. 2(i) shows the departure from equilibrium of the vibrational energy, $\bar{\sigma} - \sigma$, plotted along the negative characteristics emanating from the wedge surface. This is a very effective way of showing (in a qualitative manner) all the decay processes in the flow. The development of the equilibrium core (where $\sigma = \bar{\sigma}$) can be traced simply and the decay of $\bar{\sigma} - \sigma$ on the wedge surface can be seen from the variations on $y = 0$. The maximum value of the departure from equilibrium is always embedded in the relaxation region so that tracing the path of the maxima gives essentially the shock wave trajectory. The approach of the maximum to

its ultimate value at infinity (which we denote by $(\bar{\sigma}-\sigma)_{max\infty}$) determines the rate at which the shock wave develops. The decay of the alpha-shock is also adequately expressed by following the variations where the negative characteristics terminate. Notice how the alpha-shock reaches zero strength before the maximum value of the departure from equilibrium has reached its asymptotic value at infinity. This is true for all the computed flows which are fully dispersed at infinity and is far more apparent as the wave strength is decreased. The non-uniformities in the flow variables far downstream but near the wedge surface are not exhibited on this graph (since all the flow far downstream is in equilibrium) but will be discussed in section (3).

The quantitative results for these decay processes are best analysed by first normalizing quantities and then plotting on a logarithmic scale. We shall represent all decay processes by use of the departure from equilibrium $\bar{\sigma}-\sigma$ and shall normalize this quantity for the specific process under discussion in the following ways. To illustrate the shock wave development we plot $\frac{(\bar{\sigma}-\sigma)_{max} - (\bar{\sigma}-\sigma)_{max\infty}}{(\bar{\sigma}-\sigma)_0 - (\bar{\sigma}-\sigma)_{max\infty}}$ against y. In this expression $(\bar{\sigma}-\sigma)_{max}$ represents the maximum value of $\bar{\sigma}-\sigma$ along a positive characteristic and $(\bar{\sigma}-\sigma)_{max\infty}$ is the corresponding quantity at infinity. Since initially the maximum of $\bar{\sigma}-\sigma$ is located at the alpha-shock, this expression varies between 1 and 0. The alpha-shock decay is represented by plotting $\frac{(\bar{\sigma}-\sigma)_a}{(\bar{\sigma}-\sigma)_0}$ against y (for fully dispersed waves at infinity) and by plotting $\frac{(\bar{\sigma}-\sigma)_a - (\bar{\sigma}-\sigma)_{a\infty}}{(\bar{\sigma}-\sigma)_0 - (\bar{\sigma}-\sigma)_{a\infty}}$ against y (for partly dispersed shock waves at infinity). Here $(\bar{\sigma}-\sigma)_a$ represents the departure from equilibrium at the alpha-shock and $(\bar{\sigma}-\sigma)_{a\infty}$ is the corresponding value at infinity. The approach towards the equilibrium state on the wedge surface (and hence the appropriate relaxation distance) is investigated by plotting $\frac{(\bar{\sigma}-\sigma)_w}{(\bar{\sigma}-\sigma)_0}$ against x. Suffix w refers to quantities along the wedge surface.

For each decay process in this example the accuracy of the calculations made with steps corresponding to $^1/50$th of the total σ variation on the surface is checked by using steps corresponding to $^1/10$th and $^1/250$th of the σ variation. By plotting all the results in the above manner we shall be able to define precisely what we mean by development and decay distances which have, of necessity, been employed rather vaguely in the previous text.

The results for the 3 main decay processes are displayed in figs.2(l), 2(m) and 2(n). Base e logarithms will be employed in mathematical expressions. If we refer to fig. 2(l) we see that to a very good approximation the decay on the wedge surface is exponential. This is found to be generally true for all the flows computed so that we shall be able to give an analytical expression for the rate of decay from the tip gradients given in section (4). The effect of inaccuracies is clearly exhibited by comparing the calculations made with $^1/10$th the total variation of σ per step with those having $^1/250$th of the total σ variation per step. Notice, however, that these inaccuracies are only apparent when the flow along the surface is very nearly in equilibrium. We would expect, in fact, the numerical results on the wedge surface to be the most accurate since essentially we are integrating the streamline equations along a known boundary.

In fig. 2(m) the alpha-shock decay is plotted and on the same graph the linear decay rate is exhibited (see Chapter 5). This enables us to distinguish the non-linear effects which clearly cause a slower rate of decay. The linear theory is reasonably accurate near the tip but further out in the flow the results are best represented by a rather smaller, constant rate of decay. These conclusions are justified with calculations for 3 different step sizes. Deviations from the line establishing the slower rate of decay are shown to be due to inaccuracies in the calculations

rather than to a renewed 'speeding up' of the decay process. We can explain the two rates of decay physically by recognizing the fact that the linear theory takes into consideration only those negative characteristics that originate at distances infinitesimally close to the wedge tip. This is a good approximation only for extremely weak wave flows. The modification that results for stronger wave flows is that all or the majority of the negative characteristics originating from the wedge surface must be taken into account. The characteristics that originate further downstream carry smaller disturbances into the flow so that we might expect a slowing down in the decay of the alpha-shock (which is controlled by these signals). To determine the character of the alpha-shock decay we have only to fix the 2 lines that signify the 2 decay rates. The first line always passes through the point where $\frac{(\bar{\sigma}-\sigma)_a}{(\bar{\sigma}-\sigma)_o} = 1$ and $y = 0$ and its gradient is known analytically from the tip gradients which are established in section (4). We shall call this the initial line. The second line can be located by specifying its gradient and ordinate of intersection with $y = 0$. We shall call this second line the far-field line. The alpha-shock decay distance will then be defined as the abscissa of the ordinate on the far-field line for which $\frac{(\bar{\sigma}-\sigma)_a}{(\bar{\sigma}-\sigma)_o} = 0.01$. For instance for this example the decay distance would be 42.

Fig. 2(n) gives very much the same kind of results for the wave development. There are 2 characteristic rates of decay but the far-field line is not predicted as accurately as it was for the alpha-shock. This is principally because the calculations are extended to much greater distances from the wedge surface but also because exact boundary conditions on the alpha-shock are not available. Nevertheless the convergence of the calculations for smaller step sizes is clearly established and deviations from the far-field line justly attributed to errors. Notice that the inaccuracy in the last point on the graph computed with $^1/_{50}$th of the σ

variation per step is only 2 per cent. Fig. 2(n) also illustrates rather more precisely some of the features present in fig. 2(i). The separation of the inflexion point in the vibrational energy from the alpha-shock and the slower wave development are now clearly defined. The characteristic features of these graphs can be interpreted in the same manner as those for the alpha-shock. We shall define the development distance as the abscissa of the ordinate on the far field line for which $\frac{(\bar{\sigma}-\sigma)_{max}}{(\bar{\sigma}-\sigma)_{max\infty}} = 1.1$. This definition ensures that the characteristics shock wave profile has essentially the same shape and width as the shock wave at infinity. With the above definition, for this example the development distance is 80. Reference to fig.2(j) shows that this is quite a realistic distance in terms of comparison of shock wave shape with that at infinity.

SECTION (3)

Entropy gradients in the equilibrium flow far downstream from the shock wave

The term entropy will be employed as in the previous text when referring to the real gas entropy. In the high Mach number flows computed by Sedney, South and Gerber (1962), the appearance of entropy gradients far downstream was attributed to the initial gradients resulting from the streamlines having passed through a strong but decaying alpha-shock. A linearized analysis by Lee (1964), using the frozen flow at the wedge tip as reference state, shows that indeed all the gradients in this 'entropy layer' are proportional to the alpha-shock curvature (except, of course, for the pressure and flow deflection which are uniform in this region).

Entropy is produced across the alpha-shock and in the non-equilibrium relaxation region of the flow. For the strong shock flows discussed by Sedney et al. the former is no doubt the dominant mechanism; for weak wave

flows, however, the entropy jumps across the alpha-shock are of third order in the alpha-shock strength. We shall show that the major contributions to the entropy production arise from the gas relaxation and in particular from the departure from equilibrium in the vibrational energy initiated by the alpha-shock. On the wedge surface this effect is of second order in the alpha-shock strength.

We shall define the 'entropy layer' as the region far downstream over which the entropy is non-uniform. This layer has a thickness which is comparable to the shock wave development distance because essentially it is a manifestation of the wave development process. We shall define the 'alpha-gas entropy layer' as the region far downstream over which other thermodynamic variables than the entropy are non-uniform. This layer has a thickness which is of the same magnitude as the alpha-shock decay distance, which for very weak wave flows is much less than the shock wave development distance.

To examine the situation precisely we need to know the magnitudes of the entropy productions due to relaxation and due to the irreversible processes occurring within the alpha-shock. On the wedge surface there is an entropy jump across the alpha-shock followed by a continuous entropy production due to relaxation. Far downstream there is no entropy production because the gas is in equilibrium. There must also be an entropy increase through the shock wave at infinity. This is due solely to relaxation effects (when the shock wave is fully dispersed) but can be calculated without any knowledge of the non-equilibrium processes by using the equilibrium shock relations. We can then make an interesting physical check on the mechanism of entropy production by showing that the integrated entropy production due to the relaxation processes occurring within the shock wave is asymptotically equal to the entropy jump given by the equilibrium shock relations.

The increment in real gas entropy due to a small change of vibrational energy is given by (see Vincenti and Kruger (1965))

$$ds = \left(\frac{1}{T_{vib}} - \frac{1}{T}\right) d\sigma$$

Since

$$\bar{\sigma} = \bar{\sigma}_\infty + c_{vib}(T-1)$$

and $$\sigma = \bar{\sigma}_\infty + c_{vib}(T_{vib}-1)\ ,$$

the above expression can be written as

$$ds = \frac{c_{vib}(\bar{\sigma}-\sigma)\, d\sigma}{(c_{vib}+\bar{\sigma}-\bar{\sigma}_\infty)(c_{vib}+\sigma-\bar{\sigma}_\infty)}$$

The entropy change across a weak alpha-shock wave is given by (see Liepmann and Roshko (1967))

$$\Delta s = \frac{\gamma_f(\gamma_f+1) M_{f\infty}^3}{12\,(M_{f\infty}^2-1)^{\frac{3}{2}}}\,\theta_w^3 + O(\theta_w^4)$$

The contribution from the gas relaxation on the wedge surface, however, is given by

$$c_{vib}\int_{\sigma=\bar{\sigma}_\infty}^{\sigma=\bar{\sigma}} \frac{(\bar{\sigma}-\sigma)\, d\sigma}{(c_{vib}+\bar{\sigma}-\bar{\sigma}_\infty)(c_{vib}+\sigma-\bar{\sigma}_\infty)} \qquad 3.1$$

From this expression we can construct an approximate analytic solution. We assume that

$$(\bar{\sigma}-\sigma) = (\bar{\sigma}-\sigma)_0\, e^{-\frac{x}{\bar{x}_w}} \qquad \text{(see fig. 2(1))}$$

where $\bar{x}_w$ is the relaxation distance on the wedge surface. We shall use the rate equation in the form

$$\bar{V}\, d\sigma = \frac{\rho(\bar{\sigma}-\sigma)\, dx}{\cos\theta_w}$$

substituting these expressions for $(\bar{\sigma}-\sigma)$ and $d\sigma$ into 3.1 gives

$$\int_{s=s_0}^{s=s} ds = c_{vib}\int_{x=0}^{x=x} \frac{\rho(\bar{\sigma}-\sigma)^2\, dx}{\bar{V}\cos\theta_w\,(c_{vib}+\bar{\sigma}-\bar{\sigma}_\infty)(c_{vib}+\sigma-\bar{\sigma}_\infty)}$$

Neglecting terms in the integrand of $O(\theta_w^3)$ gives

$$\int_{s=s_0}^{s=s} ds = \frac{c_{v,b}^{-1}\rho_0(\bar{\sigma}-\sigma)_0^2}{\bar{V}_0 \cos\theta_w} \int_{x=0}^{x=x} e^{-\frac{2x}{\bar{x}_w}} dx$$

Hence

$$s - s_0 = \frac{\rho_0(\bar{\sigma}-\sigma)_0^2 \bar{x}_w \left(1 - e^{-\frac{2x}{\bar{x}_w}}\right)}{2\bar{V}_0 \cos\theta_w c_{v,b}}$$

Writing $(\bar{\sigma}-\sigma)_0 = c_{v,b}(T_0 - 1)$ gives

$$s - s_0 = \frac{c_{v,b}\rho_0(T_0-1)^2 \bar{x}_w}{2\bar{V}_0 \cos\theta_w}\left(1 - e^{-\frac{2x}{\bar{x}_w}}\right)$$

As $x \to \infty$ the entropy production on the wedge surface tends to the value

$$\frac{c_{v,b}\rho_0(\bar{T}_0-1)^2 \bar{x}_w}{2\bar{V}_0 \cos\theta_w} \qquad 3.2$$

For $c_{v,b} = O(1)$ this expression is $O(\theta_w^2)$ and hence much larger than the entropy production term across the alpha-shock which is $O(\theta_w^3)$. For an actual comparison see fig. 2(o). Notice that 3.2 implies that

$$\frac{(s-s_0)}{(s-s_0)^*} = \left(\frac{\theta_w}{\theta_w^*}\right)^2$$

The entropy jump across the shock wave at infinity is approximately the same (it is in fact slightly smaller) as that across the frozen shock at the tip. The overall flow deflection is the same and differences in the two contributions can only arise due to the differences between the equilibrium and frozen values in the coefficient of θ_w. The 'entropy layer' must therefore involve a transition from an entropy value on the wedge surface which is of order θ_w^2 to a value at infinity which is of order θ_w^3. This implies that the entropy layer thickness is of the same magnitude as the development length of the shock wave. By determining the streamline trajectories in the flow and then integrating expression 3.1 along them we can calculate the entropy variations far downstream. This

is done in fig.2(s) and supports our physical arguments.

The mechanism for the entropy production is known; in particular we can calculate the entropy production across the shock wave at infinity either by integrating 3.1 through the wave interior and finding the asymptote or by simply applying the conservation equations across the non-equilibrium region.

If we choose the former we get

$$S = c_{vib} \int_{\sigma=\bar{\sigma}_\infty}^{\sigma=\bar{\sigma}} \frac{\rho(\bar{\sigma}-\sigma)^2 \, d\sigma}{V \cos\theta \, (c_{vib}+\bar{\sigma}-\bar{\sigma}_\infty)(c_{vib}+\sigma-\bar{\sigma}_\infty)}$$

(taking the freestream entropy as zero)

An upper bound for this expression is

$$\frac{c_{vib}^{-1}(\bar{\sigma}-\sigma)^2_{max\infty} \, L}{V_\infty \cos\theta_w} \qquad 3.3$$

where L is a streamline wave thickness.

If we calculate the entropy production from the conservation equations we get

$$S = \frac{\gamma_e(\gamma_e+1) \, m_{e\infty}^3 \, \theta_w^3}{12 \, (m_{e\infty}^2-1)^{\frac{3}{2}}} + O(\theta_w^4) \qquad 3.4$$

The results of Chapter 3 show that we can write

$$(\bar{\sigma}-\sigma)_{max\infty} = \frac{\gamma_e(\gamma_e(\gamma_e-1)^{-1}-1)^2(\gamma_e+1)^2 m_{e\infty}^4 \theta_w^2}{8(m_{e\infty}^2-1)(2\gamma_e(\gamma_e-1)^{-1}-1)} + O(\theta_w^3)$$

Hence if we insert this expression into 3.3 and compare with 3.4 we see that we must have (for $c_{vib} << 1$)

$$L \sim \frac{c_{vib}}{\theta_w}$$

which has physical justification (see Hodgson and Johannesen (1971)). An exact comparison between the two methods for calculating the entropy jump is shown in fig.2(p).

Alpha-gas entropy

The significance of the alpha-gas entropy lies in the fact that it is directly related to those thermodynamic properties of the fluid which are the same for both the real gas and the alpha-gas. The real gas temperature and velocity changes, for instance, are related to changes in the alpha-gas entropy by the energy equation. That is,

$$c_{pa} T + \sigma + \tfrac{1}{2} V^2 = \text{constant}$$

Differentiating gives

$$c_{pa}\, dT + d\sigma + V dV = 0$$

Dividing by T,

$$c_{pa}\left(\frac{dT}{T}\right) + \left(\frac{V}{T}\right) dV = -\frac{d\sigma}{T} = ds_a$$

The alpha-gas entropy increments can be either positive or negative depending on whether the vibrational energy is decreasing or increasing. For the flow of a relaxing gas through an expansion, the alpha-gas entropy increases while in shock wave relaxation regions the opposite is true. The changes in the real gas entropy, however, can never be negative and in non-equilibrium regions the entropy always increases.

The alpha-gas entropy productions along the wedge surface and through the shock-wave at infinity have the same magnitude (see figs. 2(o), 2(p)). Approximate values (which are upper bounds) are respectively

$$\left| -\frac{1}{T_e} \left(\bar{\sigma}_e - \bar{\sigma}_\infty \right) \right| = O(\theta_w)$$

and

$$\left| -\frac{1}{T_\infty} \left(\bar{\sigma}_e - \bar{\sigma}_\infty \right) \right| = O(\theta_w)$$

(we are assuming that any variations in temperature far downstream are small compared to the total temperature jump across the flow). Any contributions to the total alpha-gas entropy production on the wedge surface from alpha-gas entropy jumps across the alpha shock are negligible since these are 2 orders of magnitude in the wedge angle smaller. The small entropy jumps

across the alpha-shock are important, however, in explaining the formation of the alpha-gas entropy layer. Here we are considering differences in quantities which have equal magnitude (namely the alpha-gas entropy productions at infinity and along the wedge surface) and consequently any 'small' effects are not negligible.

Inspection of fig.2(q) shows that the alpha-gas entropy layer thickness is comparable to the alpha-shock decay distance. The contribution towards the total alpha-gas entropy production on the wedge surface by the frozen shock at the wedge tip is 0.000096. This has the right sign but is not wholly sufficient to account for the variations of the alpha-gas entropy far downstream. We observe, however, that the alpha-gas entropy production integral depends on the local temperature which is slightly higher at the tip because of the relatively strong alpha-shock there. This effect would tend to increase the alpha-gas entropy production on streamlines near the wedge surface. We can justify these assumptions rather better by showing that the rate of approach of the alpha-gas entropy to its equilibrium value far downstream but high above the wedge surface is similar to the rate of decay of the alpha-shock measured in terms of the temperature. This comparison is given in fig. 2(r). T_d is the temperature immediately downstream of the alpha-shock. The variable S_{aw} denotes the value of the alpha-gas entropy on the wedge surface. The variable S_{ae} denotes the equilibrium value of the alpha-gas entropy far downstream but high above the wedge surface.

The alpha-gas entropy is related to the pressure and density by the relation

$$S_a = \log p^{(\gamma_f-1)^{-1}} - \log \rho^{\frac{\gamma_f}{(\gamma_f-1)}} \qquad + \text{constant}$$

Far downstream the pressure is constant so that variations in alpha-gas entropy correspond to variations in density. Similarly from the equation of state the density variations are related to the temperature variations

and so on. The alpha-gas entropy layer therefore has the same thickness as the temperature, density and velocity layers which exist far downstream. The thickness of these layers is comparable to the alpha-shock decay distance. The real gas entropy layer which measures the relative magnitude of the non-equilibrium on successive streamlines extends over the whole flowfield.

SECTION (4)

First order wedge tip gradients and their use in providing analytic expressions for the initial decay and development rates; solution on the wedge surface

The shock wave development and alpha-shock decay have been investigated in terms of their initial and far-field decay rates. No general expression for the far-field decay rates is at present available but the first order wedge tip gradients are well known (see Capiaux and Washington (1963)). We shall adapt these so that they give analytic expressions for the initial decay and development processes.

If z is distance coordinate along the alpha-shock and K_S denotes the alpha-shock curvature then the pressure gradients at the wedge tip are given by

$$\left(\frac{\partial p}{\partial e}\right)_0 = \frac{-(\gamma_4-1)\rho_0^2(\bar{e}_0-e_0)}{\bar{V}_0\left(\cos^2\mu_0 + \rho_0\bar{V}_0^2\cos\epsilon(\phi_0-\theta_0)\sin^2\mu_0\left(\frac{d\theta}{dp}\right)_0\right)} \qquad 4.1$$

and

$$\left(\frac{\partial p}{\partial z}\right)_0 = \left(\frac{\partial p}{\partial e}\right)_0 \cos(\phi_0-\theta_0)$$

with

$$K_S = \frac{\left(\frac{\partial p}{\partial e}\right)_0 \cos(\phi_0-\theta_0)}{\left(\frac{dp}{d\phi}\right)_0}$$

The gradients we require are

$$\frac{d\left(\log_e \frac{(\bar{\sigma}-\sigma)}{(\bar{\sigma}-\sigma)_0}\right)}{dx}, \qquad \text{for the wedge surface decay}$$

$$\frac{d\left(\log_e \frac{(\bar{\sigma}-\sigma)}{(\bar{\sigma}-\sigma)_0}\right)}{dy}, \qquad \text{for the alpha-shock decay}$$

$$\frac{d\left(\log_e \frac{(\bar{\sigma}-\sigma)-(\bar{\sigma}-\sigma)_{a\infty}}{(\bar{\sigma}-\sigma)_0-(\bar{\sigma}-\sigma)_{a\infty}}\right)}{dy}, \qquad \text{for the partly dispersed wave alpha-shock decay}$$

$$\frac{d\left(\log_e \frac{(\bar{\sigma}-\sigma)_{max}-(\bar{\sigma}-\sigma)_{max\infty}}{(\bar{\sigma}-\sigma)_0-(\bar{\sigma}-\sigma)_{max\infty}}\right)}{dy}, \qquad \text{for the shock wave development}$$

These gradients can be evaluated at the tip in the following manner. From the energy equation we have

$$c_{pa}T + \sigma + \tfrac{1}{2}\bar{V}^2 = \text{constant}$$

Differentiating and substituting $dT = \frac{1}{c_{vib}}d\bar{\sigma}$ gives

$$\frac{c_{pa}}{c_{vib}}d\bar{\sigma} + d\sigma + \bar{V}d\bar{V} = 0 \qquad 4.2$$

By employing the rate equation for $d\sigma$ and eliminating $\bar{V}d\bar{V}$ in terms of $-\frac{1}{\rho}dp$ we get

$$\frac{c_{pa}}{c_{vib}}d(\bar{\sigma}-\sigma) + \frac{\rho(\bar{\sigma}-\sigma)}{\bar{V}}\left(1+\frac{c_{pa}}{c_{vib}}\right)dl - \frac{1}{\rho}dp = 0$$

Utilizing the expression for the pressure gradient along the wedge surface (equation 4.1) gives

$$\left(\frac{d(\bar{\sigma}-\sigma)}{dl}\right)_0 = -\frac{\rho_0(\bar{\sigma}_0-\sigma_0)}{\bar{V}_0}\left(1+\frac{c_{vib}}{c_{pa}}\right) - \frac{(\gamma_f-1)\rho_0(\bar{\sigma}_0-\sigma_0)\left(\frac{c_{vib}}{c_{pa}}\right)}{\bar{V}_0\left(\cos^2\mu_0 + \rho_0\bar{V}_0^2\cot(\phi_0-\theta_0)\sin^2\mu_0\left(\frac{d\theta}{dp}\right)_0\right)}$$

Hence the gradient we require on the wedge surface is

$$\left(\frac{d\left(\log\frac{(\bar{\sigma}-\sigma)}{(\bar{\sigma}-\sigma)_0}\right)}{dx}\right)_0 = \frac{1}{(\bar{\sigma}-\sigma)_0}\left(\frac{d(\bar{\sigma}-\sigma)}{dx}\right)_0$$

$$= -\frac{\rho_0}{\bar{V}_0\cos\theta_w}\left(\left(1+\frac{c_{vib}}{c_{pa}}\right)+\frac{(\gamma_f-1)\left(\frac{c_{vib}}{c_{pa}}\right)}{\left(\cos^2\mu_0+\rho_0\bar{V}_0^2\cot(\phi_0-\theta_0)\sin^2\mu_0\left(\frac{d\theta}{d\phi}\right)_0\right)}\right)$$

The initial wave development and alpha-shock decay gradients can be found in a similar manner. In particular we notice that initially the maximum departure from equilibrium always occurs on the alpha-shock. Hence we need only to find $\left(\frac{d(\bar{\sigma}-\sigma)}{dy}\right)_0$. Referring to equation 4.2 we have

$$\frac{c_{pa}}{c_{vib}}\,d\bar{\sigma} + d\sigma + \bar{V}\,d\bar{V} = 0$$

Along the alpha-shock $d\sigma = 0$ so we have

$$\frac{c_{pa}}{c_{vib}}\,d(\bar{\sigma}-\sigma) + \bar{V}\,d\bar{V} = 0$$

Since $\frac{d}{dz} = K_s\frac{d}{d\phi}$ then

$$\frac{c_{pa}}{c_{vib}}\left(\frac{d(\bar{\sigma}-\sigma)}{dz}\right)_0 + \bar{V}_0 K_s\left(\frac{d\bar{V}}{d\phi}\right)_0 = 0$$

But

$$K_s = \frac{\left(\frac{\partial p}{\partial e}\right)_0\cos(\phi_0-\theta_0)}{\left(\frac{dp}{d\phi}\right)_0}$$

Hence

$$\frac{c_{pa}}{c_{vib}}\left(\frac{d(\bar{\sigma}-\sigma)}{dz}\right)_0 = \frac{-\bar{V}_0\left(\frac{\partial p}{\partial e}\right)_0\cos(\phi_0-\theta_0)\left(\frac{d\bar{V}}{d\phi}\right)_0}{\left(\frac{dp}{d\phi}\right)_0}$$

Inserting $dz = \frac{dy}{\sin\phi_0}$ gives

$$\frac{c_{pa}}{c_{vib}}\left(\frac{d(\bar{\sigma}-\sigma)}{dy}\right)_0 = \frac{-\bar{V}_0\left(\frac{\partial p}{\partial e}\right)_0\cos(\phi_0-\theta_0)\left(\frac{d\bar{V}}{d\phi}\right)_0}{\sin\phi_0\left(\frac{dp}{d\phi}\right)_0}$$

The initial alpha-shock decay and wave development rates can therefore be obtained from the above expression by noticing that

$$\left(\frac{d\log\frac{(\bar{\sigma}-\sigma)}{(\bar{\sigma}-\sigma)_0}}{dy}\right)_0 = \frac{1}{(\bar{\sigma}-\sigma)_0}\left(\frac{d(\bar{\sigma}-\sigma)}{dy}\right)_0$$

and

$$\left(\frac{d\log\frac{(\bar{\sigma}-\sigma)_{max}-(\bar{\sigma}-\sigma)_{max\infty}}{(\bar{\sigma}-\sigma)_0-(\bar{\sigma}-\sigma)_{max\infty}}}{dy}\right)_0 = \frac{1}{((\bar{\sigma}-\sigma)_0-(\bar{\sigma}-\sigma)_{max\infty})}\left(\frac{d(\bar{\sigma}-\sigma)}{dy}\right)_0$$

In the next Chapter we shall use these expressions to give a precise evaluation of the initial decay rates.

Simple solution on the wedge surface

The characteristic results indicate (see next Chapter, but for a specific example in fig.2(1)) that to a very good approximation the departure from local equilibrium of the vibrational energy along the wedge surface decays exponentially with distance. We therefore assume that the departure from equilibrium is given by

$$(\bar{\sigma}-\sigma) = (\bar{\sigma}-\sigma)_0\, e^{-\frac{x}{\bar{x}_w}}$$

The relaxation distance $\bar{x}_w$ is given by the tip gradients discussed above. It is

$$\bar{x}_w^{-1} = \frac{\rho_0}{\bar{V}_0\cos\theta_w}\left(\left(1+\frac{c_{vib}}{c_{pa}}\right)+\frac{(\gamma_f-1)\left(\frac{c_{vib}}{c_{pa}}\right)}{\left(\cos^2\mu_0+\rho_0\bar{V}_0^2\cot(\phi_0-\theta_0)\sin^2\mu_0\left(\frac{d\theta}{dp}\right)_0\right)}\right)$$

In order to derive a solution, however, we must make another assumption. This is because the assumption introduced above can be shown (see section (1) of Chapter 3) to be a degenerate form of the rate equation. The variations of pressure, density, temperature and velocity along the wedge surface are given approximately by

$$p_e - p_0 = \left(\frac{\gamma_e M_{e\infty}^2}{(M_{e\infty}^2-1)^{\frac{1}{2}}} - \frac{\gamma_f M_{f\infty}^2}{(M_{f\infty}^2-1)^{\frac{1}{2}}}\right)\theta_w ,$$

$$\rho_e - \rho_0 = \left(\frac{m_{e\infty}^2}{(m_{e\infty}^2 - 1)^{\frac{1}{2}}} - \frac{m_{f\infty}^2}{(m_{f\infty}^2 - 1)^{\frac{1}{2}}} \right) \theta_w ,$$

$$T_e - T_0 = \left(\frac{(\gamma_e - 1) m_{e\infty}^2}{(m_{e\infty}^2 - 1)^{\frac{1}{2}}} - \frac{(\gamma_f - 1) m_{f\infty}^2}{(m_{f\infty}^2 - 1)^{\frac{1}{2}}} \right) \theta_w ,$$

and $$\bar{V}_e - \bar{V}_0 = \left(\frac{-1}{(m_{e\infty}^2 - 1)^{\frac{1}{2}}} + \frac{1}{(m_{f\infty}^2 - 1)^{\frac{1}{2}}} \right) \theta_w .$$

The percentage variation in the pressure is largest and it is this quantity for which we seek a solution. Consequently, we cannot assume that the velocity is constant because then the streamline momentum equation implies that the pressure should be constant (see section (1) of Chapter 1 for the streamline equations). The percentage variations in the density and temperature are similar; we assume that the density is constant. The streamwise momentum equation can then be integrated and gives

$$\bar{p} - p_0 = \tfrac{1}{2} \rho_0 (\bar{V}_0^2 - \bar{V}^2)$$

The temperature is obtained from the equation of state. That is

$$\bar{T} = \frac{\bar{p}}{\rho_0}$$

The energy equation is

$$c_{pa} \bar{T} + \sigma + \tfrac{1}{2} \bar{V}^2 = c_{pa} + \bar{\sigma}_\infty + \tfrac{1}{2} \bar{V}_\infty^2$$

since $\bar{\sigma} = \bar{\sigma}_\infty + c_{vib} (\bar{T} - 1)$ then

$$c_{pa} \bar{T} + c_{vib} (\bar{T} - 1) + \sigma - \bar{\sigma} + \tfrac{1}{2} \bar{V}^2 = c_{pa} + \tfrac{1}{2} \bar{V}_\infty^2 .$$

That is

$$(c_{pa} + c_{vib}) \bar{T} + \sigma - \bar{\sigma} + \tfrac{1}{2} \bar{V}^2 = c_{pa} + c_{vib} + \tfrac{1}{2} \bar{V}_\infty^2 .$$

Eliminating the velocity and temperature by the use of the equation of state and integrated streamline momentum equation gives

$$(c_{pa}+c_{v,b})\frac{p}{\rho_0}+(\sigma-\bar{\sigma})+\tfrac{1}{2}\bar{V}_0^2-\frac{(p-p_0)}{\rho_0}=c_{pa}+c_{v,b}+\tfrac{1}{2}\bar{V}_\infty^2$$

Collecting terms gives

$$p\left(\frac{c_{v,b}+c_{pa}}{\rho_0}-\frac{1}{\rho_0}\right)=(\bar{\sigma}-\sigma)-\frac{p_0}{\rho_0}+(c_{pa}+c_{v,b})+\tfrac{1}{2}\left(\bar{V}_\infty^2-\bar{V}_0^2\right)$$

Inserting the expression for $(\bar{\sigma}-\sigma)$ gives

$$p=\frac{\rho_0(\bar{\sigma}-\sigma)_0\,e^{-\frac{x}{x_w}}}{(c_{v,b}+c_{pa})}+\frac{\rho_0\left(c_{pa}+c_{v,b}-\bar{T}_0+\frac{1}{2}\left(\bar{V}_\infty^2-\bar{V}_0^2\right)\right)}{(c_{v,b}+c_{va})}$$

This solution is plotted in fig. 2(t) where it is compared to the linear theory (see section (2) Chapter 5). It is seen to be a closer approximation to the characteristics results.

As $x\to\infty$ the pressure tends to the value

$$\frac{\rho_0\left(c_{pa}+c_{v,b}-\bar{T}_0+\frac{1}{2}\left(\bar{V}_\infty^2-\bar{V}_0^2\right)\right)}{(c_{v,b}+c_{va})}$$

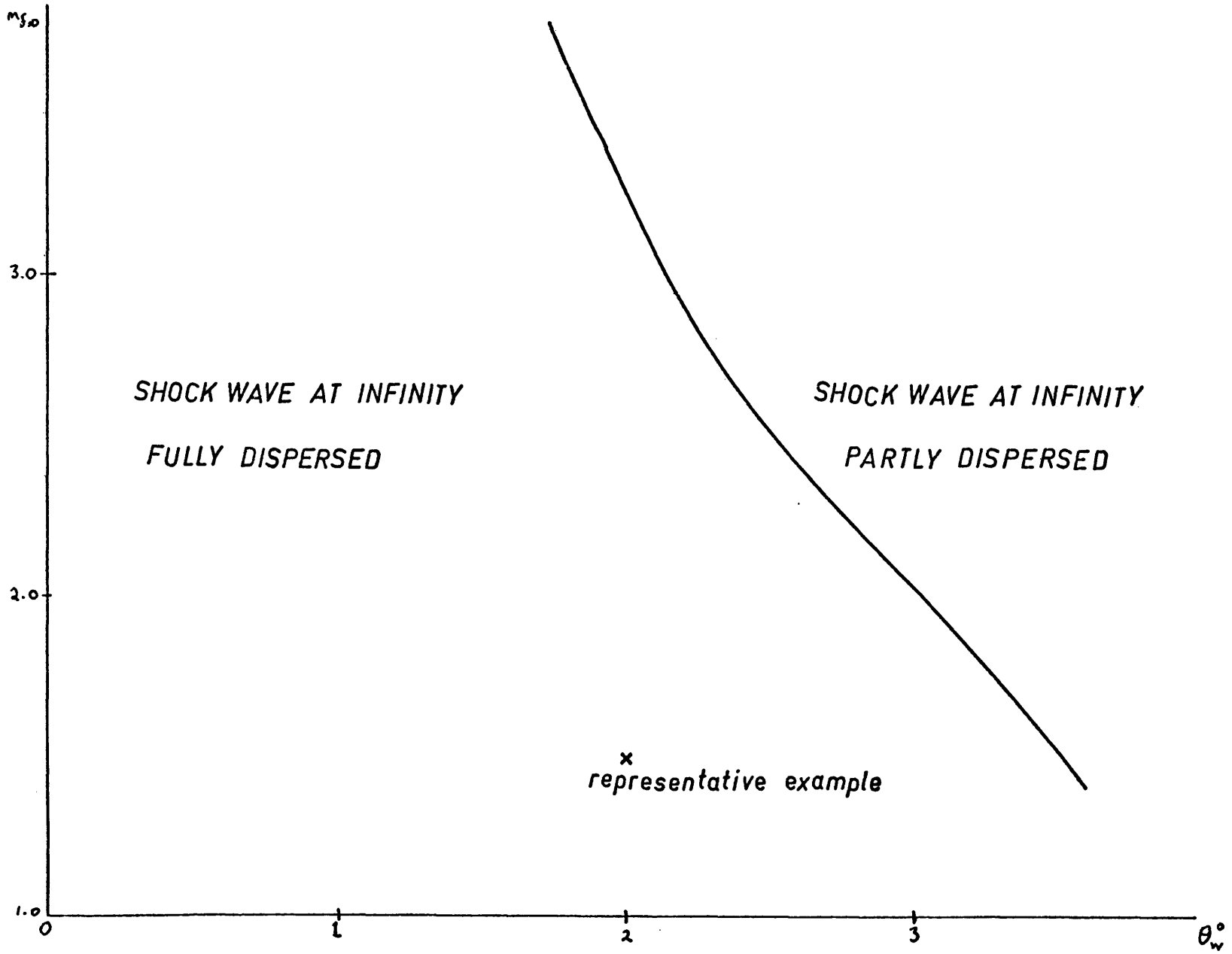

FIGURE 2(a). THE $M_{\infty} - \theta_w$ PLANE FOR $c_{v,b} = 2.12$.

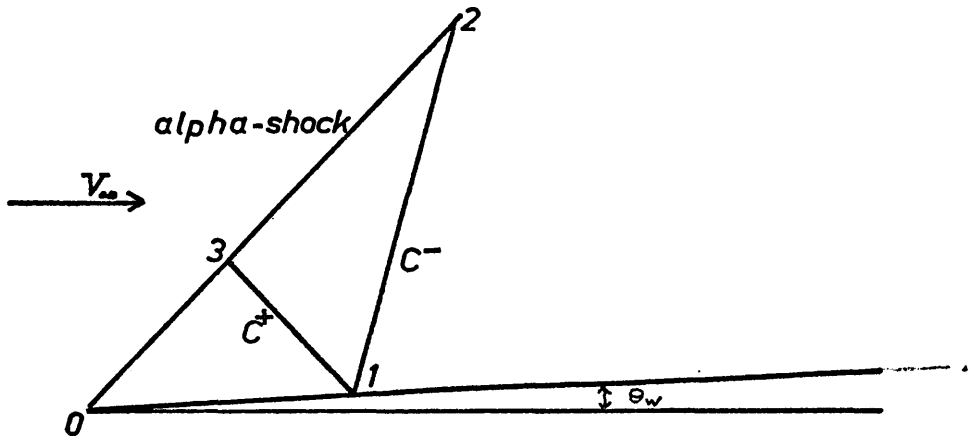

FIGURE 2(b) STARTING TRIANGLE

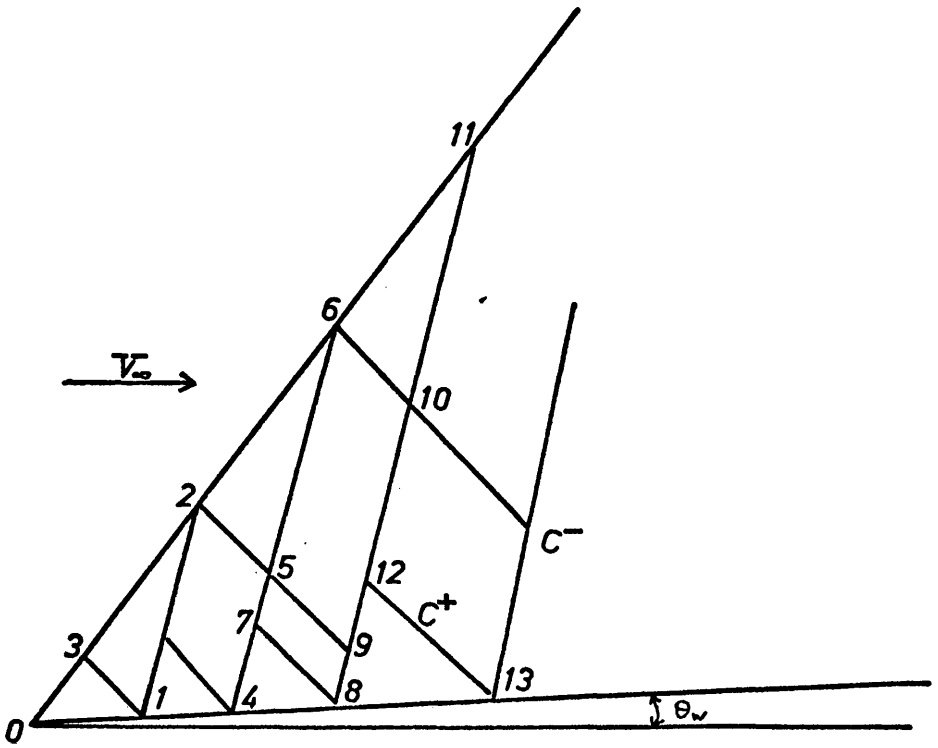

FIGURE 2(c) SCHEMATIC MESH
(points computed as numbered)

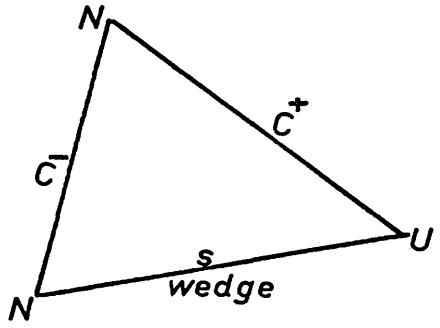

FIGURE 2(d) BODY POINT

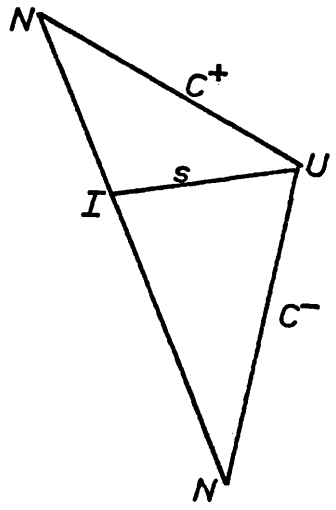

FIGURE 2(e) FIELD POINT

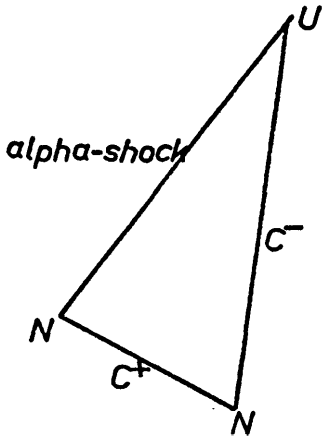

FIGURE 2(f) SHOCK POINT

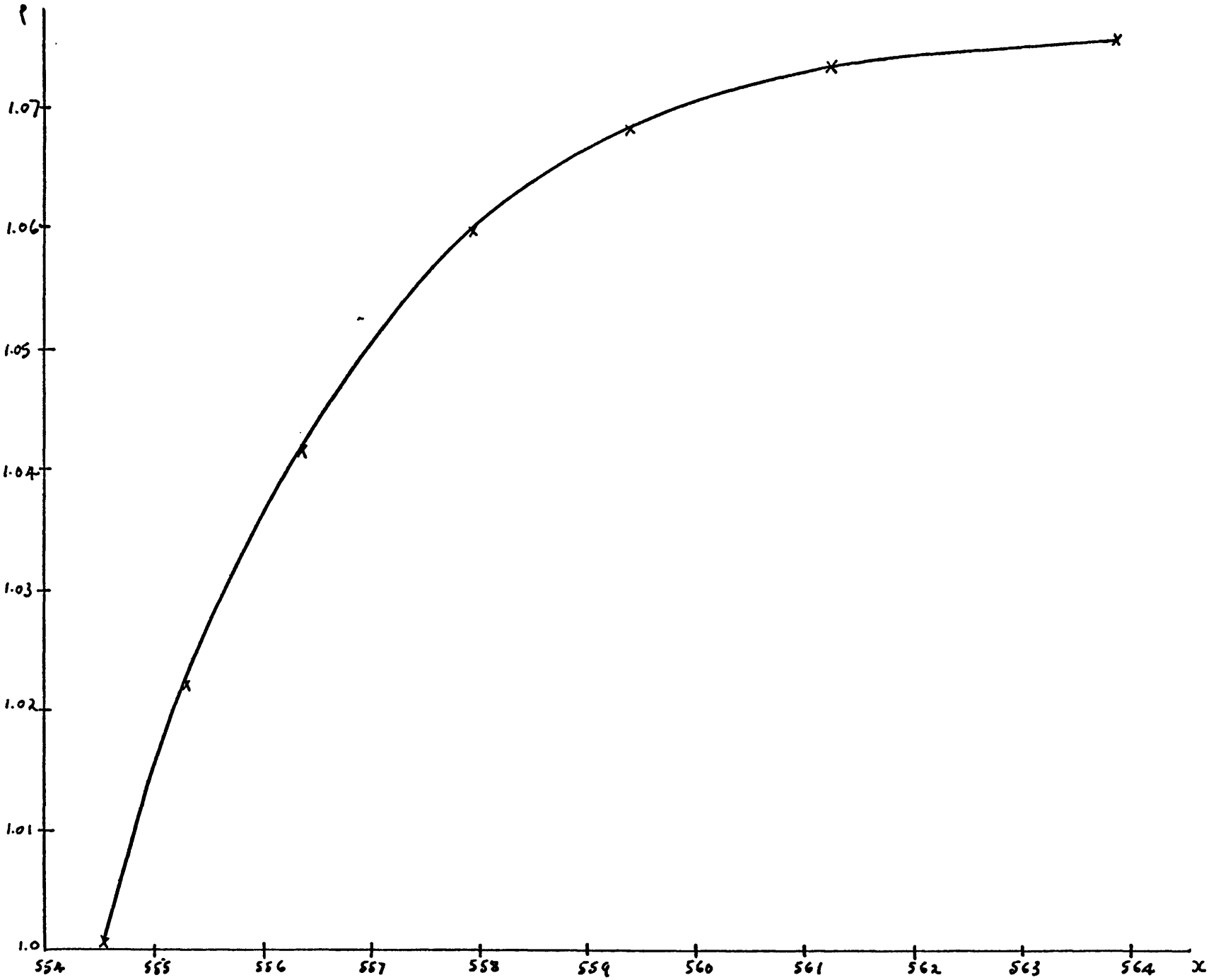

FIGURE 21g). COMPARISON OF THE CHARACTERISTICS SOLUTION WITH THE EXACT SOLUTION AT INFINITY. ($\theta_w = 1.47°$, $m_{\infty} = 2.6$ and $c_{v1b} = 1$). x, characteristics solution.

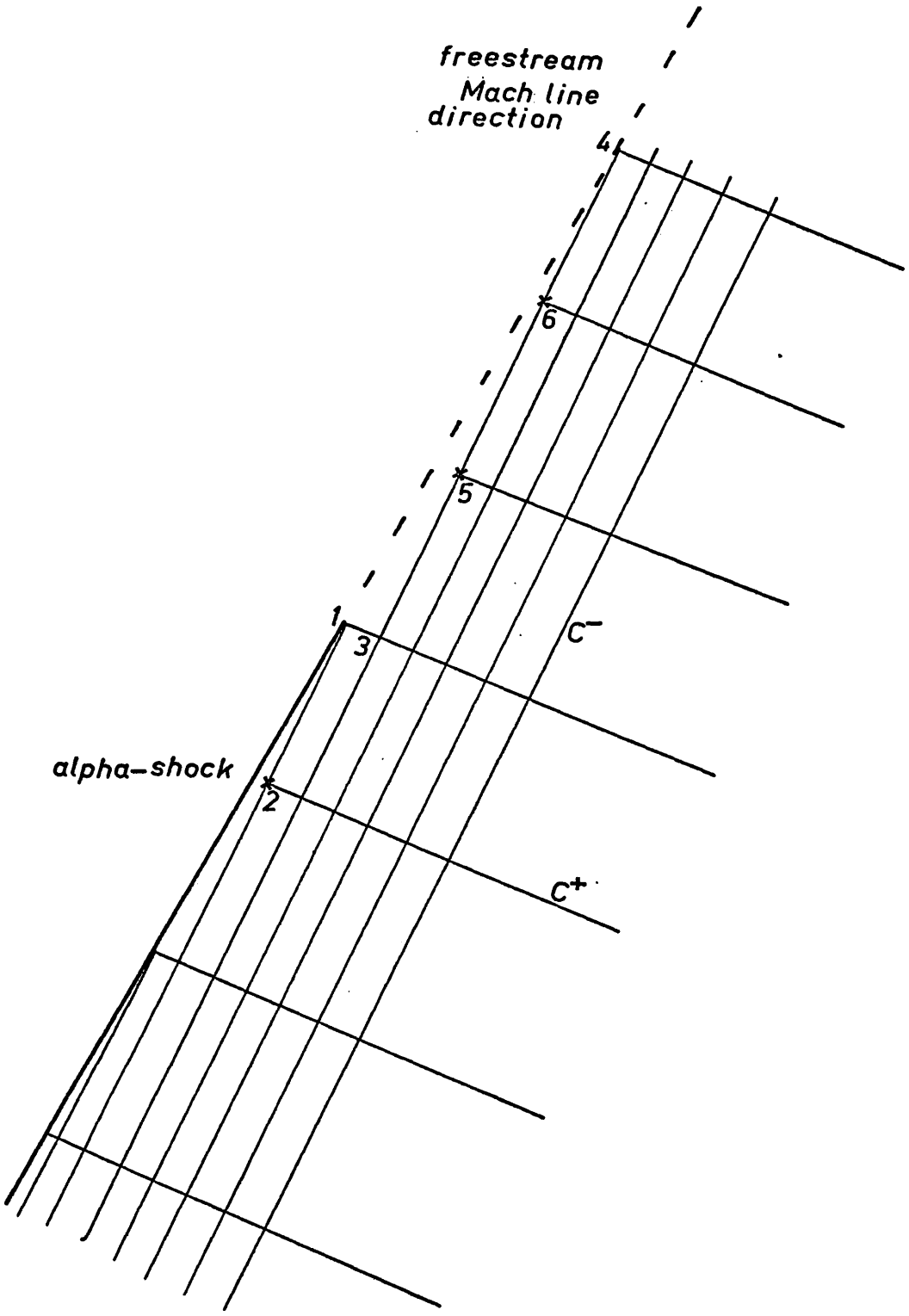

FIGURE 2(h) SHOCK MESH FOR VERY WEAK WAVE FLOWS

×, interpolated point

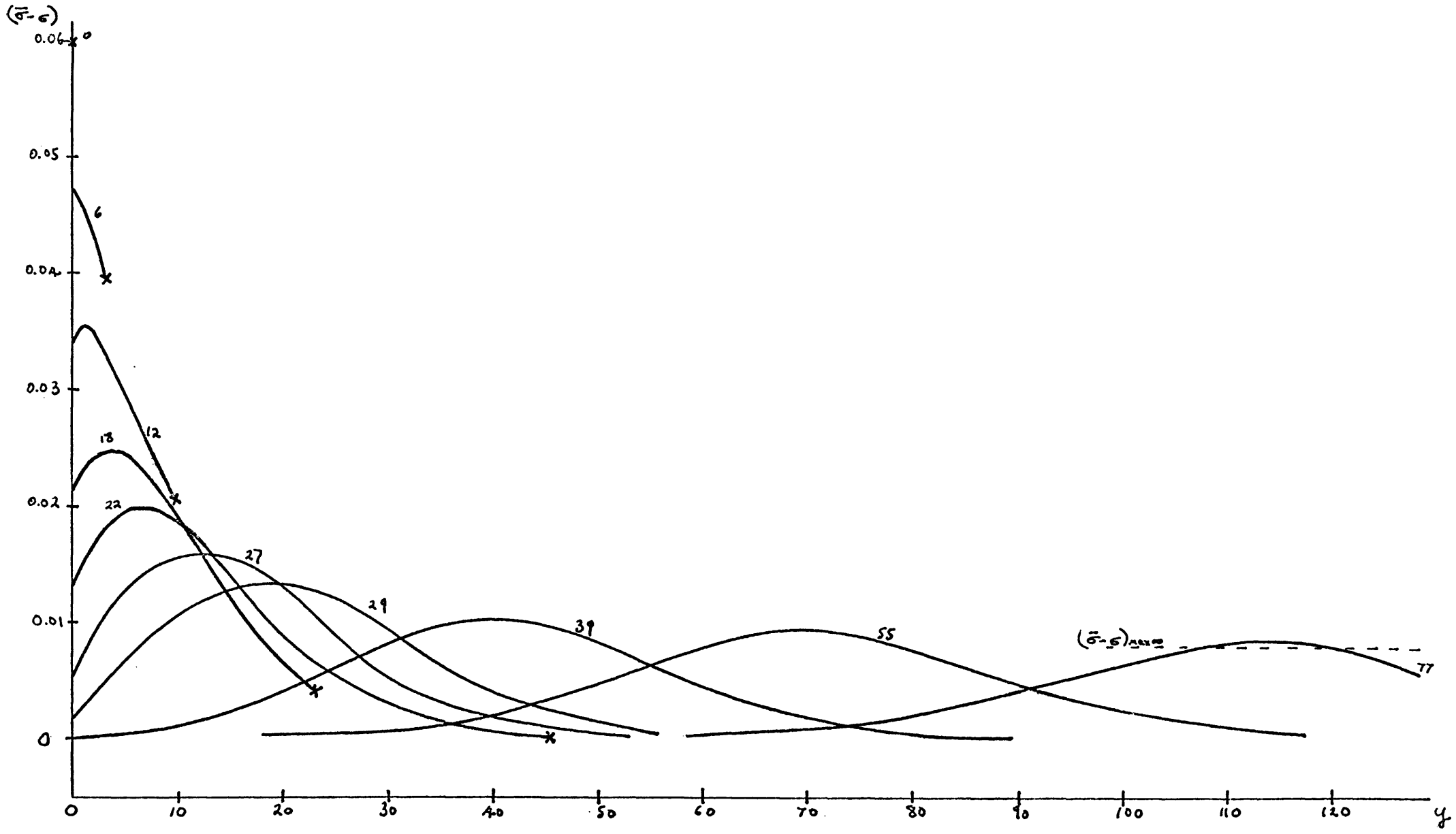

FIGURE 2(i). VARIATION OF THE DEPARTURE FROM LOCAL EQUILIBRIUM ON SUCCESSIVE C^- (numbered).
..., point on the alpha-shock.

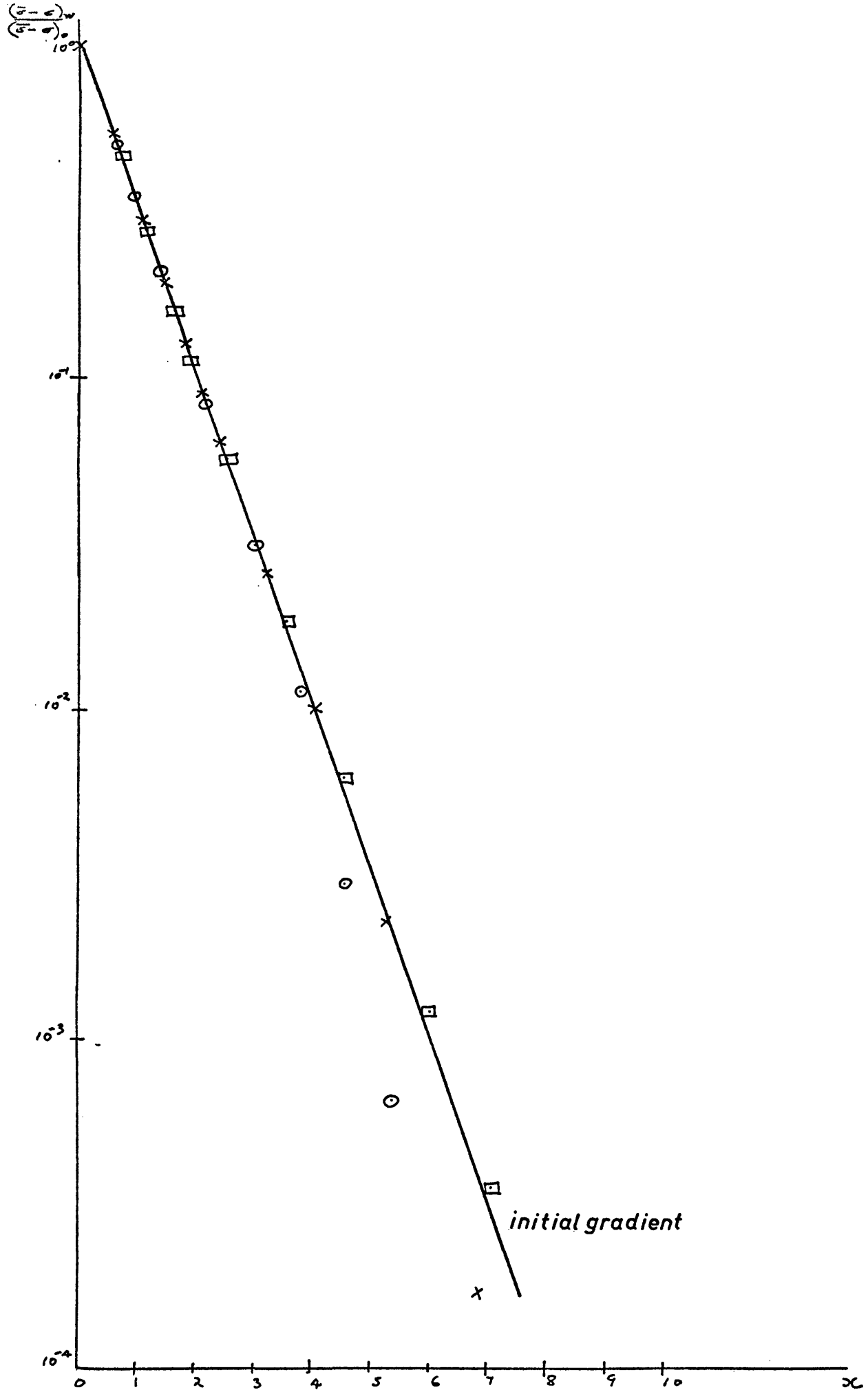

FIGURE 2(i). VARIATION OF THE DEPARTURE FROM LOCAL EQUILIBRIUM ON THE WEDGE SURFACE. ⊙, $^1/_{10}{}^{th}$ per step . x, $^1/_{50}{}^{th}$ per step . ⊡, $^1/_{250}{}^{th}$ per step.

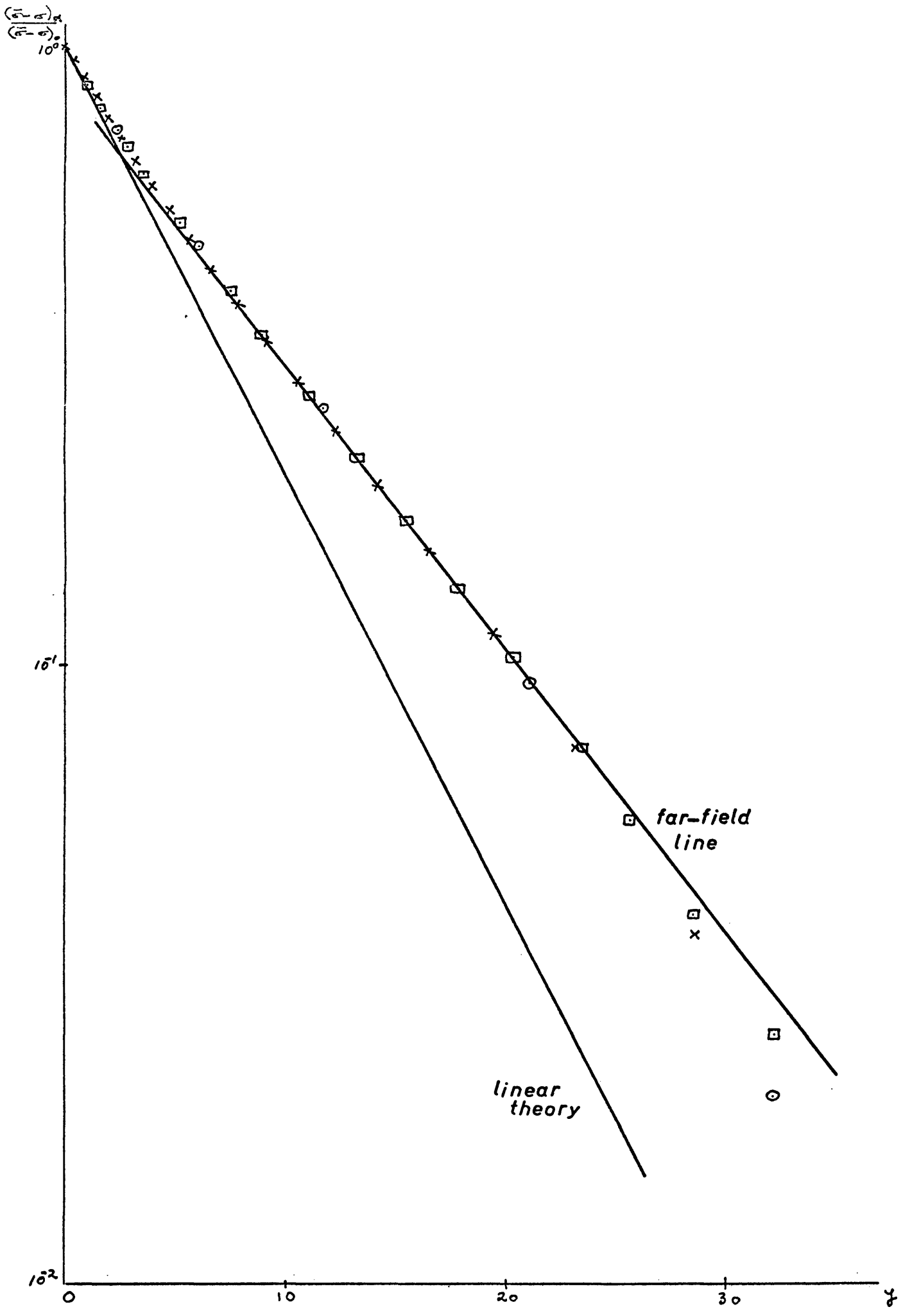

FIGURE 2(m). ALPHA-SHOCK DECAY.

⊙, $^{1}/_{10}^{th}$ per step. ×, $^{1}/_{50}^{th}$ per step. ⊡, $^{1}/_{250}^{th}$ per step.

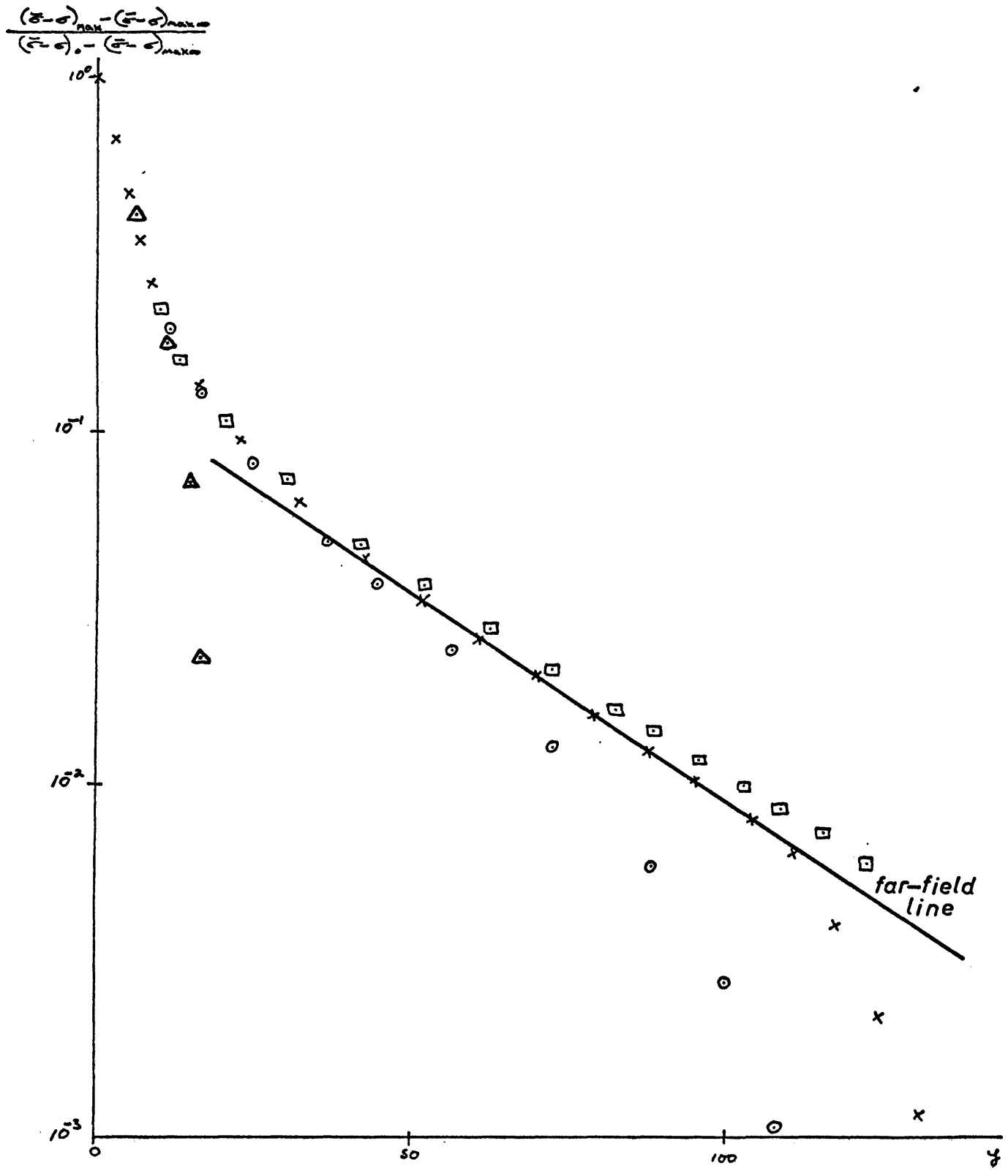

FIGURE 2(n). SHOCK WAVE DEVELOPMENT.

△, alpha-shock decay $(\bar{\sigma}-\sigma)_{max} = (\bar{\sigma}-\sigma)_\alpha$.

⊙, $1/10^{th}$ per step. ×, $1/50^{th}$ per step.

⊡, $1/250^{th}$ per step.

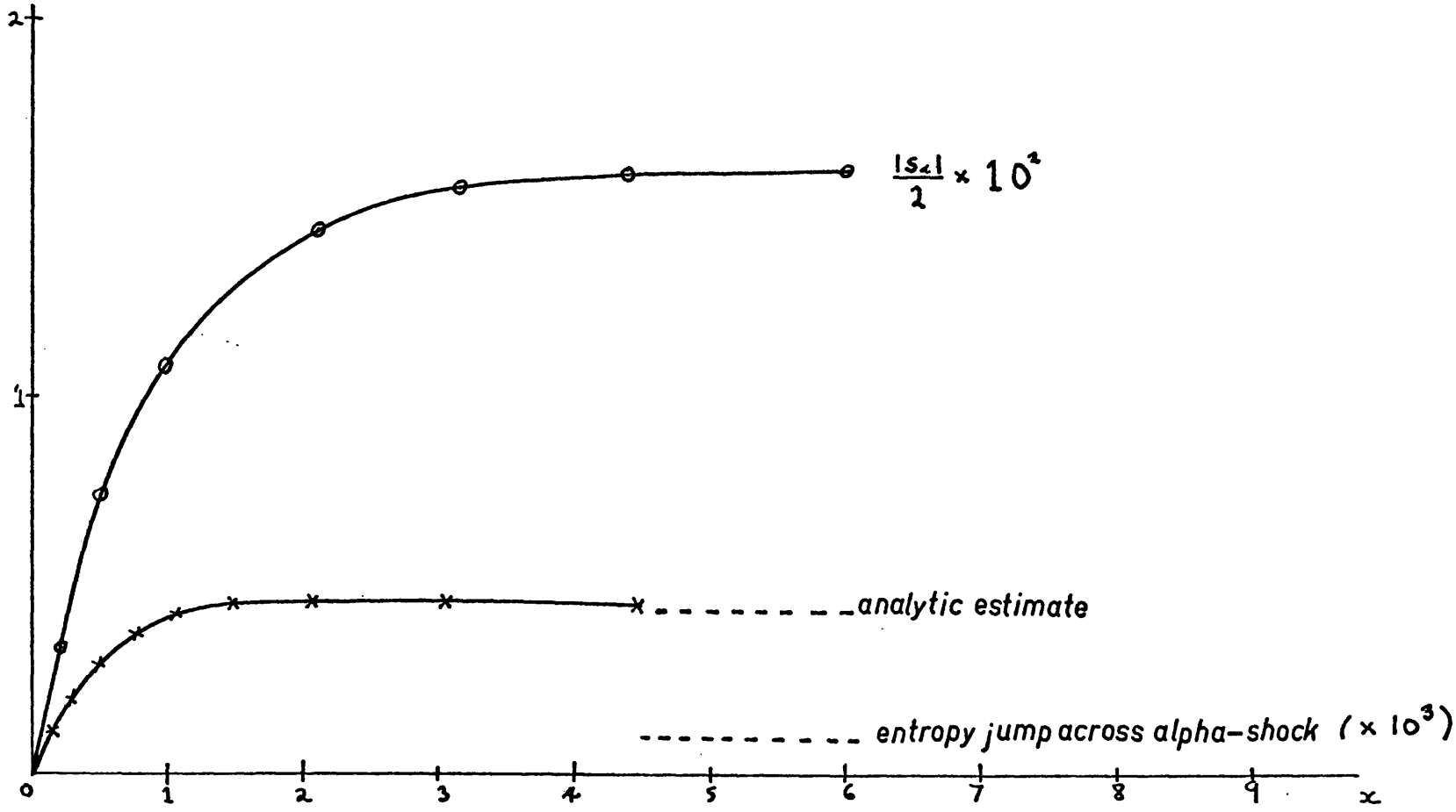

FIGURE 2(o). REAL GAS AND ALPHA-GAS ENTROPY VARIATIONS ON THE WEDGE SURFACE.
—x—, entropy production due to relaxation ($\times 10^3$).

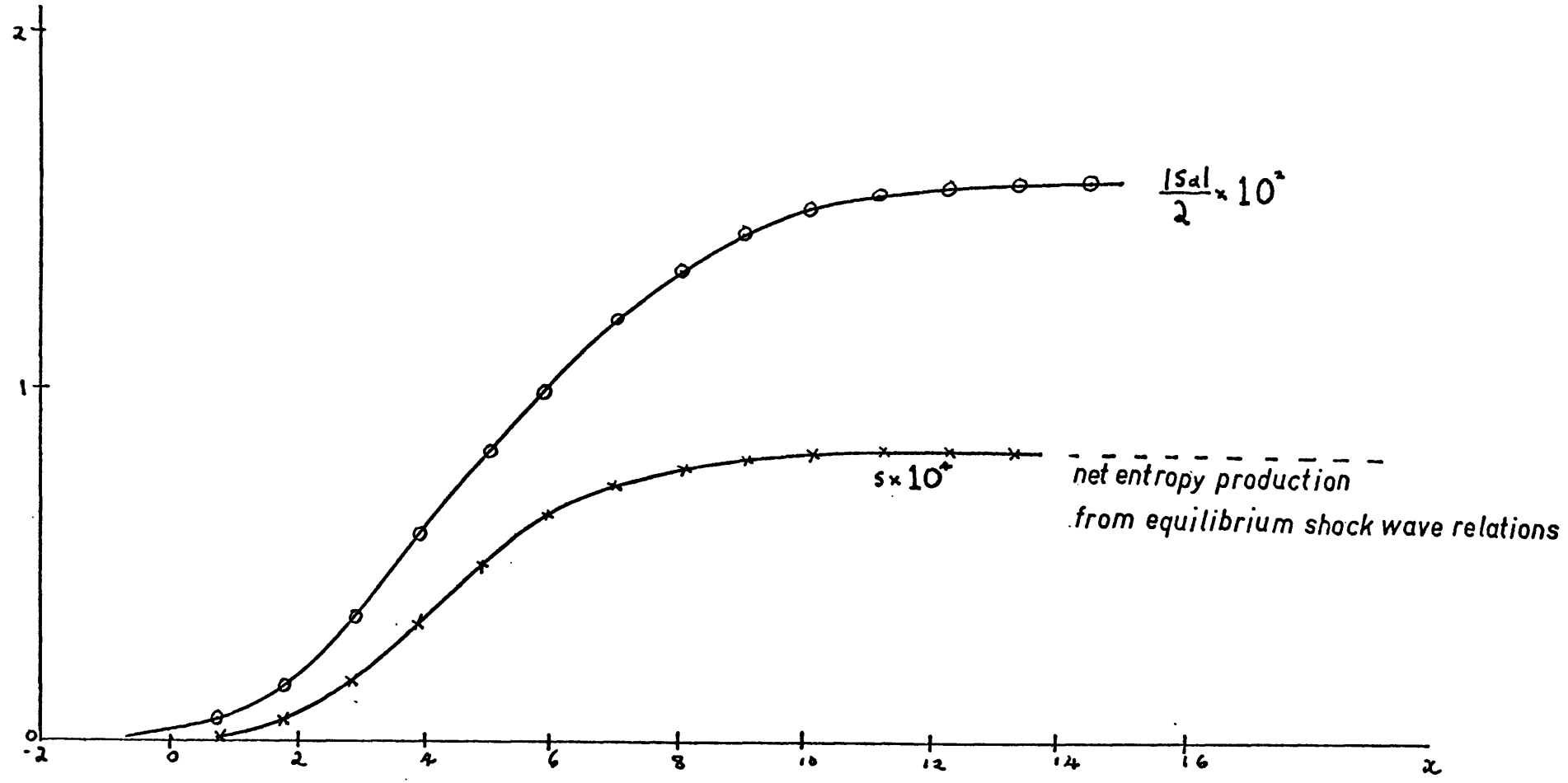

FIGURE 2(p). REAL GAS AND ALPHA-GAS ENTROPY VARIATIONS AT INFINITY.

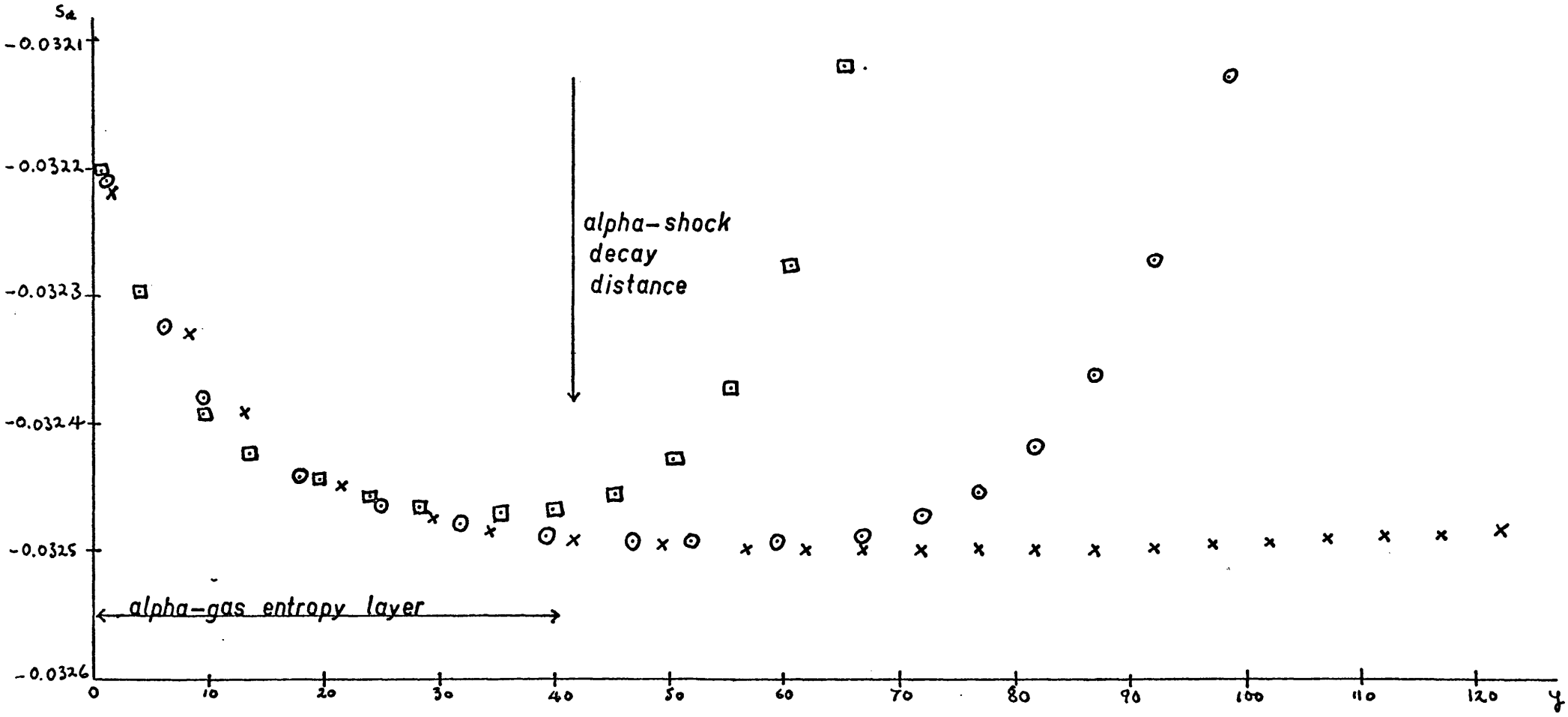

FIGURE 2(q). VARIATION OF THE ALPHA-GAS ENTROPY ON THE C^- EMANATING FAR DOWNSTREAM ON THE WEDGE SURFACE. ⊡, $80^{th}C^-$ from the wedge tip. ⊙, $90^{th}C^-$. ×, $110^{th}C^-$.

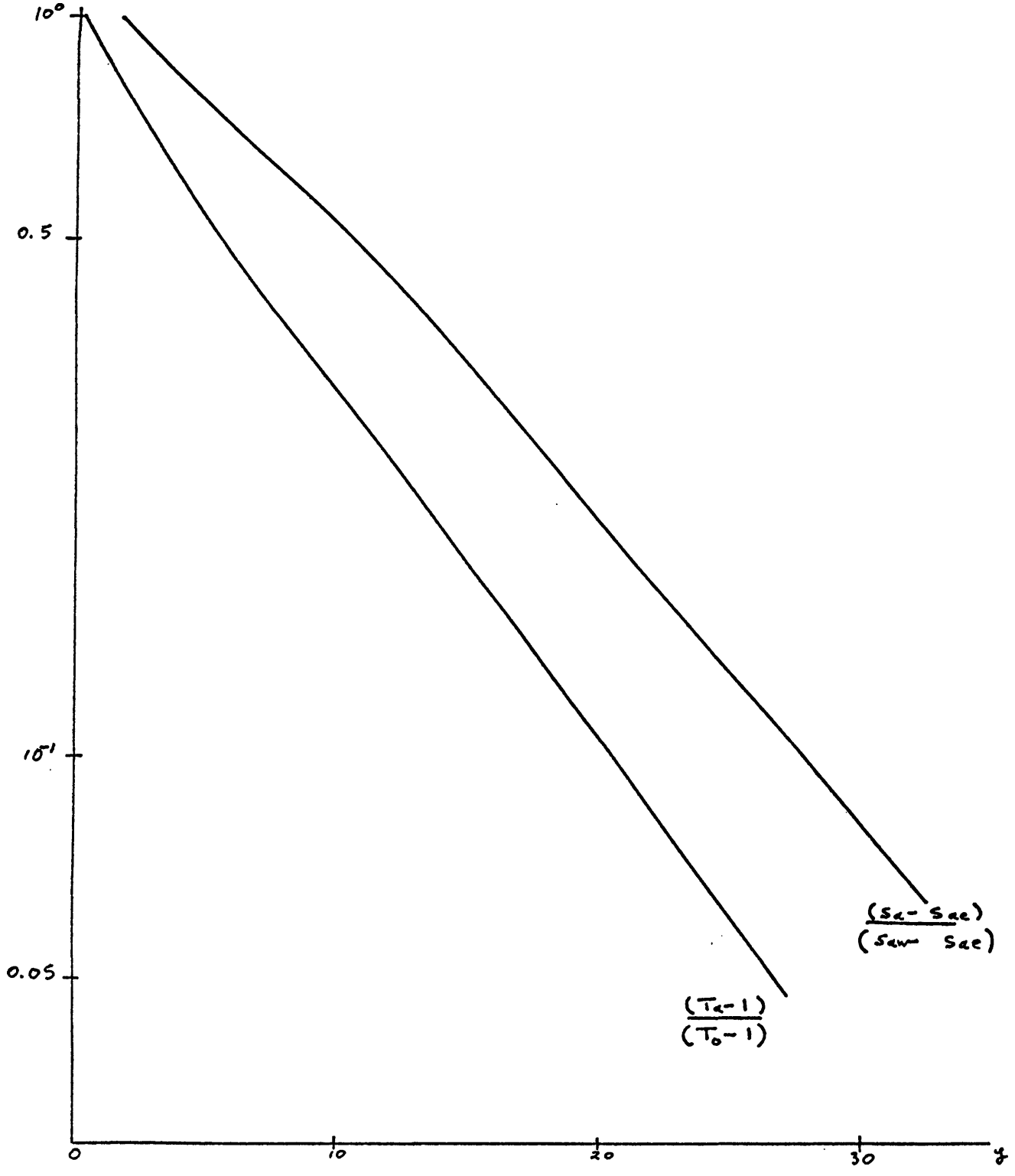

FIGURE 2(r). COMPARISON OF THE VARIATIONS ALONG THE ALPHA-SHOCK AND THROUGH THE ALPHA-GAS ENTROPY LAYER.

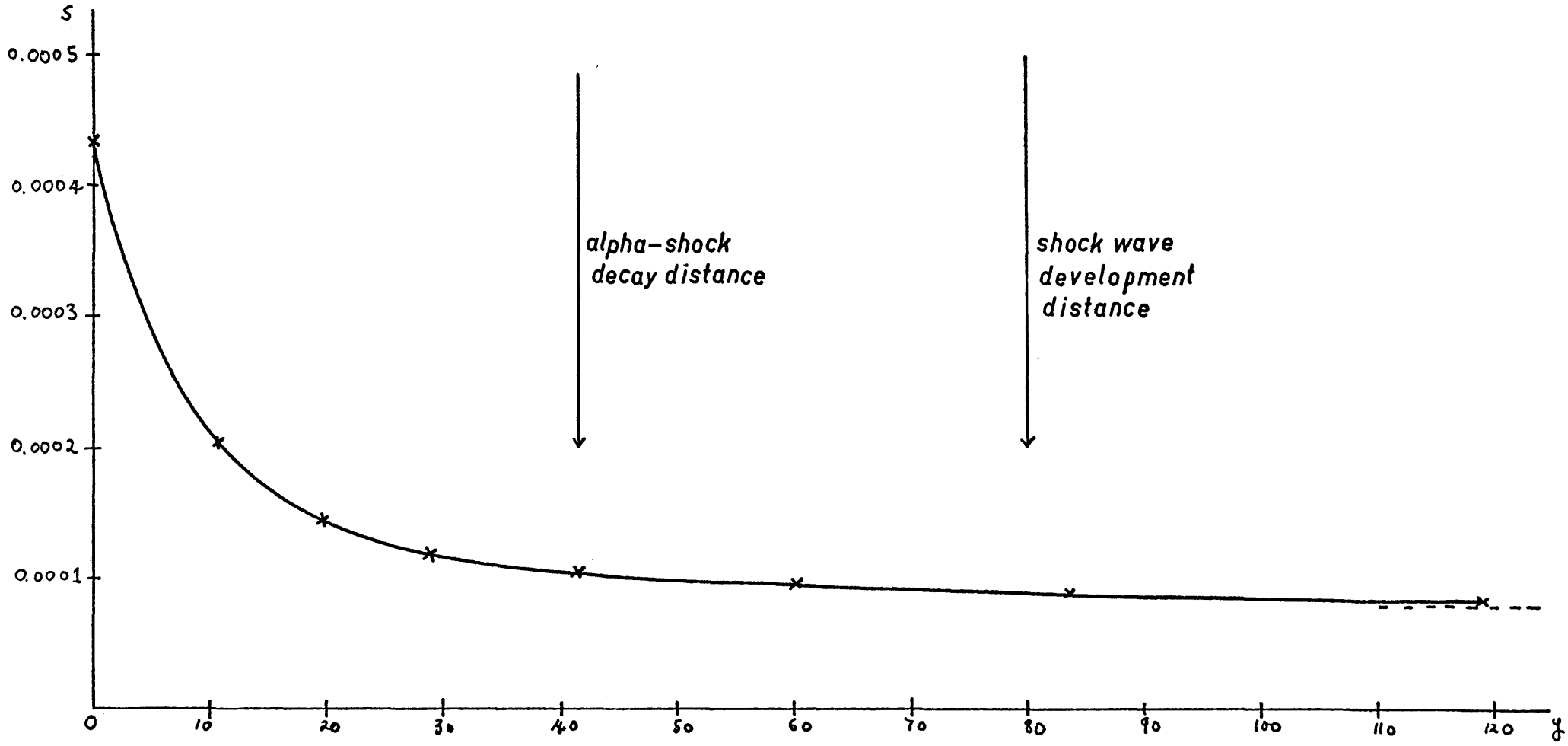

FIGURE 2(s). REAL GAS ENTROPY LAYER. - - - , entropy jump across shock wave at infinity.

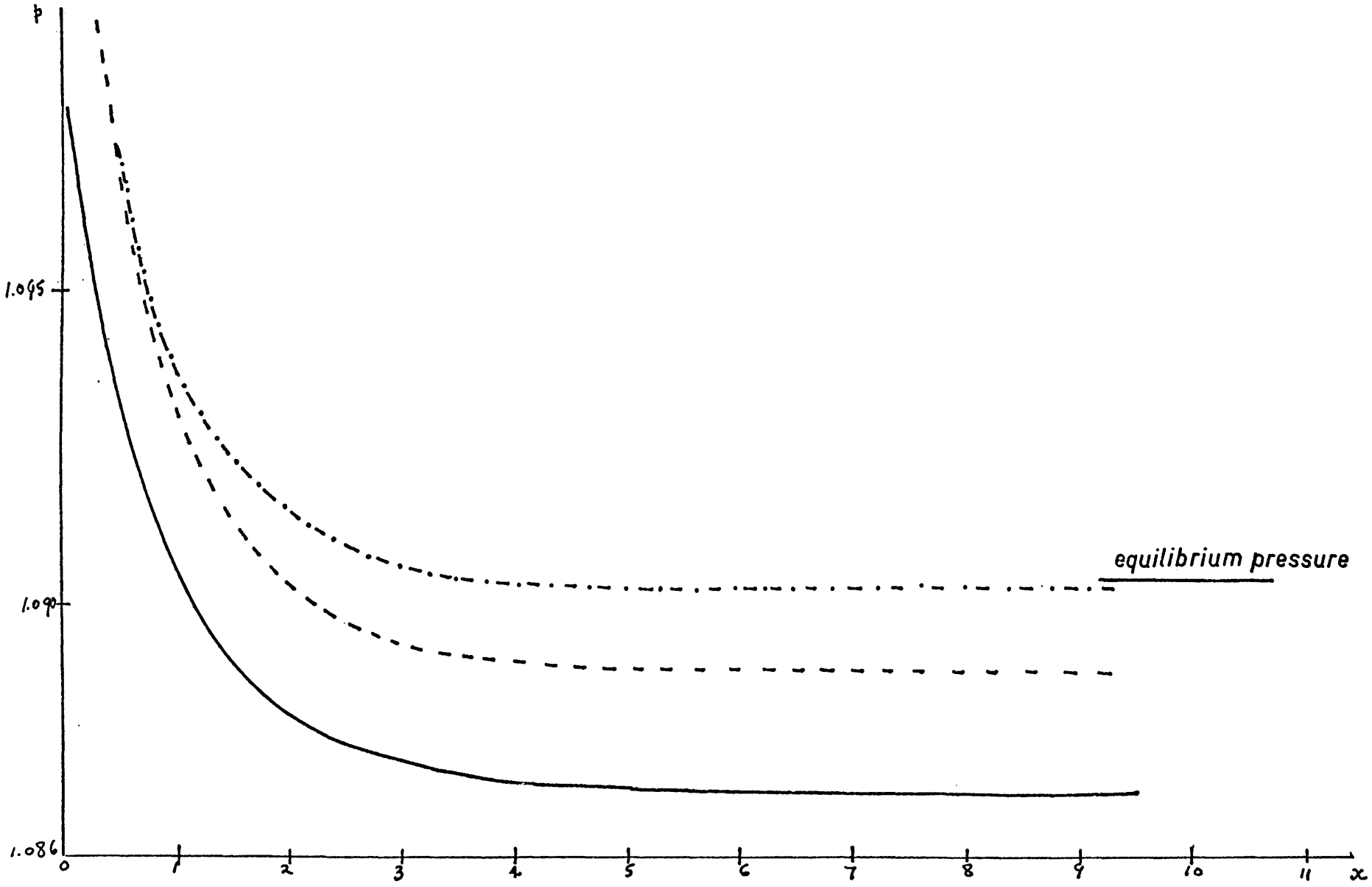

FIGURE 2(t). PRESSURE VARIATION ON THE WEDGE SURFACE. -·- , characteristics solution. - - , constant density solution. — , linear theory

CHAPTER 3

RESULTS FOR FLOWS WITH $c_{v,b} = 0.5, 1, 2$ AND 3 ; APPROXIMATE SIMILARITY REPRESENTATION.

INTRODUCTION

Chapter 3 presents all the results of the numerical computations. Specifically we are interested in the variations on the wedge surface, the alpha-shock decay and the shock wave development. Consequently, a section is devoted to the detailed representation of each of the above physical phenomena. The results are plotted, where possible, in concise similarity form by scaling with respect to critical quantities. For the alpha-shock variations we can employ the weak wave linear theory (see Chapter 5) to give alternative scalings. Section (4) assumes that the similarity exhibited in sections (1), (2) and (3) is exact and pursues the consequences. This leads to simple scaling laws for obtaining critical quantities of interest at any $M_{f\infty}$ or $C_{v,b}$.

SECTION (1)

Results for the variations along the wedge surface

A critical quantity (indicated by a * superscript) has been defined in section (4) of Chapter 1. In this Chapter these quantities will be employed as scaling factors which permit a concise representation of the numerical results in similarity form. The nature of the similarity will be discussed in section (4).

For all the computed flows, we have found that to a good approximation the variation of the departure from equilibrium along the wedge surface is exponential. We shall therefore write

$$(\bar{\sigma} - \sigma) = (\bar{\sigma} - \sigma)_{\circ}\, e^{-\frac{x}{\bar{x}_w}} \qquad 1.1$$

where $\bar{x}_w$ is the relaxation length on the wedge surface. An analytic expression for $\bar{x}_w$ can be obtained from the wedge tip gradients given

in section (4) of Chapter 2. That is

$$\bar{\kappa}_w^{-1} = -\frac{d \log(\bar{\sigma}-\sigma)_0}{d\alpha} = \frac{\rho_0}{V_0 \cos\theta_w}\left(1 + \frac{c_{vib}}{c_{pa}} + \frac{(\gamma_f-1)\left(\frac{c_{vib}}{c_{pa}}\right)}{\left(\cos^2\mu_0 + \rho_0 V_0^2 \cot(\phi_0-\theta_0)\sin^2\mu_0 \left(\frac{d\theta}{dp}\right)_0\right)}\right) \quad 1.2$$

We can explain the dependence on c_{vib} physically by realizing that if $c_{vib} << 1$ then it is essentially σ that relaxes (with very little change in $\bar{\sigma}$) but that for $c_{vib} >> 1$ the opposite is true. Since the alpha-gas entropy layer effects are small we can say that $\sigma \to \bar{\sigma}_e$ on the wedge surface as $\alpha \to \infty$. The small angle expansion for $(\bar{\sigma}-\sigma)_0$ is

$$(\bar{\sigma}-\sigma)_0 = c_{vib}(T_0-1)$$

$$= \frac{c_{vib}(\gamma_f-1)M_{f\infty}^2 \theta_w}{(M_{f\infty}^2-1)^{\frac{1}{2}}} + O(\theta_w^2)$$

Hence $$\frac{(\bar{\sigma}-\sigma)_0}{(\bar{\sigma}-\sigma)_0^*} = \left(\frac{\theta_w}{\theta_w^*}\right) + O\left(\theta_w \frac{\theta_w}{\theta_w^*}\right)$$

This form is plotted in fig. 3(a) and compared with exact results from the characteristics solution. We can therefore write

$$\frac{\bar{\sigma}_e - \sigma_0}{(\bar{\sigma}-\sigma)_0} \approx \frac{c_{vib}(\gamma_e-1)M_{e\infty}^2 (M_{f\infty}^2-1)^{\frac{1}{2}}}{c_{vib}(\gamma_f-1)M_{f\infty}^2 (M_{e\infty}^2-1)^{\frac{1}{2}}} \frac{\theta_w}{\theta_w}$$

$$\approx \frac{\gamma_f(\gamma_e-1)}{\gamma_e(\gamma_f-1)} \quad 1.3$$

The quantities $\bar{\sigma}_0 - \bar{\sigma}_e$ and $\bar{\sigma}_e - \sigma_0$ measure the amounts by which $\bar{\sigma}$ and σ respectively have relaxed. It is plausible to assume, therefore, that at any station on the wedge surface (excepting the tip) the ratio of the amounts by which $\bar{\sigma}$ and σ have relaxed is a constant determined by the

value the ratio takes as $x \to \infty$. That is

$$\frac{\bar{\sigma}_o - \bar{\sigma}}{\sigma - \sigma_o} = \frac{\bar{\sigma}_o - \bar{\sigma}_e}{\bar{\sigma}_e - \sigma_o} \approx \frac{(\gamma_f - \gamma_e)}{\gamma_f(\gamma_e - 1)}$$

Hence

$$d(\bar{\sigma} - \sigma) = -\left(1 + \frac{(\gamma_f - \gamma_e)}{\gamma_f(\gamma_e - 1)}\right) d\sigma$$

From the rate equation $d\sigma = \frac{\rho}{\bar{V}\cos\theta_w}(\bar{\sigma} - \sigma)\,dx$ so substituting above for $d\sigma$ gives

$$d(\bar{\sigma} - \sigma) = -\frac{\rho}{\bar{V}\cos\theta_w}\left(1 + \frac{(\gamma_f - \gamma_e)}{\gamma_f(\gamma_e - 1)}\right)(\bar{\sigma} - \sigma)\,dx$$

Assuming that to the approximations made $\rho = \rho_o$, $\bar{V} = \bar{V}_o$ and integrating we get

$$(\bar{\sigma} - \sigma) = (\bar{\sigma} - \sigma)_o\, e^{-\frac{\rho_o}{\bar{V}_o \cos\theta_w}\left(1 + \frac{\gamma_f - \gamma_e}{\gamma_f(\gamma_e - 1)}\right)x}$$

from which

$$\bar{x}_w^{-1} = \frac{\rho_o}{\bar{V}_o \cos\theta_w}\left(1 + \frac{c_{vib}}{c_{pa}}\right) \qquad 1.4$$

This is (as we shall see) a reasonable approximation to 1.2 since the term involving $(\gamma_f - 1)$ is small.

We can also show that $\bar{x}_w$ should have the form given by equation 1.4 by requiring 1.1 to be compatible with the rate equation. That is substituting 1.1 into the rate equation we get

$$d\sigma = \frac{\rho}{\bar{V}\cos\theta_w}(\bar{\sigma} - \sigma)_o\, e^{-\frac{x}{\bar{x}_w}}\,dx$$

Integrating (assuming $\rho = \rho_o$, $\bar{V} = \bar{V}_o$) gives

$$\sigma = -\frac{\rho_o(\bar{\sigma} - \sigma)_o\, \bar{x}_w\, e^{-\frac{x}{\bar{x}_w}}}{\bar{V}_o \cos\theta_w} + \text{constant}$$

when $x \to \infty$, $\sigma \to \bar{\sigma}_e$ so that

constant = $\bar{\sigma}_e$.

When $x = 0$, $\sigma = \sigma_0$. Hence

$$\bar{x}_w^{-1} = \frac{\rho_0(\bar{\sigma}-\sigma)_0}{\bar{V}_0 \cos\theta_w (\bar{\sigma}_e - \sigma_0)}$$

$$= \frac{\rho_0}{\bar{V}_0 \cos\theta_w}\left(1 + \frac{(\bar{\sigma}_0 - \bar{\sigma}_e)}{(\bar{\sigma}_e - \sigma_0)}\right)$$

$$= \frac{\rho_0}{\bar{V}_0 \cos\theta_w}\left(1 + \frac{c_{vib}}{c_{pa}}\right)$$

This also implies that σ relaxes in the same manner as $\bar{\sigma}-\sigma$ with the same relaxation length.

The exact expression for $\bar{x}_w$ given in 1.2 is plotted in figs.3(b) and 3(c) and shows excellent agreement with the characteristics results. The variations with the wedge angle are essentially due to the term containing $(\gamma_f - 1)$ in 1.2 and hence are absent in the above approximate derivations. We can simplify 1.2 by writing it as a power series in the wedge angle. That is we express all variables in power series of the wedge angle with the freestream as reference state, substitute into 1.2 and take successive approximations. This gives (for the first approximation)

$$\bar{x}_w^{-1} = \frac{1}{\bar{V}_\infty}\left(1 + \frac{c_{vib}}{c_{pa}} + \frac{(\gamma_f - 1)\left(\frac{c_{vib}}{c_{pa}}\right)}{\left(\cos^2\mu_\infty + \bar{V}_\infty^2 \cot\mu_\infty \sin^2\mu_\infty \left(\frac{d\theta}{d\rho}\right)_\infty\right)}\right)$$

This is the value predicted by linear theory (see Chapter 5, section (2)).

Since $\sin^2\mu_\infty = \frac{1}{M_{f\infty}^2}$, $\cos^2\mu_\infty = \frac{(M_{f\infty}^2 - 1)}{M_{f\infty}^2}$

and $\left(\frac{d\rho}{d\theta}\right)_\infty = \frac{\gamma_f M_{f\infty}^2}{(M_{f\infty}^2 - 1)^{\frac{1}{2}}}$

we get

$$\bar{x}_w^{-1} = \frac{1}{\gamma_f^{\frac{1}{2}} m_{f\infty}} \left(1 + \frac{c_{vib}}{c_{pa}} + \frac{(\gamma_f - 1) m_{f\infty}^2 \left(\frac{c_{vib}}{c_{pa}}\right)}{2(m_{f\infty}^2 - 1)} \right)$$

The critical value of this quantity is just its value at the critical Mach number. That is, (denoting the value of $\bar{x}_w$ predicted by linear theory with the additional suffix 1)

$$\frac{\bar{x}_{we}}{\bar{x}^*_{we}} = \frac{m_{f\infty}}{m^*_{f\infty}} \left(\frac{1 + \frac{c_{vib}}{c_{pa}} + \frac{(\gamma_f - 1) m_{f\infty}^2 \left(\frac{c_{vib}}{c_{pa}}\right)}{2(m^{*2}_{f\infty} - 1)}}{1 + \frac{c_{vib}}{c_{pa}} + \frac{(\gamma_f - 1) m_{f\infty}^2 \left(\frac{c_{vib}}{c_{pa}}\right)}{2(m_{f\infty}^2 - 1)}} \right)$$

$$= \frac{m_{f\infty}}{m^*_{f\infty}} \left(\frac{1 + \frac{(\gamma_f - 1) m^{*2}_{f\infty} \left(\frac{c_{vib}}{c_{pa}}\right)}{2\left(\frac{c_{vib}}{c_{pa}} + 1\right)(m^{*2}_{f\infty} - 1)}}{1 + \frac{(\gamma_f - 1) m_{f\infty}^2 \left(\frac{c_{vib}}{c_{pa}}\right)}{2\left(\frac{c_{vib}}{c_{pa}} + 1\right)(m_{f\infty}^2 - 1)}} \right).$$

The bracket multiplying $\frac{m_{f\infty}}{m^*_{f\infty}}$ is close to 1. For our calculations we can assess the deviation from 1 by choosing $c_{vib} = 1$, $m^*_{f\infty} = 1.4$ and $m_{f\infty} = 3.8$. We then have $\frac{\bar{x}_{we}}{\bar{x}^*_{we}} = 1.04 \left(\frac{m_{f\infty}}{m^*_{f\infty}} \right)$.

Hence approximately

$$\frac{\bar{x}_{we}}{\bar{x}^*_{we}} = \left(\frac{m_{f\infty}}{m^*_{f\infty}} \right)$$

The comparison between this rule and the characteristics is given in fig. 3(d). In particular we expect this rule to be most accurate for $m_{f\infty} \approx m^*_{f\infty} >> 1$ and $c_{vib} << 1$. This example illustrates a simple but approximate similarity when quantities are scaled with respect to their appropriate critical values. For the cases treated in the next

sections no general analytic expressions are as yet available and it is difficult to decide on the exact nature of the similarity. In particular, any deviations from the assumed similarity curve may be attributed to errors in the characteristic calculations.

To illustrate rather more clearly the dependence on θ_w, we expand the expression for $\bar{x}_w$ to first order in θ_w. We employ the small angle expansions

$$\rho_0 = 1 + \frac{m_{f\infty}^2}{(m_{f\infty}^2-1)^{\frac{1}{2}}}\theta_w + O(\theta_w^2)$$

$$\bar{V}_0 = \bar{V}_\infty - \frac{\bar{V}_\infty}{(m_{f\infty}^2-1)^{\frac{1}{2}}}\theta_w + O(\theta_w^2)$$

$$m_{f0}^2 = m_{f\infty}^2 - \frac{\left((\gamma_f-1)m_{f\infty}^2+2\right)m_{f\infty}^2}{(m_{f\infty}^2-1)^{\frac{1}{2}}}\theta_w + O(\theta_w^2)$$

$$\phi_0 = \mu_\infty + \frac{(\gamma_f+1)m_{f\infty}^2}{4(m_{f\infty}^2-1)}\theta_w + O(\theta_w^2)$$

$$p_0 = 1 + \frac{\gamma_f m_{f\infty}^2}{(m_{f\infty}^2-1)^{\frac{1}{2}}}\theta_w + \gamma_f m_{f\infty}^2\left(\frac{(\gamma_f+1)m_{f\infty}^4 - 4(m_{f\infty}^2-1)}{4(m_{f\infty}^2-1)^2}\right)\theta_w^2 + O(\theta_w^3)$$

(see Liepmann and Roshko (1967) p. 93 and p.389)

Substituting these expressions into 1.2, expanding and neglecting terms of order θ_w^2 gives

$$\bar{x}_w = \frac{\gamma_f^{\frac{1}{2}} m_{f\infty}\cos\theta_w}{\left(1+\frac{c_{vib}}{c_{pa}}+\frac{(\gamma_f-1)m_{f\infty}^2\left(\frac{c_{vib}}{c_{pa}}\right)}{2(m_{f\infty}^2-1)}\right)}\left(1-\theta_w\left(\frac{m_{f\infty}^2+1}{(m_{f\infty}^2-1)^{\frac{1}{2}}}+\frac{(\gamma_f-1)m_{f\infty}^4\left(m_{f\infty}^4(\gamma_f-1)-\frac{m_{f\infty}^2}{4}(9\gamma_f-7)-2\right)}{2(m_{f\infty}^2-1)^{\frac{3}{2}}\left(2\left(\frac{c_{vib}}{c_{pa}}+1\right)(m_{f\infty}^2-1)+\frac{c_{vib}}{c_{pa}}(\gamma_f-1)m_{f\infty}^2\right)}\right)\right)$$

Hence $\bar{x}_w$ decreases with increasing θ_w. Reference to fig. 3(c) shows that this expression is sufficient to account for the variation of relaxation distance with wedge angle.

SECTION 2

Results for the alpha-shock decay

A logarithmic plot of the variations along the alpha-shock has been given in section (2) of the last chapter. It was explained there that we could fix the initial and far-field decay rate lines on the graph simply by knowing their gradients and the intercept of the far-field line on the line y = 0. In this section we shall be concerned with plotting these 3 quantities and in particular we shall illustrate the essential non-linear features by comparison with the linear theory (see Chapter 5) for the weak alpha-shock decay. This theory predicts a single decay rate given by

$$\bar{y}_{ae}^{-1} = \frac{(\gamma_f - 1)}{2\gamma_f^{\frac{1}{2}}} \frac{c_{vib}}{c_{pa}} \frac{m_{f\infty}}{(m_{f\infty}^2 - 1)^{\frac{1}{2}}}$$

where $\bar{y}_{ae}$ represents the linear decay distance.

We shall represent the initial and far-field line gradients in terms of decay distances represented by $\bar{y}_{a0}$ and $\bar{y}_a$ respectively. The intercept of the far-field line on the line y = 0 we shall denote by the symbol b_a. With this notation the equations to the initial and far-field lines are

$$\frac{(\bar{\sigma} - \sigma)}{(\bar{\sigma} - \sigma)_0} = e^{-\frac{y}{\bar{y}_{a0}}}$$

and $$\frac{(\bar{\sigma} - \sigma)}{(\bar{\sigma} - \sigma)_0} = e^{-\left(\frac{y}{\bar{y}_a} - b_a\right)}$$ respectively for fully dispersed shocks at infinity and

$$\frac{(\bar{\sigma} - \sigma) - (\bar{\sigma} - \sigma)_{a\infty}}{(\bar{\sigma} - \sigma)_0 - (\bar{\sigma} - \sigma)_{a\infty}} = e^{-\frac{y}{\bar{y}_{a0}}}$$

and $$\frac{(\bar{\sigma} - \sigma) - (\bar{\sigma} - \sigma)_{a\infty}}{(\bar{\sigma} - \sigma)_0 - (\bar{\sigma} - \sigma)_{a\infty}} = e^{-\left(\frac{y}{\bar{y}_a} - b_a\right)}$$

for partly dispersed shocks at infinity.

The variation of the far-field decay distances with respect to the parameters θ_w, $M_{f\infty}$ and c_{vib} are illustrated in figs.3(e) and 3(f). Fig. 3(e) indicates how $\bar{y}_d$ varies with θ_w and c_{vib}. The decay distance decreases as c_{vib} increases. The linear decay distances (which are independent of θ_w) are plotted on the same graph and are good approximations only for $\frac{\theta_w}{\theta_w^*} << 1$. The non-linear effects are clearly exhibited in the sharp rise of the curves to a maximum when $\theta_w = \theta_w^*$. In fig. 3(f) the variation with θ_w and $M_{f\infty}$ is shown. The curves are very much similar in shape with the maximum corresponding always to critical conditions. The Mach number dependence for large Mach numbers is weak; the linear theory predicts the same effect, essentially due to functional relationships like $\frac{M_{f\infty}}{(M_{f\infty}^2-1)^{\frac{1}{2}}}$

It is clear that if an exact similarity scaling with respect to the critical values exists then in particular it must scale the linear results which represent the limits to the curves as $\frac{\theta_w}{\theta_w^*} \to 0$. This means, of course, that we can just scale quantities on the linear results and get an equivalent similarity representation. This procedure is preferable because the linear scalings are known exactly. Indeed fig.3(j) indicates that there is considerable scatter in the critical values. This scatter is partly accounted for by inaccuracies in the characteristics results. More accurate calculations with $^1/250$th of the variation of σ per step (for the $c_{vib} = 3$ flows) indicate that the decay distances increase above the values calculated with $^1/50$th of the variation of σ per step. The results are still scattered, however, but this could be due to the calculations still not being sufficiently accurate or possibly due to the calculations not having progressed far enough (because of computer time restrictions). We must emphasise, however, that these inaccuracies are only present for the computed flows with $\theta_w = \theta_w^*$. All other calculations are adequately represented with the larger step size.

Fig. 3(g) shows the quantities b_a plotted against $\frac{\theta_w}{\theta_w^*}$. In both figs. 3(g) and 3(j) the similarity representation is good except for $\theta_w = \theta_w^*$. In fig. 3(g) more accurate calculations indicate that the scatter is due, in part, to errors in the characteristics results. Notice that it is not necessary to scale the quantity b_a because all results tend to 0 as $\frac{\theta_w}{\theta_w^*} \to 0$. The linear scalings are represented in fig. 3(h).

We shall investigate the initial decay distances ($\bar{y}_{a0}$) by use of the wedge tip gradients. Linear theory predicts no θ_w dependence and so in fig. 3(i) would give the line $\frac{\bar{y}_{a0}}{\bar{y}_{a0}^*} = 1$. We can see, however, that there is quite a marked variation both with θ_w and c_{w_b}, especially for the frozen Mach number of 1.4. The appropriate wedge tip gradient has already been derived in section (4) of Chapter 2. Confining our attention (for the moment) to fully dispersed wave flows at infinity we have

$$\frac{1}{\bar{y}_{a0}} = -\frac{1}{(\bar{\sigma}-\sigma)_0}\left(\frac{d(\bar{\sigma}-\sigma)}{dy}\right)_0$$

$$= -\frac{c_{w_b}}{c_{p_a}}\left(\frac{\rho_0^3 \bar{V}_0}{p_0 - \frac{\rho_0 \bar{V}_0^2}{\gamma_f} - \frac{p_0 \rho_0 \bar{V}_0^2 \cot(\phi_0-\theta_0)}{\left(\frac{dp}{d\theta}\right)}}\right)\left(\frac{dT}{d\theta}\right)\left(\frac{dp}{d\theta}\right)\frac{\cos(\phi_0-\theta_0)}{\sin\phi_0}$$

$$= -\frac{c_{w_b}}{c_{p_a}}\left(\frac{\rho_0^3 \bar{V}_0}{p_0 \frac{dp}{d\theta} - \frac{\rho_0 \bar{V}_0^2}{\gamma_f}\frac{dp}{d\theta} - p_0 \rho_0 \bar{V}_0^2 \cot(\phi_0-\theta_0)}\right)\frac{dT}{d\theta}\frac{\cos(\phi_0-\theta_0)}{\sin\phi_0}$$

If we expand this expression as a power series in the wedge angle then we expect to recover the linear decay rate in the first approximation. The first approximation is

$$\frac{1}{\bar{y}_{a0}} = -\frac{c_{w_b}}{c_{p_a}}\left(\frac{\bar{V}_\infty}{\frac{\gamma_f m_{f\infty}^2}{(m_{f\infty}^2-1)^{\frac{1}{2}}} - \frac{\gamma_f m_{f\infty}^4}{(m_{f\infty}^2-1)^{\frac{1}{2}}} - \gamma_f m_{f\infty}^2 (m_{f\infty}^2-1)^{\frac{1}{2}}}\right)(\gamma_f - 1) m_{f\infty}^2$$

$$= -\frac{c_{vib}}{c_{pa}} \bar{V}_\infty (\gamma_f - 1) m_{f\infty}^2 \left(\frac{(m_{f\infty}^2 - 1)^{\frac{1}{2}}}{2\gamma_f m_{f\infty}^2 (1 - m_{f\infty}^2)} \right)$$

$$= \frac{c_{vib}}{c_{pa}} \frac{(\gamma_f - 1)}{2\gamma_f^{\frac{1}{2}}} \frac{m_{f\infty}}{(m_{f\infty}^2 - 1)^{\frac{1}{2}}}$$

From fig. 3(i) we see that the initial decay distances vary linearly with θ_w. It is therefore sufficient to expand $\bar{J}_{a0}^{-1}$ to $O(\theta_w)$. The small angle expansions that we shall need are,

$$\rho_0 = 1 + \frac{m_{f\infty}^2}{(m_{f\infty}^2 - 1)^{\frac{1}{2}}} \theta_w + O(\theta_w^2)$$

$$\bar{V}_0 = \bar{V}_\infty - \frac{\bar{V}_\infty \theta_w}{(m_{f\infty}^2 - 1)^{\frac{1}{2}}} + O(\theta_w^2)$$

$$\phi_0 = \mu_\infty + \frac{(\gamma_f + 1) m_{f\infty}^2 \theta_w}{4(m_{f\infty}^2 - 1)} + O(\theta_w^2)$$

$$p_0 = 1 + \frac{\gamma_f m_{f\infty}^2}{(m_{f\infty}^2 - 1)^{\frac{1}{2}}} \theta_w + \gamma_f m_{f\infty}^2 \left(\frac{(\gamma_f + 1) m_{f\infty}^4 - 4(m_{f\infty}^2 - 1)}{4(m_{f\infty}^2 - 1)^2} \right) \theta_w^2 + O(\theta_w^3)$$

$$\bar{T}_0 = 1 + \frac{(\gamma_f - 1) m_{f\infty}^2 \theta_w}{(m_{f\infty}^2 - 1)^{\frac{1}{2}}} + \left(\frac{(\gamma_f - 1)}{2} m_{f\infty}^2 \left(\frac{(\gamma_f + 1) m_{f\infty}^4 - 4(m_{f\infty}^2 - 1)}{2(m_{f\infty}^2 - 1)^2} \right) - \frac{m_{f\infty}^4 (\gamma_f - 1)}{2(m_{f\infty}^2 - 1)} \right) \theta_w^2 + O(\theta_w^3)$$

The coefficient of θ_w can be found from $\left(\frac{d}{d\theta} \left(\frac{1}{\bar{J}_{a0}} \right) \right)_{\theta_w = 0}$. Carrying out the necessary algebraic manipulations finally gives

$$\bar{J}_{a0}^{-1} = \frac{c_{vib}}{c_{pa}} \frac{(\gamma_f - 1) m_{f\infty}}{2\gamma_f^{\frac{1}{2}} (m_{f\infty}^2 - 1)^{\frac{1}{2}}} \left(1 + \frac{m_{f\infty}^2}{(m_{f\infty}^2 - 1)^{3/2}} \left(\frac{m_{f\infty}^2}{8} (5 - 3\gamma_f) + \gamma_f \right) \theta_w \right)$$

or

$$\bar{J}_{a0} = \frac{2 c_{pa} \gamma_f^{\frac{1}{2}} (m_{f\infty}^2 - 1)^{\frac{1}{2}}}{c_{vib} (\gamma_f - 1) m_{f\infty}} \left(1 - \frac{m_{f\infty}^2}{(m_{f\infty}^2 - 1)^{3/2}} \left(\frac{m_{f\infty}^2}{8} (5 - 3\gamma_f) + \gamma_f \right) \theta_w \right)$$

We can see from this that there is no possibility of the critical scaling being a similarity scaling if the θ_w term is not negligible. This is quite clearly the case when

the frozen Mach number is 1.4 and θ_w^* comparatively large (notice that θ_w^* does have a maximum near $m_{f\infty} = 1.4$). In scaled form

$$\frac{\bar{y}_{a0}}{\bar{y}_{a0}^*} = \frac{1 - \frac{\bar{m}_{f\infty}^2}{(\bar{m}_{f\infty}^2-1)^{3/2}}\left(\frac{\bar{m}_{f\infty}^2}{8}(5-3\gamma_f)+\gamma_f\right)\left(\frac{\theta_w}{\theta_w^*}\right)\theta_w^*}{1 - \frac{\bar{m}_{f\infty}^2}{(\bar{m}_{f\infty}^2-1)^{3/2}}\left(\frac{\bar{m}_{f\infty}^2}{8}(5-3\gamma_f)+\gamma_f\right)\theta_w^*}$$

The gradient of the line with $\frac{\theta_w}{\theta_w^*}$ as independent variable is

$$\frac{-\frac{\bar{m}_{f\infty}^2}{(\bar{m}_{f\infty}^2-1)^{3/2}}\left(\frac{\bar{m}_{f\infty}^2}{8}(5-3\gamma_f)+\gamma_f\right)\theta_w^*}{1 - \frac{\bar{m}_{f\infty}^2}{(\bar{m}_{f\infty}^2-1)^{3/2}}\left(\frac{\bar{m}_{f\infty}^2}{8}(5-3\gamma_f)+\gamma_f\right)\theta_w^*}$$

For $m_{f\infty} = 1.4$, $c_{vib} = 3$ and $\theta_w^* = 4.4^\circ$ the gradient is then $-0.34(6)$ and compares favourably with the characteristics results plotted in fig. 3(i).

For partly dispersed shock wave flows at infinity the initial decay distance is given by

$$\bar{y}_{a0}^{-1} = -\frac{1}{(\bar{\sigma}-\sigma)_0 - (\bar{\sigma}-\sigma)_{a\infty}}\left(\frac{d(\bar{\sigma}-\sigma)}{dy}\right)_0$$

Hence

$$\frac{\text{Initial decay distance for partly dispersed wave}}{\text{Initial decay distance for fully dispersed wave}} = \frac{(\bar{\sigma}-\sigma)_0 - (\bar{\sigma}-\sigma)_{a\infty}}{(\bar{\sigma}-\sigma)_0}$$

We shall now expand this quantity in terms of θ_w. We have already shown that (section (1))

$$(\bar{\sigma}-\sigma)_0 = \frac{c_{vib}(\gamma_f-1)\bar{m}_{f\infty}^2\theta_w}{(\bar{m}_{f\infty}^2-1)^{\frac{1}{2}}} + O(\theta_w^2)$$

The temperature ratio across the alpha-shock at infinity is

$$T_{a\infty} = 1 + \frac{2(\gamma_f-1)(m^2_{fn\infty}-1)(\gamma_f m^2_{fn\infty}-1)}{(\gamma_f+1)^2 m^2_{fn\infty}}$$

The normal frozen Mach number at infinity can be expanded as

$$m^2_{fn\infty} = \frac{\gamma_e}{\gamma_f} + \frac{\gamma_e}{\gamma_f}\frac{\gamma_e+1}{2}\frac{m^2_{e\infty}}{(m^2_{e\infty}-1)^{\frac{1}{2}}}\theta_w + \frac{\gamma_e}{\gamma_f}\frac{(\gamma_e+1)m^2_{e\infty}}{2(m^2_{e\infty}-1)}\left(\frac{\gamma_e+1}{4}\frac{m^4_{e\infty}}{(m^2_{e\infty}-1)}-1\right)\theta_w^2 + O(\theta_w^3)$$

We shall write this as

$$m^2_{fn\infty} = 1 + c_1(\theta_w-\theta_w^*) + c_2(\theta_w-\theta_w^*)^2 + O(\theta_w-\theta_w^*)^3$$

where $$c_1 = \frac{\gamma_e}{\gamma_f}\frac{\gamma_e+1}{2}\frac{m^2_{e\infty}}{(m^2_{e\infty}-1)^{\frac{1}{2}}} + \frac{2\gamma_e}{\gamma_f}\theta_w^*\frac{(\gamma_e+1)m^2_{e\infty}}{2(m^2_{e\infty}-1)}\left(\frac{\gamma_e+1}{4}\frac{m^4_{e\infty}}{(m^2_{e\infty}-1)}-1\right) + O(\theta_w^{*2})$$

and $$c_2 = \frac{\gamma_e}{\gamma_f}\frac{(\gamma_e+1)m^2_{e\infty}}{2(m^2_{e\infty}-1)}\left(\frac{\gamma_e+1}{4}\frac{m^4_{e\infty}}{(m^2_{e\infty}-1)}-1\right) + O(\theta_w^*)$$

Inserting this expansion into the expression for $T_{a\infty}$ and expanding to $O(\theta_w - \theta_w^*)^2$ gives

$$T_{a\infty} = 1 + \frac{2(\gamma_f-1)}{(\gamma_f+1)}c_1(\theta_w-\theta_w^*) + \frac{2(\gamma_f-1)}{(\gamma_f+1)^2}\left((\gamma_f+1)(c_2-c_1^2)+\gamma_f c_1^2\right)(\theta_w-\theta_w^*)^2$$

Hence

$$(\bar{\sigma}-\sigma)_{a\infty} = \frac{2(\gamma_f-1)}{(\gamma_f+1)}c_1(\theta_w-\theta_w^*)c_{vib} + \frac{2c_{vib}(\gamma_f-1)}{(\gamma_f+1)^2}\left((\gamma_f+1)(c_2-c_1^2)+\gamma_f c_1^2\right)(\theta_w-\theta_w^*)^2$$

To a first approximation we can write

$$\frac{(\bar{\sigma}-\sigma)_{a\infty}}{(\bar{\sigma}-\sigma)_0} = \frac{2\frac{(\gamma_f-1)}{(\gamma_f+1)}c_1(\theta_w-\theta_w^*)c_{vib}}{c_{vib}\frac{m^2_{f\infty}}{(m^2_{f\infty}-1)^{\frac{1}{2}}}(\gamma_f-1)\theta_w} + O\left(\left(1-\frac{\theta_w^*}{\theta_w}\right)(\theta_w-\theta_w^*)\right)$$

Neglecting terms of $O\left(\theta_w^*\left(1-\frac{\theta_w^*}{\theta_w}\right)\right)$ above means that

$$c_1 = \frac{\gamma_e}{\gamma_f}\,\frac{\gamma_e+1}{2}\,\frac{m_{e\infty}^2}{(m_{e\infty}^2-1)^{\frac{1}{2}}}$$

so that

$$\frac{(\bar{\sigma}-\sigma)_{a\infty}}{(\bar{\sigma}-\sigma)_0} = \left(1-\frac{\theta_w^*}{\theta_w}\right)\frac{(\gamma_e+1)}{(\gamma_f+1)}\frac{(m_{f\infty}^2-1)^{\frac{1}{2}}}{(m_{e\infty}^2-1)^{\frac{1}{2}}} + O\left(\theta_w^*\left(1-\frac{\theta_w^*}{\theta_w}\right)\right)$$

But

$$\frac{(\gamma_e+1)}{(\gamma_f+1)}\frac{(m_{f\infty}^2-1)^{1/2}}{(m_{e\infty}^2-1)^{1/2}} = 1 + O(\theta_w^*)$$

Hence

$$\frac{(\bar{\sigma}-\sigma)_{a\infty}}{(\bar{\sigma}-\sigma)_0} = \left(1+\frac{\theta_w^*}{\theta_w}\right) + O\left(\theta_w^*\left(1-\frac{\theta_w^*}{\theta_w}\right)\right)$$

This gives

$$\frac{(\bar{\sigma}-\sigma)_0-(\bar{\sigma}-\sigma)_{a\infty}}{(\bar{\sigma}-\sigma)_0} \approx \frac{\theta_w^*}{\theta_w}$$

We notice that the critical value of this quantity is 1 so that it can be regarded as a scaled quantity. For the moderate and high Mach number flows (where $\frac{\bar{y}_{a0}}{\bar{y}_{a0}^*}$ is nearly 1), the above expression can be used as an approximate similarity rule. The function is plotted in fig. 3(i) and compared with the available characteristic results.

SECTION (3)

Results for the fully dispersed and the partly dispersed shock wave development

We shall analyze the results for the shock wave development in the same way as for the alpha-shock decay. That is we shall specify the gradients of the initial and far-field lines and the intercept of the far-field line with y = 0. The initial and far-field development distances (inverse gradients) will be represented by the symbols $\bar{y}_0$ and $\bar{y}$ respectively. The intercept on y = 0 will be denoted by b. With this notation the equations

to the initial and far-field lines are

$$\frac{(\bar{\sigma}-\sigma)_{max}-(\bar{\sigma}-\sigma)_{max\infty}}{(\bar{\sigma}-\sigma)_0-(\bar{\sigma}-\sigma)_{max\infty}} = e^{-\frac{y}{y_0}}$$

and $$\frac{(\bar{\sigma}-\sigma)_{max}-(\bar{\sigma}-\sigma)_{max\infty}}{(\bar{\sigma}-\sigma)_0-(\bar{\sigma}-\sigma)_{max\infty}} = e^{-\left(\frac{y}{y_0}-b\right)}$$ respectively.

Here $(\bar{\sigma}-\sigma)_{max}$ is the maximum value of the departure from equilibrium on the positive characteristics reflected from the alpha-shock. Initially this maximum always occurs at the alpha-shock itself so that the initial shock wave development gradients are the initial alpha-shock decay gradients scaled by the factor

$$\frac{(\bar{\sigma}-\sigma)_0}{(\bar{\sigma}-\sigma)_0-(\bar{\sigma}-\sigma)_{max\infty}}$$

A simplified expression for $(\bar{\sigma}-\sigma)_0$ has been given in section (1). The exact value of $(\bar{\sigma}-\sigma)_{max\infty}$ was found in section (3) of Chapter 1. Here we shall expand this in terms of the wedge angle.

The exact value is

$$(\bar{\sigma}-\sigma)_{max\infty} = \frac{\left(\gamma_f^2 M_{fn\infty}^4 (c_{pa}+c_{vib}-1)^2 - 2\gamma_f M_{fn\infty}^2 (c_{pa}+c_{vib})(c_{pa}+c_{vib}-1) + (c_{pa}+c_{vib})^2\right)}{2\gamma_f M_{fn\infty}^2 \left(2(c_{pa}+c_{vib})-1\right)}$$

The normal frozen Mach number at infinity has the expansion

$$\gamma_f M_{fn\infty}^2 = \gamma_e + k_1\theta_w + k_2\theta_w^2 + O(\theta_w^3)$$

where

$$k_1 = \frac{\gamma_e(\gamma_e+1)}{2}\frac{M_{e\infty}^2}{(M_{e\infty}^2-1)^{1/2}}$$

and

$$k_2 = \frac{\gamma_e(\gamma_e+1)}{2}\frac{M_{e\infty}^2}{(M_{e\infty}^2-1)}\left(\frac{\gamma_e+1}{4}\frac{M_{e\infty}^4}{(M_{e\infty}^2-1)}-1\right)$$

(These coefficients are perhaps most easily obtained by comparing

$$\phi_e = 1 + \frac{\gamma_e M_{e\infty}^2}{(M_{e\infty}^2-1)^{1/2}}\theta_w + \frac{\gamma_e M_{e\infty}^2}{(M_{e\infty}^2-1)}\left(\frac{\gamma_e+1}{4}\frac{M_{e\infty}^4}{(M_{e\infty}^2-1)}-1\right)\theta_w^2 + O(\theta_w^3)$$

given in Liepmann and Roshko (1967) p.389 with

$$\begin{aligned} p_e &= 1 + \frac{2\gamma_e}{\gamma_e+1}\left(M_{n\infty}^2 - 1\right) \\ &= 1 + \frac{2}{\gamma_e+1}\left(k_1\theta_w + k_2\theta_w^2\right) + O(\theta_w^3) \end{aligned} \Bigg)$$

We might expect $(\bar{\sigma}-\sigma)_{max\infty}$ to be $O(\theta_w^2)$ because we could define a streamline wave thickness at infinity by

$$\left(\bar{\sigma}_e - \bar{\sigma}_\infty\right)\left(\frac{dx}{d\sigma}\right)_{\text{inflexion point}}$$

This is approximately equal to (by using the rate equation)

$$\frac{-\bar{V}_\infty\left(\bar{\sigma}_e - \bar{\sigma}_\infty\right)}{(\bar{\sigma}-\sigma)_{max\infty}} = \frac{O\left(c_{vib}\theta_w\right)}{(\bar{\sigma}-\sigma)_{max\infty}}$$

Since the wave thickness is $O\left(\frac{c_{vib}}{\theta_w}\right)$ (see, for instance, Hodgson and Johannesen (1971)) then $(\bar{\sigma}-\sigma)_{max\infty}$ is $O(\theta_w^2)$

Inserting the expansion for $M_{fn\infty}$ into the exact expression for $(\bar{\sigma}-\sigma)_{max\infty}$ gives

$$\frac{\left(\left(\gamma_e + k_1\theta_w + k_2\theta_w^2\right)^2\left(c_{pa}+c_{vib}-1\right)^2 - 2\left(\gamma_e + k_1\theta_w + k_2\theta_w^2\right)\left(c_{pa}+c_{vib}\right)\left(c_{pa}+c_{vib}-1\right) + \left(c_{pa}+c_{vib}\right)^2\right)}{2\left(\gamma_e + k_1\theta_w + k_2\theta_w^2\right)\left(2\left(c_{pa}+c_{vib}\right)-1\right)}$$

In the numerator the coefficient of θ_w^0 is

$$\begin{aligned} &\gamma_e^2\left(c_{pa}+c_{vib}-1\right)^2 - 2\gamma_e\left(c_{pa}+c_{vib}\right)\left(c_{pa}+c_{vib}-1\right) + \left(c_{pa}+c_{vib}\right)^2 \\ &= \left(c_{pa}+c_{vib}\right)^2\left(\gamma_e^2 - 2\gamma_e + 1\right) + \left(c_{pa}+c_{vib}\right)\left(2\gamma_e - 2\gamma_e^2\right) + \gamma_e^2 \\ &= 0 \end{aligned}$$

The coefficient of θ_w^1 is

$$\begin{aligned} &2\gamma_e k_1\left(c_{pa}+c_{vib}-1\right)^2 - 2k_1\left(c_{pa}+c_{vib}\right)\left(c_{pa}+c_{vib}-1\right) \\ &= 2k_1\left(\left(c_{pa}+c_{vib}-1\right)\left(\left(\gamma_e-1\right)\left(c_{pa}+c_{vib}\right)-\gamma_e\right)\right) \\ &= 0 \end{aligned}$$

The coefficient of θ_w^2 is

$$(c_{pa}+c_{vib}-1)^2(k_1^2+2\gamma_e k_2) - 2k_2(c_{pa}+c_{vib})(c_{pa}+c_{vib}-1)$$

$$= (c_{pa}+c_{vib}-1)\left((c_{pa}+c_{vib}-1)(k_1^2+2\gamma_e k_2) - 2k_2(c_{pa}+c_{vib})\right)$$

$$= (c_{pa}+c_{vib}-1)^2 k_1^2 + k_2(c_{pa}+c_{vib}-1)\left(2\gamma_e(c_{pa}+c_{vib}-1) - 2(c_{pa}+c_{vib})\right)$$

$$= (c_{pa}+c_{vib}-1)^2 k_1^2$$

Hence the expression correct to $O(\theta_w^2)$ for $(\bar{\sigma}-\sigma)_{max\infty}$ is

$$(\bar{\sigma}-\sigma)_{max\infty} = \frac{(c_{pa}+c_{vib}-1)^2 \frac{\gamma_e^2(\gamma_e+1)^2 m_{e\infty}^4}{4(m_{e\infty}^2-1)}\theta_w^2}{2\gamma_e\left(2(c_{pa}+c_{vib})-1\right)}$$

$$= \frac{\gamma_e(\gamma_e+1)^2\left(\gamma_e(\gamma_e-1)^{-1}-1\right)^2 m_{e\infty}^4\,\theta_w^2}{8(m_{e\infty}^2-1)\left(2\gamma_e(\gamma_e-1)^{-1}-1\right)}$$

Expressing this in similarity form gives

$$\frac{(\bar{\sigma}-\sigma)_{max\infty}}{(\bar{\sigma}-\sigma)^*_{max\infty}} = \left(\frac{\theta_w}{\theta_w^*}\right)^2$$

We could anticipate such a rule by noting that

$$\frac{m_{f\infty}-\frac{\gamma_e}{\gamma_f}}{1-\frac{\gamma_e}{\gamma_f}} \approx \left(\frac{\theta_w}{\theta_w^*}\right)$$

That is shock waves at infinity having the same normal frozen Mach number (and hence the same value of $(\bar{\sigma}-\sigma)_{max\infty}$) have approximately the same ratio of $\frac{\theta_w}{\theta_w^*}$. This similarity representation is plotted in fig. 3(k) together with the numerical results.

Fig. 3(o) shows the initial shock wave development distances scaled with respect to the critical development distances. These are just the initial alpha-shock decay distances multiplied by $\frac{(\bar{\sigma}-\sigma)_0-(\bar{\sigma}-\sigma)_{max\infty}}{(\bar{\sigma}-\sigma)_0}$ The results for $m_{f\infty}$ = 2.6 and 3.8 fall on to a single curve but the

results for $M_{f\infty} = 1.4$ fall on different curves depending on the vibrational specific heat. The same behaviour was exhibited by the initial alpha-shock decay distances where the functional dependence was explained by expanding the appropriate tip gradient to first order in θ_w. It is sufficient, therefore, to consider the scaled behaviour of

$$\frac{(\bar{\sigma}-\sigma)_0 - (\bar{\sigma}-\sigma)_{max\infty}}{(\bar{\sigma}-\sigma)_0}$$

Scaling with respect to the critical values gives

$$\frac{\left(1 - \frac{(\bar{\sigma}-\sigma)_{max\infty}}{(\bar{\sigma}-\sigma)_0}\right)}{\left(1 - \frac{(\bar{\sigma}-\sigma)^*_{max\infty}}{(\bar{\sigma}-\sigma)^*_0}\right)}$$

Employing the small angle expansions for $(\bar{\sigma}-\sigma)_{max\infty}$ and $(\bar{\sigma}-\sigma)_0$ gives

$$\frac{\left(1 - \frac{(\bar{\sigma}-\sigma)_{max\infty}}{(\bar{\sigma}-\sigma)_0}\right)}{\left(1 - \frac{(\bar{\sigma}-\sigma)^*_{max\infty}}{(\bar{\sigma}-\sigma)^*_0}\right)} = \frac{\left(1 - \frac{\gamma_e(\gamma_e+1)^2(\gamma_e(\gamma_e-1)^{-1}-1)^2 m_{e\infty}^4 (m_{f\infty}^2-1)^{\frac{1}{2}}}{8(\gamma_f-1)\,cvib\,(m_{e\infty}^2-1)\,m_{f\infty}^2\,(2\gamma_e(\gamma_e-1)^{-1}-1)} \frac{\theta_w}{\theta_w^*}\theta_w^*\right)}{\left(1 - \frac{\gamma_e(\gamma_e+1)^2(\gamma_e(\gamma_e-1)^{-1}-1)^2 m_{e\infty}^4 (m_{f\infty}^2-1)^{\frac{1}{2}}}{8(\gamma_f-1)\,cvib\,(m_{e\infty}^2-1)\,m_{f\infty}^2\,(2\gamma_e(\gamma_e-1)^{-1}-1)}\theta_w^*\right)}$$

From the expansion for the normal frozen Mach number at infinity we have

$$\theta_w^* \approx \frac{2(\gamma_f-\gamma_e)(m_{e\infty}^2-1)^{1/2}}{\gamma_e(\gamma_e+1)m_{e\infty}^2}$$

$$= \frac{2\,cvib\,(\gamma_e-1)(\gamma_f-1)(m_{e\infty}^2-1)^{1/2}}{\gamma_e(\gamma_e+1)m_{e\infty}^2}.$$

Hence

$$\frac{\left(1 - \frac{(\bar{\sigma}-\sigma)_{max\infty}}{(\bar{\sigma}-\sigma)_0}\right)}{\left(1 - \frac{(\bar{\sigma}-\sigma)^*_{max\infty}}{(\bar{\sigma}-\sigma)_0}\right)} \approx \frac{\left(1 - \frac{(\gamma_e+1)(\gamma_e-1)(\gamma_e(\gamma_e-1)^{-1}-1)^2 \frac{\gamma_f}{\gamma_e}(m_{f\infty}^2-1)^{\frac{1}{2}}\left(\frac{\theta_w}{\theta_w^*}\right)}{4(2\gamma_e(\gamma_e-1)^{-1}-1)(m_{e\infty}^2-1)^{\frac{1}{2}}}\right)}{\left(1 - \frac{(\gamma_e+1)(\gamma_e-1)(\gamma_e(\gamma_e-1)^{-1}-1)^2 \frac{\gamma_f}{\gamma_e}(m_{f\infty}^2-1)^{1/2}}{4(2\gamma_e(\gamma_e-1)^{-1}-1)(m_{e\infty}^2-1)^{1/2}}\right)}$$

For $c_{vib} = 1$, $m_{f\infty} = 3.8$ the value of this expression on $\frac{\theta_w}{\theta_w^*} = 0$ is 1.35. This compares well with the results plotted in fig. 3(o). To get the gradients of the lines for $m_{f\infty} = 1.4$ we have only to add the gradient just derived to the gradient found in the last section for the initial alpha-shock decay distances. Values of $\bar{y}_o^*$ are plotted in fig. 3(p).

The shock wave development distance has been defined in section (2) of Chapter 2. We shall represent it with the symbol $\bar{y}_D$. Fig. 3(l) illustrates the variation of $\bar{y}_D$ with θ_w, c_{vib} and $m_{f\infty}$. There is very little variation with c_{vib} and the main dependence is on θ_w and $m_{f\infty}$. The result of scaling these distances with respect to the critical distances is shown in fig. 3(m). The results fall very nearly on to a single curve; the scatter that we do get is where we expect it - for $\frac{\theta_w}{\theta_w^*} \ll 1$. Here the shock waves are very weak and very wide at infinity in comparison to their width on the wedge surface. The development distance is also comparatively large and these effects combine to make the computations long and costly. One is forced, therefore, to terminate the calculations at a stage where the far-field line is tenuously predicted. One can state, however, that the values plotted are underestimates to the true development distances. From section (2) of Chapter 5, for very weak waves, the analytic estimate for the development distance is given by

$$\bar{y}_D \approx F(m_{f\infty}, c_{vib})\,\theta_w^{-2}$$

We shall tentatively assume that this holds for all $\frac{\theta_w}{\theta_w^*} \leq 1$. In our similarity form this is

$$\frac{\bar{y}_D}{\bar{y}_D^*} \approx \left(\frac{\theta_w}{\theta_w^*}\right)^{-2}$$

This function is plotted in fig. 3(m) and exhibits the qualitative θ_w dependence reasonably well.

Fig. 3(n) shows the variations of the critical shock wave development distances with frozen Mach number and vibrational specific heat. The Mach

number and vibrational specific heat dependences are very similar to those of the linear theory for alpha-shock decay (see fig. 3(h)). More will be said about the nature of the dependence on m_{f_∞}, $c_{v,b}$ and θ_w in section (4).

Fig. 3(q), which is similar to fig. 3(m), illustrates the variation of the far-field scaled shock wave development distances. The very weak wave theory (see section (2) Chapter 5) predicts that these distances should also vary like θ_w^{-2}. In fig. 3(r) the far-field critical development distances are plotted and compared to the corresponding far-field alpha-shock decay distances which are approximately a factor of 2 greater (note, however, that the critical alpha-shock decay distances are subject to the error mentioned in section (2)). Fig. 3(s) compares the scaled far-field alpha-shock decay and shock wave development distances. By use of fig. 3(r) (determine the absolute values) we see that for $\frac{\theta_w}{\theta_{w^*}} \geq 1$ $\bar{y}$ and $\bar{y}_a$ have approximately the same magnitude. For $\frac{\theta_w}{\theta_{w^*}} << 1$, $\bar{y} >> \bar{y}_a$

The values of b can be found using the plotted values of $\bar{y}$ and $\bar{y}_b$. We choose to plot $\bar{y}_b$ (instead of b) for convenience in the analysis that follows in the next section. We shall also need estimates of $\bar{y}_b$ in Chapters 4 and 5.

SECTION 4

Discussion of general similarity and extrapolation of results

We have seen in the previous 3 sections how the scaling of quantities with respect to their critical values has given some kind of similarity representation. In some cases, however, this approach has failed (see figs. 3(i) and 3(o)). To precisely analyze the nature of the similarity from the governing equations and wedge boundary condition is a formidable task. Simplifications have to be made; in particular, Blythe (1969) has

given similarity scalings for the very weak wave case. We shall tentatively assume, however, that (in the appropriate cases) the characteristic results are indications of an exact similarity and shall pursue the consequences.

First we shall consider the far-field alpha-shock decay distances which are plotted in fig. $3(\overset{\cdot}{\ast})$. We shall assume that an exact similarity does exist so that we can write

$$\frac{\bar{y}_a}{\bar{y}_a^*} = \bar{\gamma}_a\left(\frac{\theta_w}{\theta_w^*}\right)$$

In particular this must scale the linear values (which are the limiting values as $\frac{\theta_w}{\theta_w^*} \to 0$) so that

$$\frac{\bar{y}_{ae}}{\bar{y}_a^*} = \bar{\gamma}_a(0)$$

Hence the linear values can be used as scaling factors so that

$$\frac{\bar{y}_a}{\bar{y}_{ae}} = \frac{\bar{\gamma}_a\left(\frac{\theta_w}{\theta_w^*}\right)}{\bar{\gamma}_a(0)}$$

The analytic form for the linear decay distances has been given in section (2). Therefore,

$$\bar{y}_a = \frac{2\gamma_f^{1/2} c_{pa}\left(m_{f\infty}^2 - 1\right)^{\frac{1}{2}}}{(\gamma_f - 1)\, c_{vb}\, m_{f\infty}} \quad \frac{\bar{\gamma}_a\left(\frac{\theta_w}{\theta_w^*}\right)}{\bar{\gamma}_a(0)}$$

Unfortunately we can say nothing about the nature of the function $\bar{\gamma}_a\left(\frac{\theta_w}{\theta_w^*}\right)$ because the linear theory gives no indication of even the initial variation with θ_w. This expression does show, however, how the critical values vary with $m_{f\infty}$ and c_{vb}. Examination of fig. 3(r) reveals that these dependences are qualitatively correct. The inaccuracies found in the determination of the critical quantities in section (2) forbid a more precise statement.

If, however, we next consider the shock wave development then the weak wave analysis given in Chapter 5, section (2) furnishes an initial

dependence on all 3 parameters. In Chapter 5, it is shown that, for very weak waves, the development distance is a multiple of

$$\frac{B}{C^2 \left(m_{f\infty}^2 - 1\right)^{\frac{1}{2}} \theta_w^2}$$

where $$B = \frac{\gamma_f^{\frac{1}{2}} \left(\frac{m_{e\infty}^2 - 1}{m_{f\infty}^2 - 1} - 1 \right) m_{f\infty}}{\left(1 + \frac{c_{vib}}{c_{pa}}\right) \left(\frac{m_{e\infty}^2 - 1}{m_{f\infty}^2 - 1} \right)^{\frac{1}{2}}}$$

and $$C = \frac{(\gamma_e + 1)\, m_{e\infty}^4}{2 \left(m_{e\infty}^2 - 1\right) \left(m_{f\infty}^2 - 1\right)^{\frac{1}{2}}}$$

On the evidence presented in fig. 3($\frac{m}{p}$) we assume an exact similarity exists and write

$$\frac{\bar{y}_D}{\bar{y}_D^*} = \bar{y}_D \left(\frac{\theta_w}{\theta_w^*} \right)$$

This implies in general that

$$\bar{y}_D = \bar{y}_{D1}(m_{f\infty}, c_{vib})\, \bar{y}_{D2} \left(\frac{\theta_w}{\theta_w^*} \right) \theta_w^n$$

where n can take any value and $\bar{y}_{D1}$ and $\bar{y}_{D2}$ are unknown functions. This equation indicates that for similarity of the type under discussion to exist the dependences on the flow parameters must be separable into distinct functional relationships. If, as above, scalings are taken with respect to critical values at $\theta_w = \theta_w^*$ then it is the θ_w dependence that must be separable: the $m_{f\infty}$ and c_{vib} dependence can be coupled in any manner.

The expression above must agree with the weak wave analysis in the limit $\frac{\theta_w}{\theta_w^*} \to 0$. Hence we must have

$$n = -2$$

$$\bar{y}_{D2} \left(\frac{\theta_w}{\theta_w^*} \right) \to 1 \quad \text{as} \quad \frac{\theta_w}{\theta_w^*} \to 0$$

$$\bar{y}_{D1}(m_{f\infty}, c_{vib}) \propto \frac{\gamma_e^{\frac{1}{2}} c_{vib} \left(m_{e\infty}^2 - 1\right)^{\frac{3}{2}}}{(\gamma_e + 1)^2 (c_{va} + c_{vib})(c_{pa} + c_{vib}) m_{e\infty}^5}$$

Therefore

$$\bar{\gamma}_D^* = \bar{\gamma}_{D1}\left(m_{f\infty}, c_{vib}\right)\bar{\gamma}_{D2}(1)\,\theta_w^{-2}$$

$$\propto \frac{\gamma_e^{\frac{1}{2}}\, c_{vib}\,(m_{e\infty}^2-1)^{\frac{3}{2}}\,\theta_w^{*-2}}{(\gamma_e+1)^2\,(c_{va}+c_{vib})(c_{pa}+c_{vib})\,m_{e\infty}^5}$$

But $\theta_w^* \approx \dfrac{2\,c_{vib}\,(\gamma_e-1)(\gamma_f-1)(m_{e\infty}^2-1)^{\frac{1}{2}}}{\gamma_e\,(\gamma_e+1)\,m_{e\infty}^2}$ from section (3).

Substituting gives

$$\bar{\gamma}_D^* \propto \frac{\gamma_e^2(m_{e\infty}^2-1)^{\frac{1}{2}}}{c_{vib}\,m_{f\infty}}$$

$$= \frac{\gamma_f^2(m_{f\infty}^2-1)^{\frac{1}{2}}}{c_{vib}\,m_{f\infty}} + O(\gamma_f-\gamma_e)$$

That this dependence is qualitatively correct can be seen by examining fig. 3(r). Of major importance is the dependence on c_{vib} which enables us to extend the results to any vibrational specific heat of interest. We can assess the accuracy of this prediction by testing whether at constant $m_{f\infty}$, $\bar{\gamma}_D^*\, c_{vib}$ = constant. This calculation is made in Table 1 which verifies the rule especially when we remember

TABLE 1

c_{vib} =	0.5	1.0	2.0	3.0
$m_{f\infty}$ = 1.4	63.5	61.0	55.0	53.0
2.6	84.5	84.0	79.0	75.0
3.8	89.5	86.0	82.0	79.0

that only the simplified form has been used. For more accurate verification the results in Table 1 should be divided by $\gamma_e^2\,(m_{e\infty}^2-1)^{\frac{1}{2}}$ If this is done then we get the results in Table 2 which are a considerable improvement over those in Table 1.

TABLE 2

c_{vib} =		0.5	1.0	2.0	3.0
$M_{f\infty}$ =	1.4	34.6	34.6	33.0	33.0
	2.6	19.3	20.1	20.3	20.2
	3.8	13.4	13.6	13.9	13.7

For crude assessments, however, the simple rule is adequate and will be used in estimating the development distance in Chapter 5 for a flow with $c_{vib} = 0.05$.

The same arguments can be applied to the far-field shock wave development distances. The analysis in section (2) of Chapter 5 indicates that these have the same $M_{f\infty}$ and c_{vib} dependence as the shock wave development distance (in the very weak wave limit). Consequently the critical values must have the same dependence as presented above for the development distances. These results mean that we can evaluate the whole shock wave development process for any c_{vib} ; the whole alpha-shock decay process can be extrapolated using the known linear scalings.

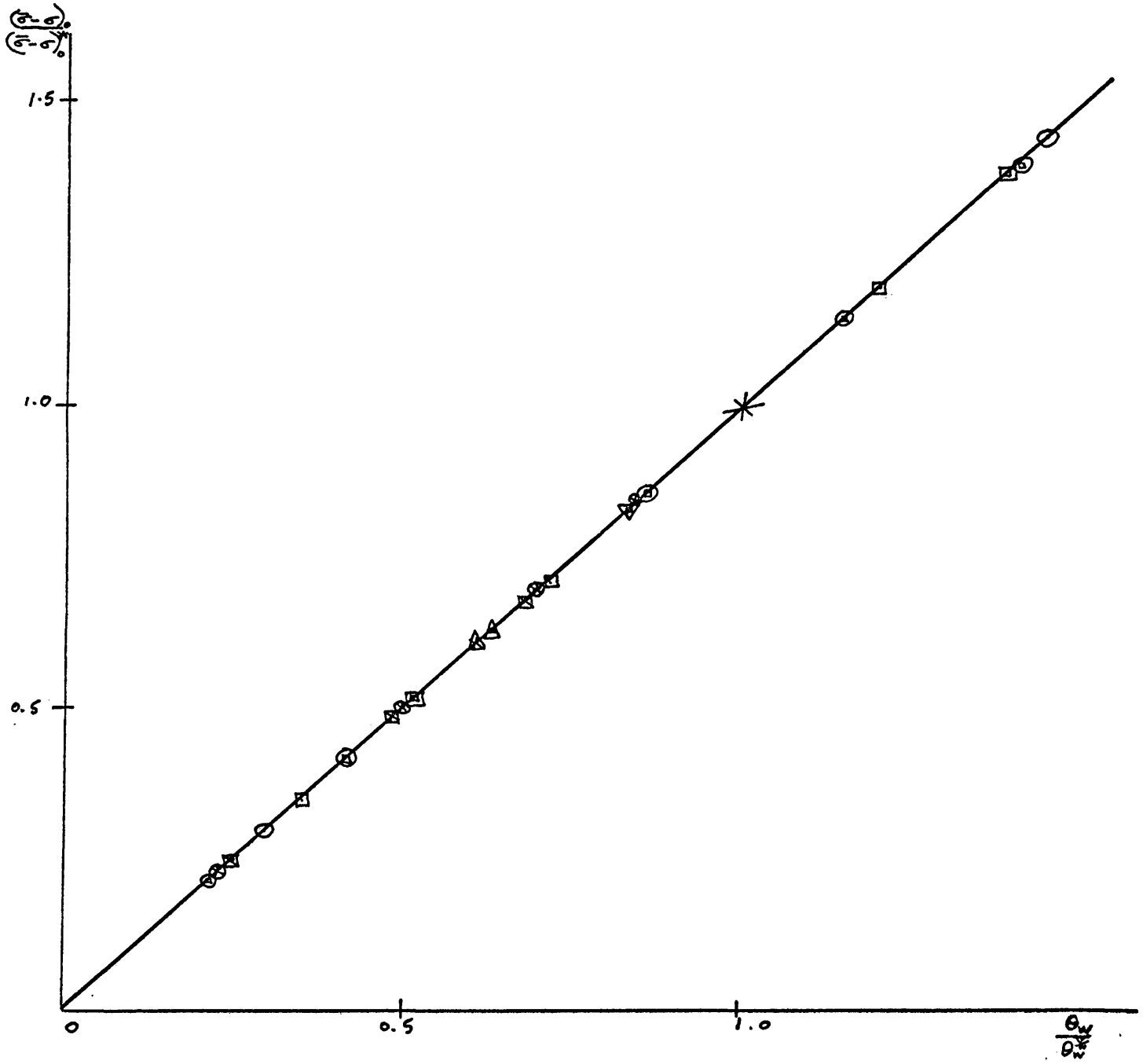

FIGURE 3(a). SIMILARITY CURVE FOR INITIAL DEPARTURE FROM EQUILIBRIUM. —, $\frac{(\bar{\varepsilon}-\sigma)_0}{(\bar{\varepsilon}-\sigma)_0^*} = \frac{\theta_w}{\theta_w^*}$.

IN THIS CHAPTER WE EMPLOY THE FOLLOWING SYMBOLISM:

$C_{vib} = 0.5$

▽, $m_{f\infty} = 1.4$

▽, $m_{f\infty} = 2.6$

▽, $m_{f\infty} = 3.8$

$C_{vib} = 1$

⊗, $m_{f\infty} = 1.4$

⊙, $m_{f\infty} = 2.6$

◎, $m_{f\infty} = 3.8$

$C_{vib} = 2$

△, $m_{f\infty} = 1.4$

△, $m_{f\infty} = 2.6$

△, $m_{f\infty} = 3.8$

$C_{vib} = 3$

⊠, $m_{f\infty} = 1.4$

⊡, $m_{f\infty} = 2.6$

▣, $m_{f\infty} = 3.8$

(for the characteristics results)

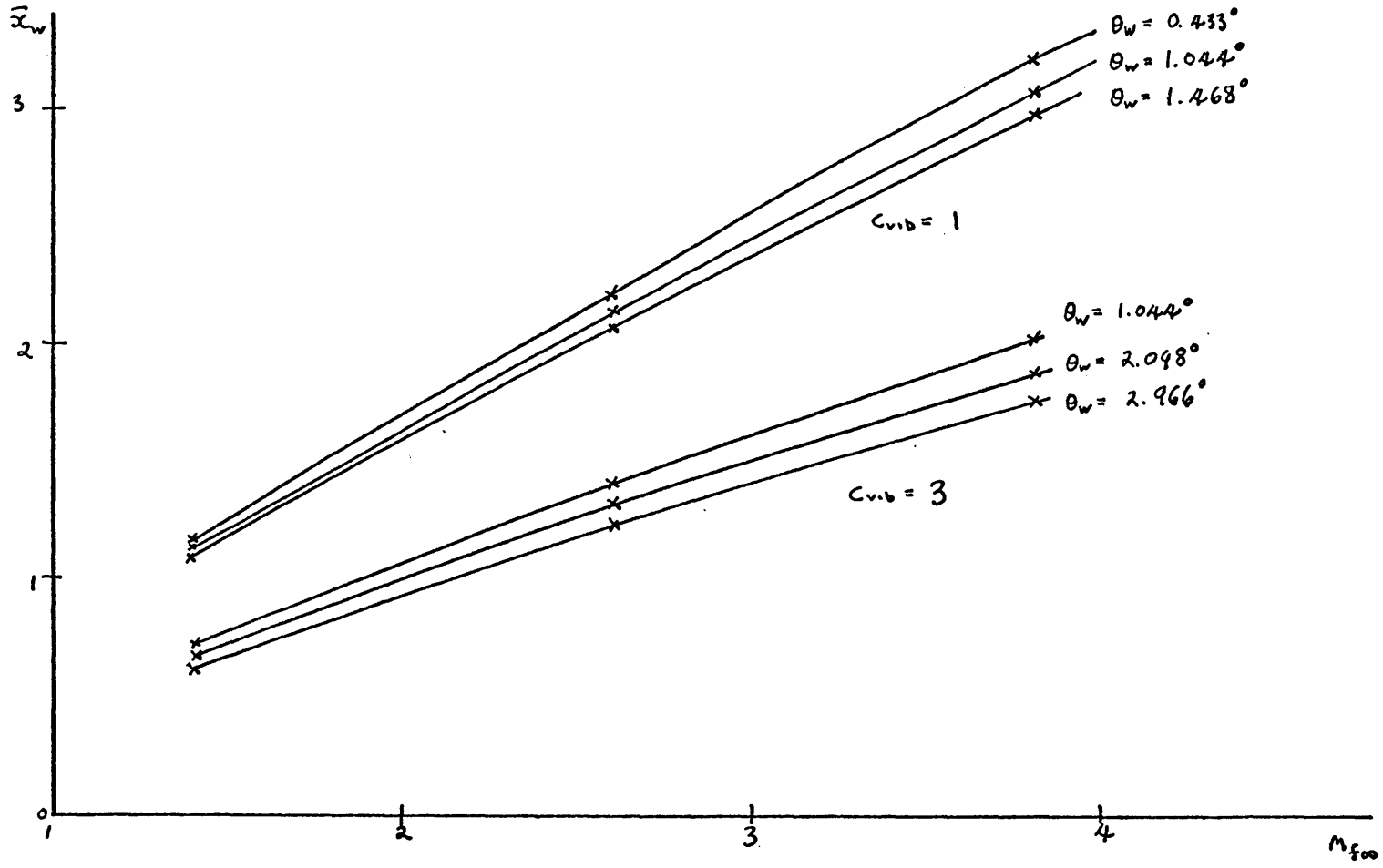

FIGURE 3(b). VARIATION OF THE RELAXATION DISTANCE ON THE WEDGE SURFACE.

x, characteristics. —, from wedge tip gradients.

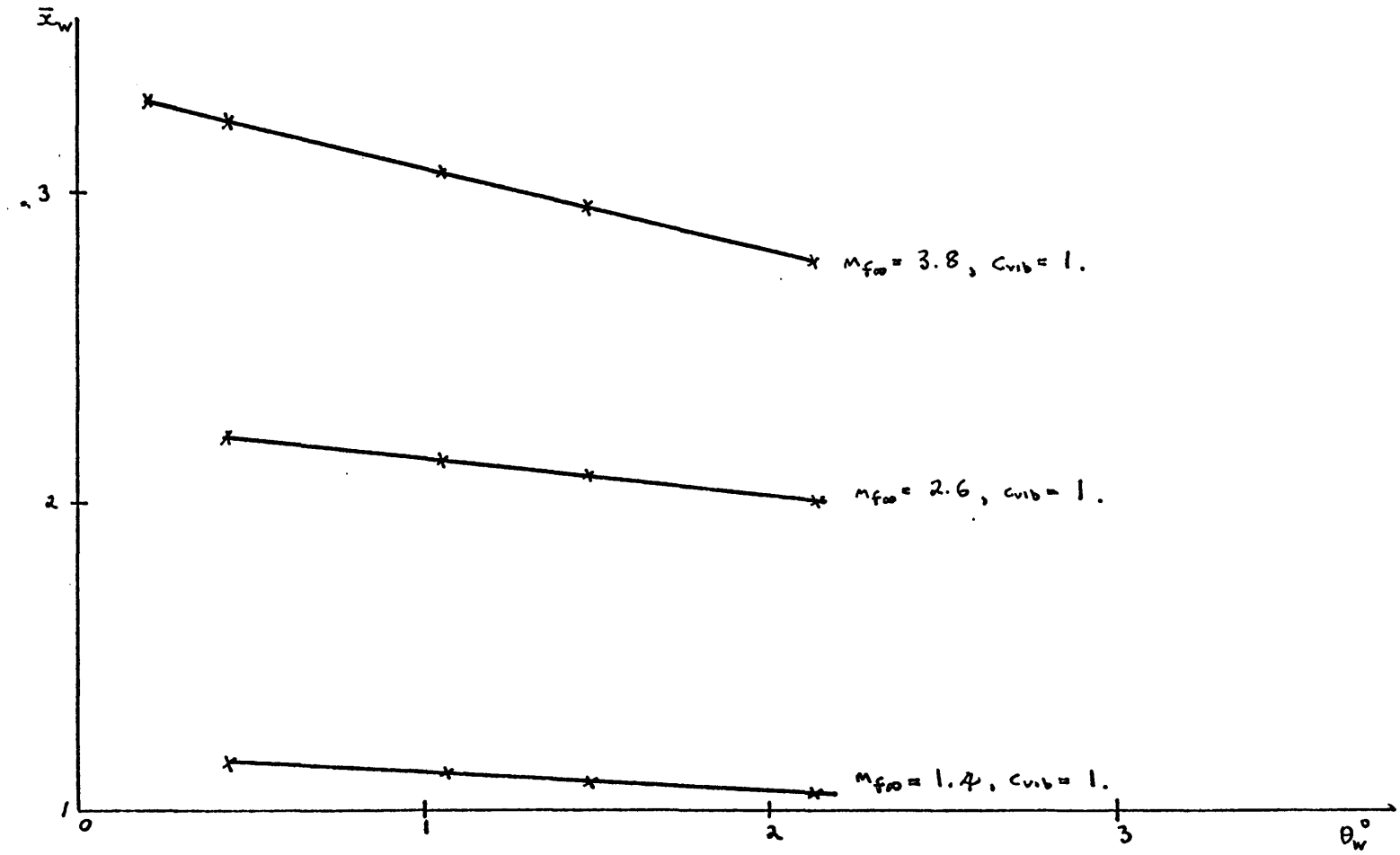

FIGURE 3(c). (see figure 3(b) for legend).

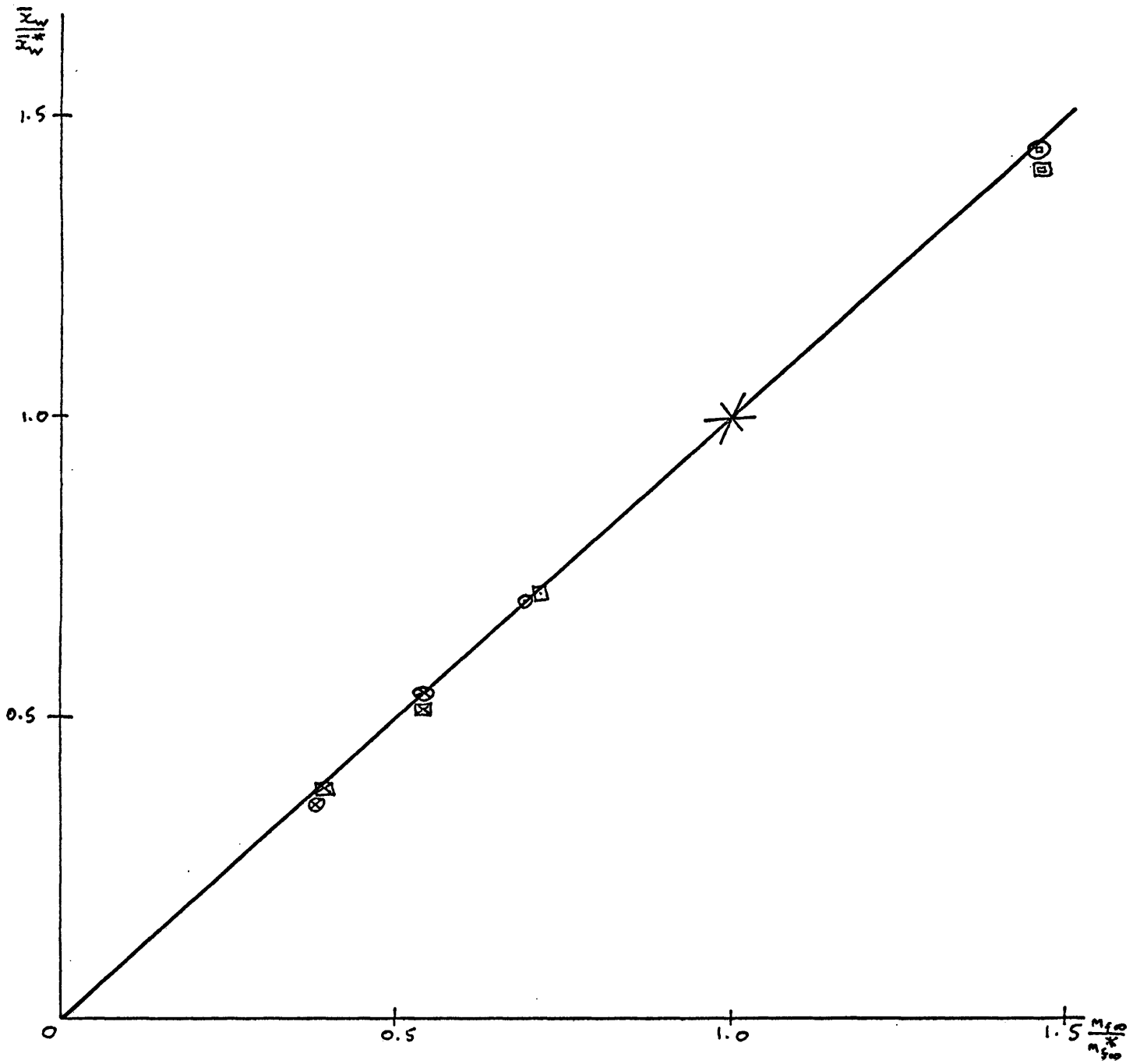

FIGURE 3(d). SIMILARITY REPRESENTATION OF THE VARIATIONS OF THE RELAXATION DISTANCE ON THE WEDGE SURFACE. —, approximate similarity rule.

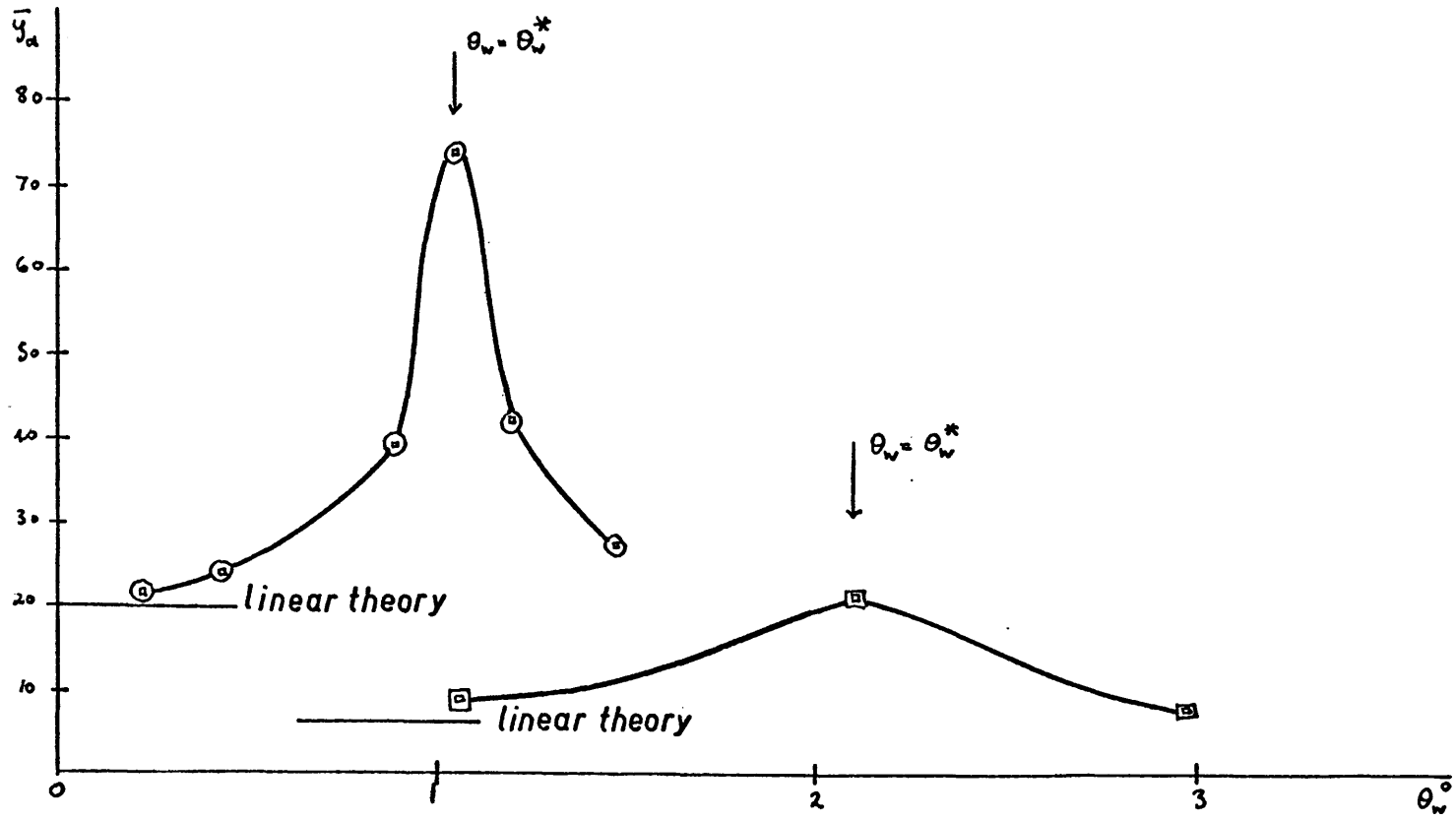

FIGURE 3(e). VARIATION OF FAR-FIELD ALPHA-SHOCK DECAY DISTANCE.

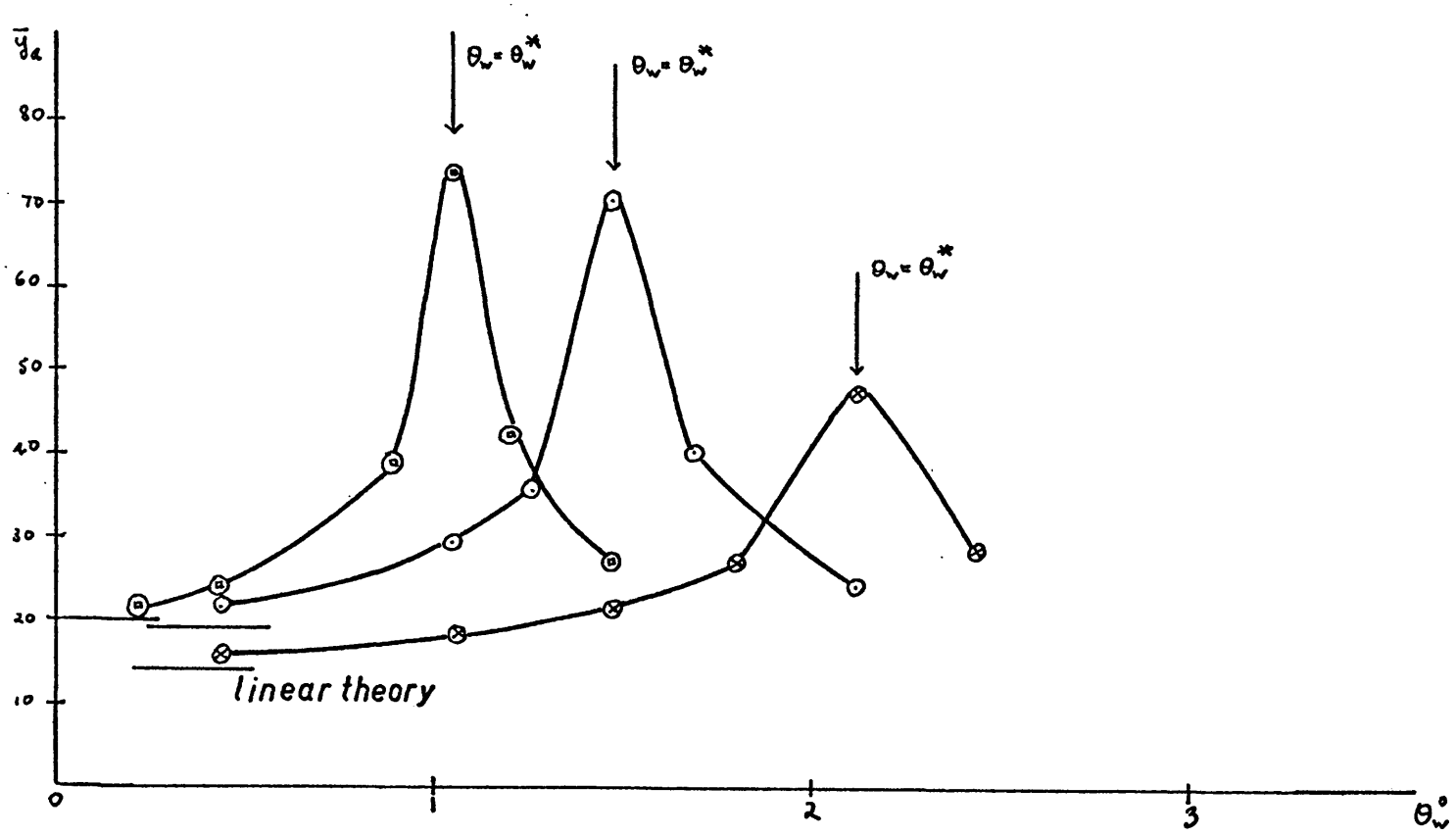

FIGURE 3(f). (see figure 3(e) for legend).

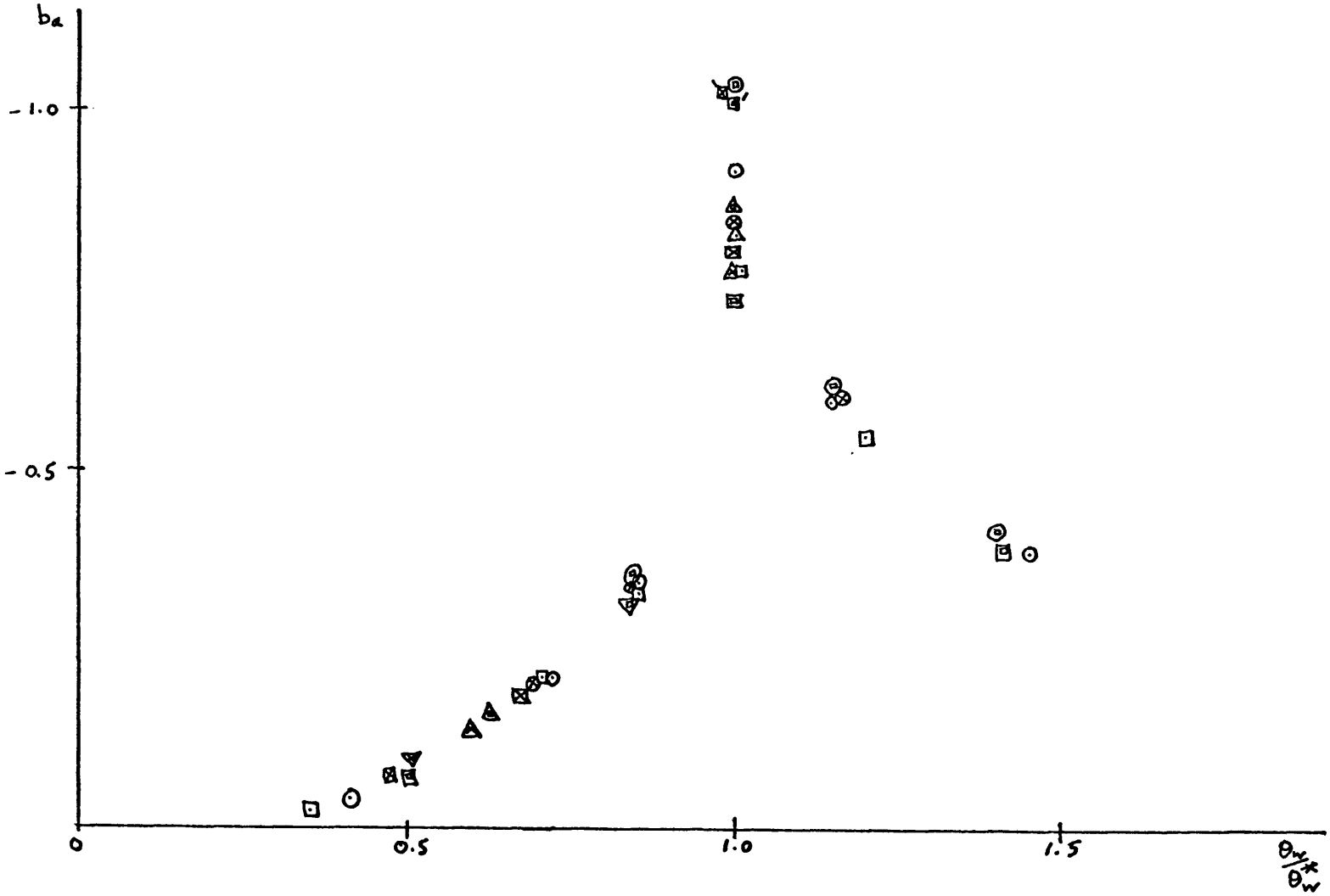

FIGURE 3(g). SIMILARITY REPRESENTATION OF THE VARIATIONS OF b_a.

The dashes indicate calculations with $1/250^{th}$ of the variation of σ per step.

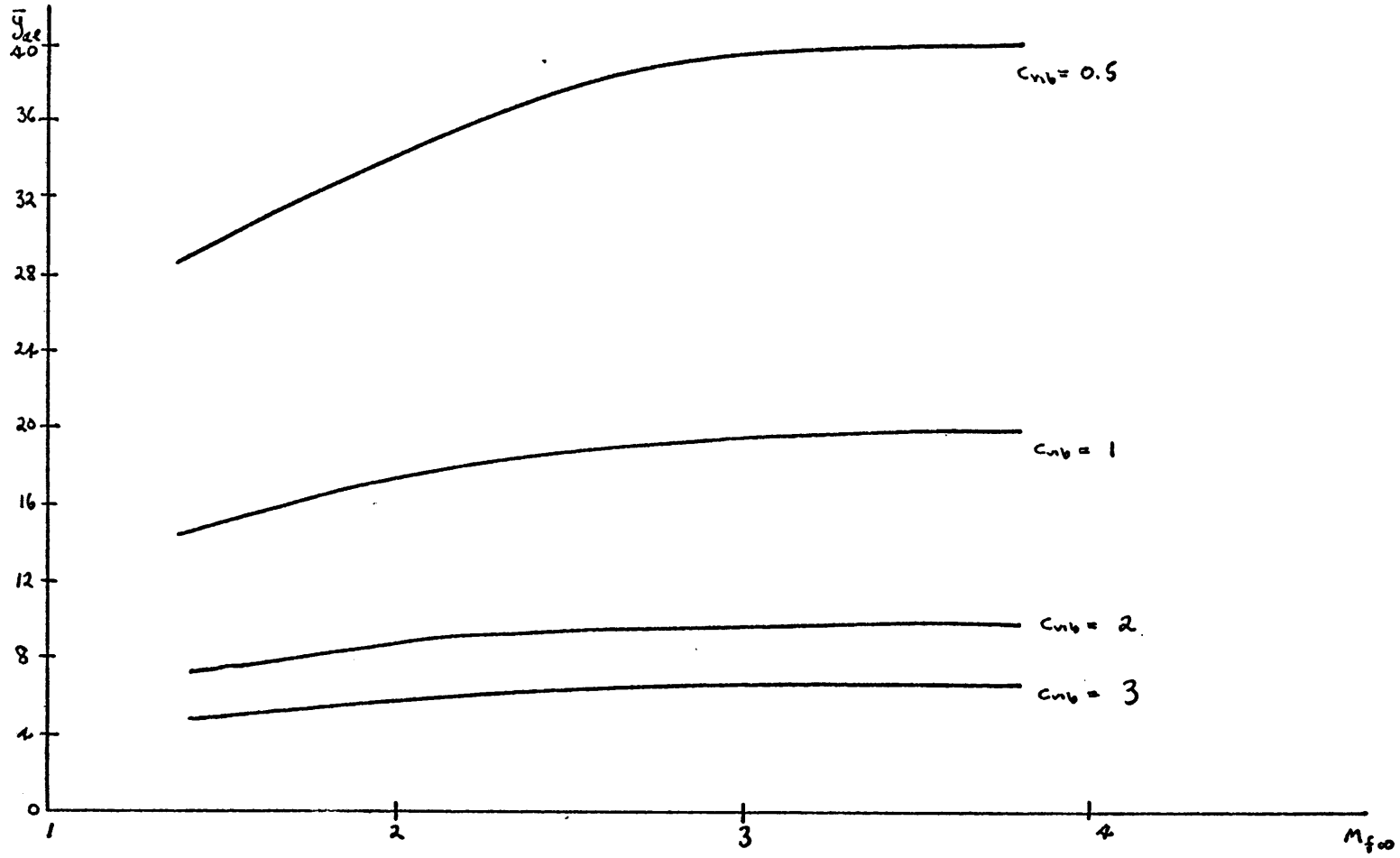

FIGURE 3(h). VARIATION OF LINEAR ALPHA-SHOCK DECAY DISTANCE.

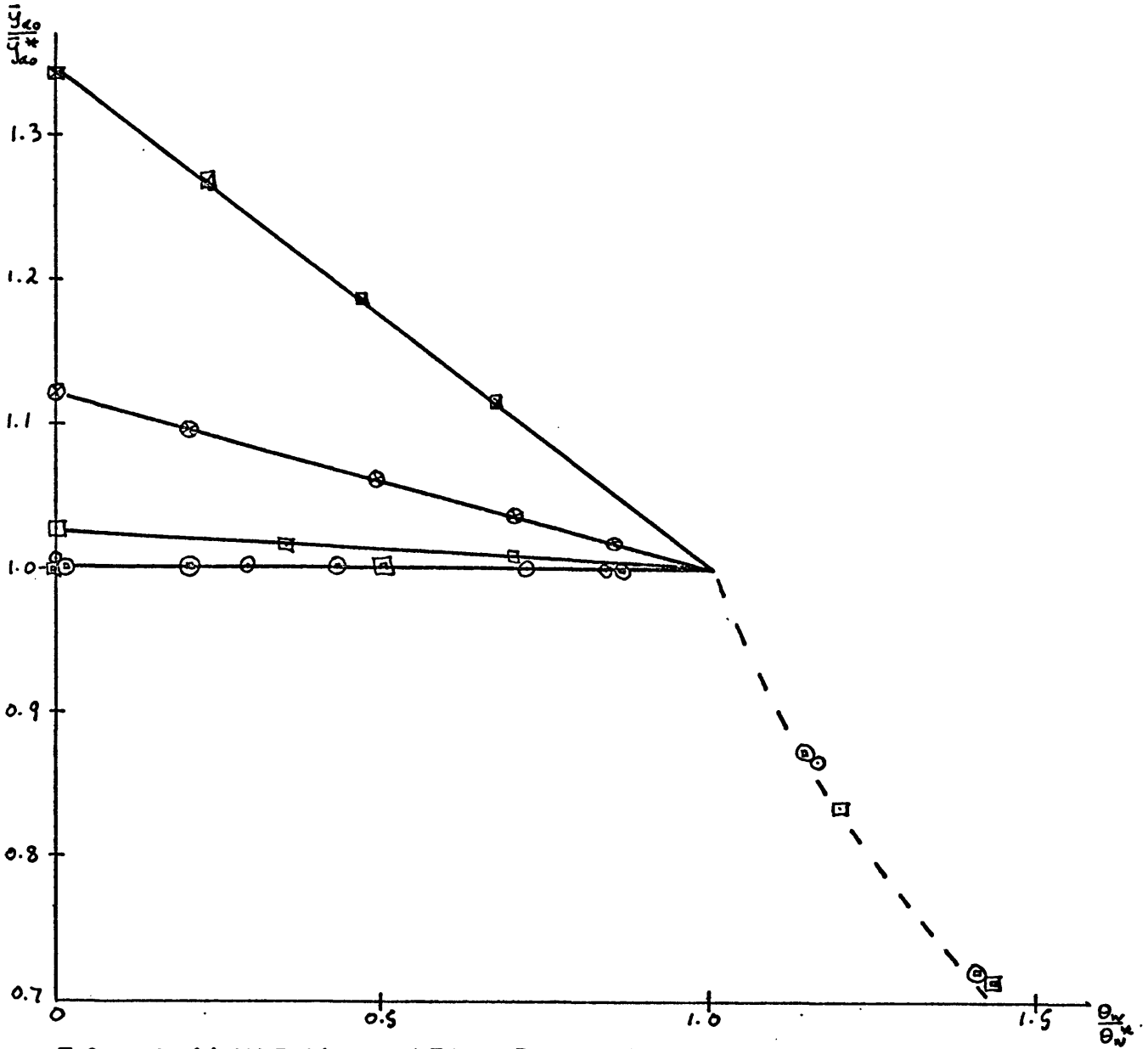

FIGURE 3(i). INITIAL, SCALED ALPHA-SHOCK DECAY DISTANCES.
—, from wedge tip gradients. - -, approximate similarity rule (for $m_{f\infty} \gg 1$)

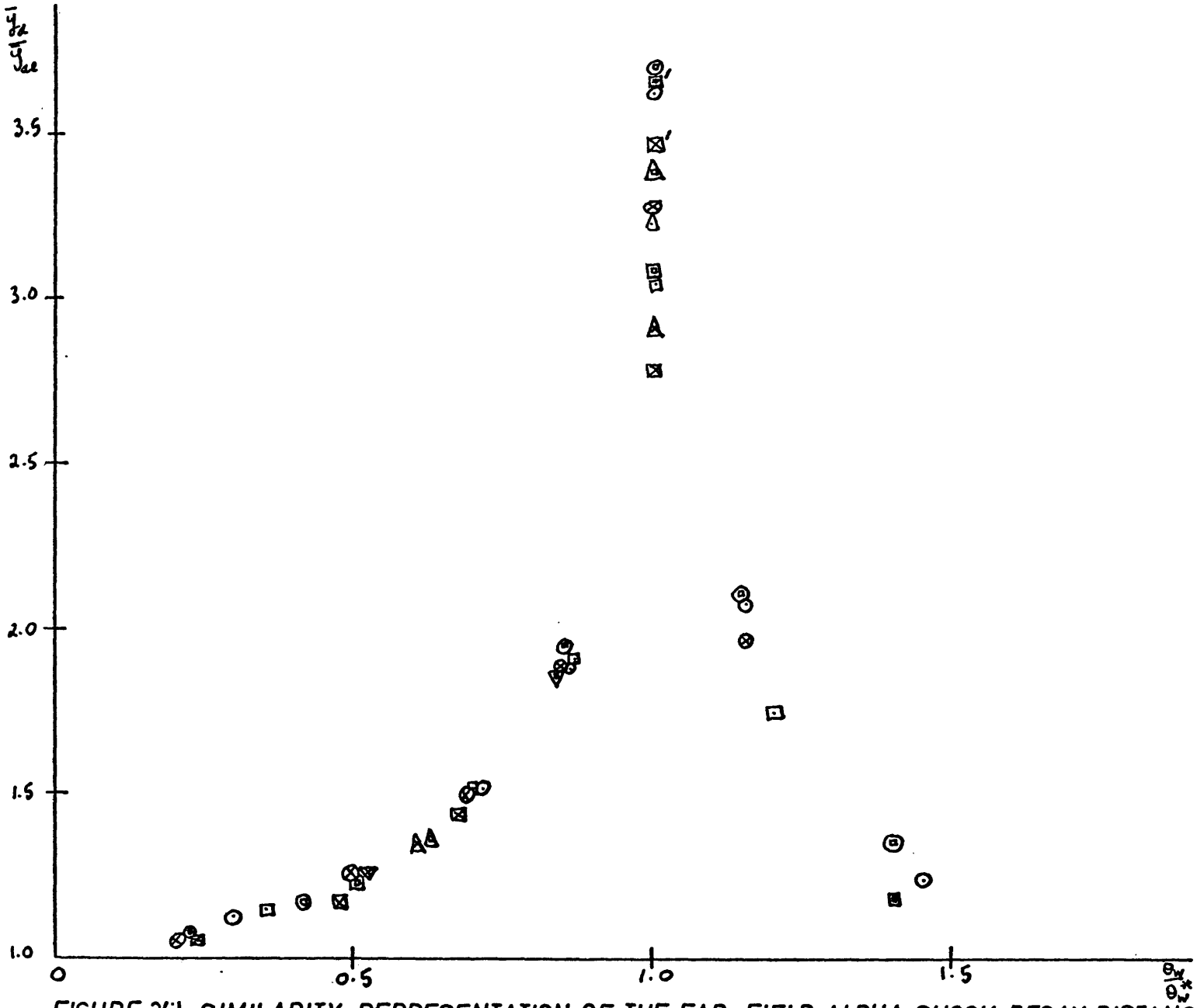

FIGURE 3(j). SIMILARITY REPRESENTATION OF THE FAR-FIELD ALPHA-SHOCK DECAY DISTANCES.
The dashes indicate calculations with $\frac{1}{250}^{th}$ of the variation of σ per step.

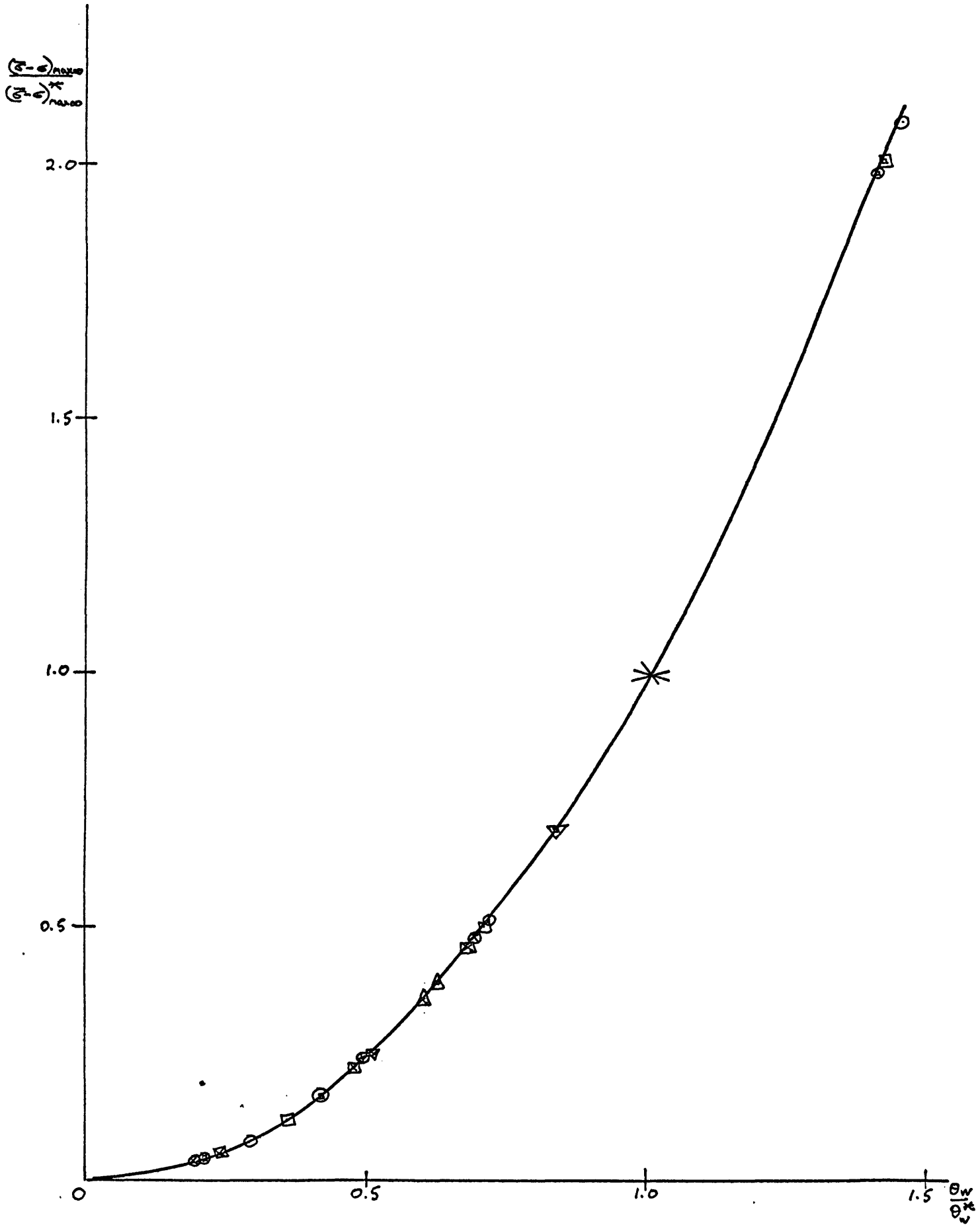

FIGURE 3(k). SIMILARITY CURVE FOR THE MAXIMUM DEPARTURE FROM EQUILIBRIUM IN THE SHOCK WAVE AT INFINITY.

—, $\frac{(\bar{\sigma}-\sigma)_{max\infty}}{(\bar{\sigma}-\sigma)^{*}_{max\infty}} = \left(\frac{\theta_w}{\theta_w^{*}}\right)^2$.

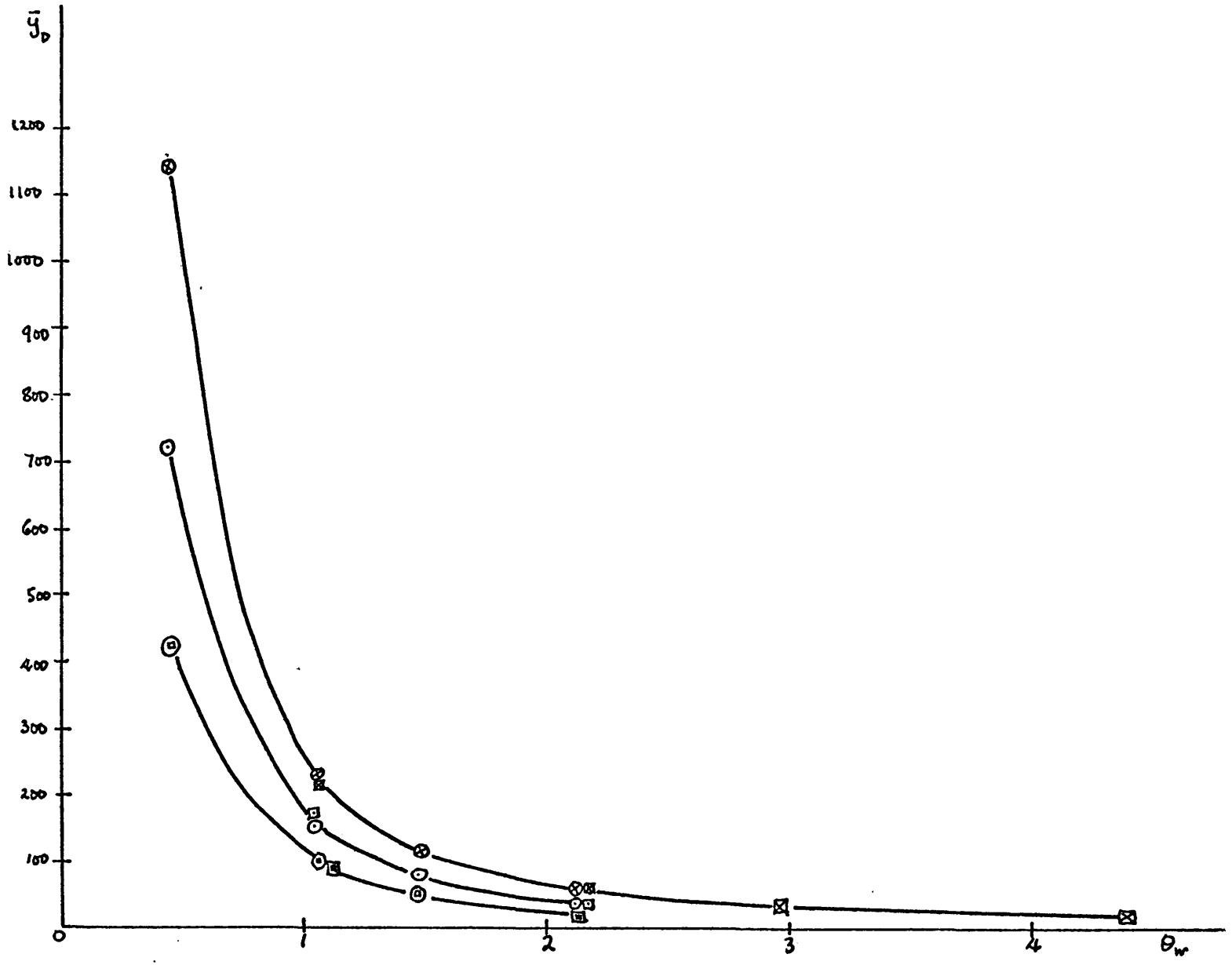

FIGURE 3(1). VARIATION OF SHOCK WAVE DEVELOPMENT DISTANCE.

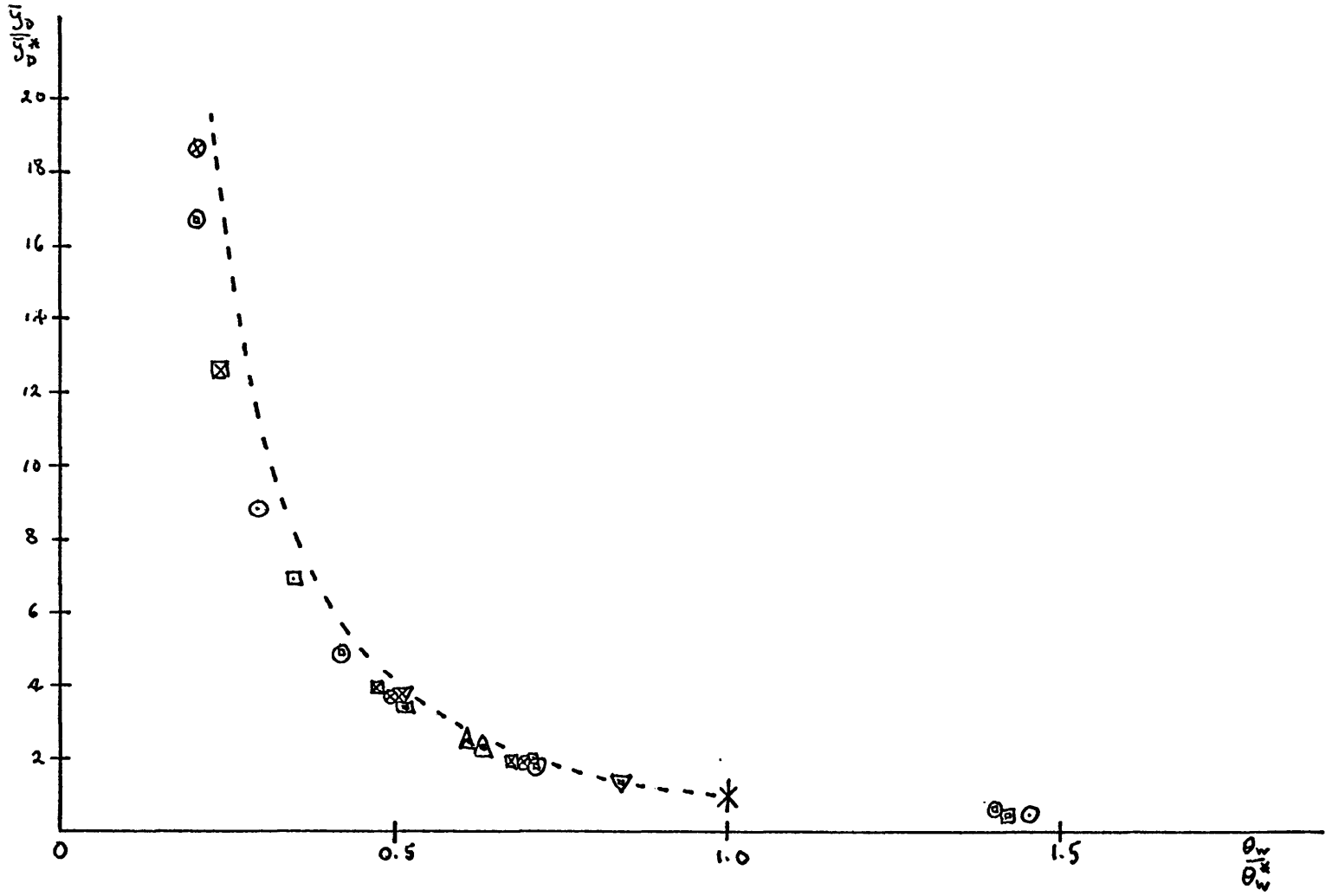

FIGURE 3(m). SIMILARITY REPRESENTATION OF THE VARIATION OF SHOCK WAVE DEVELOPMENT DISTANCE. --, $\frac{J_D}{J_D^*} = \left(\frac{\theta_w}{\theta_w^*}\right)^{-2}$.

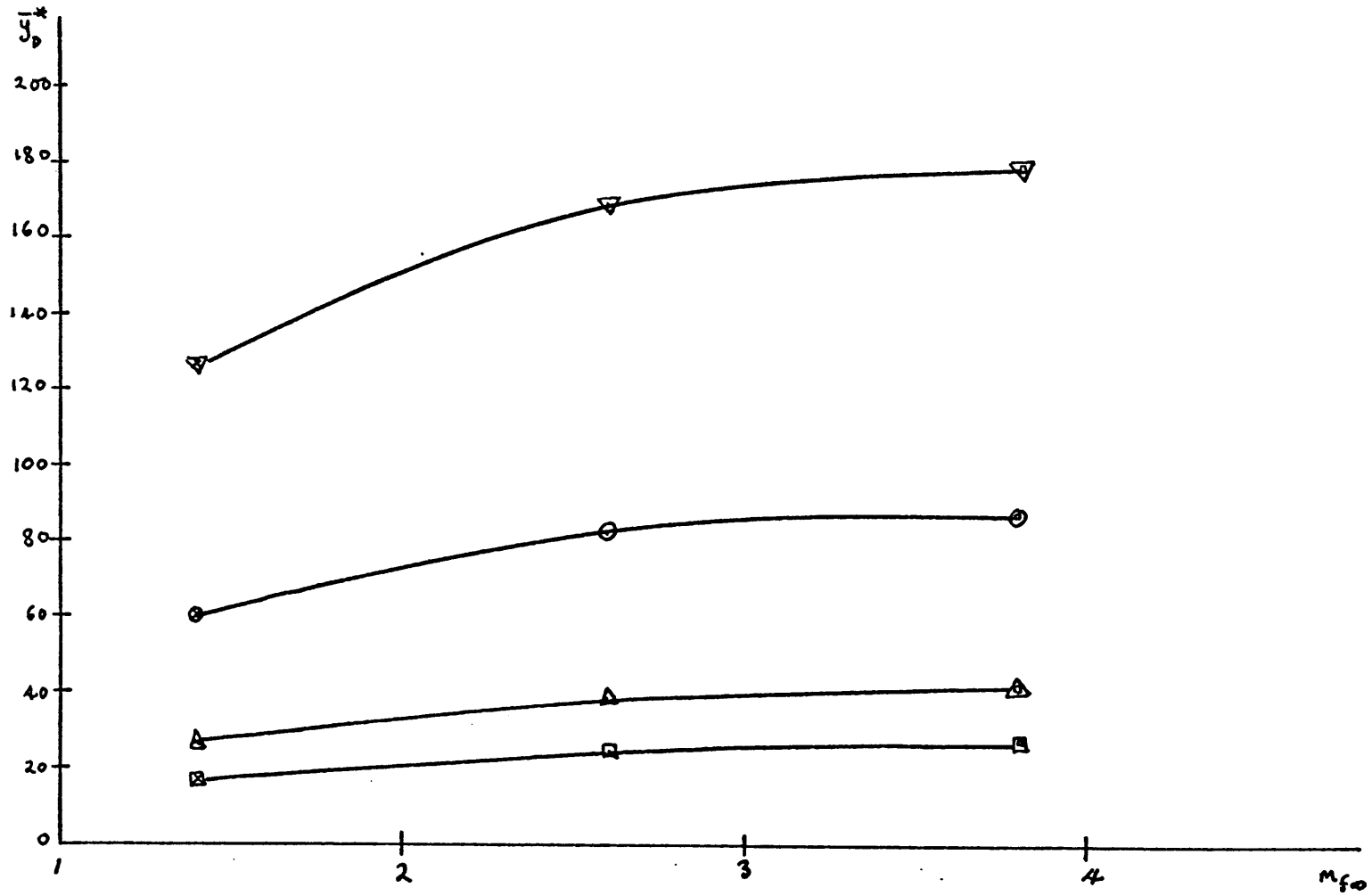

FIGURE 3(n). VARIATION OF THE CRITICAL SHOCK WAVE DEVELOPMENT DISTANCES.

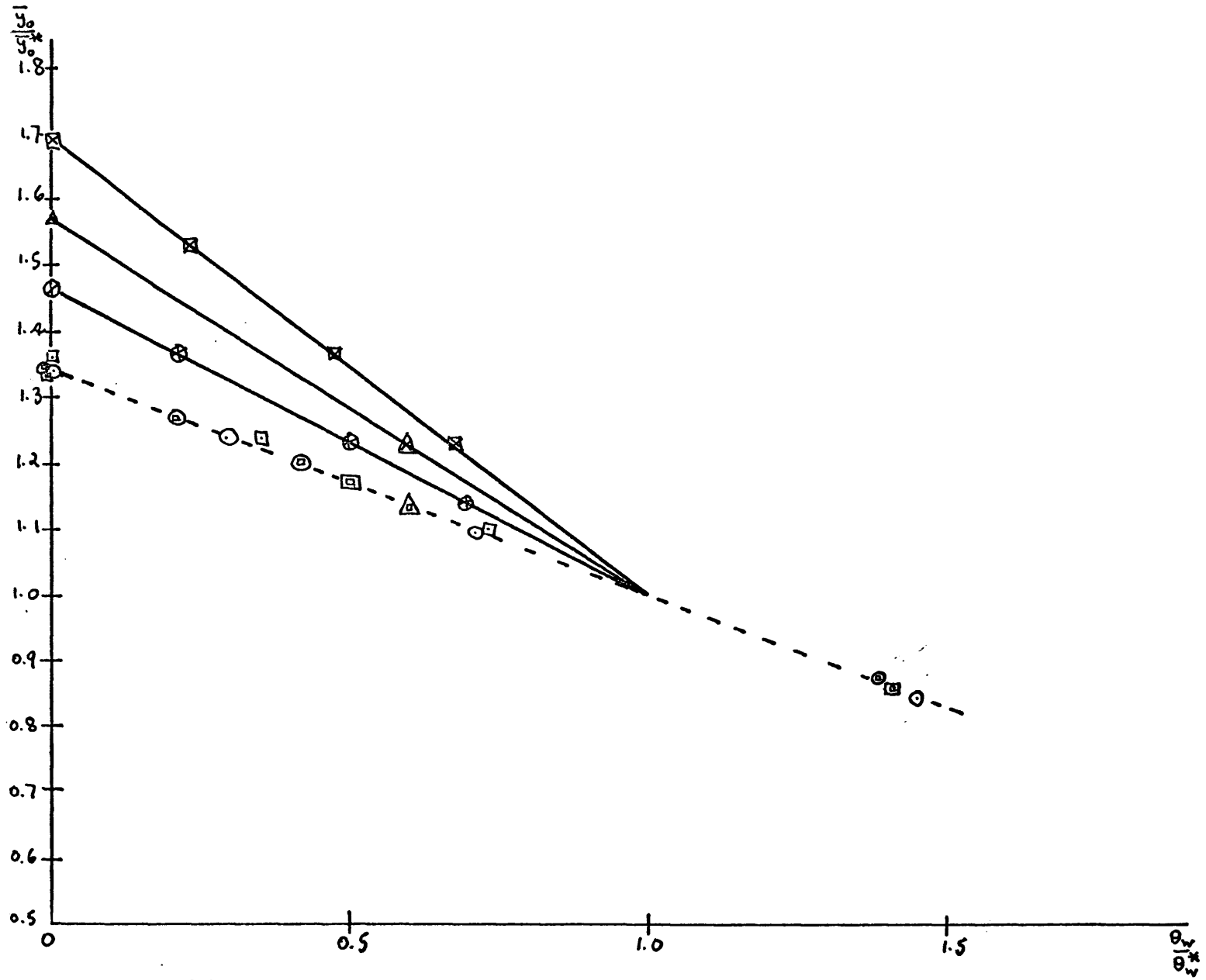

FIGURE 3(o). INITIAL, SCALED SHOCK WAVE DEVELOPMENT DISTANCES.
—, from wedge tip gradients. - -, approximate similarity rule (for $m_{f\infty} >> 1$).

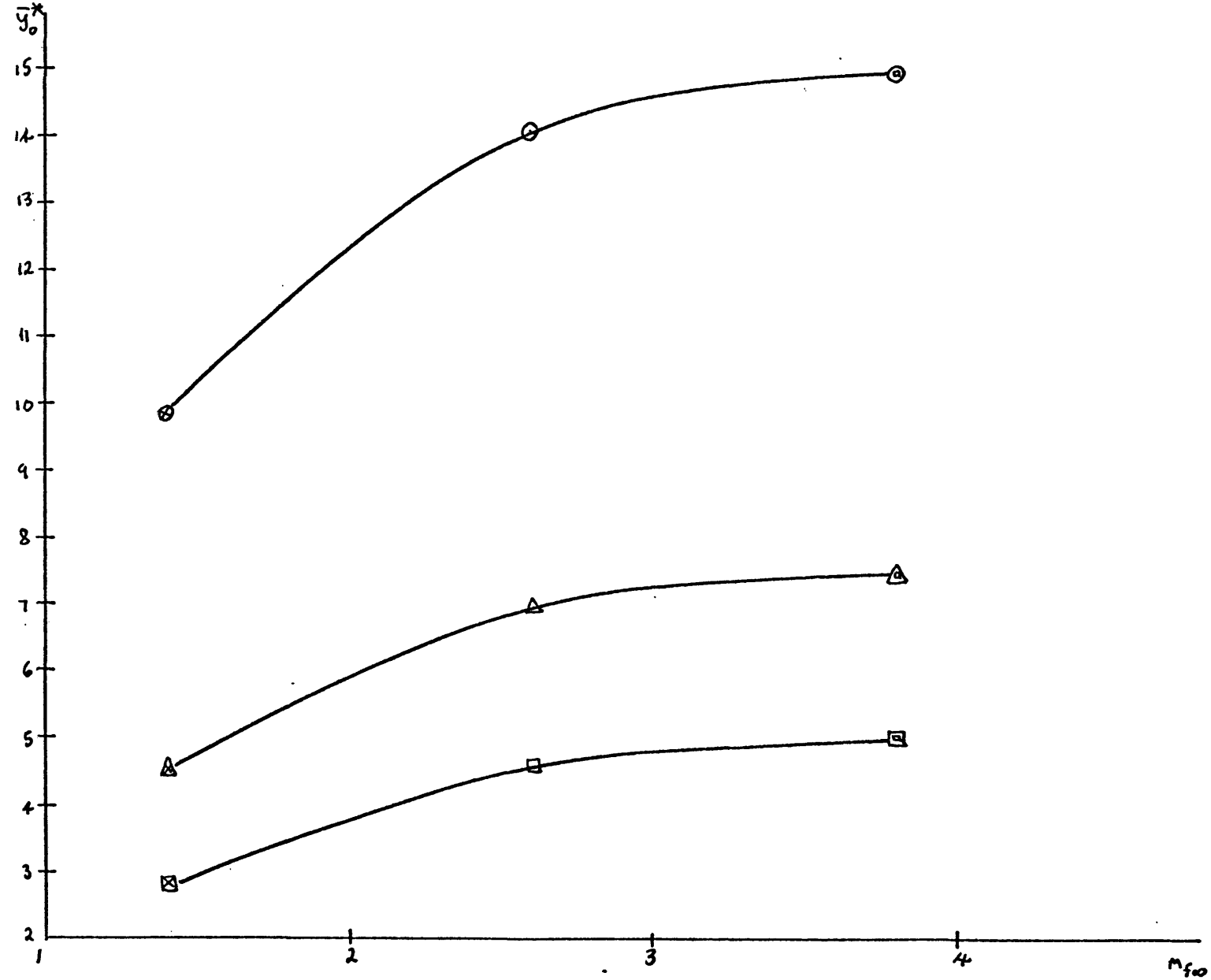

FIGURE 3(p). VARIATION OF INITIAL, CRITICAL SHOCK WAVE DEVELOPMENT DISTANCE.

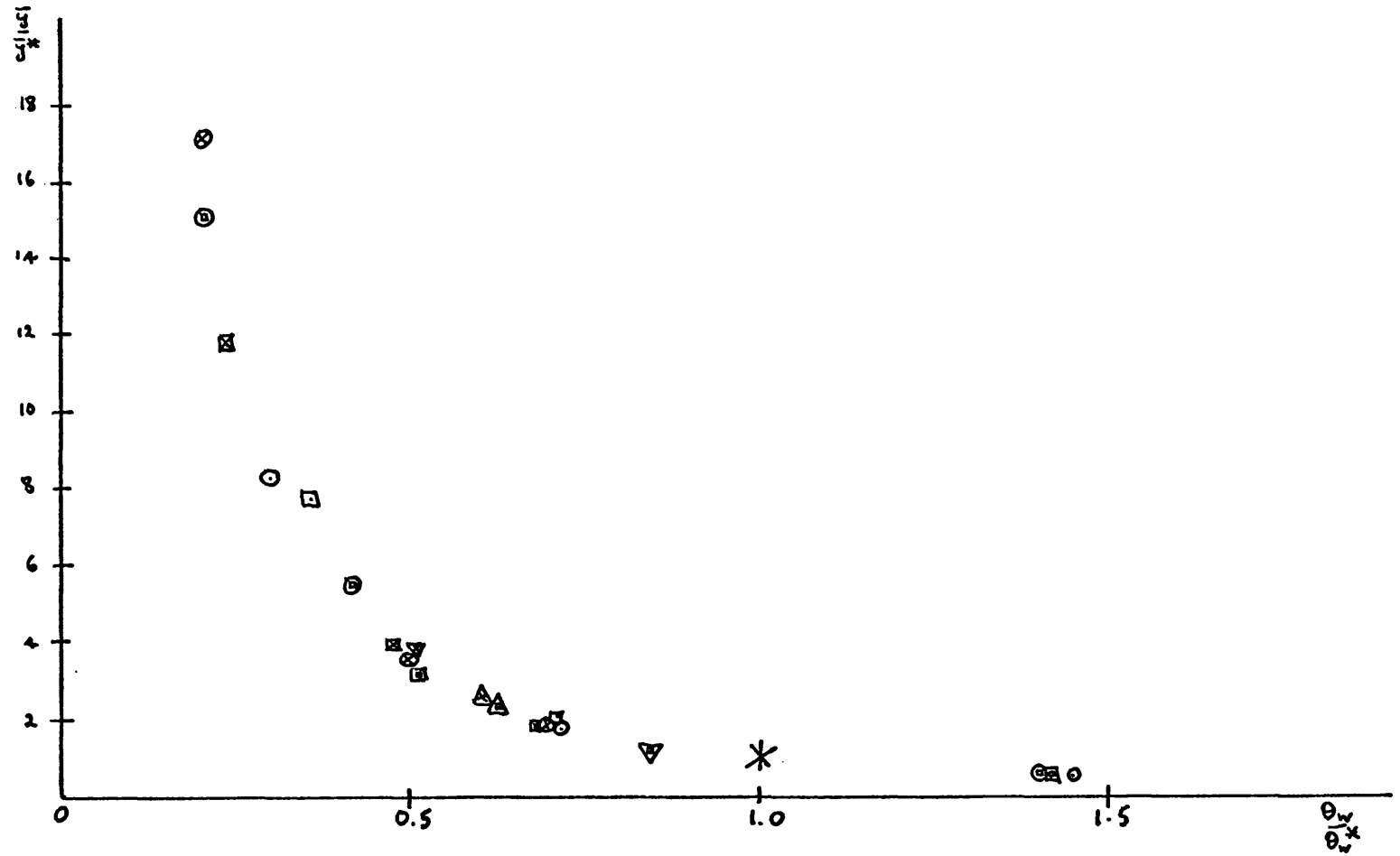

FIGURE 3(q). SIMILARITY REPRESENTATION OF THE VARIATION OF FAR-FIELD SHOCK WAVE DEVELOPMENT DISTANCE.

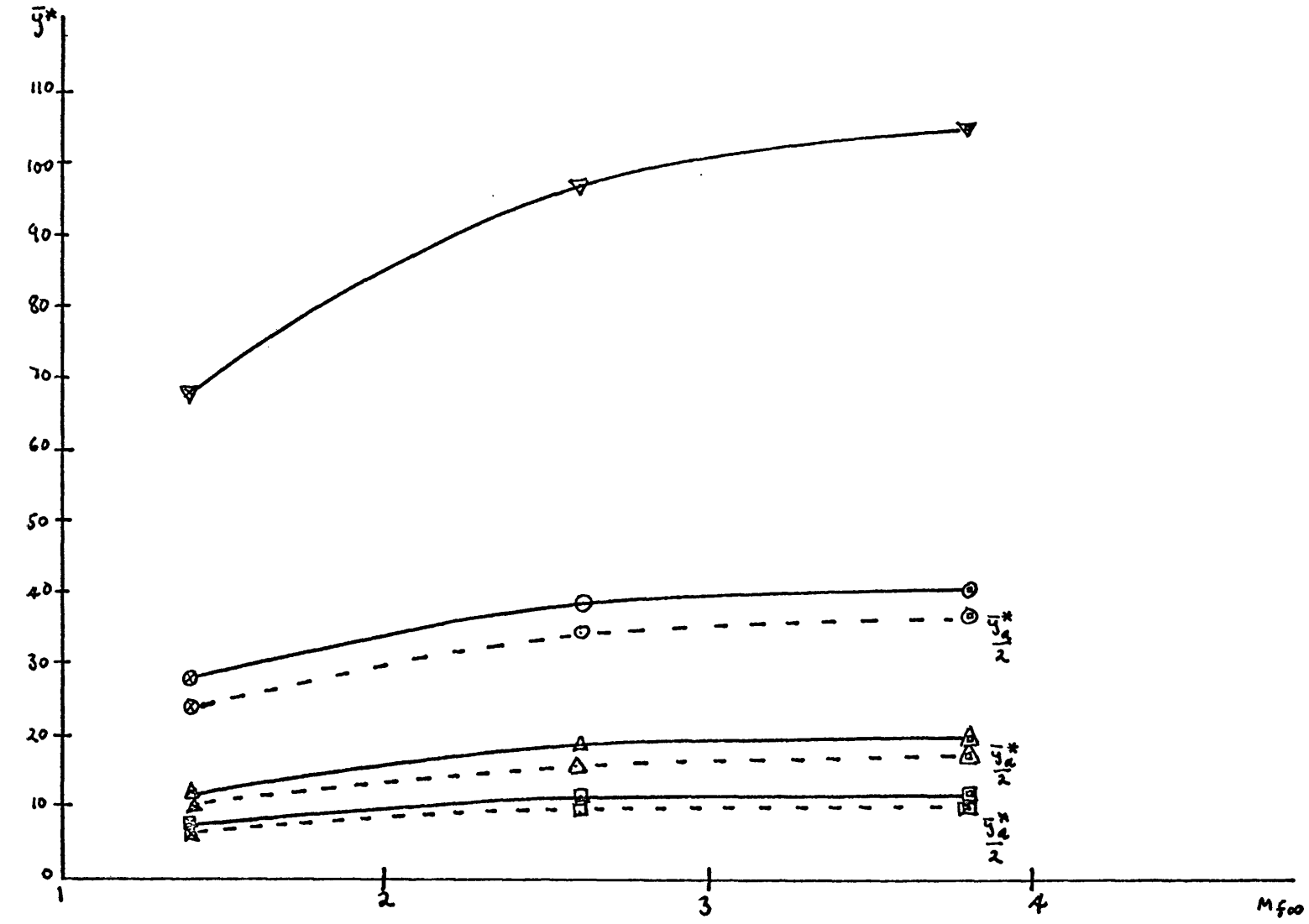

FIGURE 3(r). VARIATION OF FAR-FIELD, CRITICAL SHOCK WAVE DEVELOPMENT DISTANCE.

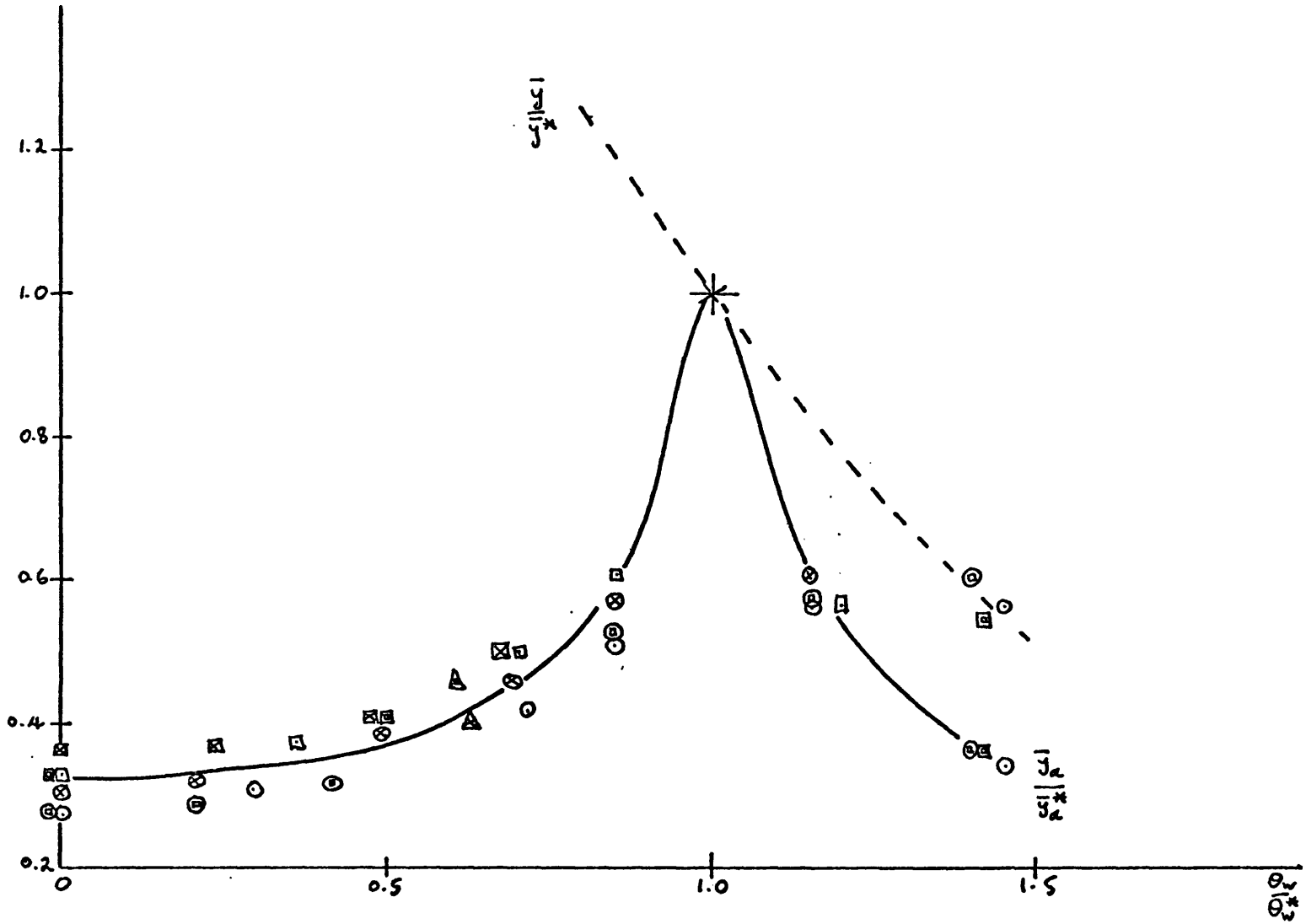

FIGURE 3(s). COMPARISON OF SCALED ALPHA-SHOCK AND SHOCK WAVE FAR-FIELD DECAY AND DEVELOPMENT DISTANCES.

C H A P T E R 4

COMPARISON OF EXPERIMENTAL RESULTS WITH THE SOLUTION BY CHARACTERISTICS.

INTRODUCTION

In section (1) we shall describe the experimental apparatus. Section (2) goes on to deal with the factors influencing the production of the desired steady flow and section (3) provides a method for determining the theoretical fringe pattern so that comparison can be made between theory and experiment.

SECTION (1)

Experimental arrangement

The Manchester University Mark 2 shock tube was used in experiments to produce the flow described in the previous Chapters. The shock tube is shown schematically in fig. 4(a). The high pressure section and first part of the low pressure section are of cylindrical cross section of 12 in. (0.305m) diameter. At a distance of 19½ tube diameters from the diaphragm station an area change scoop is used to gradually accelerate the shock into a rectangular duct of dimensions 2 in. (51mm) by 8 in. (204mm) which continues to the end of the working section. The cross sectional area then increases abruptly to 12 in. (0.305m) diameter circular in a dump chamber. The working section is filled with windows of dimensions 2 in. (51mm) by 12 in. (305mm).

The shock tube is first evacuated using rotary pumps to a pressure of about 10^{-1} N/m^2 and then diffusion pumps reduce this further to below 10^{-3} N/m^2. These very low pressures are checked with Pirani gauges. The working gases used in the experiments were CO_2 and N_2O. These gases have very similar thermodynamic properties but the former has a relaxation frequency per unit density approximately 1/6th the value of the latter (see Johannesen et al. (1962) and Bhangu (1966)). Particular attention

was paid to the purity of the gas which was slowly passed through a molecular sieve capable of reducing the dew point to 173°K. This effectively eliminates the water vapour content of the commercial gas used. This is especially important in the case of CO_2 where CO_2-H_2O collisions are known to be highly effective in providing energy exchange between the translational and rotational modes and vibration. For N_2O a crude comparison of photographed runs with dry and undried gas suggested that perhaps the effects of water vapour are less serious in this case. Nevertheless the same precautions were taken as for CO_2. In the experiments in which a pure gas was essential, the leak rate was a fraction of 0.1 N/m^2 per minute. The leak times were about 5 minutes.

The gas pressure in the low pressure section was measured on an oil manometer connected directly to the tube. The shock Mach number was found by timing the passage of the shock between 2 platinum film timing elements placed 14 in. (0.356m) apart. The signal from the last timing station, after having been passed through a suitable delay, was also used to trigger a short duration spark light source which illuminated the working section.

A wedge model was made (see fig. 4(b)) which was supported in the working section on 2 stings secured from the dump chamber. The wedge incidence was variable to such an extent that the upper face could be inclined to the freestream flow (which is defined as the uniform section of flow behind the initial shock wave) at any angle between 0° and 5°. The wedge chord was sufficiently long to ensure that there was no interaction between the expansion from the wedge trailing edge and the shock wave at the wedge tip (see fig. 4(c)), but short enough to eliminate the probability of choking in the upper channel for the freestream Mach numbers to be used. The more serious problem of choking in the channel

beneath the wedge surface was avoided by inserting a plate of thickness $\frac{1}{2}$ in. (12.7mm) and width 8 in. (0.204m) into the rectangular section of the shock tube. This plate merged smoothly with the area change and entered the working section to a position just below the wedge tip. This ensured that the expansion from the plate corner did not affect the flow on the upper surface of the wedge. The boundary layer on the plate separates at the corner as shown in fig. 4(c). From previous experiments using the plate to study expansions we were fairly certain that the channel formed between the lower surface of the wedge and separated boundary layer would be diverging (this was also a factor which influenced the choice of wedge chord). There is then no possibility of sonic flow in the lower channel for supersonic freestream flow. It was also possible to raise the wedge tip higher above the plate in order to minimise any interference to the flow above the wedge caused by the plate boundary layer.

The mechanical methods for measuring the small angles of incidence of the upper wedge face to the freestream flow were checked by an optical method. Parallel light was reflected by a plane mirror mounted in the working section on to brightly polished slip gauges placed on the upper surfaces of the wedge and plate. The inclination of the mirror to the plate was adjusted until rays of light from the plate and wedge surfaces were reflected out of the working section on to a screen. The angle between the beams emerging from the working section is twice the inclination of the upper wedge face to the horizontal. The separation of the slip gauge images on the screen is therefore simply related to the wedge incidence. By measuring the separation for several distances of the screen from a fixed reference station, one can eliminate the necessity for determining the virtual position of intersection of the two beams. These measurements were taken at the two outside edges of the wedge and

at a middle section. The 3 values so obtained for the wedge incidence were then averaged. This method was in good agreement with the mechanical methods.

Two sets of experiments were made. The first set were to ascertain whether there was enough running time (which is defined as the duration of uniform flow behind the initial shock wave) for the initially unsteady flow over the upper wedge surface to settle down into the expected steady configuration shown in fig. 4(c). To do this a conventional 2 mirror Toepler Schlieren system was employed with a parallel light beam passing perpendicularly through the working section. Both vertical and horizontal knife edges were used. The working section was focussed on to a camera plate. To accurately evaluate the density distributions within the flow a second set of experiments was made employing a Mach Zehnder interferometer with a 4 in. (0.102m) square field of view. These experiments are described in sections (2) and (3).

SECTION (2)

Running conditions and choice of gas

In this section and section (3) non-dimensional quantities will be hatted.

The schlieren runs were made with N_2 as the driver gas and N_2O as the driven gas. In these experiments the purity of the gas was not important.

The starting flow is well illustrated by the schlieren plates 1, 2 and 3. The wedge tip was placed $^1/_5$th in. (5.1mm) above the plate edge and no special attention was paid to the leading edge thickness which was about 0.2mm. In the second set of experiments the wedge tip had to be raised to about 9mm from the plate edge in order to clear

the plate boundary layer and the wedge tip was sharpened to 0.04mm. Performance calculations for the running of the tube were based on earlier experiments in the department using the plate to study expansions. In plates 1, 2 and 3 the upper wedge surface is inclined at 3° to the freestream flow the the ratio of area at the wedge trailing edge to area at the wedge tip is 0.95. To avoid choking the freestream Mach number must be above 1.25. Higher freestream Mach numbers imply higher shock Mach numbers and a reduced running time. Crudely the running time can be expressed as

$$\Delta t_R = \frac{L_{AW}}{\left(\frac{\rho_{e2}}{\rho_{e1}}\right) M_s a_{e1}}$$

where L_{AW} is the distance from the termination of the area change to the working section, Ms is the initial (equilibrium) shock Mach number and suffixes 1 and 2 refer to conditions ahead of and behind the shock.

The formation of the steady flow about the wedge is, however, intimately related to the time taken for propagation of pressure pulses between wedge surface and working section roof. This is clearly illustrated in plates 1, 2 and 3. These pressure disturbances travel at the frozen gas sound speed a_{f2} so that an estimate of the time for the formation of the steady oblique pattern would be a multiple of

$$\Delta t_F = \frac{L_{WW}}{a_{f2}}$$

where L_{WW} is the distance from the wedge surface to the working section roof. We can write this expression as

$$\Delta t_F = \frac{L_{WW}}{a_{f1}} \left(\frac{T_{e1}}{T_{e2}}\right)^{\frac{1}{2}} = \frac{L_{WW}}{a_{f1}} \left(\frac{p_{e1}}{p_{e2}}\right)^{\frac{1}{2}} \left(\frac{\rho_{e2}}{\rho_{e1}}\right)^{\frac{1}{2}}$$

An important consideration is how $\frac{\Delta t_F}{\Delta t_R}$ varies with incident shock Mach number. According to the above model we can write

$$\frac{\Delta t_F}{\Delta t_R} = \left(\frac{\gamma_e}{\gamma_f}\right)^{\frac{1}{2}} \frac{L_{WW}}{L_{AW}} M_s \left(\frac{\rho_{e2}}{\rho_{e1}}\right)^{\frac{3}{2}} \left(\frac{p_{e1}}{p_{e2}}\right)^{\frac{1}{2}}$$

Using Rees (1968) results for equilibrium flow ratios for normal shocks we can show that this expression increases with increasing Mach number. This suggests that experiments should be confined to low freestream Mach numbers. Experiments carried out with initial shock Mach numbers of about 4 (corresponding to freestream flows of about Mach 2) gave unsatisfactory results because of interference from the secondary contact surface (caused by the area change) before the flow was steady. The best results were obtained with initial shock Mach numbers of about 3 (as in plates 1 to 8) corresponding to freestream flows of about Mach 1.7. The running times are then in the region of 600 μs. Plate 4 shows the flow initiated by a shock of Mach number 2.9 250 μs after it passed over the wedge tip. Plate 5 shows the same flow 420 μs after the initial shock wave passed over the wedge tip. In ideal gas flows over wedge surfaces it is well known that any apparent thickening of the shock wave is due to sidewall boundary layer interaction. In our experiments, however, there is the additional shock thickening due to relaxation. These two effects are highly coupled because the relaxation effects ease the pressure gradients through the shock and consequently render any shock-boundary layer interaction less severe. In plates 1 to 5 the bluntness effects are clearly visible from the expansion along the separation bubble near the wedge tip. Of particular interest is the reflected wedge tip shock which still seems to be in the process of forming in both plates 4 and 5.

Having established that the flow would not choke and selected a suitable Mach number range for which the observed flow was steady, a second set of experiments was made using an interferometer to evaluate the density distributions. It was decided that the undisturbed fringes should be vertical (by aligning them with the vertical face of the plate) so that the thickness of the boundary layers on the plate and working section roof could be estimated. The boundary layers on the working section windows would

presumably have similar thicknesses. This could be important in gauging the effects of shock-boundary layer interaction on the expected two-dimensional flow over the upper wedge surface. Filtered light of wavelength 442.5 nm. and bandwidth 4 nm. was used so that the whole density flowfield could be evaluated.

The flow coordinates have been non-dimensionalized in the following manner

$$\left\{ \begin{matrix} x \\ y \end{matrix} \right\} = \frac{(RT_\infty)^{\frac{1}{2}}}{\rho_\infty \underline{\Phi}_\infty} \left\{ \begin{matrix} \hat{x} \\ \hat{y} \end{matrix} \right\} \equiv \frac{(RT_\infty)^{\frac{3}{2}}}{\rho_\infty \underline{\Phi}_\infty} \left\{ \begin{matrix} \hat{x} \\ \hat{y} \end{matrix} \right\}$$

In the shock tube, for fixed initial Mach number, it is most convenient to vary ρ_∞ (by changing the pressure in the low pressure section) or $\underline{\Phi}_\infty$ (by changing the gas). To vary T_∞ would involve heating or cooling the low pressure gas prior to the passage of the initial shock. Ideally one would like to be able to choose a pressure for which the shock wave development length is less than the distance between upper wedge surface and working section roof. This value of the pressure, however, must not scale the relaxation length so dratically that density measurements are difficult to make. The working section windows can withstand an excess pressure of just 1 atmosphere and the fringe shift across the flow also depends on freestream pressure. These factors must be taken into consideration and optimized. The gases CO_2 and N_2O were chosen because their similar thermodynamic properties (but differing relaxation frequencies) enables one to scale the flow dimensions without changing the freestream pressure. These gases also have large vibrational specific heats at moderate temperatures (the characteristic temperature of vibration of the bending modes for CO_2 is 959°K. The bending modes for N_2O have a characteristic temperature of 847°K).

The results of Chapter 3 indicate clearly how the flow wave development distance decreases with increasing vibrational specific heat. One

therefore has the chance with these gases of being able to investigate the portion of flow of interest within the confines of the working section. The value of θ_w^* also increases as ϵ_{vib} increases (for constant freestream Mach number) so that one can use wedge angles of a few degrees, with a measurable fringe shift across the flow.

Thermodynamic data referring to vibrational specific heats and flow changes across normal shock waves (in CO_2 and N_2O) were obtained from Rees (1968). Data on vibrational relaxation frequencies were found from Bhangu (1966) (for N_2O) and Johannesen et al. (1962) (for CO_2).

The first runs were with N_2O in the low pressure section at a pressure of 2.30 kN/m^2. The upper face of the wedge was set at 2^o incidence and the driver section was filled to a pressure of 140 kN/m^2 with N_2. The initial shock Mach number was measured as 2.92 corresponding to an equilibrium Mach 1.68 flow over the upper wedge surface. The vibrational specific heat, relaxation frequency per unit density, pressure and temperature in the freestream were calculated as 2.28R, 5.3×10^6 s^{-1} $amagat^{-1}$, 21.8 kN/m^2 and 583^oK. These conditions correspond to a fully dispersed wave flow at infinity with $\frac{\theta_w}{\theta_{w^*}} \simeq 0.5$. The results of Chapter 3 indicate that in this instance the development distance is approximately 60mm whereas the distance available in the working section is only 30mm. This flow is shown in plate 6. The second set of runs were with CO_2 as the driven gas. The starting conditions were almost identical to those when N_2O was used. The initial shock Mach number was measured as 2.92. The vibrational specific heat, relaxation frequency per unit density, pressure and temperature in the freestream were calculated as 2.19R, 0.89×10^6 s^{-1} $amagat^{-1}$, 22.4 kN/m^2 and 597^oK. The value of the gas constant per unit mass was taken as $189 J/kg^oK$ (both N_2O and CO_2 have the same molecular weight). For this flow the development

distance is 320mm. The relaxation regions are also correspondingly magnified. Comparison of plates 6 and 7 amply illustrate the scaling function of the relaxation frequency. Plate 8 shows the N_2O flow with an 'infinite fringe' setting. Here fringes correspond to constant density contours.

These flows will be discussed in more detail in the next section where a comparison is made with a theoretical prediction of the density distribution by the method of characteristics. The theory assumes that the flow is perfectly two-dimensional, that the wedge tip has no bluntness and that viscous effects can be neglected.

SECTION (3)

Method for finding the fringe system from the computed density field; comparison of theory and experiment for 2 gas flows

The method of characteristics (with $^1/_{50}$th of the variation of σ per step) was used to compute the theoretical density field for the shock tube runs in CO_2 and N_2O described in the last section. These computations gave the density at the mesh points along the negative characteristics and from this information the fringe system can be found as follows.

Let the undisturbed fringe spacing be d and assign to each freestream fringe a number given by its x coordinate $x_{fr\infty}$. The locus of a freestream fringe through the non-equilibrium regions of flow is consequently assigned the same number as the freestream fringe. The fringe shift along the locus is measured as the number of freestream fringes that the locus is displaced from the freestream fringe with the same number. This is a local quantity and will be denoted by $\Delta N(x, y)$. The relation that must hold along the locus of a fringe is therefore

$$\Delta N(x,y) \times d = x - x_{fr\infty} \qquad 3.1$$

The fringe shifts are, however, related to the density field by the Gladstone-Dale law so that

$$\Delta N(x,y) = \frac{DK}{\lambda \rho_0} \left(\rho(x,y) - \rho_\infty \right) \qquad 3.2$$

where D is the width of the shock tube working section. K is the Gladstone-Dale constant for the light of wavelength λ and ρ_0 is the density of the gas at N.T.P. We employed light of the same wavelength as Johannesen et al. (1962) (who give $\frac{DK}{\lambda}$ equal to 209.2 for CO_2) and Bhangu (1966) (who gives $\frac{DK}{\lambda}$ equal to 240 for N_2O).

We therefore evaluate the density field in terms of fringe shifts from 3.2 and then satisfy 3.1 directly. In order to obtain a solution to 3.1 we must assume that the changes between neighbouring mesh points are linear. Then at each mesh point on a negative characteristic in the flow we test whether the quantity

$$\Delta N(x,y) \times d - x + x_{fr\infty}$$

is positive or negative and if it is positive at one mesh point and negative at its neighbour then it must be zero inbetween. Let suffix j indicate the j^{th} mesh point from the wedge surface along a negative characteristic. Then fringe coordinates (x_{fr}, y_{fr}) must satisfy

$$\left(\Delta N(x_j, y_j) \times d - x_j + x_{fr\infty} \right) \left(\Delta N(x_{j+1}, y_{j+1}) \times d - x_{j+1} + x_{fr\infty} \right) \leq 0$$

and

$$x_{fr} = x_j - \frac{\left(\Delta N(x_j, y_j) \times d - x_j + x_{fr\infty} \right) (x_{j+1} - x_j)}{\left(\Delta N(x_{j+1}, y_{j+1}) \times d - x_{j+1} - \Delta N(x_j, y_j) \times d + x_j \right)}$$

$$y_{fr} = y_j - \frac{\left(\Delta N(x_j, y_j) \times d - x_j + x_{fr\infty} \right) (y_{j+1} - y_j)}{\left(\Delta N(x_{j+1}, y_{j+1}) \times d - x_{j+1} - \Delta N(x_j, y_j) \times d + x_j \right)}$$

These equations furnish the locus of the freestream fringe with x coordinate $x_{fr\infty}$. The process can then be repeated to determine all fringes.

For ease of observation the experimental and theoretical fringe patterns were magnified by a factor of 10.1. The first results we compare are for N_2O. Fig. 4(d) shows what a fringe would look like at 'infinity' (in this case at approximately 60mm above the wedge). Fig. 4(e) gives a more detailed comparison between theory and ezperiment. Of particular importance here are the effects of the wedge bluntness which can be seen by observing plate 6 near the wedge tip. Bardsley (1951) and Bardsley and Mair (1952) have studied bluntness effects in ideal gas flows. Their results indicate that boundary layer separation at the body nose will not occur if the Reynolds number based on the leading edge thickness is below 1000. In our experiments this Reynolds number was calculated as 200. Even so, close examination of plates 6 and 7 does indicate an expansion region downstream of the wedge tip. Sharp (1959) has given a characteristics calculation of the flow of an ideal gas over a separation bubble.

For blunted wedge ideal gas flow the bow shock decays to an oblique shock giving a flow deflection parallel to the wedge surface. Moreover, for the supersonic flow, disturbances are propagated along the Mach lines so that to any straight portion of the body there corresponds a uniform section of the shock. If one compares the detached shock with the oblique shock from a perfectly sharp wedge with tip lined with the blunt wedge face then the shock due to the blunt wedge will lie above that due to the sharp one. The situation when the gas is relaxing, though more complicated is qualitatively the same. The shock displacement due to bluntness is apparent in fig. 4(e) where the theoretical shock locations (see fringe 1) lie below those due to experiment. The fringe

shift is also larger initially than one would expect. Fringes 3 and 4 give good agreements between theory and experiment but fringe 5 is not so good. This could be due to the shock wave still being unsteady. The photographs were taken 300 μs after the initial shock passed over the wedge tip. This time is sufficient for a disturbance from the wedge to propagate 4 times between wedge surface and working section roof. The running time is about 600 μs . This effect could also be due to shock-boundary layer interaction on the working section roof. The thickening of the boundary layer can be seen quite clearly in plate 6.

Fig. 4(f) gives the same comparison for CO_2. Because the relaxation frequency is about $^1/6$th of that for N_2O the relaxation effects take place over correspondingly magnified distances. The same effects are discussed for N_2O are present here (see fringe 1) but the interaction of the shock wave with the side window boundary layers is much more clearly exhibited. M^{c}Cabe (1966) has studied such three-dimensional interactions in ideal supersonic gas flows round wedges. The interaction is the more severe the steeper the pressure gradient and hence is shown better in fig. 4(f) since the alpha-shock has not yet decayed. The region of the interaction spreads with distance from the wedge surface. This is possibly the reason why the fringes are not visibly discontinuous at the alpha-shock. M^{c}Cabe finds that the shock strength is maintained during the interaction so that comparison of fringes 2, 3 and 4 gives reasonable agreement between theory and experiment for the alpha-shock decay. The variations within the relaxation region are also predicted with reasonable accuracy.

In conclusion the agreement between the theory and experiment has been shown to be qualitatively good. Any discrepancies between theory and experiment have been due to limitations in the experiment's being able

to faithfully reproduce the desired flow. We are confident that the theory gives a more exact evaluation of the flow than experiment and consequently the bulk of our results are numerical.

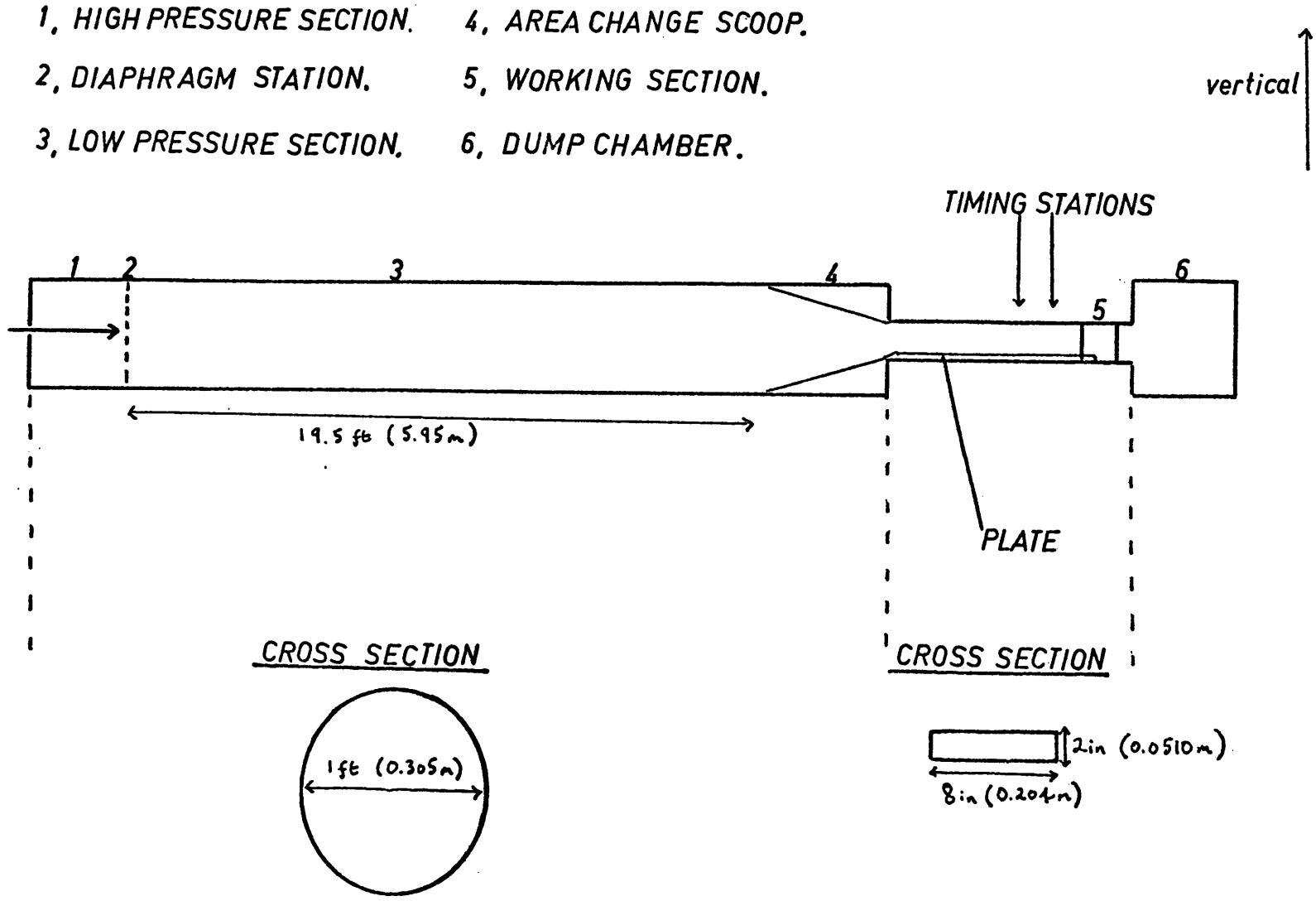

FIGURE 4(a). MANCHESTER UNIVERSITY MARK 2 SHOCK TUBE. (vertical scale exaggerated)

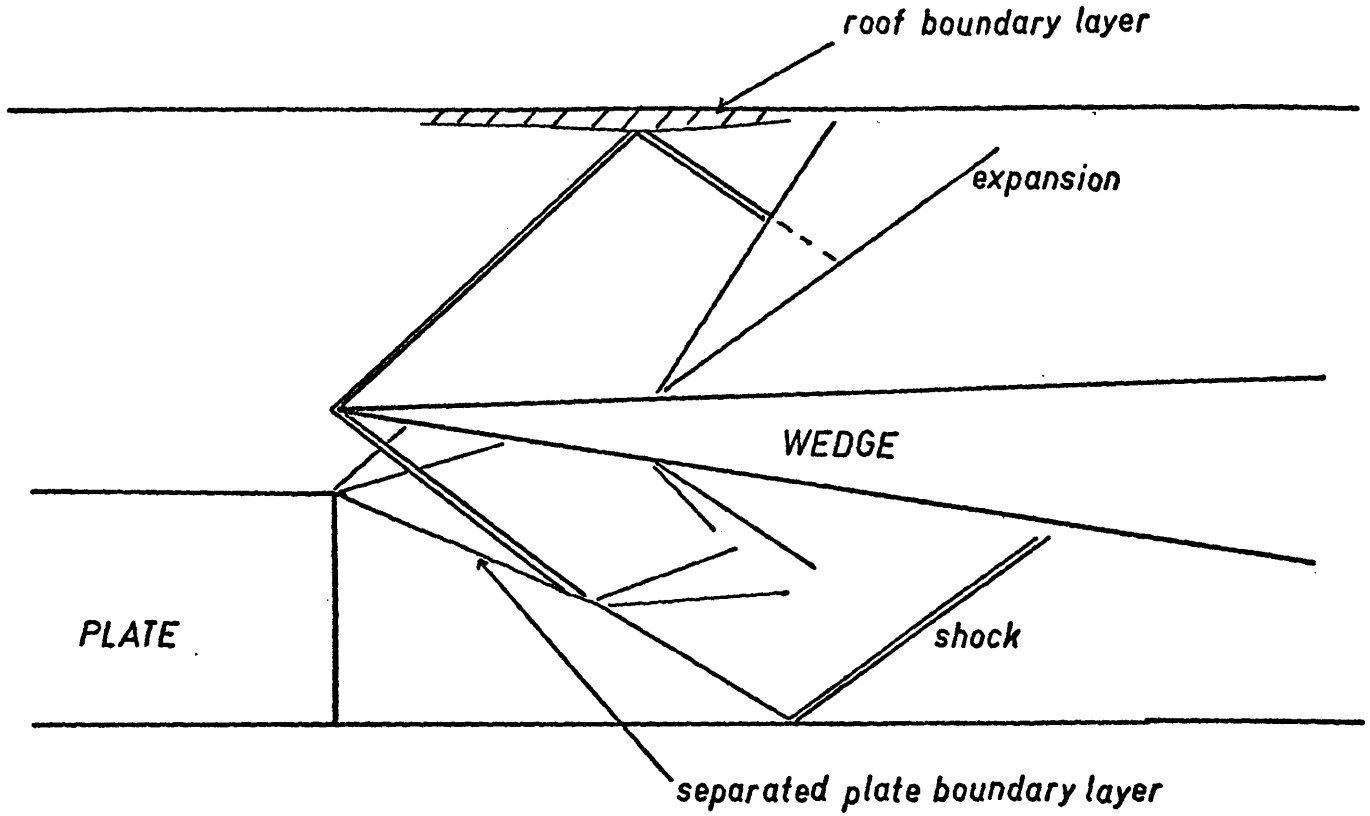

FIGURE 4(c). SIMPLIFIED FLOW PATTERN.

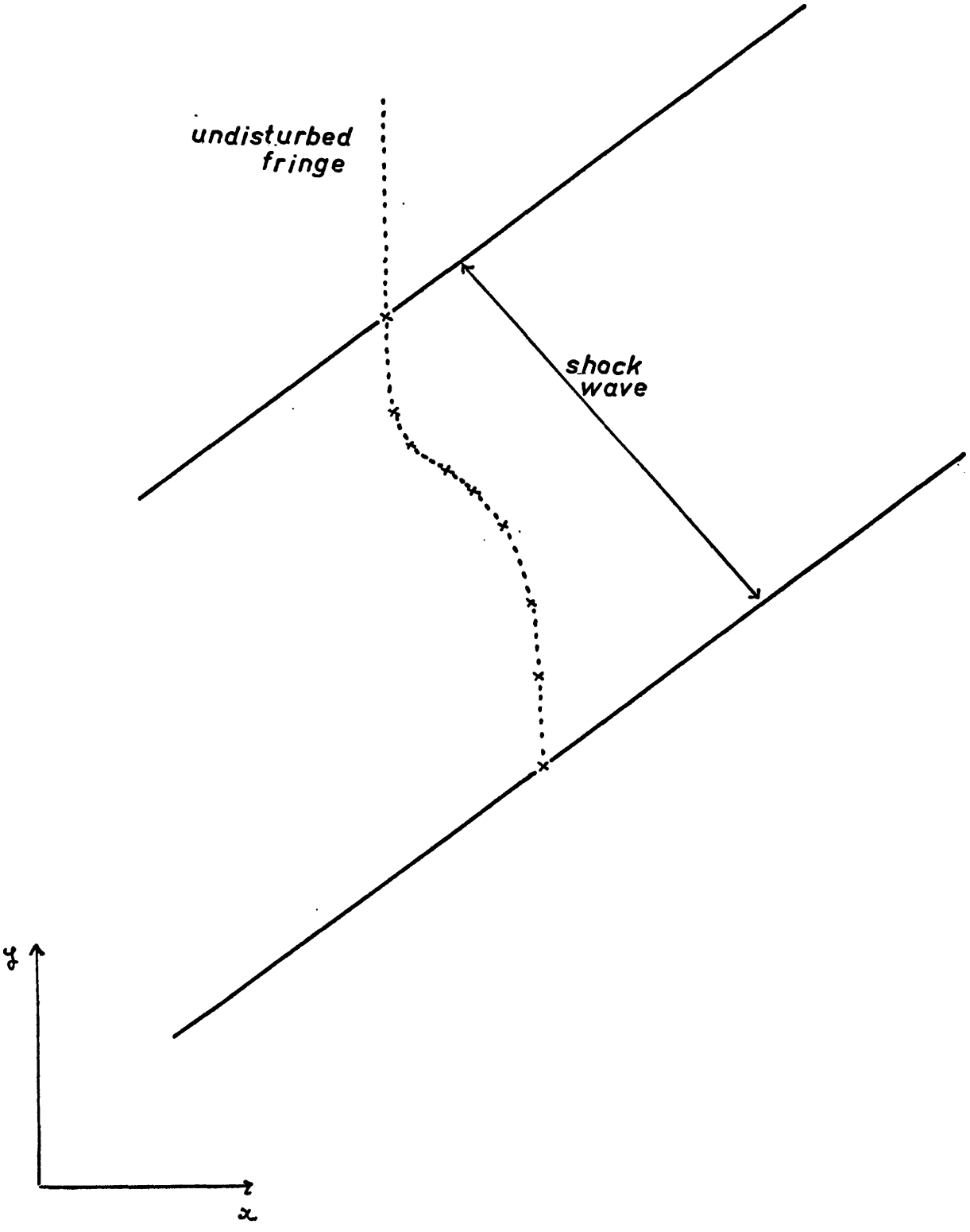

FIGURE 4(d). LOCUS OF A FRINGE THROUGH THE SHOCK WAVE AT INFINITY. $\theta_w = 2°$, $m_{\infty} = 1.68$ and $c_{vib} = 2.28$. Gas, N_2O. Magnification, 10.1. d=12.5 mm.

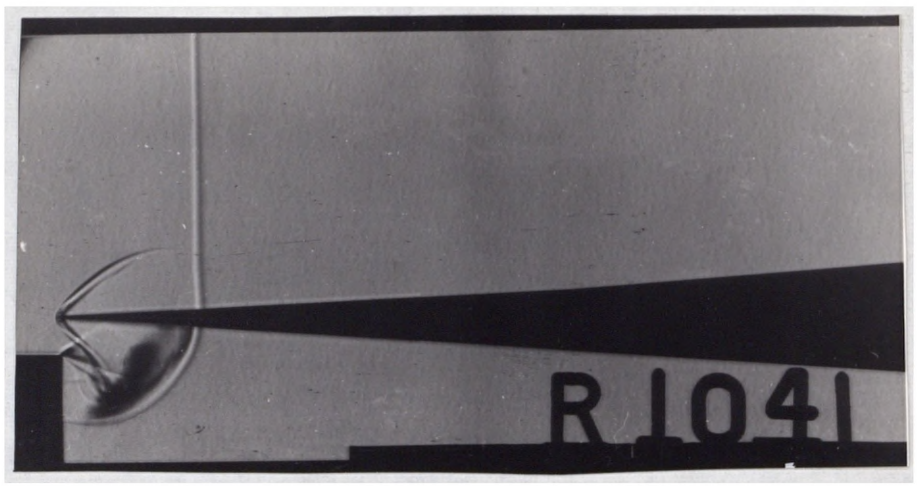

PLATE 1

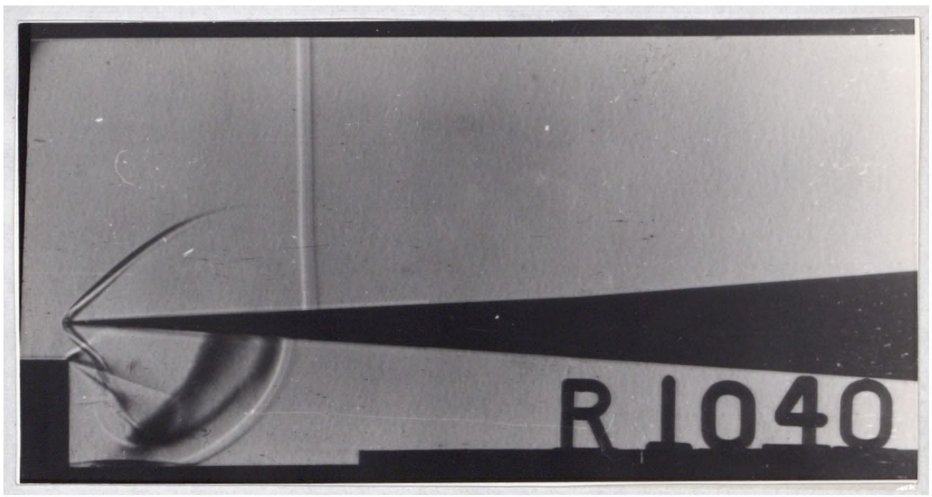

PLATE 2

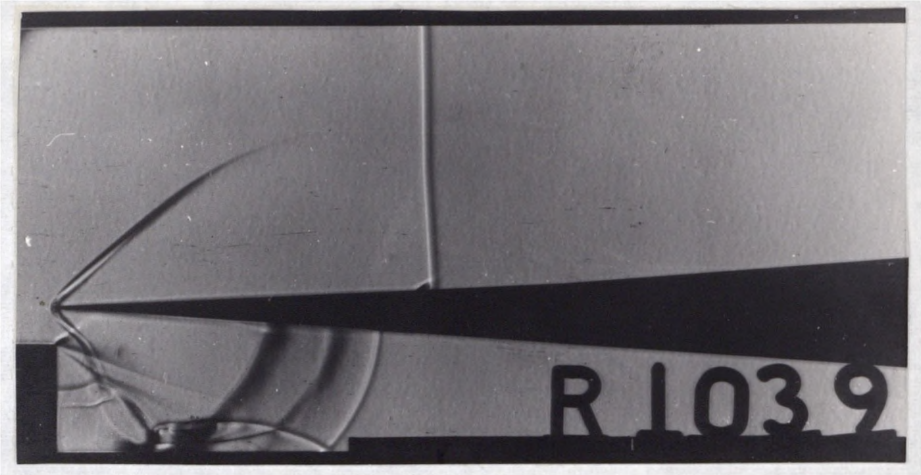

PLATE 3

PLATE 4

PLATE 5

PLATE 6

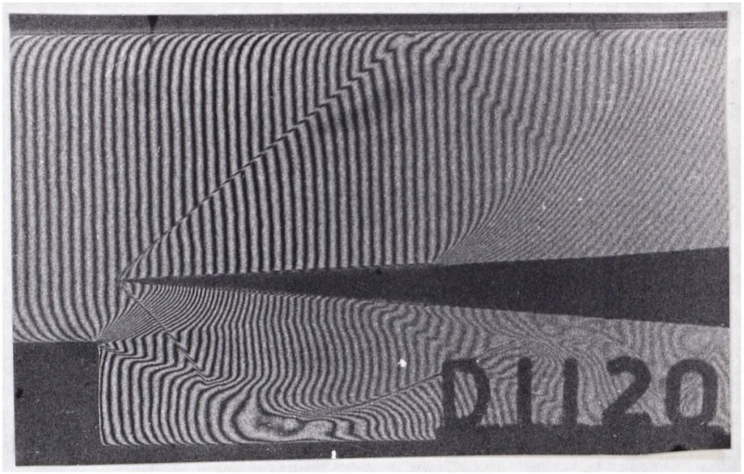

PLATE 7

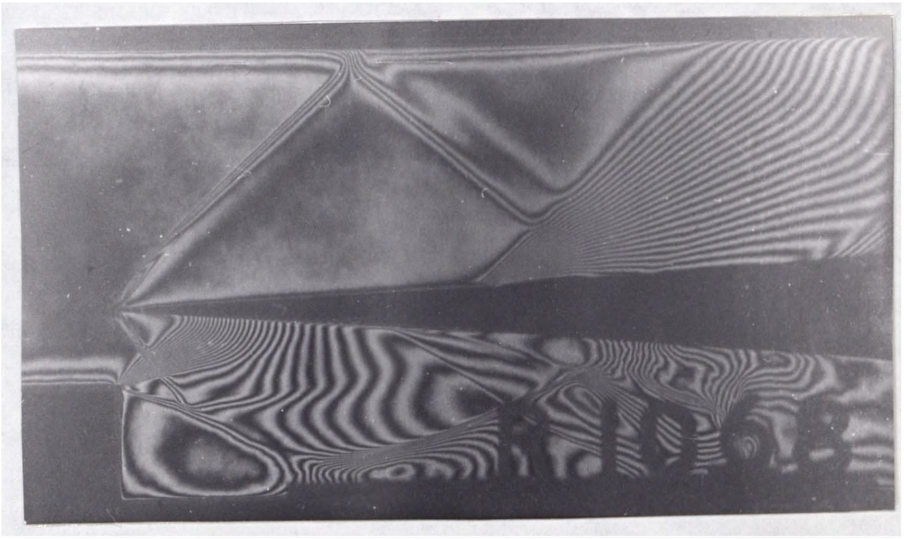

PLATE 8

CHAPTER 5

ANALYTIC PROCEDURES FOR WEAK WAVE RELAXING GAS FLOW OVER A WEDGE.

SECTION (1)

INTRODUCTION

So far a numerical solution, together with certain restricted analytic results, has been presented. In sections (1) and (2) we shall discuss in more detail the analytic approximation schemes that are available for solving weak wave relaxing gas flows over wedge surfaces. The comparison made in section (3) between the numerical method of characteristics and the analytic method of matched asymptotic expansions gives some idea of the accuracy involved. However, because the characteristic calculations cannot be extended to extremely weak wave flows (for reasons of cost) the comparison is perhaps not as good as it could be. Section (4) investigates the application of Whitham's rule to the decay of alpha-shocks in relaxing gases. In particular this rule furnishes the variation in alpha-shock angle with distance from the wedge surface. We start in section (1) with all variables in dimensional form. We can then discuss, without confusion, the length scales introduced into the flow when the gas is relaxing.

A review of non-linear wave propagation has been given by Lick (1971). Here we shall be specifically concerned with the flow of a relaxing gas about a thin pointed wedge.

If we consider the two-dimensional supersonic ideal gas flow about a pointed wedge of infinite chord then since there are no length scales in the problem the flow must be conical and consequently uniform downstream of the shock. If, however, the gas is relaxing then we introduce a time scale into the problem given by $\frac{1}{\rho_\infty \Phi_\infty}$ (the relaxation time). The gas consequently relaxes over a distance (measured in the freestream direction) $L_1 = \frac{V_\infty}{\rho_\infty \Phi_\infty}$ which furnishes the basic length scale in the flow. However, if we wish to characterize the whole flow

then we must introduce additional length scales L_2 and L_3 based on the shock wave width at infinity and shock development distance respectively. For weak wave flows we shall show in section (2) that $L_2 = 0\left(\frac{L_1}{\theta_w}\right)$ and $L_3 = 0\left(\frac{L_1}{\theta_w^2}\right)$. The thermodynamic variables and the velocity are non-dimensionalized as in section (1) of Chapter 1. If we non-dimensionalise the coordinates with respect to L_1 and assume a power series representation for each of the thermodynamic and velocity variables then we expect the approximations obtained by substitution of the power series into the governing equations to be valid only near the wedge surface. The first approximation in such a scheme made by neglecting terms of $O(\theta_w^2)$ gives the well known linear solution. This solution has been obtained by Chu (1958) and Clarke (1960); the results were generalized by Vincenti (1962) to the case where the freestream is not in equilibrium. Explicit exact solutions to the linear problem can be obtained along the leading Mach line (which is the linear approximation to the alpha-shock) and along the wedge surface. Generally, however, the solution is not explicit but approximations that do render it so have been made by Moore and Gibson (1960) and Sussman and Baron (1967). The correct equilibrium flow far downstream is predicted though the alpha-gas entropy layer is uniform since in this approximation the flow is irrotational. Lee (1964) by employing a linear perturbation about the frozen flow at the wedge tip was able to investigate the variations through the alpha-gas entropy layer in certain restricted cases.

The equivalent approximations have also been tried in characteristic coordinates. Lin's (1954) linear characteristic perturbation method gave a uniformly valid solution to the ideal gas flow over aerofoil sections whereas the straightforward linear theory was correct only near the aerofoil. The same procedure, however, does not give a uniformly valid solution when the gas is relaxing (see Clarke (1965), Lick (1967)

and Chu (1970)). An asymptotic analysis of the far-field behaviour of the solution (Clarke (1965)) shows that the width of the relaxation region grows like the square root of the distance from the wedge surface. The straightforward linear analysis exhibits the same type of deficiency in the far-field solution (Moore and Gibson (1960)). This is due to not including in the first approximation those non-linear terms which grow to first order over large distances. An analysis by Romberg (1970a) gives a set of corrected first order equations in characteristic coordinates, though no solution is given.

To gain any insight into the far-field flow we must non-dimensionalize the coordinates with respect to the length scales L_2 (x coordinate) and L_3 (y coordinate). L_2 is derived from the known solution at infinity. L_3 is found by considering when the linear solution is inconsistent with the L_2 scale. The solution in the far-field can be obtained by the method of matched asymptotic expansions (see Van Dyke (1964)). Having located where the non-uniformity in the linear ('outer') solution arises, we define new coordinates of O(1) in this region. The thermodynamic and velocity variables are non-dimensionalized in the same way as before and the same power series representation is used though the coefficients are now written as functions of the new coordinates. The power series are substituted into the governing equations and coefficients of θ_w are equated to zero. Physically, this procedure re-estimates the magnitude of the gradients in the flow. The linear theory assumes that x and y derivatives are of the same order and hence is not a valid approximation in the far-field; the new procedure correctly assumes that the y derivatives are an order of magnitude smaller in the wedge angle than the x derivatives.

Solutions by the method of matched asymptotic expansions for the near and far-field flow have been obtained by Ockendon and Spence (1969)

for the one-dimensional unsteady case and by Blythe (1969) who treats both the one-dimensional unsteady and two-dimensional steady problems. We have mentioned that the steady and unsteady flows are closely related. It will be sufficient here to regard the piston Mach number in the unsteady case to correspond to the wedge angle in the steady case and the y coordinate to be 'time-like'. Ockendon and Spence give an analysis in terms of 2 small parameters. For simplicity they consider small values of the vibrational specific heat. For small times they find that the flow is essentially linear but for intermediate and large times non-linear effects are important unless the wave is very weak $\left(\frac{\theta_w}{\theta_w^*} \ll 1 \right)$. With this restriction the flow is linear except in the far-field at times of the order of the inverse piston Mach number squared where Burgers's equation is valid. Blythe (1969) derives essentially the same results as Lick (1969) who has solved the same problem by the method of multiple scales. This method dispenses with the need for matching by assuming from the outset a generalized perturbation expansion in several stretched coordinates. For example for steady two-dimensional supersonic flow of a relaxing gas we would expand the pressure as

$$p = \sum_{n=0}^{N} \theta_w^n p_n \left(x_0, x_1 \ldots x_{N-1} ; y_0, y_1 \ldots y_{N-1} \right)$$

where we assume

$$x_n = \theta_w^n x \quad \text{and} \quad y_n = \theta_w^n y .$$

Substitution of expansions like these into the governing equations of motion give the usual linear solution in the first approximation and Burgers's equation for the far-field flow (where $y = O(1/\theta_w^2)$) in the third approximation. This is providing that the shock wave is weak enough for non-linear effects to be important only in the far-field. To ensure that the expansions are uniformly valid the ratios $\frac{p_n}{p_{n-1}}$, $n = 1, 2, 3 \ldots$ must remain of O(1) as $\theta_w \to 0$. The requirement for this is that (Van Dyke 1964) "each approximation shall be no more singular than its predecessor - or vanish no more slowly - as $\theta_w \to 0$ for arbitrary values

of the independent variables. The same shall be true of all derivatives". This method has also been successfully applied by Chong and Sirovich (1971) to steady supersonic two-dimensional flows governed by the Navier Stokes equations.

Romberg (1970b) has applied the method of matched asymptotic expansions to the one-dimensional unsteady flow of a binary mixture of relaxing gases created by an impulsively started piston. In particular he gives numerical results for air (considered as a mixture of oxygen and nitrogen) in the form of constant time profiles. Care must be taken in interpreting the results given by the composite expansion. One cannot use this expansion to correct for non-linear effects in regions where one supposes initially that the linear theory is valid. For instance, the composite expansion will inevitably smooth out the transition from outer to inner solution. We therefore might well expect that the composite expansion does not exactly reproduce the linear variations on the alpha-shock but we cannot attribute these small deviations to non-linear effects because the non-linear solution is continuous.

In section (2) we shall give the mathematical results for the two-dimensional steady linear flow and non-linear far-field flow. These results are essentially the same as for the corresponding one-dimensional unsteady case treated by the authors mentioned above. In section (3) we shall apply these results to a particular example which is checked by characteristics. The example chosen must be a very weak wave flow in order that Burgers's equation describes the non-linear flow but we shall also make the vibrational specific heat small so that we can check extrapolations of the numerical results with the approximate analysis.

SECTION (2)

Linear solution and far-field non-linear solution

The linear theory for the flow of a relaxing gas about a wedge is well known and we shall only extract those results that are pertinent. We shall employ rectangular Cartesian coordinates with origin at the wedge tip and x -axis in the freestream direction. The upper wedge face makes an angle θ_w with the x -axis and all variables are non-dimensionalized as in section (1) of Chapter (1). If θ_w is very small (to be qualified later) then we can expand all the thermodynamic variables in power series with the freestream quantities as reference state. For instance we can expand the pressure as

$$p = 1 + p_1 \theta_w + p_2 \theta_w^2 + \ldots\ldots$$

where the coefficients p_i $(i = 1,2,3..)$ are functions of x and y.

If we substitute expansions like these into the governing equations given in section (1) of Chapter 1 and neglect terms of $O(\theta_w^2)$ (assuming all gradients are $O(1)$ in the disturbed flowfield) we get a system of linear partial differential equations. Transforming to the 'shock orientated' coordinate system given by

$$\xi = x - \sqrt{m_{f\infty}^2 - 1}\, y$$

$$\eta = \sqrt{m_{f\infty}^2 - 1}\, y$$

and making use of the fact that to the above approximation the flow is irrotational by defining a potential ϕ^p such that

$$u_1 = \phi^p_x \qquad \text{and} \qquad v_1 = \phi^p_y$$

or in the new coordinates

$$u_1 = \phi^p_\xi \qquad \text{and} \qquad v_1 = \sqrt{m_{f\infty}^2 - 1}\,(\phi^p_\eta - \phi^p_\xi)$$

we can derive the potential equation

$$\frac{c_{pa} V_\infty}{(c_{pa} + c_{vb})}\left(2\phi^p_{\eta\xi\xi} - \phi^p_{\xi\eta\eta}\right) + \frac{(m_{e\infty}^2 - 1)}{(m_{f\infty}^2 - 1)}\phi^p_{\xi\xi} + 2\phi^p_{\eta\xi} - \phi^p_{\eta\eta} = 0$$

(see Der (1961))

The boundary conditions for the velocity components are

$$u_1, v_1 \to 0 \quad \text{as} \quad \eta \to \infty$$

$$v_1 = 1 \quad \text{on} \quad \eta = 0$$

which in terms of a potential are

$$\phi^b \to 0 \quad \text{as} \quad \eta \to \infty$$

$$\sqrt{m_{f\infty}^2 - 1}\ \left(\phi_\eta^b - \phi_\xi^b \right) = 1 \quad \text{on } \eta = 0$$

With these boundary conditions the potential equation can be solved by Laplace transform so that if

$$\bar{\phi}^b = \int_0^\infty e^{-s\xi} \phi^b \, d\xi$$

Then we get

$$\bar{\phi}^b = -\frac{1}{\sqrt{m_{f\infty}^2 - 1}} \frac{1}{s^2} \sqrt{\frac{\frac{s}{A} + 1}{\frac{s}{A} + b}}\ e^{s\left(1 - \sqrt{\frac{\frac{s}{A} + b}{\frac{s}{A} + 1}}\right)\eta}$$

where $A = \dfrac{(c_{pa} + c_{vb})}{c_{pa} V_\infty}$

and $b = \dfrac{(m_{e\infty}^2 - 1)}{(m_{f\infty}^2 - 1)}$

This transform is too difficult to invert in general but 'exact' results are available on the shock ($\xi = 0$) and on the wedge surface ($\eta = 0$).

On $\xi = 0$ one gets

$$\phi_\xi^b = -\frac{1}{\sqrt{m_{f\infty}^2 - 1}}\ e^{-\frac{A(b-1)}{2}\eta} \qquad \text{(see Der (1961))} \quad 2.1$$

and on $\eta = 0$ (with the usual notation for Bessel functions)

$$\phi_\xi^b = -\frac{1}{\sqrt{m_{f\infty}^2 - 1}}\ e^{-\frac{(b+1)}{2}\xi}\ I_0\left(\frac{(b-1)}{2}\xi\right) - \frac{1}{\sqrt{m_{f\infty}^2 - 1}} \int_0^\xi e^{-\frac{(b+1)}{2}\omega} I_0\left(\frac{(b-1)}{2}\omega\right) d\omega$$

(see Clarke (1960))

In this linearized theory $p_1 = -\gamma_f m_{f\infty}^2 u_1$ so that the pressure can easily be found from the velocity perturbation.

An approximate solution to the linear problem can be obtained by expanding the transform $\bar{\phi}^b$ in powers of $(b - 1)$. If we use the matching techniques of Sussman and Baron (1967) we get

$$\bar{\phi}^{\flat} = -\frac{1}{(m_{f\infty}^2-1)^{\frac{1}{2}}}\frac{1}{s^2}\, e^{-\frac{s\tau'}{2(\frac{s}{A}+1)}}\left(1+(b-1)\left(\frac{s\tau'}{8(\frac{s}{A}+1)^2}-\frac{1}{2(\frac{s}{A}+1)}\right)+O\left((b-1)^2\right)\right)$$

where $\tau' = (b-1)\tau$

This inverts as

$$\phi_\xi^{\flat} = -\frac{1}{(m_{f\infty}^2-1)^{\frac{1}{2}}}\, e^{-\frac{A(b-1)\tau}{2}} e^{-A\xi} I_0\left(2\left(\frac{A^2(b-1)\tau}{2}\right)^{\frac{1}{2}}\right)$$

$$-\frac{1}{(m_{f\infty}^2-1)^{\frac{1}{2}}}\, e^{-\frac{A(b-1)\tau}{2}} e^{-A\xi}\int_0^{\xi} A e^{A\xi_0} I_0\left(2\left(\frac{A^2(b-1)\tau(\xi-\xi_0)}{2}\right)^{\frac{1}{2}}\right)d\xi_0$$

$$+\frac{1}{2(m_{f\infty}^2-1)^{\frac{1}{2}}}(b-1)\, e^{-\frac{A(b-1)\tau}{2}} e^{-A\xi}\int_0^{\xi} A e^{A\xi_0} I_0\left(2\left(\frac{A^2(b-1)\tau(\xi-\xi_0)}{2}\right)^{\frac{1}{2}}\right)d\xi_0$$

$$-\frac{A^2(b-1)^2\tau}{(m_{f\infty}^2-1)^{\frac{1}{2}}\,8}\, e^{-\frac{A(b-1)\tau}{2}} e^{-A\xi}\int_0^{\xi} I_0\left(2\left(\frac{A^2(b-1)\tau(\xi-\xi_0)}{2}\right)^{\frac{1}{2}}\right)d\xi_0 \qquad 2.3$$

The first 2 terms were obtained by Moore and Gibson (1960) and correspond to the solution of the telegraph equation

$$\frac{2}{A}\,\phi^{\flat}_{\tau'\xi\xi} + \phi^{\flat}_{\xi\xi} + 2\,\phi^{\flat}_{\tau'\xi} = 0$$

The extra terms are added to assess the accuracy of the solution to the telegraph equation. This solution is valid for $\tau' = O\left((b-1)^{-1}\right)$

The far-field behaviour of the linear theory can be obtained by applying the method of steepest descents to the Laplace inversion integral. This gives (Clarke (1965))

$$u_1 = \phi^{\flat}_{\xi} = -\frac{1}{2(m_{\infty}^2-1)^{\frac{1}{2}}}\,\mathrm{erfc}\left(\frac{\bar{\xi}}{\sqrt{\frac{2(b-1)\tau}{b^{\frac{1}{2}}A}}}\right)+O\left(\frac{1}{\sqrt{\tau}}\right) \qquad 2.4$$

where

$$\bar{\xi} = x - (m_\infty^2-1)^{\frac{1}{2}} y .$$

We can derive the thickness of this wave by using the gradient at the inflexion point $\bar{\xi} = 0$. The value we get is

$$\Delta_1 = \frac{1}{2}\sqrt{\frac{2(b-1)\eta}{b^{\frac{1}{2}}A}}$$

If we assume that $\frac{\theta_w}{\theta_w^{*}} << 1$ then we obtain for the structure of the shock wave at infinity

$$u_1 = -\left(1 + \exp\left(\frac{-(\gamma_e+1)\gamma_e m_{e\infty}^2 (m_{f\infty}^2-1)}{2(\gamma_e-1)^2 (m_{e\infty}^2-1)^{\frac{3}{2}} \bar{V}_\infty c_{vib}} x'\right)\right)^{-1} \qquad 2.5$$

(see Lighthill (1956)) where x' is a coordinate measured in the freestream direction. If we estimate the thickness of this shock wave as before by using the gradient at the inflexion point $x' = 0$ we get

$$\Delta_2 = \frac{8\,(m_{e\infty}^2-1)^{\frac{3}{2}}(\gamma_e-1)^2 \bar{V}_\infty c_{vib}}{(\gamma_e+1)\gamma_e m_{e\infty}^2 (m_{f\infty}^2-1)\,\theta_w}$$

If we assume $c_{vib} << 1$ then we get

$$\Delta_2 = \frac{8\,(m_{e\infty}^2-1)^{\frac{1}{2}}(\gamma_f-1)^2 \bar{V}_\infty c_{vib}}{(\gamma_f+1)\gamma_e m_{e\infty}^2\,\theta_w}$$

$$= \frac{8}{15}\cdot\frac{\bar{V}_\infty c_{vib}\,(m_{e\infty}^2-1)^{\frac{1}{2}}}{\gamma_e m_{e\infty}^2\,\theta_w}$$

which is the same expression as obtained by Hodgson and Johannesen (1971).

Comparing Δ_1 and Δ_2 we see that the linear theory is necessarily invalid when

$$\frac{1}{2}\sqrt{\frac{2(b-1)\eta}{b^{\frac{1}{2}}A}} > \frac{8\,(m_{e\infty}^2-1)^{\frac{3}{2}}(\gamma_e-1)^2 \bar{V}_\infty c_{vib}}{(\gamma_e+1)\gamma_e m_{e\infty}^2 (m_{f\infty}^2-1)\,\theta_w}$$

or

$$\eta > \frac{16\times 16\,(m_{e\infty}^2-1)^3(\gamma_e-1)^4 \bar{V}_\infty^2 c_{vib}^2\, b^{\frac{1}{2}}A}{2(b-1)(\gamma_e+1)^2\gamma_e^2 m_{e\infty}^4 (m_{f\infty}^2-1)^2\,\theta_w^2}$$

$$= \frac{8\times 16\,(\gamma_e-1)^2\gamma_e^{\frac{1}{2}}(m_{e\infty}^2-1)^{\frac{7}{2}} c_{vib}}{m_{e\infty}^5(\gamma_e+1)^2(m_{f\infty}^2-1)^{\frac{3}{2}}\,\theta_w^2}$$

The above equation is $O\left(\frac{\theta_w^*}{\theta_w}\frac{1}{\theta_w}\right)$. If $\frac{\theta_w}{\theta_w^*} << 1$ (which from section (2) of Chapter 3 is the condition that linear theory be a good approximation at the alpha-shock) then the above expression is $O(\theta_w^{-2})$.

The fundamental assumption made in deriving the linear results was that the gradients were O(1). This is inconsistent with the linear solution itself. For instance, for large y

$$\frac{\partial u_1}{\partial x} \propto \frac{1}{\sqrt{y}}$$

When $y = O(\theta_w^{-2})$ this gradient is $O(\theta_w)$ and linearization can no longer be justified.

In accordance with the method of matched asymptotic expansions new coordinates of O(1) in the region of non-uniformity are defined. That is

$$\bar{\xi}_i = \theta_w \bar{\xi}$$

$$\eta_i = \theta_w^2 \eta$$

The thermodynamic variables are expanded in power series of the wedge angle as before. These expansions are substituted into the exact governing equations written in terms of the new coordinates ('inner coordinates') and coefficients of the wedge angle set equal to 0.

Taking the first approximation gives

$$\frac{\partial u_1}{\partial \bar{\xi}_i} - \sqrt{m_{e\infty}^2 - 1}\,\frac{\partial v_1}{\partial \bar{\xi}_i} + \frac{\partial \rho_1}{\partial \bar{\xi}_i} = 0,$$

$$\frac{\partial p_1}{\partial \bar{\xi}_i} + \gamma_e m_{e\infty}^2 \frac{\partial u_1}{\partial \bar{\xi}_i} = 0,$$

$$\frac{\partial p_1}{\partial \bar{\xi}_i} - \frac{\gamma_e m_{e\infty}^2}{\sqrt{m_{e\infty}^2 - 1}}\frac{\partial v_1}{\partial \bar{\xi}_i} = 0,$$

$$\frac{\gamma_e}{(\gamma_e - 1)}\bar{T}_1 + \bar{V}_\infty^2 u_1 = 0$$

and $$p_1 - \rho_1 - \bar{T}_1 = 0$$

These equations are not linearly independent (see Moran and Shen (1966) who encountered a similar problem) and hence no solution can be obtained from them. For waves propagating in one direction, however, they can be integrated to give (on simplification)

$$\left.\begin{aligned} p_1 &= -\gamma_e m_{e\infty}^2 u_1 , \\ v_1 &= -\sqrt{m_{e\infty}^2 - 1}\, u_1 , \\ T_1 &= -\frac{(\gamma_e - 1)}{\gamma_e} V_\infty^2 u_1 , \\ \text{and} \quad \rho_1 &= -m_{e\infty}^2 u_1 \end{aligned}\right\} \qquad 2.6$$

Hence once u_1 is found the remaining variables are calculated from the relations for equilibrium flow.

Taking the next approximation and substituting the above relations gives finally

$$\frac{\partial u_1}{\partial \eta_i} + \frac{(\gamma_e + 1) m_{e\infty}^4}{2 (m_{e\infty}^2 - 1)^{\frac{1}{4}} (m_{f\infty}^2 - 1)^{\frac{1}{4}}} u_1 \frac{\partial u_1}{\partial \bar{\xi}_i} = \frac{1}{2} \frac{(b-1)}{A b^{\frac{1}{2}}} \frac{\partial^2 u_1}{\partial \bar{\xi}_i^2}$$

where the coefficient of $\frac{\partial^2 u_1}{\partial \bar{\xi}_i^2}$ has been written in a form appropriate for comparison with the linear theory. The above equation is Burgers's equation for two-dimensional steady supersonic flow. For the one-dimensional unsteady case see Ockendon and Spence (1969), Blythe (1969) and Lick (1967).

Initial conditions for the solution of Burgers's equation are (as supplied by the linear theory)

$$\begin{aligned} u_1 &\to 0 \quad \text{as} \quad \bar{\xi}_i \to -\infty , \\ u_1 &\to -\frac{1}{\sqrt{m_{e\infty}^2 - 1}} \quad \text{as} \quad \bar{\xi}_i \to +\infty \end{aligned}$$

$$\text{and} \qquad u_1 = -\frac{1}{2\sqrt{m_{e\infty}^2 - 1}} \operatorname{erfc}\left(\frac{\bar{\xi}_i}{\sqrt{\frac{2(b-1)}{b^{\frac{1}{2}} A} \eta_i}} \right) \quad \text{as} \quad \eta_i \to 0$$

If we make the transformation

$$u_{11} = -\sqrt{m_{e\infty}^2 - 1}\, u_1$$

$$\bar{\xi}_{i1} = -\bar{\xi}_i$$

then Burgers's equation becomes

$$\frac{\partial u_{11}}{\partial \eta_i} + \frac{(\gamma_e+1) m_{e\infty}^4}{2(m_{e\infty}^2-1)(m_{f\infty}^2-1)^{\frac{1}{2}}} u_{11} \frac{\partial u_{11}}{\partial \bar{\xi}_{i1}} = \frac{1}{2} \frac{(\beta-1)}{A\beta^{\frac{1}{2}}} \frac{\partial^2 u_{11}}{\partial \bar{\xi}_{i1}^2}$$

and the boundary conditions reduce to those of the one-dimensional unsteady case.

If we define

$$B = \frac{(\beta-1)}{A\beta^{\frac{1}{2}}}$$

and $$C = \frac{(\gamma_e+1) m_{e\infty}^4}{2(m_{e\infty}^2-1)(m_{f\infty}^2-1)^{\frac{1}{2}}}$$

then the solution is (see Ockendon and Spence (1969))

$$u_{11} = \left(1 + \frac{\exp\left(\frac{C}{B}\left(\bar{\xi}_{i1} - \frac{1}{2} C\eta_i\right)\right) \operatorname{erfc}\left(\frac{-\bar{\xi}_{i1}}{\sqrt{2B\eta_i}}\right)}{\operatorname{erfc}\left(\left(\bar{\xi}_{i1} - C\eta_i\right)/\sqrt{2B\eta_i}\right)} \right)^{-1}$$

or

$$u_1 = \frac{-1}{\sqrt{m_{e\infty}^2-1}} \left(1 + \frac{\exp\left(-\frac{C}{B}\left(\bar{\xi}_i + \frac{1}{2} C\eta_i\right)\right) \operatorname{erfc}\left(\frac{\bar{\xi}_i}{\sqrt{2B\eta_i}}\right)}{\operatorname{erfc}\left(-\left(\bar{\xi}_i + C\eta_i\right)/\sqrt{2B\eta_i}\right)} \right)^{-1} \qquad 2.7$$

As $\eta_i \to \infty$

$$u_1 \to -\frac{1}{\sqrt{m_{e\infty}^2-1}} \left(1 + \exp\left(-\frac{C}{B}\left(\bar{\xi}_i + \frac{1}{2} C\eta_i\right)\right) \right)^{-1} \qquad 2.8$$

The same result can be derived (see equation 2.5) by approximating the conservation equations in the limit $\frac{\theta_w}{\theta_w^*} << 1$.

We can therefore estimate the formation time by comparing wave thicknesses based on gradients at the mid-point in the u_1 velocity profile. We can do this by noticing that when

$$\bar{\xi}_i = -\frac{1}{2} C\eta_i$$

$u_1 = -\frac{1}{2\sqrt{m\tilde{c}_0 - 1}}$ both for the asymptotic solution ($\eta_i \to \infty$) and for the solution of Burgers's equation.

For the asymptotic wave thickness we get

$$\frac{4B}{C} \qquad \text{(at constant } \eta_i\text{)} \qquad 2.9(a)$$

Taking the derivative with respect to ξ_i of the solution for u_1 gives

$$\left.\frac{\partial u_1}{\partial \bar{\xi}_i}\right|_{\bar{\xi}_i = -\frac{1}{2}c_{1i}} = \frac{1}{\sqrt{m\tilde{c}_0 - 1}} \; \frac{\frac{c}{B} - 2e^{-\frac{\tilde{c}\eta_i}{8B}}\left(\operatorname{erfc}\frac{-c_{1i}^{\frac{1}{2}}}{2\sqrt{2B}}\right)^{-1}(2B\eta_i)^{-\frac{1}{2}}}{4} \qquad 2.9(b)$$

Hence the wave thickness for the solution of Burgers's equation is

$$\frac{(4B/c)}{1 + \left(\frac{2B}{c}\right)e^{-\frac{c\eta_i}{8B}}\left(\operatorname{erfc}\frac{-c_{1i}^{\frac{1}{2}}}{2\sqrt{2B}}\right)^{-1}(2B\eta_i)^{-\frac{1}{2}}} \qquad 2.9(c)$$

If η_i = constant x $\frac{B}{C^2}$ then the denominator is independent of B or C. Hence the formation distance is given by

$$\eta = \text{constant x } \frac{B}{C^2\theta_w^2}$$

which is a multiple of the estimated distance for the breakdown of the linear theory. The constant can then by chosen to ensure that the denominator is sufficiently close to 1 that the asymptotic wave thickness is reached.

Expression 2.9(c) is, however, much more important because it does indicate the manner in which the shock wave approaches its asymptotic state. When the results for the wave development were determined from the characteristics solution (Chapters 2 and 3) we plotted maximum departures

from equilibrium in the vibrational energy (along positive characteristics) against y. For weak waves this procedure is approximately equivalent to plotting maximum departures from equilibrium along the streamlines. To see this let F(x,y) = constant and G(x,y) = constant be the equations to a positive and negative characteristic respectively. Then

$$\frac{\partial(\bar{\sigma}-\sigma)}{\partial e} = \frac{\partial(\bar{\sigma}-\sigma)}{|\partial F|}\frac{|dF|}{de} + \frac{\partial(\bar{\sigma}-\sigma)}{|\partial G|}\frac{|dG|}{de}$$

The moduli are used for convenience.

If $\bar{\sigma}-\sigma$ is a maximum on the streamline then

$$\frac{\partial(\bar{\sigma}-\sigma)}{\partial e} = 0$$

or

$$\frac{\partial(\bar{\sigma}-\sigma)}{|\partial F|}\frac{|dF|}{de} + \frac{\partial(\bar{\sigma}-\sigma)}{|\partial G|}\frac{|dG|}{de} = 0 \qquad 2.10$$

Clearly if we consider the surface

$$\bar{\sigma}-\sigma = E(F, G)$$

then it must appear as a sharp ridge at the origin extending in decreasing height to a rounded ridge at infinity. We cannot therefore have any local maxima of $\bar{\sigma}-\sigma$. Hence we cannot have $\frac{\partial(\bar{\sigma}-\sigma)}{|\partial F|}$ and $\frac{\partial(\bar{\sigma}-\sigma)}{|\partial G|}$ simultaneously zero (except at the foot of the ridge and at infinity). Since $\frac{|dF|}{de} \approx \frac{|dG|}{de}$ 2.10 can only be satisfied if $\frac{\partial(\bar{\sigma}-\sigma)}{|\partial F|}$ and $\frac{\partial(\bar{\sigma}-\sigma)}{|\partial G|}$ are close to 0 but of opposite sign. A maximum of $\bar{\sigma}-\sigma$ on the streamlines therefore corresponds closely to a maximum of $\bar{\sigma}-\sigma$ on the positive characteristics. Furthermore, the maxima themselves must be nearly equal.

Since maximum values of $\bar{\sigma}-\sigma$ on the streamlines can be related to maximum values of the gradient in vibrational energy by using the rate equation, then our procedure is approximately equivalent to plotting maximum gradients on streamlines against y. For $\frac{\theta_w}{\theta_w^*} << 1$ a maximum

gradient in one thermodynamic variable corresponds to a maximum gradient in any other thermodynamic variable because all variables are simply related by equations 2.6. Moreover in this limit, and close to equilibrium, inflexion points in the velocity (say) profile occur when the velocity takes the mean of its values at either end of the wave. We can therefore use equation 2.9(b) to derive an analytic estimate for the far-field shock wave development rate. This estimate is applicable to the work in section (3) of Chapter 3 for $\frac{\theta_w}{\theta_w^*} << 1$.

If we subtract from 2.9(b) its asymptotic value we get

$$\frac{1}{2\sqrt{m_{\infty}^2-1}}\, e^{-\frac{c^2\eta_i}{8B}} \left(\operatorname{erfc} -\frac{c\eta_i^{\frac{1}{2}}}{2\sqrt{2B}}\right)^{-1} (2B\eta_i)^{-\frac{1}{2}}$$

Taking the logarithm and differentiating with respect to η_i gives

$$-\frac{c^2}{8B} - \left(\operatorname{erfc} -\frac{c\eta_i^{\frac{1}{2}}}{2\sqrt{2B}}\right)^{-1} e^{-\frac{c^2\eta_i}{8B}} \frac{c}{4\sqrt{2B\eta_i}} - \frac{1}{2\eta_i}$$

As $\eta_i \to \infty$ the gradient tends to the constant value

$$-\frac{c^2}{8B} \quad \text{or} \quad -\frac{c^2\theta_w^2\sqrt{m_{f\infty}^2-1}}{8B}$$ taking gradients with respect to y.

This lends support to our interpretation of the numerical results.

We can compare this result to our numerical results for weak wave flows. Notice, however, that in this limit ($\frac{\theta_w}{\theta_w^*} << 1$) it is the numerical results that are necessarily inaccurate because calculations must be stopped (for reasons of cost) before one can predict with certainty the direction of the far-field line. The weakest wave flow for which we have numerical results is given by $\frac{\theta_w}{\theta_w^*} = 0.2$, $m_{f\infty} = 3.8$, $c_{v,b} = 1.0$. With natural base logarithms the gradient is -17×15^{-4}. The analytic far-field estimate is -5.4×10^{-4}. We have mentioned before that inaccuracy (or perhaps more specifically 'incompleteness') in the numerical results leads to underestimations of the true development distances. In

the above case the analytic result predicts a development distance about 3 times the value derived from the characteristics.

In the next section we shall compare these results in detail with a numerical calculation by characteristics.

SECTION 3

Comparison of the method of characteristics with the method of matched asymptotoc expansions for the flow $\theta_w = 0.019^o$, $M_{f\infty} = 2.6$ and $c_{v,b} = 0.050$.

In this section we shall compare the numerical method of characteristics with the analytic method of matched asymptotic expansions by inspecting weak shock wave profiles at constant y. The essential mathematical results have been given in section (2). The flow we have chosen has $\frac{\theta_w}{\theta_w^*} = 0.2$; numerical computations for flows much weaker than this are extremely costly.

To gain some idea of the length scales involved in this flow we shall extrapolate the results for the computed flows with larger values of the vibrational specific heat. This will also serve as a useful check on our similarity representation. The flow dimensions we are interested in are the wave development distance (which we shall represent as the distance for which $\frac{(\bar{\sigma}-\sigma)_{max}}{(\bar{\sigma}-\sigma)_{max\infty}} = 1.1$), the width of the non-equilibrium region on the wedge surface (we shall choose the distance for which 90 per cent of the change in $(\bar{\sigma}-\sigma)$ has taken place) and the asymptotic wave width.

For $c_{v,b} = 1.0$ and $M_{f\infty} = 2.6$ the wave development distance defined in the above manner is 84. If we use the result of section (4) Chapter 3 that the critical development distance varies inversely with

$c_{v,b}$ then for $c_{v,b} = 0.05$ we get

$$\bar{y}_b^* = 1680$$

If we use fig. 3(m) with $\frac{\theta_w}{\theta_w^*} = 0.2$ then

$$\frac{\bar{y}_b}{\bar{y}_b^*} \approx 18$$

Hence $\bar{y}_b \approx 3 \times 10^4$.

The results of section (1) Chapter 3 give the width of the non-equilibrium region on the wedge surface as approximately equal to 7.

The asymptotic shock wave thickness as given by the expression in section (2) for $c_{v,b} << 1$ is approximately 60.

In fig. 5(a) the linear pressure profile on the wedge surface obtained from expression 2.2 is compared to the pressure profile calculated by characteristics. The linear theory overestimates the pressure drop, though the variation with distance is predicted reasonably well. In section (4) of Chapter 2, however, we showed how a very much more simplified solution gave more accurate results. Fig. 5(b) compares the linear theory and characteristics on the alpha- shock. The linear results are given by expression 2.1. We can see that the linear theory is reasonably accurate even for large y ($\approx$ 1000). This is to be expected since we have already established in Chapter 3 that non-linear effects on the alpha-shock are small for very weak waves.

Expression 2.3 gives minimal gains in accuracy over the solution to the telegraph equation (represented by the first 2 terms). We can expect this solution to be a valid approximation to the linear theory for $y = O((b-1)^{-2})$ i.e. for $y \approx$ 10,000. This solution is plotted in figs.5(c), 5(d) and 5(e) and checked with characteristics results. The agreement is initially very good but falls off with increasing distance from the wedge surface. The solution does give, however, a good qualitative representation

of the initial wave development process. In fig. 5(e) we see how this solution approaches the asympotic representation of the linear theory. In fig. 5(d) non-linear effects in the geometrical location of flow properties are clearly exhibited, though in this case they are not serious. For stronger shock wave flows it is this type of non-uniformity which necessitates the use of an intermediate expansion with y scaled on $1/\theta_w$.

For large y the linear solution grows in width like $\sqrt{y}$ and is centred on the equilibrium characteristic. The matched expression 2.7 corrects for this by relocating the wave trajectory and by including a first approximation to the non-linear terms which ultimately balance the diffusive effects of the relaxation. This solution is plotted in figs. 5(e), 5(f) and 5(g). The agreement with the characteristics is very good and the asymptotic representation (given by expression 2.8) is compared to an exact integration of the conservation, rate and state equations in fig. 5(h). A comparison of fig. 5(g) with fig. 5(h) shows that for $y \approx 40{,}000$ the wave is almost fully developed. This agrees very well with the extrapolated estimate from the characteristics results.

We can represent these results by a single composite expansion valid over the whole flowfield. We can construct these composite expansions in many ways (see Van Dyke (1964)). In this case a simple one to choose is

$$u_c = u_o + u_i - [u_i]_o$$

where suffix c represents the composite expansion, suffixes o and i represent the outer (linear) and inner (non-linear) solutions, and $[u_i]_o$ represents the inner solution expressed in outer variables $(\bar{\xi}, \tau)$ and expanded to $O(\theta_w)$. In this case

$$[u_i]_o = -\frac{1}{2\sqrt{m_\infty^2 - 1}} \operatorname{erfc}\left(\frac{\bar{\xi}}{\sqrt{\frac{2(b-1)\tau}{b^2 A}}}\right)$$

which is just the asymptotic representation of the linear solution

given by expression (2.4). Hence the composite solution is given by adding together the solution of Burgers's equation and the approximate linear solution and subtracting the asymptotic linear solution. For instance, by inspecting fig. 5(c) we see that the composite solution is virtually the same as the approximate linear solution. For large y (see fig. 5(e)) the composite solution reduces to the solution of Burgers's equation. For intermediate distances (see fig. 5(d)) the composite expansion smooths out the otherwise abrupt change from outer to inner expansion.

We can see quite clearly by examining fig. 5(d) at the alpha-shock how the composite expansion represents a slower decay rate than that given by linear theory. It is quite wrong to interpret this as a true non-linear effect (see Romberg (1970b)). It is merely a consequence of the smoothing out process inherent in representing the results by a composite expansion.

In conclusion the method of matched asymptotic expansion gives reasonable agreement with the method of characteristics, the approach to a final asymptotic state being correctly predicted. In this example, non-linear effects, though small, were present for intermediate distances. For much weaker flows we expect these effects to be absent and consequently the analytic representation to be that more accurate.

SECTION (4)

The use of Whitham's rule in weak wave relaxing gas flows

Whitham (1958) gave a simple rule for determining the motion of a shock wave through a region of non-uniform area or flow when disturbances are propagated predominantly along one set of characteristics. The rule is to solve the characteristic compatibility relation in conjunction with the shock wave equations. Lick (1966) has shown how a more general approach to shock expansion theory incorporates Whitham's rule at the shock front.

We shall be concerned in this section with applying Whitham's rule to the decay of weak alpha-shocks in relaxing supersonic two-dimensional steady flows over wedge surfaces. Lick's approach (which is successful for area-change interactions) of using the equation which is strictly valid only along a minor characteristic as an approximation valid throughout the flow fails here because the pertinent relation to be applied at the shock is that along the major (negative) characteristic. On the line given by

$$\frac{dy}{dx} = \tan(\theta+\mu)$$

we have

$$\frac{dp}{\rho V^2 \tan\mu} + d\theta = \frac{-(\gamma_f-1)\rho(\bar{\sigma}-\sigma)\,dy}{V^3 \sin\mu \sin(\theta+\mu)}$$

where

$$dp = \frac{\partial p}{\partial x}dx + \frac{\partial p}{\partial y}dy$$

Writing the characteristic relation in terms of partial derivatives therefore gives

$$\frac{1}{\rho V^2 \tan\mu}\left(\frac{\partial p}{\partial x}\frac{dx}{dy} + \frac{\partial p}{\partial y}\right) + \left(\frac{\partial \theta}{\partial x}\frac{dx}{dy} + \frac{\partial \theta}{\partial y}\right) = \frac{-(\gamma_f-1)\rho(\bar{\sigma}-\sigma)}{V^3 \sin\mu \sin(\theta+\mu)}$$

or, since $\frac{dx}{dy} = \cot(\theta+\mu)$

$$\frac{1}{\rho V^2 \tan\mu}\left(\frac{\partial p}{\partial x}\cot(\theta+\mu)+\frac{\partial p}{\partial y}\right)+\left(\frac{\partial\theta}{\partial x}\cot(\theta+\mu)+\frac{\partial\theta}{\partial y}\right)=\frac{-(\gamma_f-1)\rho(\bar{\sigma}-\sigma)}{V^3\sin\mu\sin(\theta+\mu)}$$

If we apply the same characteristic relation along the alpha-shock for which $\frac{dy}{dx} = \tan\phi$ then we get

$$\frac{1}{\rho V^2 \tan\mu}\left(\frac{\partial p}{\partial x}\cot\phi+\frac{\partial p}{\partial y}\right)+\left(\frac{\partial\theta}{\partial x}\cot\phi+\frac{\partial\theta}{\partial y}\right)=\frac{-(\gamma_f-1)\rho(\bar{\sigma}-\sigma)}{V^3\sin\mu\sin\phi}.$$

In doing this we have neglected terms like

$$\frac{1}{\rho V^2\tan\mu}\left(\cot(\theta+\mu)-\cot\phi\right)\frac{\partial p}{\partial x}$$

which are small (i.e. $O(\theta_w)$) provided the alpha-shock is very weak. Physically, only those characteristics which are close to the wedge tip are responsible for the alpha-shock decay. This suggests that a first approximation to the development of the alpha-shock may be made by solving

$$\frac{dp}{\rho V^2\tan\mu}+d\theta=\frac{-(\gamma_f-1)\rho(\bar{\sigma}-\sigma)\,dy}{V^3\sin\mu\sin\phi}$$

along the alpha-shock together with the shock relations which we can write as

$$p = p(\theta),$$
$$V = V(\theta) \quad \text{etc.}$$

This gives the differential equation for the variation in flow deflection along the shock as

$$\frac{d\theta}{dy}\left(1+\frac{\frac{dp}{d\theta}}{\rho(\theta)V(\theta)^2\tan\mu(\theta)}\right)=\frac{-(\gamma_f-1)\rho(\theta)\left(\bar{\sigma}(\theta)-\bar{\sigma}_\infty\right)}{V(\theta)^3\sin\mu(\theta)\sin\phi(\theta)} \qquad 4.1$$

This equation is best integrated numerically; basically we expect the results to be equivalent to a perturbation about the freestream in characteristic coordinates. Clarke's (1965) results show that such a perturbation scheme gives identical results to the linear theory at the alpha-shock if the linearized characteristics are replaced by the more exact ones. We would therefore expect Whitham's rule to give essentially the same decay rate for the thermodynamic variables as predicted by linear theory. This conclusion is supported by fig. 5(i) which compares Whitham's rule with linear theory and characteristics for a weak wave flow with $\frac{\theta_w}{\theta_w^*} = 0.2$. If we linearize Whitham's rule with the freestream as reference state and expansion parameter θ_w then we get (from 4.1)

$$\frac{d\theta}{dy}\left(1+1\right) = \frac{-(\gamma_f-1)^2 c_{vib}\, m_{f\infty}^2\, \theta}{V_\infty^3 \sin^2\mu_\infty\, (m_{f\infty}^2-1)^{\frac{1}{2}}}$$

That is

$$\frac{d\theta}{dy} = -\frac{(\gamma_f-1) c_{vib}\, m_{f\infty}\, \theta}{2\,\gamma_f^{\frac{1}{2}} c_{pa} (m_{f\infty}^2-1)^{\frac{1}{2}}}$$

Integrating and applying the boundary condition $\theta = \theta_w$ on $y = 0$ gives

$$\theta = \theta_w\, e^{\frac{-(\gamma_f-1) c_{vib}\, m_{f\infty}\, y}{2\,\gamma_f^{\frac{1}{2}} c_{pa} (m_{f\infty}^2-1)^{1/2}}}$$

which is identical to the expression for the alpha-shock decay given by linear theory.

The exact formulation of Whitham's rule does, however, give the variation of shock angle ϕ with distance y. Fig. 5(j) compares Whitham's rule with characteristics. The agreement is quite reasonable and we might expect similar results for even stronger alpha-shocks.

If we denote variables on a negative characteristic which has coordinates (x_w , y_w) on the wedge surface with subscript ch and define

$$\psi = -x + x_w + \int_{y_w}^{y} \frac{dy}{\tan(\theta_{ch}+\mu_{ch})}$$

and

$$\bar{Y} = y$$

then we can expand variables from this characteristic in power series like

$$p = p_{ch}(\bar{Y}) + \psi p_1(\bar{Y}) + \psi^2 p_2(\bar{Y}) + \ldots$$

for $\psi << 1$

If the alpha-shock wave is very weak ($\frac{\theta_w}{\theta_*} << 1$) then the value of ψ on the alpha-shock is very small. Then, following Whitham (1958), substituting expansions like the one above into the governing equations and putting $\psi = 0$ gives as a first approximation to the variations along the alpha-shock ,

$$p = p_{ch}(\bar{Y}) = 1 + \frac{2\gamma_f}{(\gamma_f+1)}\left(M_{f\infty}^2 \sin^2\phi_f - 1\right) \quad \text{etc.}$$

with

$$\frac{1}{\rho_{ch}\bar{V}_{ch}^2 \tan\mu_{ch}} \frac{\partial p_{ch}}{\partial \bar{Y}} + \frac{\partial \theta_{ch}}{\partial \bar{Y}} = \frac{-(\gamma_f-1)\rho_{ch}(\bar{\sigma}_{ch}-\sigma_{ch})}{\bar{V}_{ch}^3 \sin\mu_{ch} \sin(\theta_{ch}-\mu_{ch})}$$

This set of equations constitues Whitham's rule. We also obtain a set of linear equations relating the suffix 1 quantities to the suffix ch quantities. These relations determine the gradient functions at the alpha-shock wave in terms of the shock wave curvature. We might therefore try to improve the first approximation by using the gradients to estimate the variables on the characteristic more accurately. However, examination of fig. 5(i) shows that this procedure results in a negligible improvement.

Chou and Chu (1971) have investigated the decay of weak alpha-shock waves in axisymmetric non-equilibrium flow by a systematic perturbation scheme in semicharacteristic coordinates. The solution proceeds by Laplace transform which can only be inverted (in our notation) for $\Psi << 1$ in which case the results reduce to Whitham's rule in the limit of frozen flow. We have seen here, however, how Whitham's rule can be applied to the non-equilbrium flow to good approximation for $\Psi << 1$ and how the variation of shock angle with distance is correctly predicted. Chou and Chu compare their theoretical results with the experimental determination of the variation of alpha-shock angle with radial distance, and find excellent agreement. A direct application of Whitham's rule to the non-equilbrium flow must give the same results as the first simplified approximation in the perturbation analysis and is probably sufficient for adequate comparison with experiments of the type cited by the above authors.

CONCLUSIONS

The method of characteristics has been used to solve the two-dimensional steady, supersonic flow of a relaxing gas about a thin wedge. The essential non-linear effects in the shock development and alpha-shock decay have been established and represented in an approximate similarity form with the critical values as scaling factors. The consequences of assuming this similarity to be exact have been investigated and lead to simple scaling laws which enable critical shock development and alpha-shock decay distances to be found for any $M_{f\infty}$ or c_{vib}. The characteristics results have also been compared with experimental flows and with analytical results valid when $\frac{\theta_w}{\theta_w^*} << 1$. Both comparisons are favourable.

The flow over a wedge surface is perhaps the most simplified two-dimensional problem that one can study but nevertheless when the gas is relaxing the problem is difficult and no generally applicable analytic solutions are available. The present numerical calculations, however, can quite easily be extended to flows over pointed two-dimensional bodies of any prescribed shape providing that subsonic flow at the body tip does not occur. The same numerical method could also be applied to flows of binary relaxing gas mixtures over wedge surfaces by including an extra rate equation. Flows of this nature are possibly important in determining the separate effects of O_2 and N_2 on wave propagation in the atmosphere.

The work presented has been restricted by the time available. There remain areas where further work is necessary to establish the accuracy of our results and the validity of our conclusions. The precise analogies between the numerical results for the one-dimensional unsteady and the two-dimensional steady flows also need to be investigated. Certainly some crude comparisons between the 2 sets of results show remarkable similarity. Fully dispersed wave flows at infinity in the wedge problem are also possible for hypersonic freestream Mach numbers. There is then the rather interesting problem of applying both the weak-wave and hypersonic approximations simultaneously.

We can also hope that these results provide a stimulus for renewed analytic attacks on the problem. The essential characteristics of the solution have been given and these should provide a satisfactory basis for further approximation schemes.

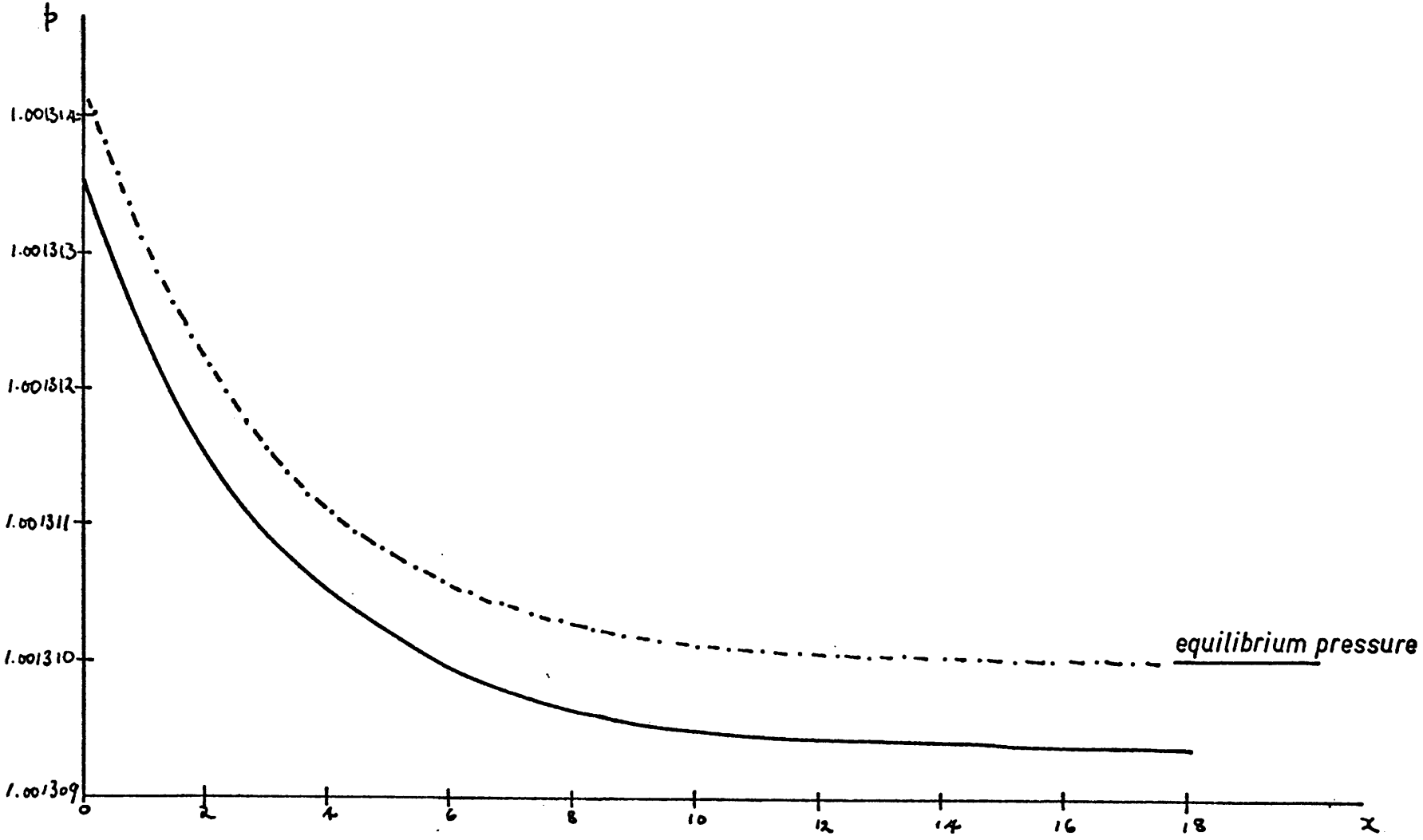

FIGURE 5(a). PRESSURE VARIATION ON THE WEDGE SURFACE .-·- , characteristics .
—, linear theory.

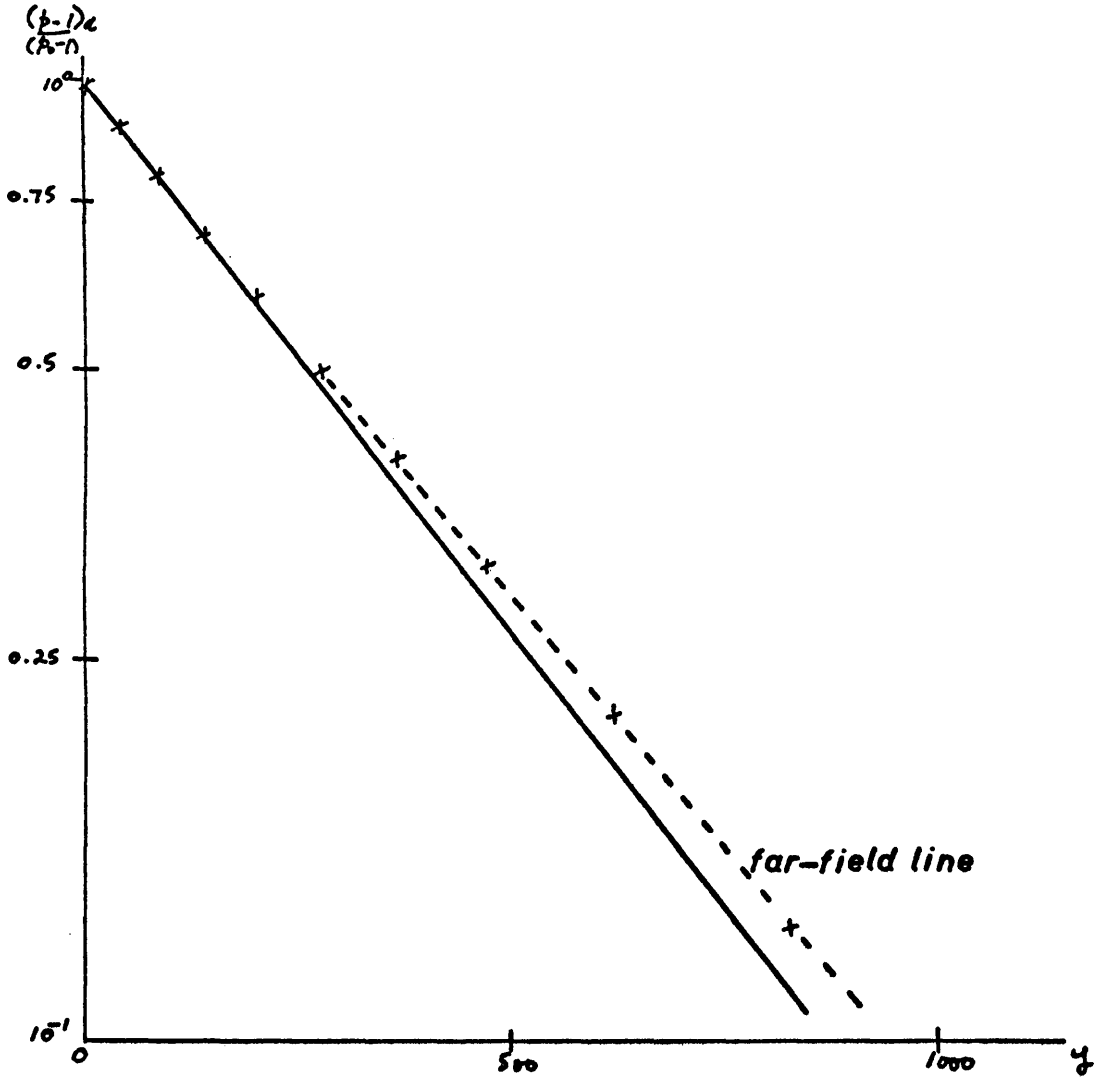

FIGURE 5(b). PRESSURE VARIATION ALONG THE ALPHA-SHOCK.
x, characteristics. —, linear theory.

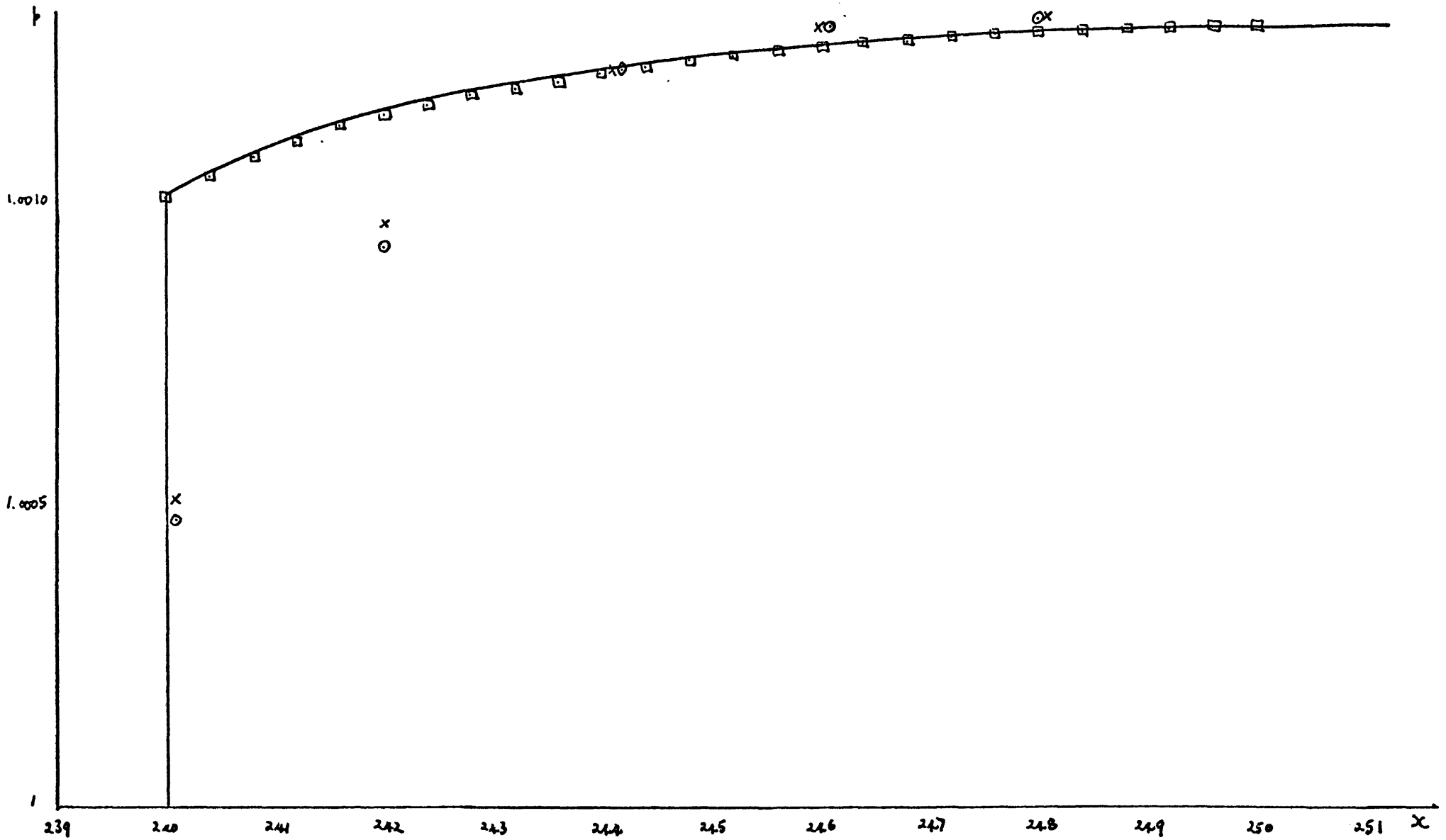

FIGURE 5(c). CONSTANT y PRESSURE PROFILES. y=100. —, characteristics. □, approximate linear solution. ⊙, asymptotic linear solution. ×, solution to Burgers's equation.

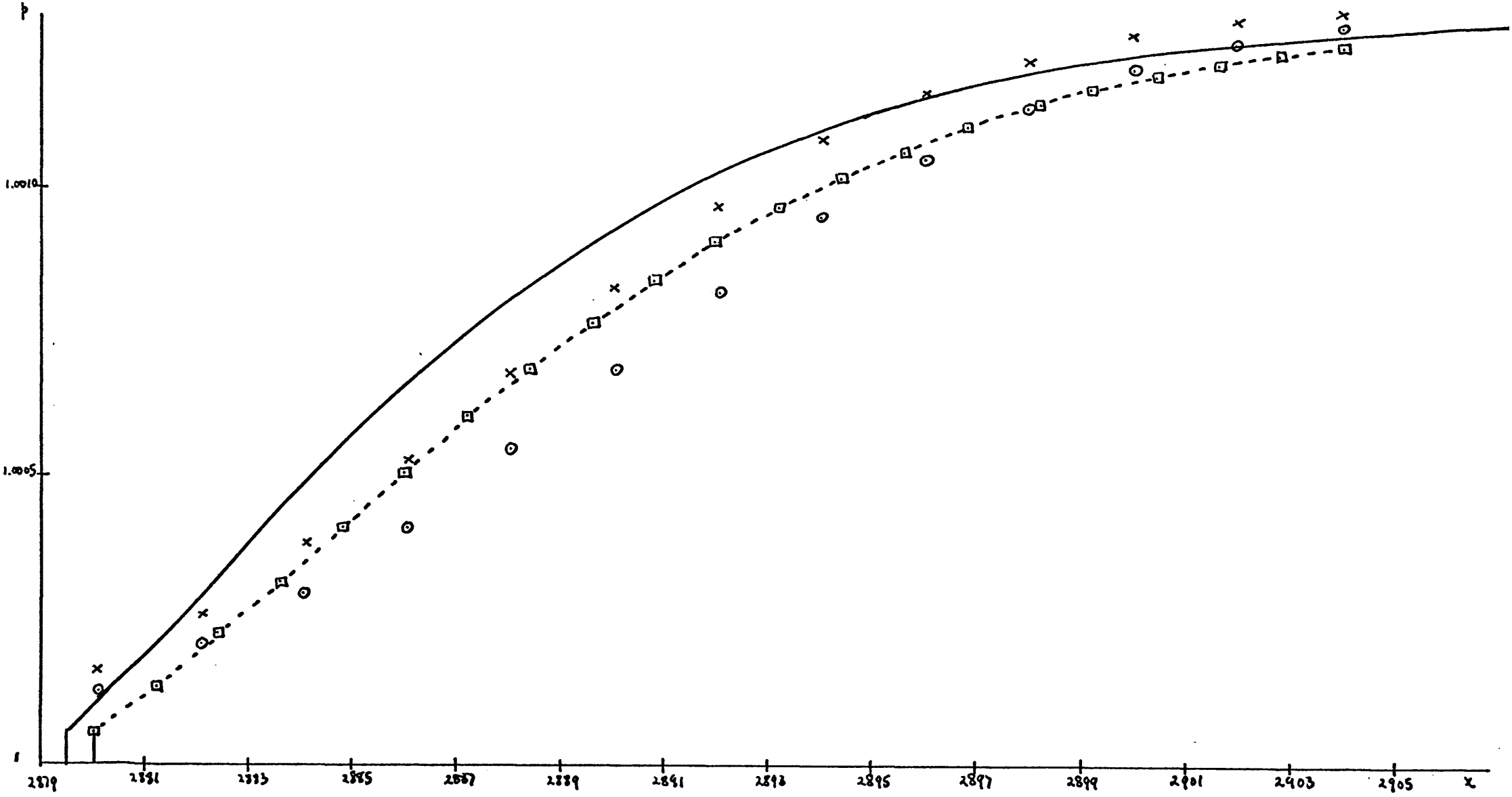

FIGURE 5(d). $y = 1200$. (see figure 5(c) for legend).

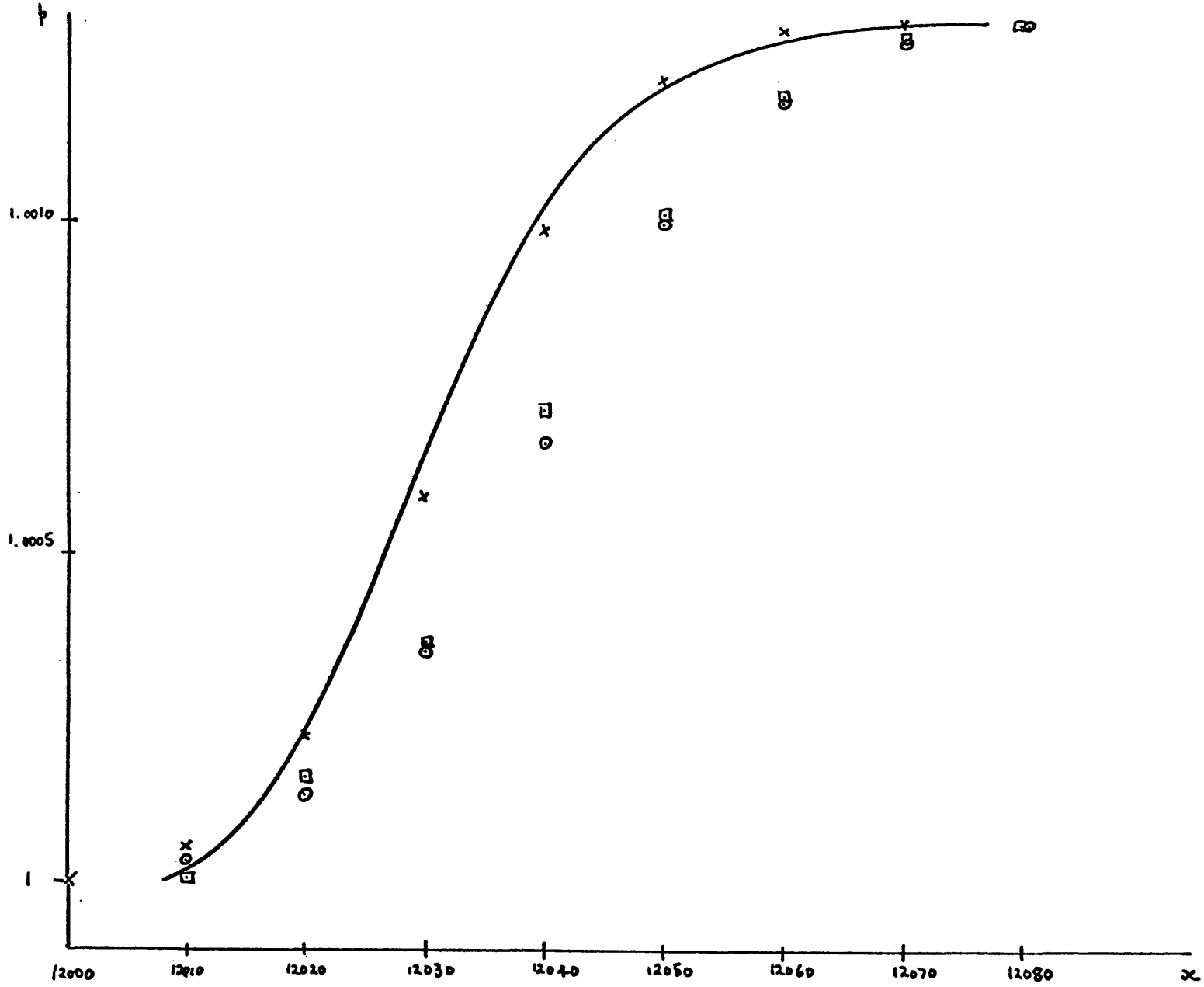

FIGURE 5(e). $y = 5000$. (see figure 5(c) for legend).

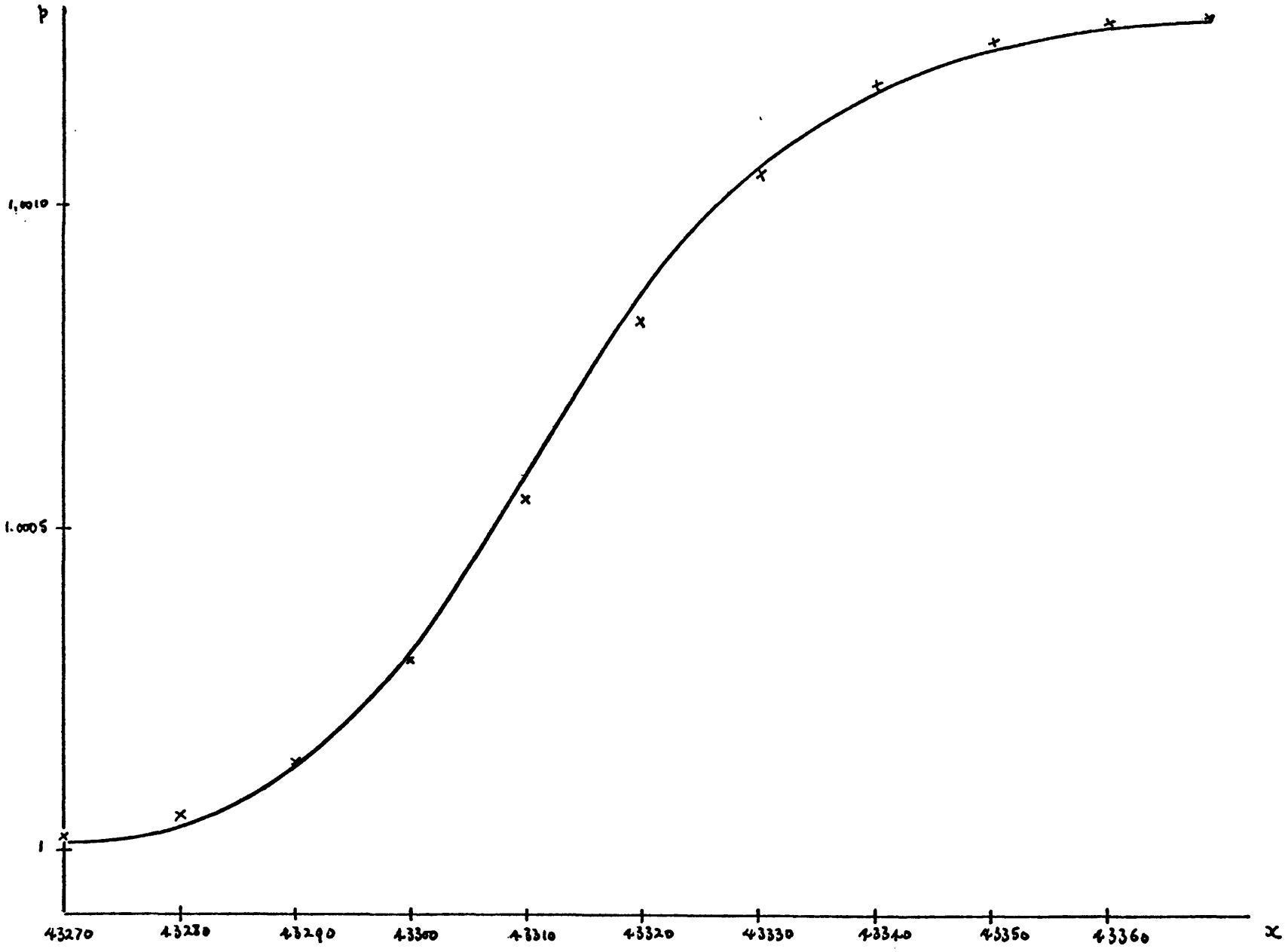

FIGURE 5(f). $y = 18000$. (see figure 5(c) for legend).

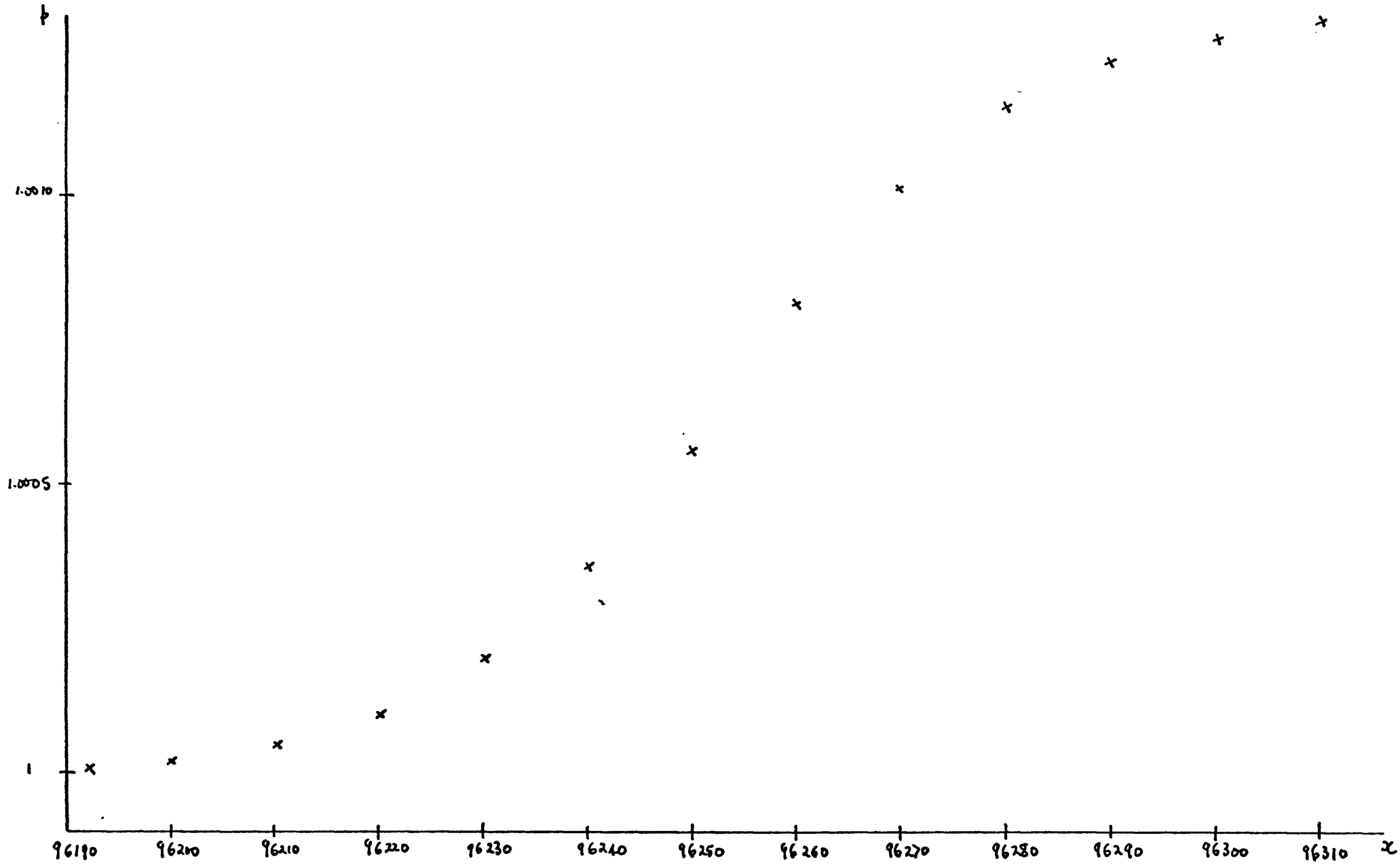

FIGURE 5(g). $y = 40000$. (see figure 5(c) for legend).

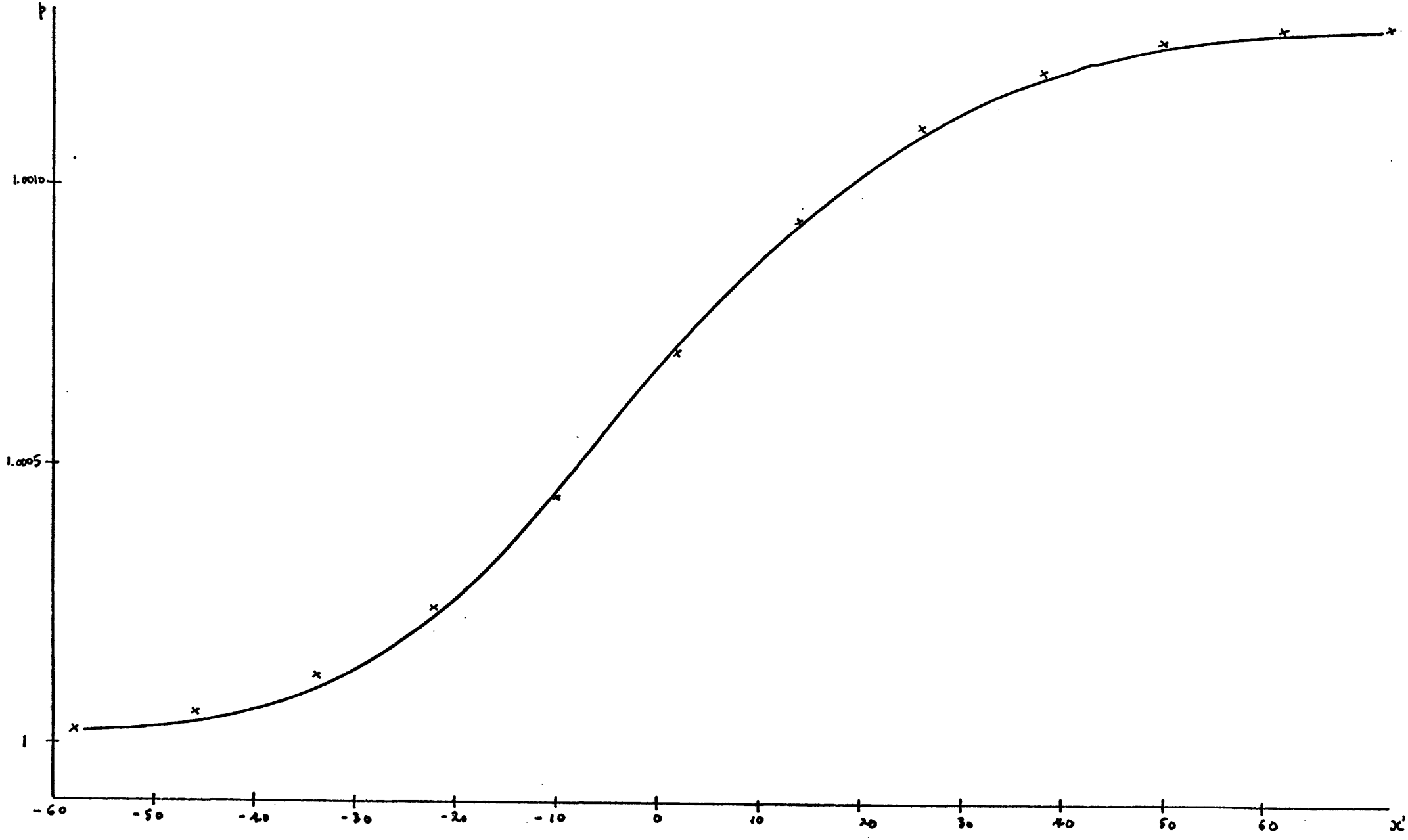

FIGURE 5(h). COMPARISON OF EXACT SOLUTION AT INFINITY WITH ASYMPTOTIC SOLUTION OF BURGERS'S EQUATION.
—, exact solution. ×, asymptotic solution of Burgers's equation.

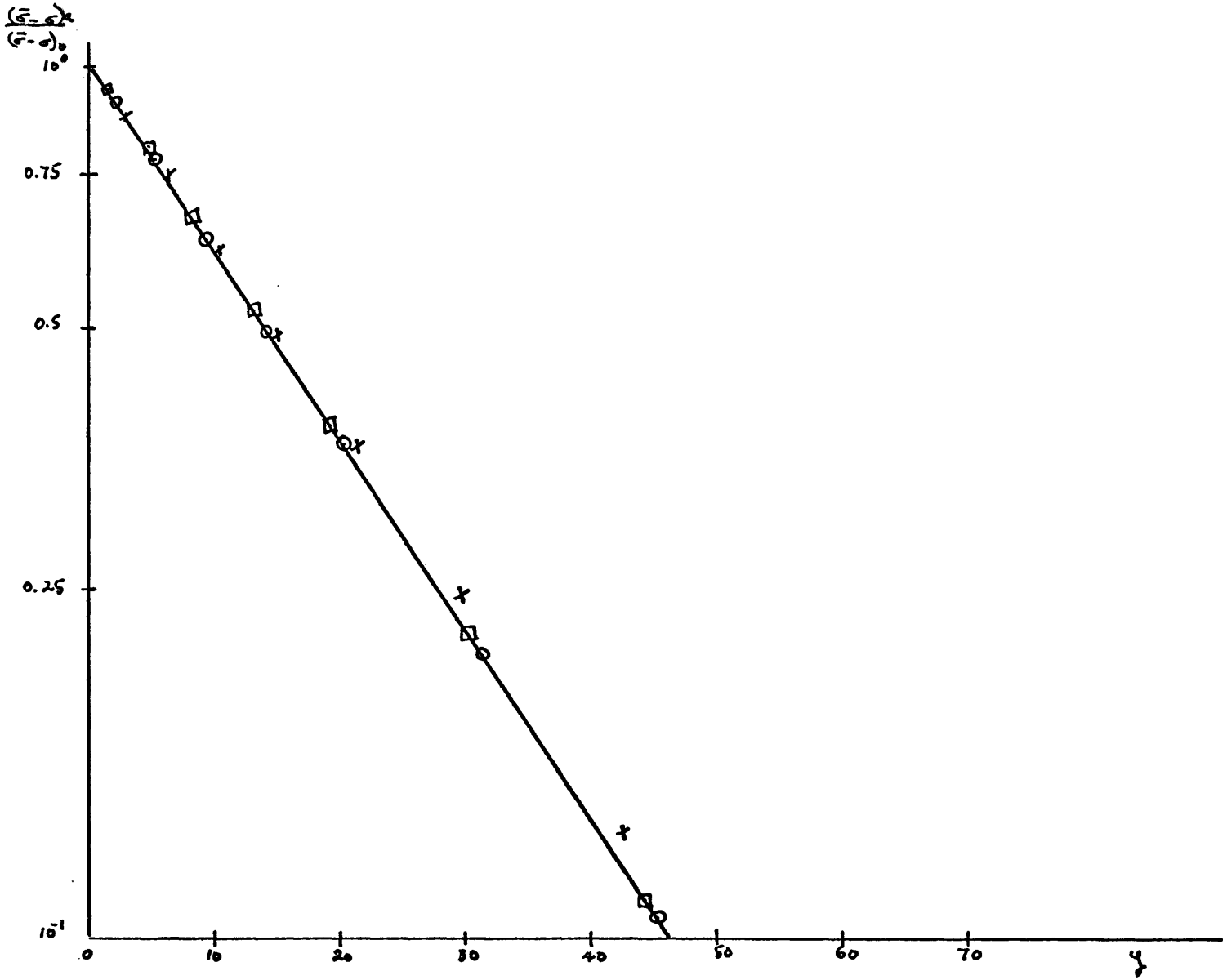

FIGURE 5(i). ALPHA-SHOCK DECAY. ($\theta_w = 0.212°$, $m_{\infty} = 3.80$ and $c_{wb} = 1$).

×, characteristics. —, linear theory. ⊙, first approximation (Whitham's rule).
⊡, second approximation.

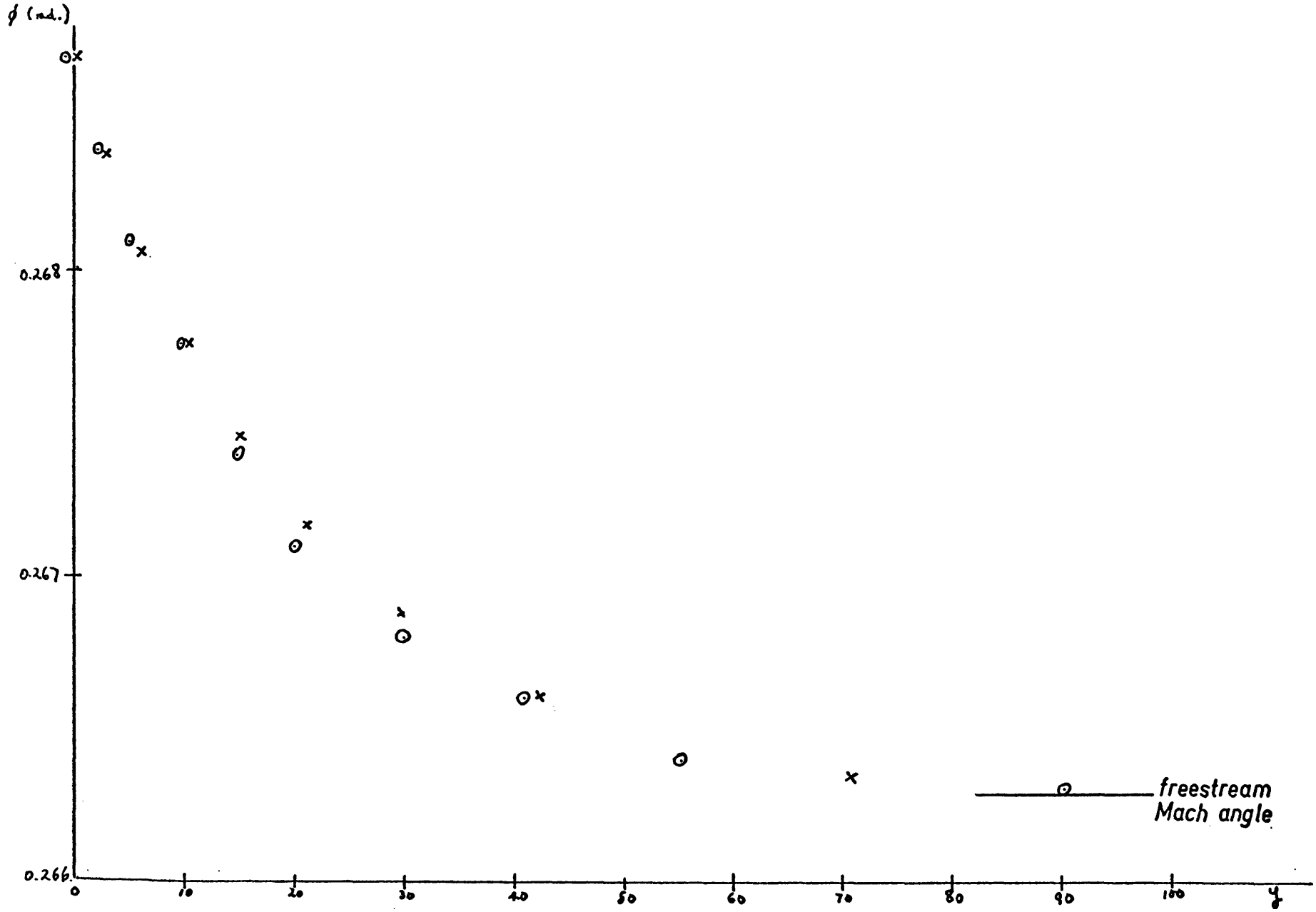

FIGURE 5(j). (see figure 5(i) for legend).

APPENDIX 1

The relationship between the wedge angle, equilibrium Mach number, vibrational specific heat and shock wave angle is given by

$$\tan\theta_w = 2\cot\phi_e \frac{(M_{e\infty}^2 \sin^2\phi_e - 1)}{\left(M_{e\infty}^2(\gamma_e + \cos 2\phi_e) + 2\right)}$$

Dividing by $\sin^2\phi_e$ and noting that

$$\sin^{-2}\phi_e = \operatorname{cosec}^2\phi_e = 1 + \cot^2\phi_e$$ we get

$$\tan\theta_w = \frac{2\cot\phi_e\,(M_{e\infty}^2 - 1 - \cot^2\phi_e)}{\left((\gamma_e+1)M_{e\infty}^2 + 2\right)(1+\cot^2\phi_e) - 2M_{e\infty}^2)}$$

Cross multiplying and collecting powers of $\cot\phi_e$ gives

$$\cot^3\phi_e + \frac{\tan\theta_w}{2}\left((\gamma_e+1)M_{e\infty}^2 + 2\right)\cot^2\phi_e - (M_{e\infty}^2 - 1)\cot\phi_e + \frac{\tan\theta_w}{2}\left((\gamma_e - 1)M_{e\infty}^2 + 2\right) = 0$$

This is a cubic equation in $\cot\phi_e$. The standard trignometrical method of solution gives

$$\cot\phi_e = \left(\frac{4n_2^2}{9} - \frac{4}{3}n_1\right)^{\frac{1}{2}} \cos\left(\frac{1}{3}\cos^{-1}\left(\frac{-4\left(\frac{2n_2^3}{27} - \frac{n_1 n_2}{3} + n_0\right)}{\left(\frac{4n_2^2}{9} - \frac{4}{3}n_1\right)^{\frac{3}{2}}}\right) + \frac{2\pi j}{3}\right) - \frac{n_2}{3}$$

where

$$n_0 = \frac{\tan\theta_w}{2}\left((\gamma_e - 1)M_{e\infty}^2 + 2\right),$$

$$n_1 = 1 - M_{e\infty}^2,$$

$$n_2 = \frac{\tan\theta_w}{2}\left((\gamma_e+1)M_{e\infty}^2 + 2\right)$$

and $j = 0, 1, 2$.

If we let $\theta_W \to 0$ then for the weak solution we expect $\cot\phi_e \to (m_{e\infty}^2 - 1)^{\frac{1}{2}}$ and for the strong solution $\cot\phi_e \to 0$

Putting $\theta_W = 0$ in the solution for $\cot\phi_e$ gives

$$\cot\phi_e = \left(\frac{4}{3}(m_{e\infty}^2-1)\right)^{\frac{1}{2}} \cos\left(\tfrac{1}{3}\cos^{-1}(0) + \frac{2\pi j}{3}\right) \quad \text{so}$$

when $j = 0$

$$\cot\phi_e = \left(\frac{4}{3}(m_{e\infty}^2-1)\right)^{\frac{1}{2}} \cos\left(\frac{\pi}{6}\right) = (m_{e\infty}^2-1)^{\frac{1}{2}}$$

Hence $j = 0$ corresponds to the weak solution.

When $j = 1$

$$\cot\phi_e = \left(\frac{4}{3}(m_{e\infty}^2-1)\right)^{\frac{1}{2}} \cos\left(\frac{\pi}{6} + \frac{2\pi}{3}\right) < 0$$

Hence $j = 1$ corresponds to no physical solution since $\phi_e < 0$ or $\phi_e > \frac{\pi}{2}$.

When $j = 2$

$$\cot\phi_e = \left(\frac{4}{3}(m_{e\infty}^2-1)\right)^{\frac{1}{2}} \cos\left(\frac{\pi}{6} + \frac{4\pi}{3}\right)$$
$$= 0$$

Hence $j = 2$ corresponds to the strong solution.

Mascitti (1968) has given a similar solution in terms of $\sin^2\phi_e$

The solution presented here for $\cot\phi_e$ involves rather simpler coefficients in the cubic.

REFERENCES

BARDSLEY, O. 1951
The conditions at a sharp leading edge in supersonic flow.
Phil. Mag. 42, 255

BARDSLEY, O. MAIR, V.A. 1952
Separation of the boundary layer at a slightly blunt leading edge in supersonic flow
Phil. Mag. 43, 344

BHANGU, J.K. 1966
Shock tube studies of vibrational relaxation in N_2O
J.F.M. 25, 817

BLYTHE, P.A. 1969
Non-linear wave propagation in a relaxing gas
J.F.M. 37, 31

CAPIAUX, R. WASHINGTON, M. 1963
Non-equilibrium flow past a wedge
A.I.A.A. J. 1, 650

CHONG, T.H. SIROVICH, L. 1971
Non-linear effects in steady supersonic dissipative gasdynamics. Part 1. Two-dimensional flow
J.F.M. 50, 161

CHOU, D.C. CHU, B.T. 1971
On the decay of weak shock waves in axisymmetric non-equilibrium flow
J.F.M. 50, 355

CHU, B.T. 1958
Wave propagation in a reacting mixture
Heat Transf. Fluid Mech. Inst., 80

CHU, B.T. 1970
Weak non-linear waves in non-equilibrium flow
Article in 'Non-equilibrium Flows'
edited by P.P. Wegener, published by Dekker, Part 2, p33

CLARKE, J.F. 1960
The linearized flow of a dissociating gas
J.F.M. 5, 577

CLARKE, J.F. 1965
On a first order wave theory for a relaxaing gas flow
Co. A. Report Acro., 182

CROW, S.C. 1969
Distortion of sonic bangs by atmospheric turbulence
J.F.M. 37, 529

DEJARNETTE, F.R. 1966
Application of Lax's finite difference method to non-equilibrium hypersonic flow problems
N.A.S.A. T.R. R.-234

REFERENCES(contd.)

DER, J.J. 1961
Linearized supersonic non-equilibrium flow past an arbitrary boundary
N.A.S.A. T.R. - 119

DER, J.J. 1963
Theoretical studies of supersonic two-dimensional and axisymmetric non-equilibrium flow including calculations of flow through a nozzle
N.A.S.A. T.R. - 164

FELDMAN, S. WIDAWSKY, A. 1962
Errors in calculating flowfields by the method of characteristics
A.R.S. J. 32, 434

GRIFFITH, W.C. KENNY, A. 1957
On fully dispersed shock waves in CO_2
J.F.M. 3, 286

HODGSON, J.P. JOHANNESEN, N.H. 1971
Real gas effects in very weak shock waves in the atmosphere and the structure of sonic bangs
J.F.M. 50, 17

JOHANNESEN, N.H. 1961
Analysis of vibrational relaxation regions by the Rayleigh line method
J.F.M. 10, 25

JOHANNESEN, N.H. ZIENKIEWICZ, H.K.
BLYTHE, P.A. GERRARD, J.H. 1962
Experimental and theoretical analysis of vibrational relaxation regions in CO_2
J.F.M. 13, 213

JOHANNESEN, N.H. BIRD, G.A. ZIENKIEWICZ, H.K. 1967
Theoretical and experimental investigations of the reflection of normal shock waves with vibrational relaxation
J.F.M. 30, 51

LEE, R.S. 1964
A unified analysis of supersonic non-equilibrium flow over a wedge: I. vibrational non-equilibrium
A.I.A.A. J. 2, 637

LICK, W. 1966
The shock expansion method and Whitham's rule
J.F.M. 25, 179

LICK, W. 1967
Wave propagation in real gases
Advances in Applied Mechanics
vol.10, Fascicle 1. Academic Press, New York.

LICK, W. 1969
Two variable expansion and singular perturbation problems
S.I.A.M. J. Appl. Math. 17, 815

REFERENCES (contd.)

LICK, W. 1970
Non-linear wave propagation
Article in 'Annual Review of Fluid Mechanics' 2, 113

LIEPMANN, H.W. ROSHKO, A. 1967
Elements of Gasdynamics. Wiley

LIGHTHILL, M.J. 1956
Viscosity in waves of finite amplitude
Article in 'Surveys in Mechanics', edited by G.K. Batchelor and R.M. Davies, Cambridge University Press

LIN, C.C. 1954
On a perturbation theory based on the method of characteristics
J. Math. and Physics 33, 117

MASCITTI, V.R. 1968
A closed-form solution to oblique shock wave properties
J. Aircraft 6, 66

M^{c}CABE, A. 1966
The three-dimensional interaction of a shock wave with a turbulent boundary layer
Aeronautical Quarterly 17, 231

MOORE, F.K. GIBSON, W.E. 1960
Propagation of weak disturbances in a gas subject to relaxation effects
J. Aerospace Sci. 27, 117

OCKENDON, H. SPENCE D.A. 1969
Non-linear wave propagation in a relaxing gas
J.F.M. 39, 329

PHINNEY, R. 1964
Non-dimensional solutions of flows with vibrational relaxation
A.I.A.A. J. 2, 240

POWERS, S.A. O'NEILL, J.B. 1962
Determination of hypersonic flowfields by the method of characteristics
A.I.A.A. J. 1, 1693

REES, T. 1968
Computer calculations of relaxation regions and equilibrium conditions for shock waves with tables for CO_2 and N_2O
R. and M. N^{o}. 3472

ROMBERG, G. 1970b
Bildung schwacher stationärer Stosswellen in relaxierenden Gasgemischen
Z.A.M.P. 21, 145

ROMBERG, G. 1970a
Über die Anwerdbarkeit des analytischen Charakteristikenverfahrens bei Welkenansbreitungen in relaxierenden Gasen
Z. Flugwiss. 18, 65

REFERENCES (contd.)

SAUERWEIN, H. 1966
The method of characteristics for the three-dimensional unsteady magnetofluid dynamics of a multi-component medium
J.F.M. 25, 17

SEDNEY, R. SOUTH, J.C. GERBER, N. 1962
Characteristic calculations of non-equilibrium flows
Rep. No. 1173, Ballistic Res. Lab.,
Aberdeen Proving Ground

SEDNEY, R. 1970
The method of characteristics.
Article in 'Non-equilibrium Flows' edited by P.P. Wegener, published by Dekker, Part 2, Chapter 4, p159

SHARP, A.W. 1959
Supersonic flow past a leading edge separation bubble
J.F.M. 5, 445

SOUTH, J.C. 1964
Application of the method of integral relations to supersonic non-equilibrium flow past wedges and cones
N.A.S.A. T.R. R.-205

SUSSMAN, M.B. BARON, J.R. 1967
Approximate analysis of linearized inviscid relaxing gas flow
Physics of Fluids 10, 2128

VAN DYKE, M. 1964
Perturbation Methods in Fluid Mechanics
Academic Press, New York.

VINCENTI, W.G. 1962
Linearized flow over a wedge in a non-equilibrium oncoming stream
J. Mecan. 1, 193

VINCENTI, W.G. KRUGER, C.H. 1965
Physical Gas Dynamics
Wiley

WHITHAM, G.B. 1958
On the propagation of shock waves through regions of non-uniform area or flow
J.F.M. 4, 337

WOOD, A.D. SPRINGFIELD, J.F. PALLEN, A.J. 1964
Determination of the effects of chemical and vibrational relaxation on an inviscid hypersonic flowfield
A.I.A.A. J. 2, 1697

ZIENKIEWICZ, H.K. JOHANNESEN, N.H. 1963
Departures from the linear equation for vibrational relaxation in shock waves in O_2 and CO_2
J.F.M. 17, 499

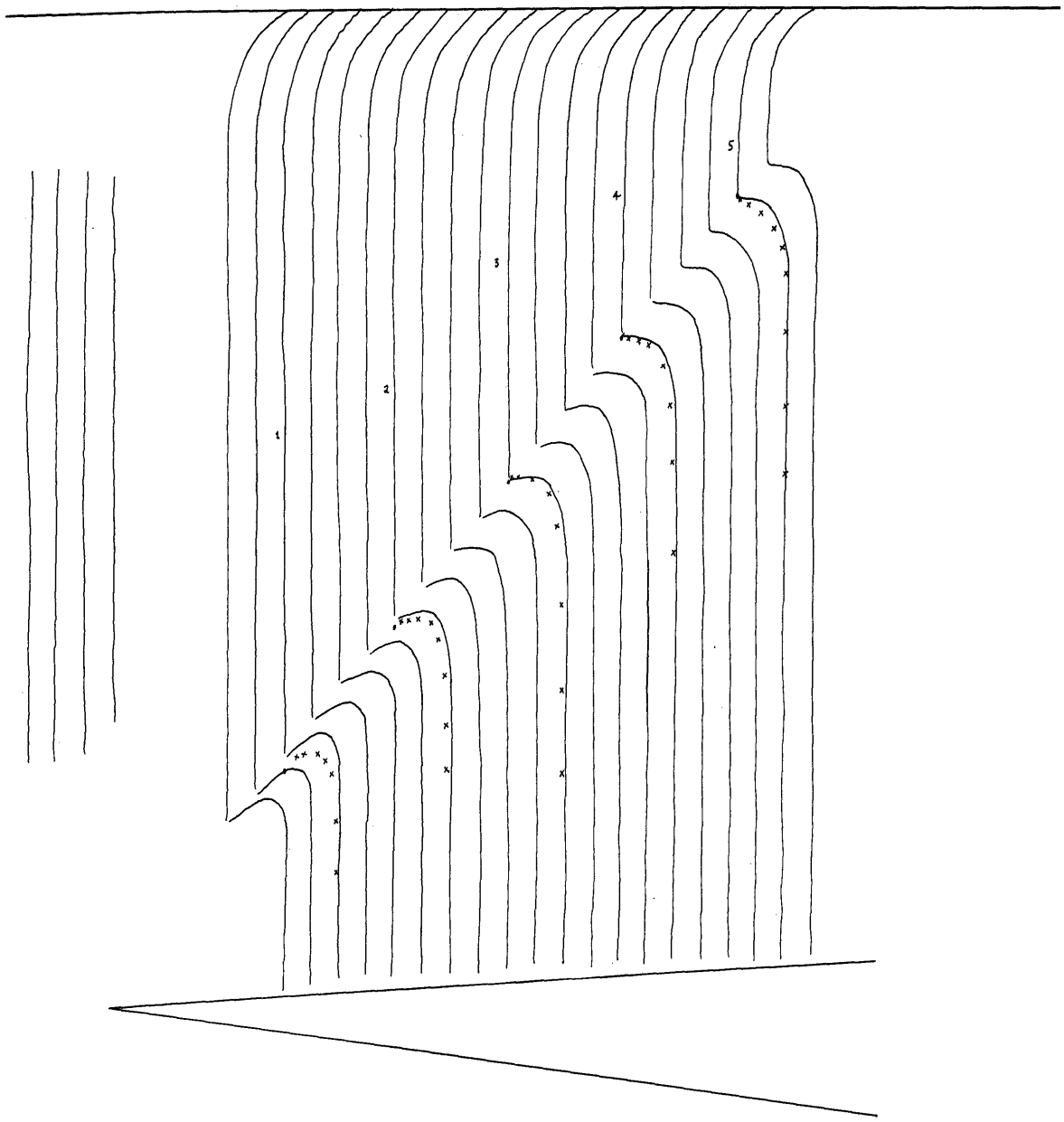

RUN NUMBER R 1119

FIGURE 4(e). COMPARISON OF EXPERIMENTAL AND THEORETICAL FRINGE PATTERNS.

($\theta_w = 2.00°$, $M_{\infty} = 1.68$ and $c_{wb} = 2.28$). —, experiment. x, theory. •, alpha-shock location (theory).

figure 4(e).

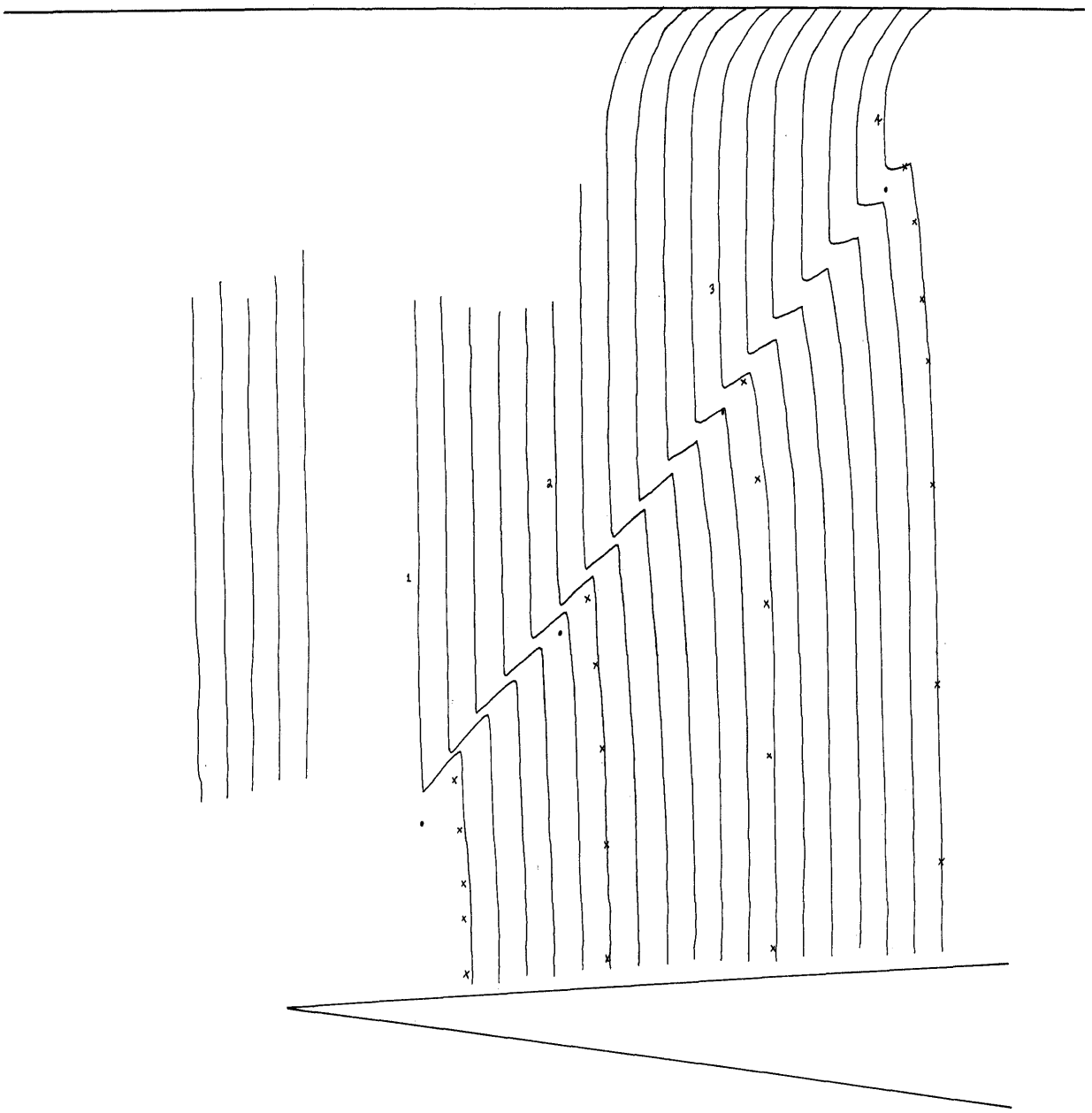

FIGURE 4(f). COMPARISON OF EXPERIMENTAL AND THEORETICAL FRINGE PATTERNS. ($\theta_w = 2.00°$, $M_{\infty} = 1.68$ and $c_{nb} = 2.19$).
— , experiment. × , theory. · , alpha-shock location (theory).

figure 4(f).

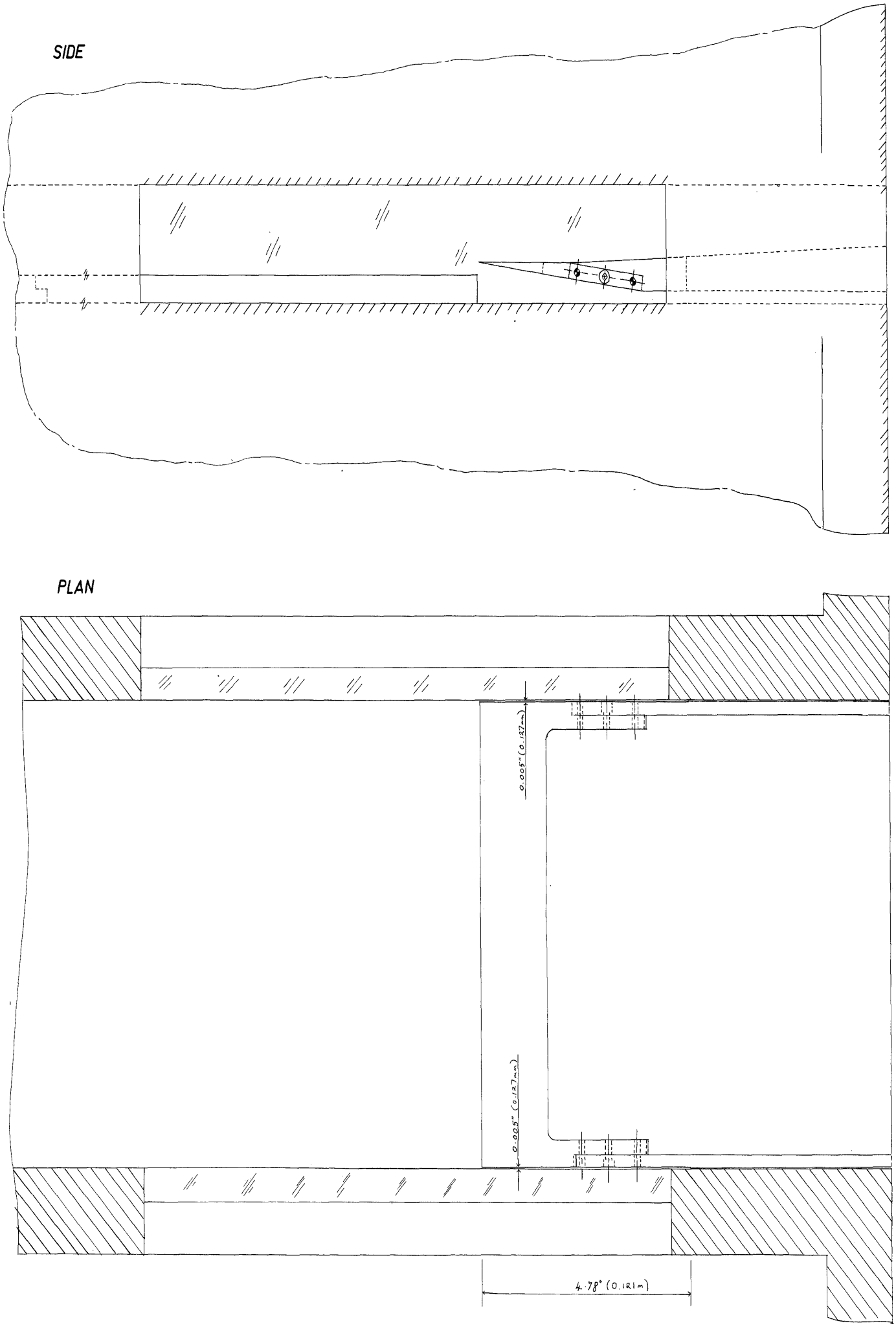

FIGURE 4(b). WEDGE MODEL IN WORKING SECTION. (Full scale).

figure 4(b).

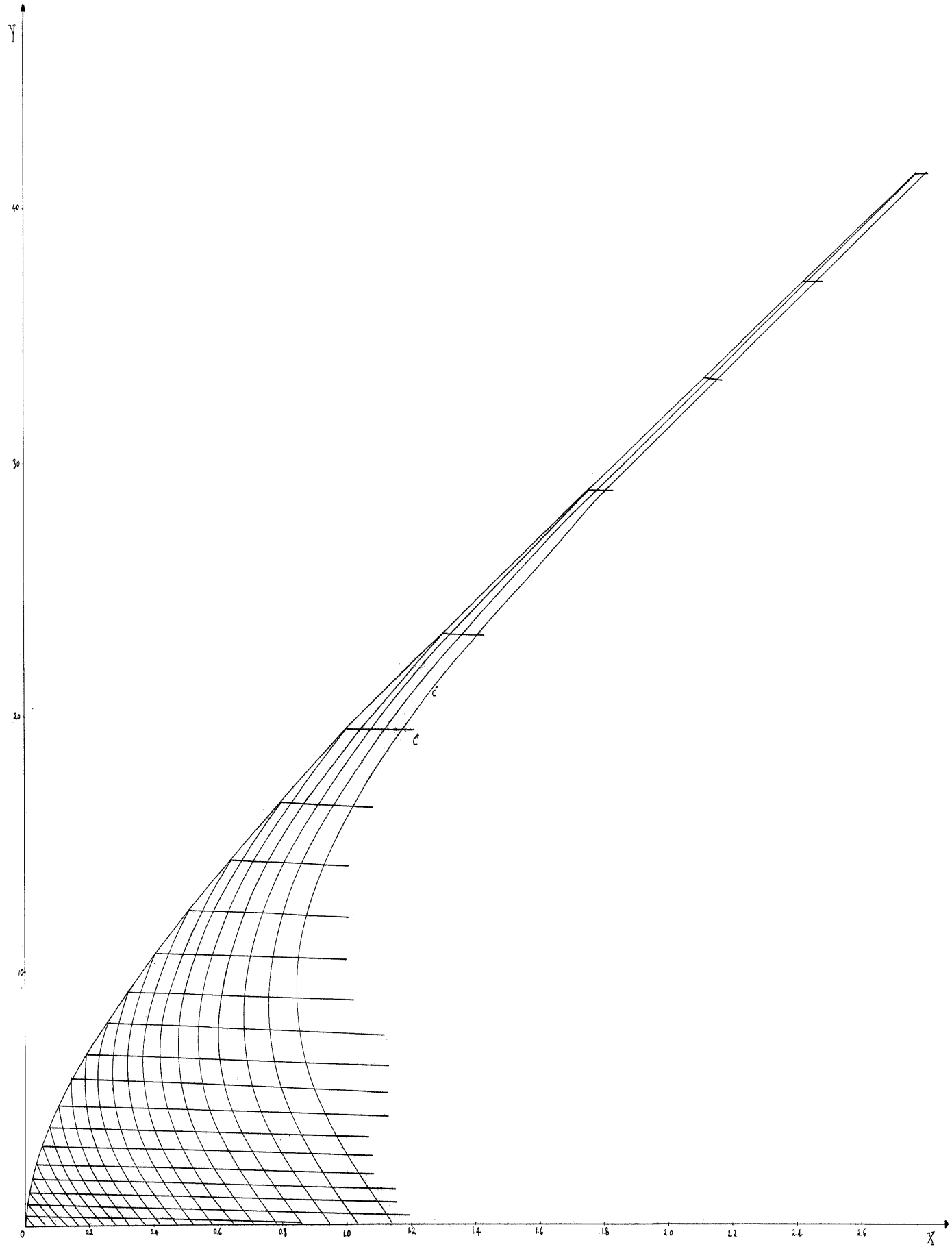

FIGURE 2(k). CHARACTERISTIC MESH ($\theta_w = 2.00°$, $n_{50} = 1.69$ and $c_{n_0} = 2.12$).

Figure.2(k).

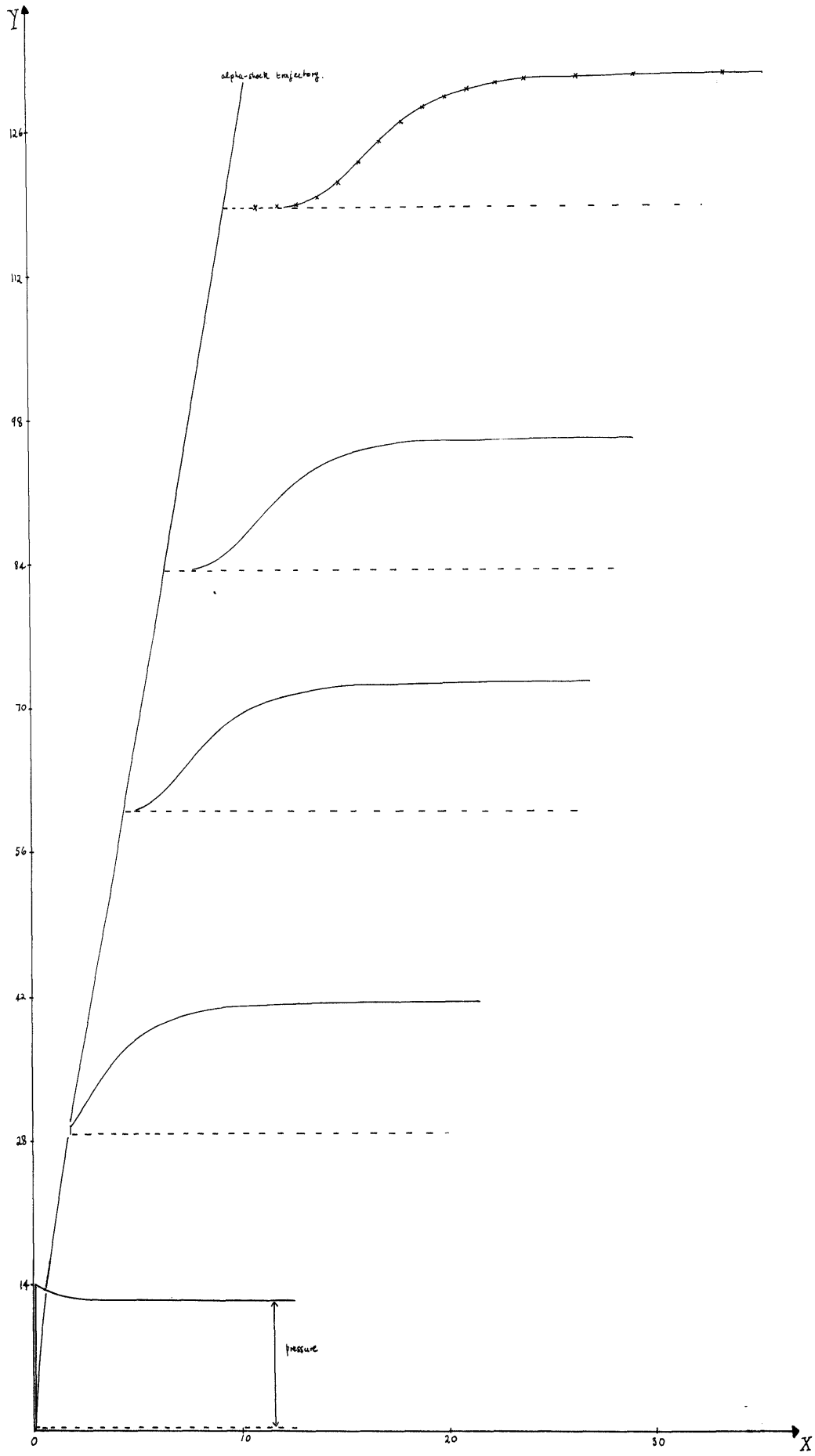

FIGURE 2(j). SHOCK WAVE DEVELOPMENT. ($\theta_w = 2.00°$, $m_{\infty} = 1.49$ and $c_{vib} = 2.12$. $p_e = 1.09$).
x ; exact solution at infinity. — , characteristics solution.

G 39103

figure 2[j].

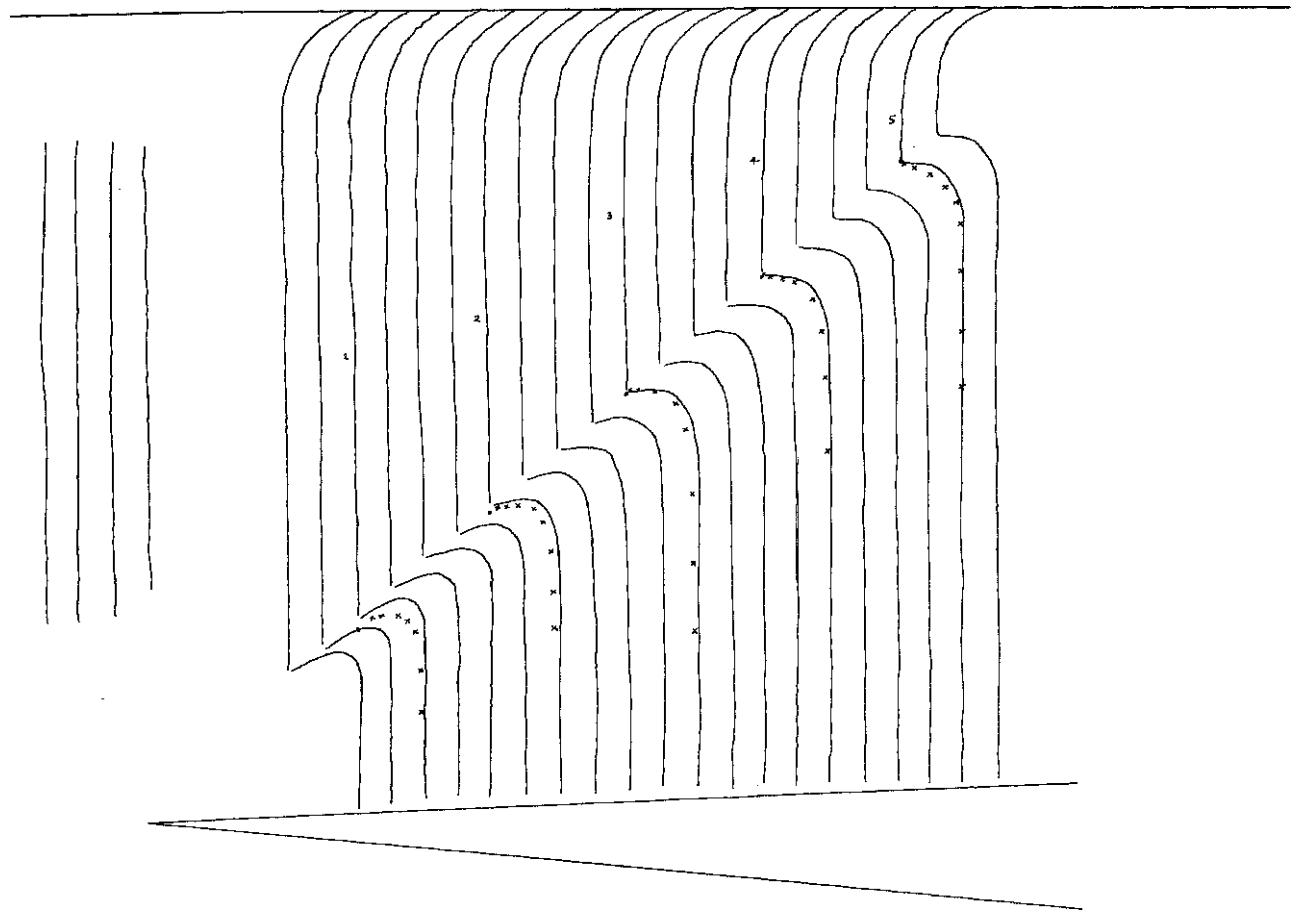

RUN NUMBER R 1119

FIGURE 4(e). COMPARISON OF EXPERIMENTAL AND THEORETICAL FRINGE PATTERNS.
($\theta_w = 2.00°$, $M_\infty = 1.65$ and $c_{wb} = 2.25$). —— , experiment. × , theory. • , alpha-shock location (theory) .

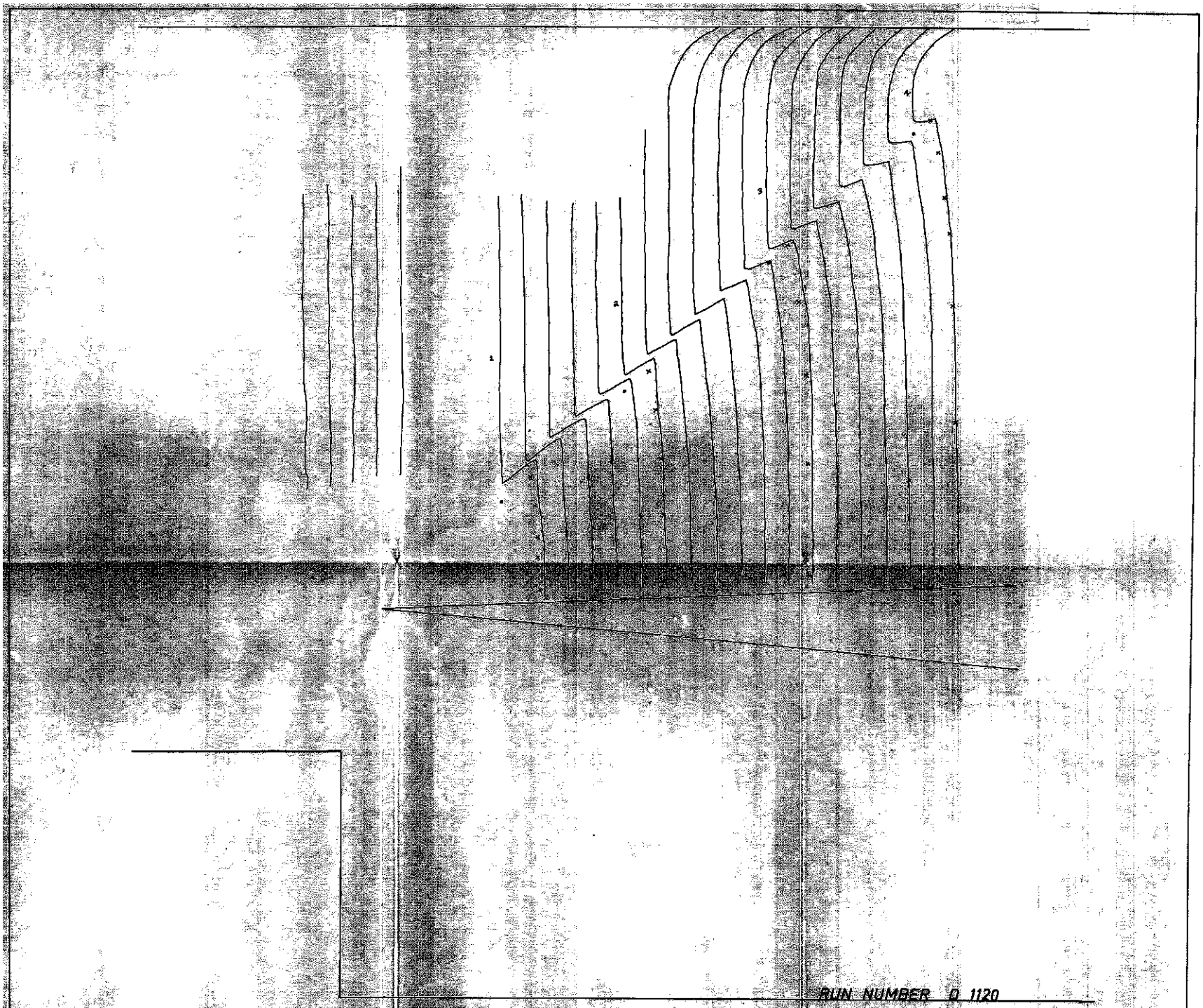

FIGURE 4(f) COMPARISON OF EXPERIMENTAL AND THEORETICAL FRINGE PATTERNS (θ_c = 2.00°, M_{max} = 1.45 and c_{max} = 2.19).
— experiment, × , theory, · , alpha-shock location (theory).

figure 4(f).

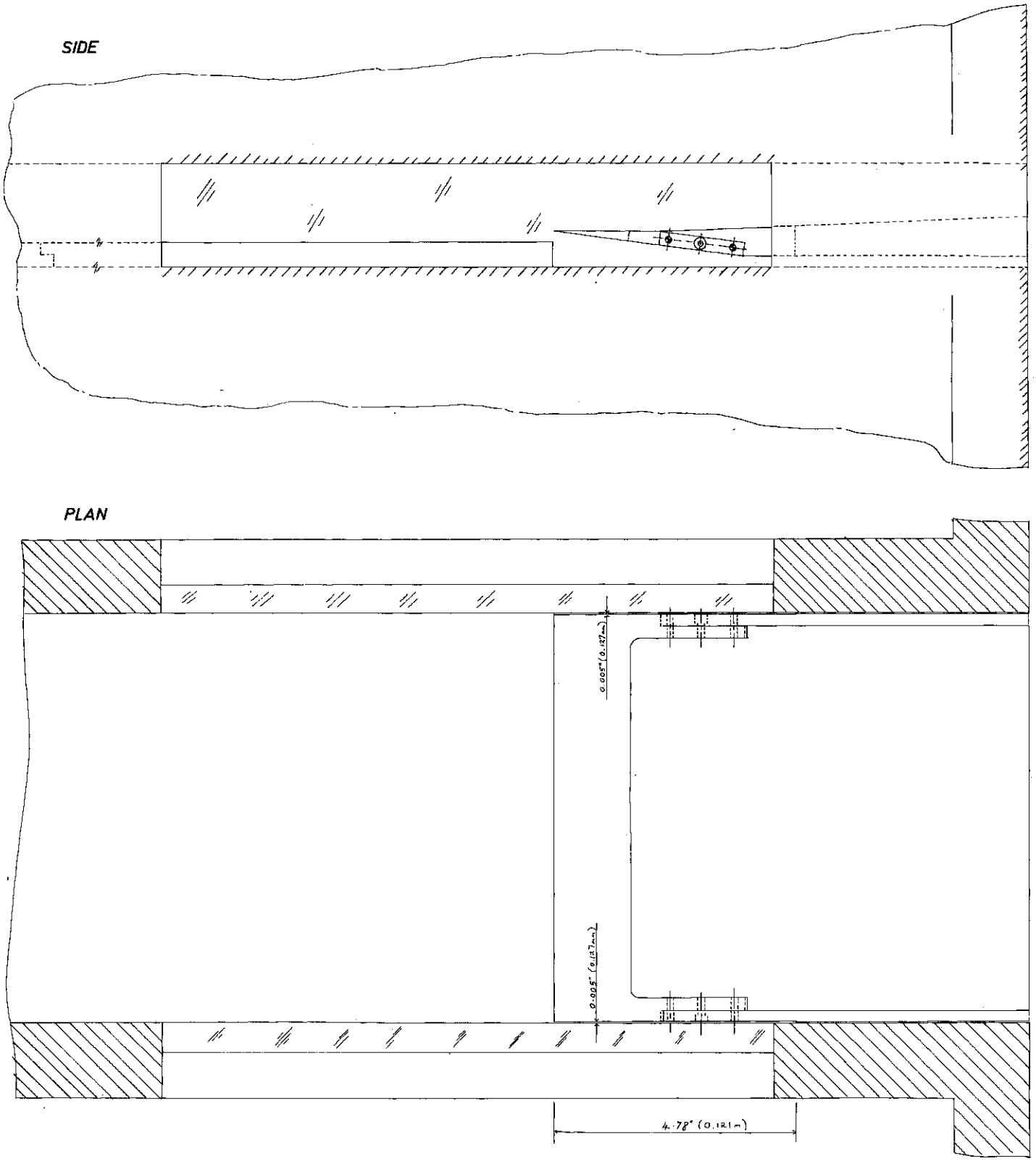

FIGURE 4(b). WEDGE MODEL IN WORKING SECTION. (Full scale).


figure_4(b)

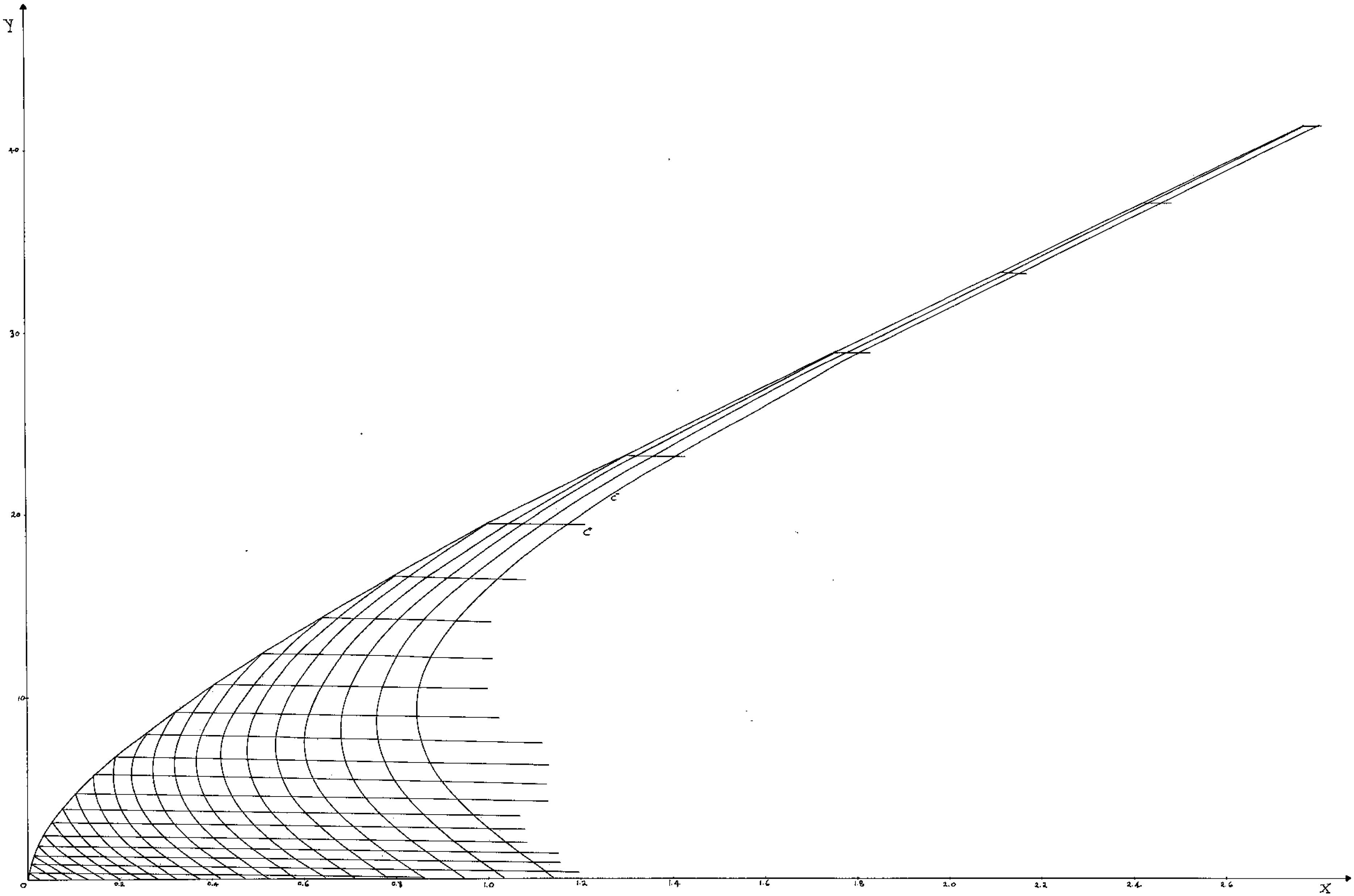

FIGURE 2(k). CHARACTERISTIC MESH. ($\theta_w = 2.00°$, $n_{gw} = 1.49$ and $c_{mb} = 2.12$).

figure 2(b).

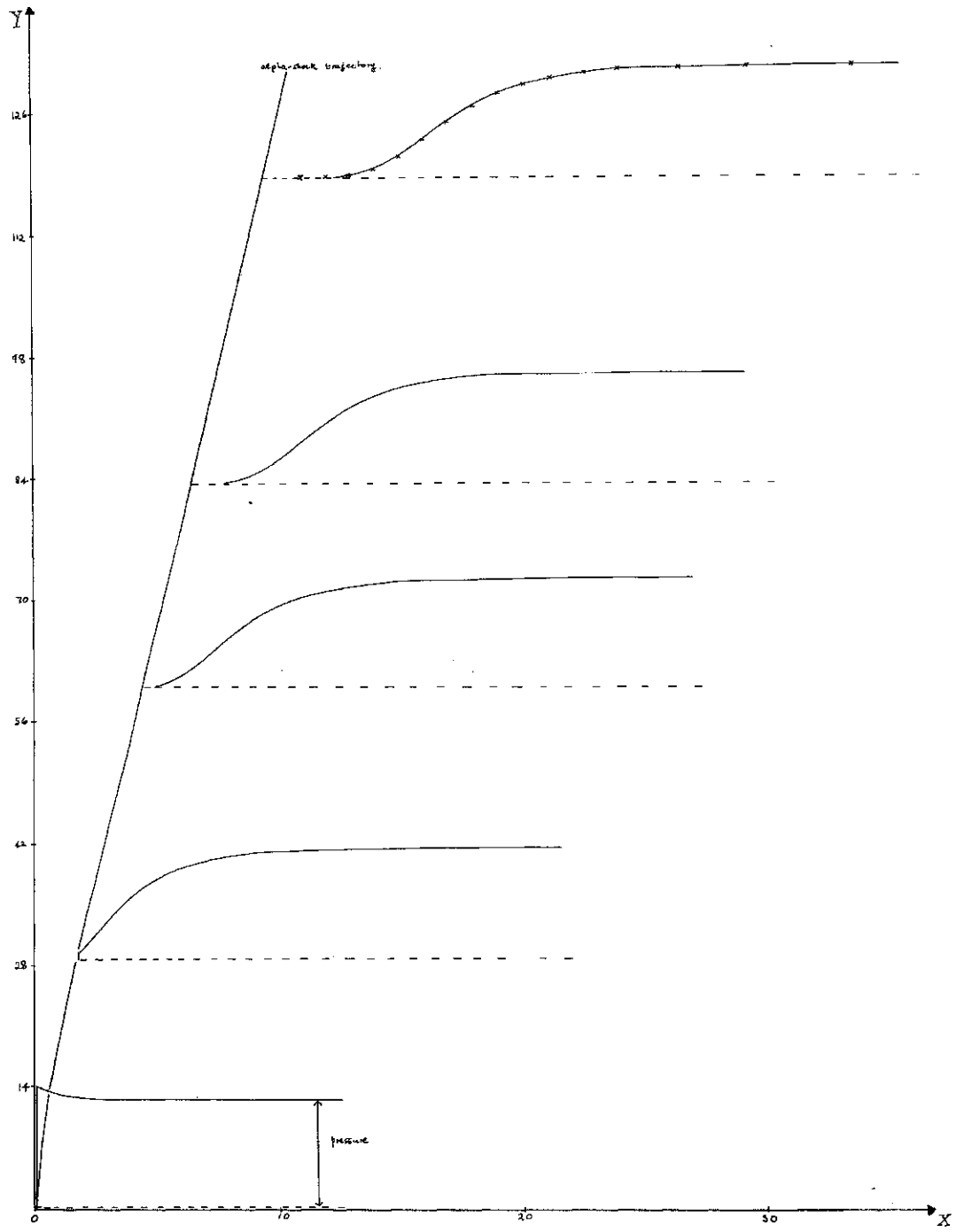

FIGURE 2(j). SHOCK WAVE DEVELOPMENT. ($\theta_c = 2.00°$, $M_{\infty} = 1.49$ and $\cos\lambda = 2.12$. $\beta_c = 1.09$).
x ; exact solution at infinity. — , characteristics solution.

G 39102

figure 2(j).